TRANSACTIONS
OF THE ASME
Series A

Journal of ENGINEERING FOR POWER

October 1961

Divisions: POWER • GAS TURBINE POWER • NUCLEAR ENGINEERING • FUELS OIL AND GAS POWER • HYDRAULIC • **Research Committees:** FURNACE PERFORMANCE FACTORS • CORROSION AND DEPOSITS FROM COMBUSTION GASES • BOILER FEEDWATER STUDIES • HIGH TEMPERATURE STEAM GENERATION • CONDENSER TUBES • PROPERTIES OF STEAM • **Committees on:** AIR POLLUTION CONTROLS SOLAR ENERGY APPLICATION • **And:** POWER TEST CODES COMMITTEES

Published Quarterly by
THE AMERICAN SOCIETY OF MECHANICAL ENGINEERS

TRANSACTIONS OF THE ASME
Series A

EDITORIAL DEPARTMENT

Editor, J. J. JAKLITSCH, JR.
Consulting Editor, LEO BLODGETT
Production, JEAN NORTH
Art Editor, HENRY BALFOUR

OFFICERS OF THE ASME

President, W. H. BYRNE
Secretary, O. B. SCHIER, II
Treasurer, E. J. KATES
Assistant Treasurer, H. J. SAUER

PUBLICATIONS COMMITTEE

Chairman, HENDLEY N. BLACKBURN
R. D. MINDLIN
MARTIN GOLAND
VITO L. SALERNO
F. J. HEINZE
Junior Representatives
J. W. FOLLANSBEE
STEWART H. ROSE

REGIONAL ADVISORY BOARD

Region I, H. M. ROGERS, JR.
Region II, ROBERT E. ABBOTT
Region III, A. F. BOCHENEK
Region IV, FRANCIS C. SMITH
Region V, WM. J. TITZEL
Region VI, C. R. EARLE
Region VII, RALPH L. SCORAH
Region VIII, G. CORRY MCDONALD
Region IX, M. S. UMBENHAUER
Region X, CARL J. ECKHARDT

Published quarterly by The American Society of Mechanical Engineers. Publication office at 20th and Northampton Streets, Easton, Pa. The editorial department is located at the headquarters of the Society, 345 East Forty-Seventh Street, New York 17, N. Y. Cable address "Mechanize," New York. Price $1.00 a copy, $10.00 annually, to members, $1.50 a copy, $6.00 annually. Add 50 cents for postage to all countries outside the United States and Canada. Changes of address must be received at Society headquarters seven weeks before they are to be effective on the mailing list. Please send old as well as new address. . . . By-Law: The Society shall not be responsible for statements or opinions advanced in papers or . . . printed in its publications (B13, Par. 4). . . . Second-class mail privileges authorized at Easton, Penna. . . . This publication is authorized to be mailed at the special rates of postage prescribed by Section 132.122 . . . © Copyrighted 1961, by The American Society of Mechanical Engineers. Reprints from this publication may be made on condition that full credit be given the TRANSACTIONS OF THE ASME, Series A—Journal of Engineering for Power, and the author, and that date of publication be stated.

TRANSACTIONS OF THE ASME
is indexed by the Engineering Index, Inc.

Journal of ENGINEERING FOR POWER

VOLUME 83 • SERIES A • NUMBER 4
October 1961

CONTENTS

331 **Vacuum Deaerator Design** (60—WA-214)
A. W. Kingsbury and E. L. Phillips

339 **Performance of Stainless-Steel Condenser Tubes** (60—WA-217)
R. H. Pell

343 **Evaluation of Steam Washers in Power-Plant Boilers** (60—WA-213)
H. A. Klein

354 **German Development in Acid Cleaning of High-Pressure Boilers** (60—WA-227)
H. G. Heitmann

363 **Acid Cleaning of Superheaters and Reheaters** (60—WA-219)
W. F. Ashton and S. M. Rose

367 **Precautions in the Use of Citric Acid for Chemical Cleaning** (60—WA-221)
E. B. Morris

371 **Inlet Guide Vane Performance of Centrifugal Blowers** (60—WA-130)
A. J. Stepanoff

381 **Dissimilarity Laws in Centrifugal Pumps and Blowers** (60—WA-145)
A. J. Stepanoff and H. A. Stahl

392 **The Significance of the Hall Effect for Three MHD Generator Configurations** (60—WA-329)
L. P. Harris and J. D. Cobine

397 **Experiments With MHD Power Generation** (60—WA-328)
S. Way, S. M. DeCorso, R. L. Hundstad, G. A. Kemeny, W. Stewart, and W. E. Young

409 **Power-Plant Performance Monitoring** (60—WA-222)
J. Kenneth Salisbury

423 **The Application of the Deviation Concept of Turbine Cycle Monitoring** (60—WA-166)
H. T. Hoffman and C. P. Welch

433 **Optimizing a Regenerative Steam-Turbine Cycle** (60—WA-179)
G. Chiantore, D. Borgese, F. Baldo, and J. H. Potter

444 **A Study of Sulfur Reactions in Furnace Deposits** (60—WA-183)
M. Weintraub, S. Goldberg, and A. A. Orning

451 **The Role of Chemical Thermodynamics in Analyzing Gas-Side Problems in Boilers** (60—WA-182)
R. H. Boll and H. C. Patel

468 **Corrosion of Superheaters and Reheaters of Pulverized-Coal-Fired Boilers, II** (60—WA-180)
Carl Cain, Jr., and Wharton Nelson

A. W. KINGSBURY
E. L. PHILLIPS
The Permutit Company, a Division of Pfaudler Permutit Inc., New York, N. Y.

Vacuum Deaerator Design

A study was made of vacuum desorption of oxygen and carbon dioxide from water using 1-in. Raschig rings in a 2-ft-diameter tower having a maximum packing height of 22 ft. The effect of various operating variables on the HTU was investigated and the data correlated to give a practical basis for designing vacuum deaerators.

THE cold-water vacuum deaerator is finding application in the treatment of industrial waters containing contaminant gases which may interfere with a chemical process or be responsible for corrosion. The study of the operating characteristics of a unit approaching industrial size was made to obtain data which could be used as a basis for practical design for oxygen or carbon-dioxide removal.

The concept of the height of a transfer unit (HTU) was used for predicting the most economical combination of tower height and size of vacuum pump for a required effluent concentration.

The basic concept as given by Chilton and Colburn [1][1] was adopted by Knoedler and Bonilla [2] in their work on vacuum desorption of oxygen using Stedman triangular packing. The height of the packed tower h, including the end effect h_e, is equal to the product of the number of transfer units $(NTU)_{OL}$ and the over-all height of a transfer unit $(HTU)_{OL}$, or

$$h + h_e = (NTU)_{OL}(HTU)_{OL} \quad (1)$$

The $(NTU)_{OL}$ is determined from the following relationship:

$$(NTU)_{OL} = 2.3 \log \frac{x_i - x_e}{x_o - x_e} \quad (2)$$

where

$(HTU)_{OL}$ = over-all height of transfer unit using liquid-phase driving force, ft
$(NTU)_{OL}$ = number of transfer units based on over-all driving force in liquid-phase concentration units
x_i = concentration of solute gas at inlet to tower, ppm
x_o = concentration of solute gas at outlet of tower, ppm
x_e = concentration of solute gas in equilibrium with gas phase in tower, ppm

Experimental Unit

The arrangement of the tower and auxiliary equipment is shown in Fig. 1. The steel column was packed to a height of 22 ft with dumped 1-in. ceramic Raschig rings. The rings were supported by a subway grating. The inlet distributor was a spray nozzle which impinged upon a baffle plate covering the vapor outlet.

The aerated plant-water supply had a high enough oxygen content for the purposes of the tests. It was necessary to add carbon dioxide from a cylinder which first discharged to an expansion tank. This was required to prevent freezing at the point of addition to the inlet water.

The effluent from the tower could be recirculated to the inlet. This procedure was used in some cases where carbon dioxide was added to water almost free of oxygen.

Vacuum was maintained in the tower by use of a 3-stage steam-ejector system. The tower pressure was regulated by using various combinations of stages and by throttling the suction of the ejectors by means of a plug valve.

Tower pressure was measured by means of a Dubrovin gage. All joints and connecting tubing were varnished to minimize the possibility of air leakage. The tower was tested by shutting off the inlet and suction valves and observing any leakage on the vacuum gage.

Test Procedures

The water used in the tests was from a surface supply which varied in temperature from winter to summer and frequently from day to day over a fairly wide range. As there was no practical way of controlling the temperature, it was impossible to hold this factor constant. Under the circumstances, it was necessary to group the test runs in various temperature ranges, using data accumulated over an extended period.

The height of the packing was varied by submerging the Raschig rings to the required level. The amount of degasification occurring in the submerged portion was insignificant.

Sampling was from the discharge of the centrifugal pump at the deaerator outlet. The pump was provided with a water seal from the pump discharge. Alternately, samples were taken directly from the tower through a pipeline extending from a gage-glass connection to floor level. A small vacuum pump was used to provide enough negative head to allow the sample to be drawn

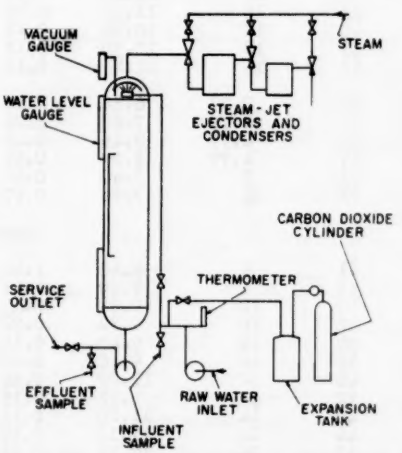

Fig. 1 Vacuum deaerator; two-ft-diameter tower filled with 22 ft of 1-in. Raschig rings

[1] Numbers in brackets designate References at end of paper.

Contributed by the Joint Research Committee on Boiler Feedwater Studies and presented at the Winter Annual Meeting, New York, N. Y., November 27–December 2, 1960, of THE AMERICAN SOCIETY OF MECHANICAL ENGINEERS. Manuscript received at ASME Headquarters, August 24, 1960. Paper No. 60—WA-214.

through a sampling flask or pipette. Samples from either point checked within the degree of accuracy of the analytical method.

Analytical Procedures

Oxygen analyses were by the Winkler method. Check analysis by the modified Schwartz-Gurney procedure [3] indicated that interferences were negligible.

Carbon dioxide was analyzed by back-titrating, after adding the sample to an excess of sodium hydroxide which had been standardized by titrating with standard acid, using phenolphthalein indicator. Blanks were run on each sample after aerating to remove free CO_2. When presence of interfering substances was indicated by an analysis for CO_2 greater than the equilibrium solubility with air, a corresponding deduction was made from the CO_2 determination.

No analysis for nitrogen was made. As the water supply was aerated, nitrogen was calculated to be present in proportion to its relative solubility in water in equilibrium with air.

Determination of NTU

In calculating the number of transfer units (NTU), it will be noted from the relationship

$$\text{NTU} = 2.3 \log \frac{x_i - x_e}{x_o - x_e} \qquad (2)$$

that, as the height of the tower increases, the residual-gas concentration x_e will approach the equilibrium concentration x_e. This places a limitation on the height of a tower which can be used for test purposes, as at low values of x_e, the term $(x_o - x_e)$ is less than the accuracy of the analytical and test procedures. The calculated NTU value is therefore meaningless. The maximum tower height at which significant data could be obtained was about 6 ft for CO_2. For oxygen, data at greater heights could be used as the analytical method is more precise.

The values of x_e for oxygen and carbon dioxide were calculated from Henry's law constants given in the literature [4]. If the calculated equilibrium solubilities were correct for this application, the concentration of the solute gas would approach the equilibrium solubility at high tower heights. This was found to be so within the limits of accuracy of the analytical methods used.

As the gas phase for most runs was a mixture of O_2, N_2, and CO_2 in addition to water vapor, the partial pressure of the gas in question was determined by calculating the mol fraction from the inlet and outlet compositions. The mol fraction multiplied by the difference between the total tower pressure and the water-vapor pressure gave the partial pressure of the gas.

Determination of HTU

If the height of a transfer unit is the same over the entire tower height, a plot of tower height versus $(\text{NTU})_{OL}$ should give a straight line. The $(\text{NTU})_{OL}$ and tower heights for oxygen given in Table 1 were plotted for a flow rate of 40 gpm per sq ft at two temperature ranges, and also at 70 gpm per sq ft, Fig. 2. The straight-line relationship is fairly good.

The HTU is the number of feet of packing height equivalent to one transfer unit. This is also expressed as the reciprocal of the slope of the line.

As the slope of the line is the same for the data for 40 gpm per sq ft at both the low and high-temperature range, it appears that for oxygen desorption the HTU is independent of the water temperature within the limits tested. This is in agreement with

Table 1 Oxygen desorption data; dumped 1-in. Raschig rings

Run #	Temp. °F.	Packing Height Ft.	Inlet O_2 ppm	Outlet O_2 ppm	Inlet CO_2 ppm	Outlet CO_2 ppm	Water Vap. Pres. mm Hg	Total Tower Pres. mm Hg	O_2 Equil. Sol. ppm	NTU
					Water Rate 40 gpm/sq ft					
51	35	4	12.60	2.40	6.5	0.5	5.2	8.8	0.095	1.69
52	35	4	12.60	2.17	6.5	0.5	5.2	8.0	0.074	1.78
53	36	6	11.70	1.37	6.0	1.0	5.3	8.4	0.083	2.19
54	36	6	11.65	1.15	6.0	1.0	5.3	8.2	0.077	2.37
55	37	8	12.00	0.82	7.5	0.5	5.6	8.8	0.082	2.78
56	38	8	12.00	0.73	8.0	1.0	5.7	8.8	0.077	2.89
57	38	10	11.10	0.32	8.0	1.5	5.7	8.8	0.076	3.79
58	38	10	11.10	0.39	7.0	1.5	5.7	8.8	0.077	3.98
48	40	12	10.90	0.22	3.5	4.0	6.2	9.1	0.070	4.27
50	43	12	10.70	0.18	5.5	0	7.1	9.6	0.060	4.48
49	38	16	11.45	0.14	2.0	0	5.8	9.5	0.106	5.80
75	69	0.77	6.84	2.10	88.3	35.3	18.0	23.5	0.026	1.19
78	65	2.77	7.62	1.06	102.8	11.4	15.6	22.0	0.031	1.99
77	64	4.77	7.45	0.48	105.4	19.1	15.6	22.0	0.030	2.81
89	57	4.77	8.89	0.69	87.7	19.2	12.1	18.0	0.038	2.60
64	72	7	7.40	0.30	64.3	16.8	20.1	32.0	0.071	3.47
66	72	14	7.20	0.10	54.3	16.5	20.1	33.0	0.084	6.10
					Water Rate 70 gpm/sq ft					
38	51	6	9.40	1.41	7.5	3.0	9.6	12.2	0.052	1.93
39	52	6	9.40	1.43	7.7	2.0	9.9	11.9	0.038	1.90
40	50	10	9.82	0.64	7.2	2.5	9.4	12.2	0.056	2.80
41	50	10	9.82	0.72	7.5	2.5	9.4	11.9	0.051	2.68
28	50	12	9.40	0.35	7.0	0.5	9.2	10.4	0.025	3.36
29	50	12	9.40	0.28	8.5	2.5	9.2	10.3	0.022	3.69
30	40	12	11.20	0.56	5.1	2.0	6.2	11.3	0.124	3.23
42	52	12	9.52	0.35	7.5	2.0	9.6	12.5	0.057	3.46
32	40	14	11.20	0.35	5.1	2.0	6.2	11.3	0.125	3.88
33	44	14	11.10	0.31	8.0	2.0	7.4	11.5	0.092	3.91
43	47	16	10.71	0.23	7.5	3.2	8.1	12.5	0.094	4.37
44	47	16	10.71	0.22	7.0	2.5	8.1	12.3	0.092	4.42
37	43	18	10.90	0.19	7.2	1.2	7.1	11.6	0.110	4.90

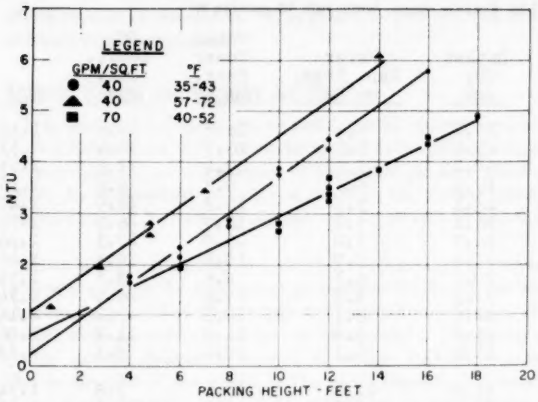

Fig. 2 Relation between number of transfer units and packing height for oxygen desorption

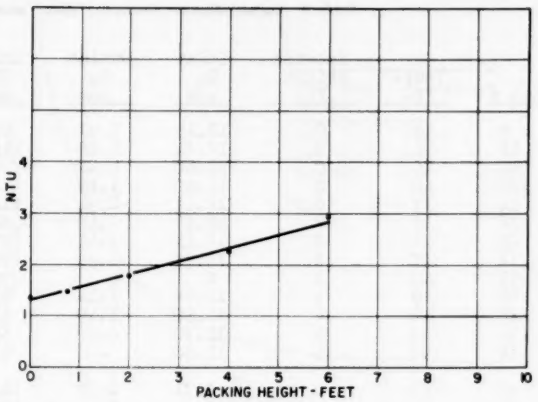

Fig. 3 Relation between number of transfer units and packing height for carbon-dioxide desorption. Flow rate, 40 gpm/sq ft; temperature, 35–40 F.

the work of Knoedler and Bonilla [2]. The increase in HTU at the higher flow rate of 70 gpm per sq ft is to be expected.

End Effect

The number of transfer units at zero tower height is a measure of the desorption capacity of the tower exclusive of the packing itself. The NTU at zero tower height multiplied by the HTU gives the feet of tower packing equivalent to the end effect. The end effect is primarily dependent on the design of the distributing system at the top of the tower. A high-velocity spray appears to be more effective than large droplets. The end effect is not proportional to the unpacked height above the Raschig rings, as most of the desorption takes place near the spray head. The end effect for oxygen desorption increases with temperature.

Oxygen Desorption

The results plotted in Fig. 2 are summarized in Table 2.

Table 2 Oxygen desorption

Flow rate gpm/ sq ft	Temp, deg F	HTU, ft	End effect NTU	End effect, ft
40	35–43	2.9	0.25	0.7
40	57–72	2.9	1.0	2.9
70	40–52	4.3	0.6	2.6

Carbon-Dioxide Desorption

The data for carbon-dioxide desorption are given in Table 3. As there was no trend of NTU versus temperature within the temperature groupings used, the NTU for each tower height were averaged for purposes of plotting. Again a reasonably good straight-line relationship was found, Figs. 3–5.

The bicarbonate alkalinity of the water used in a deaeration process will have a bearing on the degree of CO_2 removal. The water used in these tests had a natural bicarbonate alkalinity of 20 ppm (as $CaCO_3$). If the bicarbonate alkalinity were sufficiently high, some of the bicarbonates would release free CO_2 and be converted to carbonates. Nordell [5] has shown that as the alkalinity increases, aeration of the water results in a corresponding increase in conversion of bicarbonates to carbonates. As free CO_2 can only exist in trace amounts in the presence of carbonates, the HTU for CO_2 removal from a highly alkaline water is probably quite low.

Some spot checks at flow rates higher than 40 gpm per sq ft

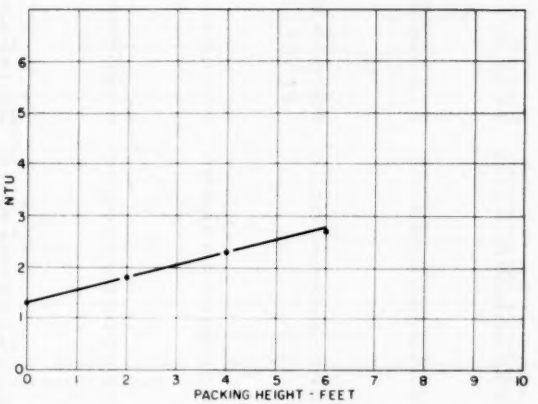

Fig. 4 Relation between number of transfer units and packing height for carbon-dioxide desorption. Flow rate, 40 gpm/sq ft; temperature 41–56 F.

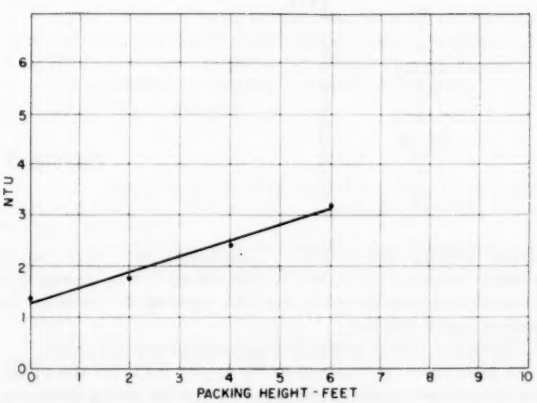

Fig. 5 Relation between number of transfer units and packing height for carbon-dioxide desorption. Flow rate, 40 gpm/sq ft; temperature 61–82 F.

Table 3 Carbon-dioxide desorption data: dumped 1-in. Raschig rings; water rate 40 gpm/sq ft

Run #	Temp. °F.	Packing Height Ft.	Inlet O_2 ppm	Outlet O_2 ppm	Inlet CO_2 ppm	Outlet CO_2 ppm	Water Vap. Pres. mm Hg	Total Tower Pres. mm Hg	CO_2 Equil. Sol. ppm	NTU
5	36	0	12.36	3.91	69.9	35.2	5.4	16.2	22.6	1.30
13	36	0	12.84	3.88	118.1	49.4	5.3	16.7	30.4	1.53
16	36	0	12.60	4.24	126	62.2	5.3	17.4	32.6	1.15
122	40	0	11.60	3.36	54.3	19.1	6.3	9.8	6.8	1.35
14	37	0.77	12.41	2.94	112.2	48.1	5.5	16.8	28.9	1.47
22	35	2	12.03	2.48	82.6	36.1	5.2	16.7	26.7	1.78
23	35	2	12.13	2.45	87.8	36.7	5.2	16.7	27.3	1.86
32	37	2	11.78	1.96	74.2	22.4	5.7	10.2	10.3	1.66
63	40	2	0	0	76.9	20.3	6.3	8.6	8.5	1.75
21	38	4	11.58	1.14	93.4	33.3	5.8	17.6	26.9	2.34
120	40	4	11.60	1.49	53.5	12.5	6.3	10.1	7.2	2.16
114	38	6	11.70	0.62	56.0	13.3	5.8	11.6	11.2	3.06
124	40	6	11.60	-	63.8	11.4	6.3	10.2	8.3	2.88
44	55	0	8.71	1.71	141	41.0	11.0	13.6	5.8	1.34
66	41	0	0	0	108.0	39.1	6.5	10.1	13.3	1.30
71	50	0	0	0	96.3	31.6	9.1	11.9	8.7	1.34
102	43	0	11.80	2.70	73.5	26.8	7.1	10.9	7.6	1.23
43	53	2	8.60	0.95	147	34.6	10.2	15.5	12.2	1.79
67	42	2	0	0	86.3	22.8	6.8	9.7	10.6	1.82
72	51	2	0	0	81.3	17.9	9.1	12.1	7.6	1.97
98	42	2	11.80	1.80	72.1	20.6	6.8	10.9	8.3	1.64
55	56	4	8.95	1.11	94.6	17.2	11.4	15.4	7.8	2.22
64	41	4	0	0	69.9	12.2	6.5	8.3	6.1	2.34
73	53	4	0	0	84.7	14.2	10.4	12.7	6.6	2.33
167	43	4	0	0	144.2	36.5	7.1	14.0	24.4	2.29
65	41	6	0	0	65.8	9.2	6.5	8.2	5.4	2.76
69	41	6	0	0	75.2	12.0	6.5	9.5	10.5	2.70
74	52	6	0	0	83.0	11.4	9.7	11.7	6.0	2.66
168	44	6	0	0	138.4	27.3	7.4	12.8	18.7	2.64
58	76	0	0	0	220	126.3	22.8	69.5	94.0	1.36
112	82	0	0	0	70.3	26.8	27.9	33.0	9.3	1.25
134	61	0	0	0	67.8	25.2	13.7	18.3	11.7	1.42
141	79	0	0	0	68.8	22.6	25.3	28.5	6.1	1.33
157	79	0	0	0	145.4	40.2	25.3	29.5	8.0	1.44
60	70	2	0	0	69.8	27.0	18.6	28.2	21.1	2.11
108	82	2	0	0	64.2	16.3	27.9	30.0	3.8	1.57
129	61	2	0	0	60.3	15.8	13.7	16.4	8.7	1.98
142	78	2	0	0	62.7	18.2	24.5	28.5	7.7	1.65
150	79	2	0	0	90.9	21.0	25.3	27.0	3.2	1.60
158	79	2	0	0	133.6	24.9	25.3	27.0	3.2	1.78
104	82	4	0	0	58.3	11.4	27.9	31.5	6.6	2.38
128	61	4	0	0	57.2	13.2	13.7	17.1	8.7	2.37
151	79	4	0	0	84.9	10.5	25.3	27.0	3.2	2.41
159	79	4	0	0	124.1	14.3	25.3	27.5	4.2	2.47
135	61	6	0	0	57.2	10.2	13.7	16.8	7.9	3.06
160	79	6	0	0	119.9	9.7	25.3	28.0	5.2	3.24

Condensed Table

35-40	0	1.33
"	0.77	1.47
"	2	1.76
"	4	2.25
"	6	2.97
41-56	0	1.30
"	2	1.81
"	4	2.30
"	6	2.69
61-82	0	1.36
"	2	1.77
"	4	2.41
"	6	3.15

showed a sharp rise in HTU. Insufficient tests were run to establish an actual value, but 40 gpm per sq ft was chosen as a practical flow-rate limitation for CO_2 removal to levels in the range of 5 ppm residual.

The results plotted in Figs. 3–5 are summarized in Table 4.

No significance is attached to the higher HTU for the 41–56-deg temperature range as compared to the 35–40-deg range, as a very slight change in the slope of the plot will have an appreciable effect on the HTU. A decrease in HTU at temperatures over 60 F is indicated.

Table 4 CO_2 desorption

Flow rate, gpm/sq ft	Temp, deg F	HTU, ft	End effect NTU	End effect, ft
40	35–40	4.0	1.3	5.2
40	41–56	4.1	1.3	5.3
40	61–82	3.3	1.3	4.3

Different spray-chamber systems above the tower packing were used for the oxygen and carbon-dioxide studies, so the end

effects cannot be compared. It is probable that the end effect will vary for different gases.

Vacuum Pumps and Packing Height

It is obvious that the pump or steam ejector chosen for maintaining the vacuum in the deaerator should have sufficient capacity to reduce the partial pressure of the solute gas to a point at which the equilibrium solubility is less than the desired effluent concentration. In terms of equation (2), x_e should be less than x_o.

When specifying a pump or ejector, it is customary to provide information as to the total vapor pressure at the pump suction, and also the pounds of water vapor and noncondensable gases of a specific average molecular weight to be handled. The pump or ejector can be defined as having a certain H_2O/NCG ratio. This is the ratio of the weight of the water vapor to the weight of the noncondensable gases, and is a measure of pump capacity.

At a given temperature the vapor pressure of the water is fixed. As the H_2O/NCG ratio increases, the vapor pressure of the noncondensable gas will therefore decrease, and with it the equilibrium solubility x_e. As x_e decreases, the required tower height also decreases. The problem of design then depends on the relative costs of using a higher packing height with a lower capacity pumping system, or a shorter tower with a larger pump.

However, there are certain limitations of tower height and pump capacity which are independent of their relative costs. These limitations are shown graphically in Figs. 6 and 7.

Fig. 6 shows the calculated curve for oxygen residual versus packing height for an H_2O/NCG ratio of 2 to 1. It is apparent that if a residual of 0.20 ppm of oxygen is desired, increasing the tower height beyond the required 10 ft will not affect the residual concentration markedly.

If a plot of H_2O/NCG ratio versus tower packing height for the required residual is made, the most effective combination of pump capacity and tower height can be shown. This has been done in Fig. 7 for an oxygen residual of 0.20 ppm. This plot shows that at H_2O/NCG ratios much below 2 to 1, the required tower heights increase rapidly. Conversely, at tower heights below 10 ft, the required H_2O/NCG ratio increases rapidly.

Examination of the curve shows that it is asymptotic. The H_2O/NCG ratio approaches a value of 1 as a limit. This occurs because, for the stated conditions, a ratio of 1 gives an equilibrium solubility of 0.20 ppm, the required effluent concentration. Any H_2O/NCG ratio below 1 cannot give a residual of 0.20 ppm, no matter how high a tower is used.

The data in the tables do not indicate any appreciable change in HTU with vapor pressure of the noncondensable gas. The tower height will therefore approach 8 ft as a limit, under conditions given in Fig. 7. If the H_2O/NCG ratio is infinite, x_e becomes zero. Examination of equation (2) shows that the NTU is then proportional to log (x_i/x_o). This relationship fixes the minimum tower height.

For the solution of a specific problem in reference to the selection of a required tower height and vacuum pump, a suggested procedure would be to plot the H_2O/NCG ratio versus tower height. The tower height can be calculated from equations (1) and (2) if x_e is known, and the appropriate HTU and end effect are selected. In determining x_e, the assumption is made that the average molecular weight of the noncondensable gas phase in the deaerator is the same as that of the influent composition. This is true for practical purposes if most of the gases are removed.

The value of x_e can be determined from the following relationship:

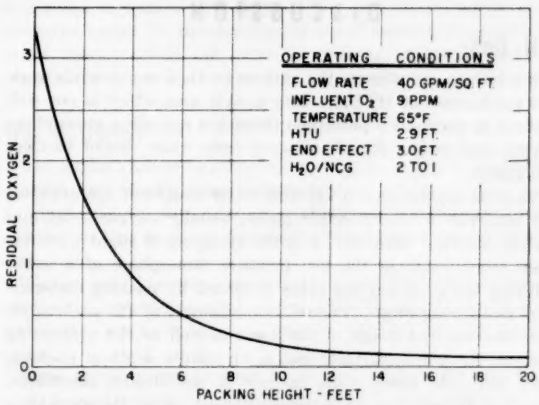

Fig. 6 Relation between residual oxygen and packing height for a given H_2O/NCG ratio

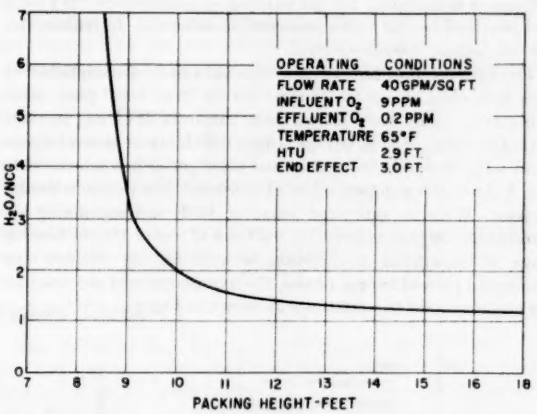

Fig. 7 Relation between the H_2O/NCG ratio and packing height for a given oxygen residual

$$x_e = \frac{abc}{def} \times \frac{10^6}{760} \tag{3}$$

where

x_e = equilibrium solubility of gas, ppm
a = molecular weight of gas
b = vapor pressure of water at operating temperature, mm Hg
c = mol fraction of solute gas in noncondensable gas phase
d = Henry's constant for gas at operating temperature, atm
e = average molecular weight of noncondensable gases
f = H_2O/NCG weight ratio

References

1 T. H. Chilton and A. P. Colburn, "Distillation and Absorption in Packed Columns," *Industrial and Engineering Chemistry*, vol. 27, 1935, pp. 255–260.

2 E. L. Knoedler and C. F. Bonilla, "Vacuum Degasification in a Packed Column," *Chemical Engineering Progress*, vol. 50, 1954, pp. 125–133.

3 ASME Power Test Code 12.3, THE AMERICAN SOCIETY OF MECHANICAL ENGINEERS, New York, N. Y., 1958.

4 J. H. Perry, "Chemical Engineers' Handbook," McGraw-Hill Book Company, Inc., New York, N. Y., third edition, 1950, pp. 674–675.

5 E. Nordell, "Water Treatment," Reinhold Publishing Company, New York, N. Y., 1951, pp. 88–89.

DISCUSSION

J. H. Duff[2]

We wish to compliment the authors on their worth-while work and publication of $HTU_{(OL)}$ data in this area which is not well covered in previously published literature regarding atmosphere oxygen and carbon dioxide removal from water, under vacuum conditions.

Vacuum deaeration is a valuable water treatment operation for the removal of objectionable gases, usually oxygen (air) and carbon dioxide. Basically, it is the stripping of slightly soluble gases from water in the low pressure atmosphere of a tower utilizing the great surface areas produced by packing materials such as Raschig rings. The relative efficiency of the packing affects the size and design of the tower as well as the evacuating system. If infinite surface, that is, an infinite depth of packing, were used, the tower could operate at equilibrium conditions. Practical systems require a driving force to drive the concentration of the unwanted gases in solution to the lowest possible limits. The magnitude of the driving force required for a given effluent is determined by the packing characteristics—$HTU_{(OL)}$ and provided by the tower pressure conditions as determined by the evacuating system selected.

The authors show how oxygen removal can be accomplished at area flow rates of up to 70 gpm per sq ft in large pilot plant apparatus. They have shown how values of $HTU_{(OL)}$ increase with flow rate. Using our own data which are in general agreement with those of the authors and other published information, Fig. 8 shows the practical effect of increased flow rate in a similar system. With air saturated water at 40 F and containing approximately 10 ppm of free CO_2, utilizing 12 feet of $1^1/_4$ in. Raschig rings, and operating at pressures to maintain an effluent containing 0.1 ppm of oxygen or less, the requirements of the evacuating system would be essentially as shown in Fig. 8.

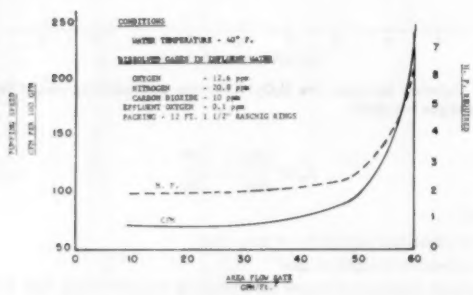

Fig. 8 Pumping speed and horsepower required versus area flow rate

Because of the increase in HTU value, the effectiveness of the packing decreases with increased flow rate. This makes it necessary to reduce the oxygen partial pressure and hence the total pressure in the tower which in turn requires a subsequent increase in volume capacity of the evacuating system. If mechanical pumps were used, the power requirements would be on the order of magnitude as shown. As can be seen from Fig. 8, there is a marked increase in power requirements as the area flow rate goes above 45–50 gpm per ft^2

If we consider a different system with carbon dioxide in appreciable concentrations as the primary contaminant to be removed, tower conditions must change because:

(*a*) Usually larger quantities of contaminant gas

(*b*) Different value for $HTU_{(OL)}$

(*c*) Different value for Henry's Law constant, namely, 0.265 mm Hg per ppm at 40 F for carbon dioxide, as compared to 12.4 mm Hg per ppm for oxygen.

Because of these factors, it can be seen in Fig. 9 that proportionally greater pumping capacity would be required for evacuation in a system involving carbon dioxide. In Fig. 8 it was shown that about 70 cfm was required to remove about 40 ppm of noncondensible gases at an area flow rate of 30 gpm per ft^2; whereas in the conditions as shown in Fig. 9, about 380 cfm are required to remove about 130 ppm of noncondensible gases. In this case, about $5^1/_2$ times more pumping capcity is required to remove about three times as much gas.

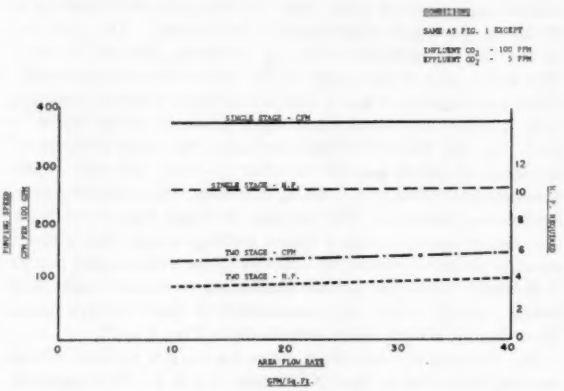

Fig. 9 Pumping speed and horsepower required versus area flow rate

Another factor involved in the selection of the evacuating system is the possible use of two-stage deaerators. These are essentially two vacuum deaerators operating in series at different pressures under gravity flow and isolated by seal arrangements. This system has the advantage of substantial reduction in pumping capacity required because the bulk of the gas is stripped in the first or high-pressure stage while the small residuals are scrubbed out in the second or low-pressure stage. Fig. 9 also shows the relative effect of using a two-stage system for carbon dioxide removal as compared to a single-stage system. In this case, each stage of the two-stage deaerator utilizes six feet of Raschig rings and the pumping capacity and power requirements are totals although approximately one half is used in each stage.

It has been our experience that in the design of most commercial vacuum deaerator installations, the flow rate is limited to the range of 30–40 gpm per ft^2:

(*a*) To provide normal engineering design factors.

(*b*) To minimize liquid entrainment and simplify the upper gas collector system.

(*c*) To provide the necessary storage in the lower sections of the pressure vessel without utilizing excessive straight heights or increased costs due to horizontal storage sections.

(*d*) To permit operation without flooding or short circuiting in the event of packing attrition.

Howard B. France[3]

The authors are to be complimented on the completeness of their report on a performance test of a vacuum deaerator. Considerable time and effort have been devoted to the accumulation of performance data, but these data are limited in application to only one type vacuum deaerator.

The purpose of the paper is somewhat obscure. While no con-

[2] Technical Manager, Graver Water Conditioning Company, New York, N. Y.

[3] Manager, Steam Process Section, Cochrane Division, Crane Company, Philadelphia, Pa. Assoc. Mem. ASME.

clusions are stated, it may be inferred that the data can be used for the design and evaluation of all vacuum deaerators. I do not believe this is so. The data are limited in application to vacuum deaerators of precisely the same design as the one which was tested, and which is illustrated in the paper. The design and performance of other types and arrangements will vary considerably.

I would like to comment on several points:

1 End effect
2 Depth of packing
3 Effect of temperature
4 Tower loading rate
5 Design for very low residual gas concentrations

Let us analyze each of these points.

The authors point out that end effect varies with the design of the spray chamber. They state that the design of this chamber was not the same for the oxygen and carbon dioxide desorption tests and, therefore, the end effects which were determined from the data are not comparable. Since the recorded end effects are of much the same order of magnitude, it may be inferred that a change in the design of the spray chamber might have only a small, and perhaps negligible, effect on performance. We find that end effect varies appreciably. We find that it varies not only with the design of the spray head and spray chamber, but also with rate of tower loading, temperature, and the amount of gases available for removal. Our data and experience contradict the authors' statement that end effect is independent of these variables.

The design of the spray head and of the entire spray chamber has a pronounced effect on the amount of gas that will remain in the liquid phase as it enters the packing section. Variation in this concentration can be much greater than is apparent from the reported data.

The required depth of packing, as determined by the authors, is definitely associated with the magnitude of end effect. Variation in end effect will change the depth of packing that is required to produce a stipulated over-all performance.

It is unfortunate that the authors' tests did not provide for the control of water temperature. Apparently, data were collected at different water temperatures and the results were grouped within certain temperature ranges. Thus, the precise effective temperature is not clearly defined. Viscosity of the fluid has a significant effect on mass transfer capability. This effect is concealed somewhat by the grouping of data within relatively broad temperature ranges. Our experience indicates that the effect of temperature is much more important than is shown by this paper.

The authors have used tower loadings of 40 and 70 gpm per square foot. These loadings seem unusually high. For a given degree of deaeration the data clearly indicate that packing depth must be high for a high tower loading or, conversely, a low tower loading permits a reduced packing depth. We customarily use more conservative tower loadings with corresponding reduction in packing depth.

The tabulated data include only moderate to large residual gas concentrations. No apparent attempt was made by the authors to reach very low residual gas concentrations, such as 0.005 cc/l. oxygen which may be required for nuclear installations. We have built several vacuum deaerators which have achieved 0.005 cc/l. oxygen, even with very low water temperatures, and it is safe to state that it would be inadvisable to extrapolate the authors' data to the design of such units.

It is not my intention to belittle the authors' efforts or their report. I do want to conclude my remarks by emphasizing that the data contained in the paper apply to a vacuum deaerator of a specific design and arrangement and that use of the data should be limited to units of that design. The data should not be used indiscriminately for sizing or evaluation of vacuum deaerators of other designs which are based on different concepts and arrangements.

Wm. B. Gurney[4]

The authors are to be complimented for a fine job in supplying us with some much needed information.

Apparently the size of the deaerator is not too important economically; that is, it can be larger without too much additional cost.

The important factors seem to be the capacity of the evacuating pumps, the temperature of the water, pH of the water, the amount and kind of gas to be removed, and the residual that can be tolerated.

For example, if a water (cation effluent) contains 200 ppm CO_2 at 40 F (and oxygen), it may be necessary to heat this water to 90 F and, therefore, obtain a much lower residual CO_2 (and O_2) with a much smaller pump than could be obtained with this same pump at 40 F.

Referring to Fig. 6 and Fig. 7, it would appear that at a temperature of 90 F the economical or practical residual and water/gas ratios would be as low as the curves show for a *practical size pump* in place of the "infinite" size pump used in the tests. Below 70 deg F the required pump capacities increase very rapidly and the pump must be three-stage to handle very high vacuums. Of course, O_2 values of 0.2 ppm are far from acceptable for boiler feedwater used in the electric utility field. It appears that some other feature is required to get the residuals (especially O_2) down easily to a lower value. Perhaps a two-stage unit or a purging gas such as steam heating elements in place of the fill is needed.

Authors' Closure

The curves of flow rate versus horsepower required given by Mr. Duff can be considered a form of a plot of HTU versus H_2O/NCG ratio, HTU being a function of flow rate, and H_2O/NCG being a function of HP requirement. By combining equations (1) and (3) of the paper, the relationship between the two terms can be calculated and a similar plot obtained.

Mr. Duff's comments on the use of a two-stage system are of interest in reference to lower power requirements. The requirements for two-stage operation can be determined by considering the deaerator as two single stage units, the effluent from one being the influent for the other. We have operated the test unit in this manner by recycling part of the effluent in order to obtain oxygen residuals below 0.005 cc/l. In cases where a low residual is required, a curve of the type shown in Fig. 7 will be shifted upwardly to the right, demonstrating that extremely high H_2O/NCG ratios with correspondingly larger pump sizes will be required. Two-stage operation will keep the H_2O/NCG ratios within reasonable limits.

The above observations also apply to Mr. France's comments on designs for obtaining low residual effluent concentrations. Following the method outlined in the paper for determination of most effective combination of pump capacity and tower height will show that practical limits exist for single stage operation. Experimental data at low residuals could not be used as explained under "Determination of NTU."

In reference to end effects, the tabulated data do show variations with respect to temperature and flow rate. We agree with Mr. France that the design of the distributing system will have an appreciable effect on the depth of packing required. This is obvious from observation of equation (1).

The temperature effect on the HTU for oxygen desorption is

[4] Gulf States Utilities Company, Beaumont, Texas. Mem. ASME.

negligible within the limits of the test. Of course the temperature is an important factor insofar as it affects the number of transfer units. For CO_2 desorption, there does appear to be an effect of temperature on the HTU, although it is not very great. Grouping of the data therefore appears justified.

It should be noted that present designs of vacuum deaerators are based on operation of a packed tower. As the basic concept of the height of a transfer unit is applicable regardless of the tower design outside of the packing itself, the operation of any tower can be predicted from a knowledge of the HTU and the number of transfer units in the end effect. The data given in the paper apply to the most commonly used packing for oxygen and carbon dioxide desorption.

Mr. Gurney's observations regarding pump requirements refer to the higher capacity as the suction pressure increases with water temperature.

It does not appear that cold water vacuum deaerators will be a factor in boiler feedwater treatment as they cannot compete with a deaerating heater, especially as the feedwater must be preheated.

ROBERT H. PELL

Manager, Power Generation,
Monongahela Power Company,
Fairmont, West Virginia

Performance of Stainless-Steel Condenser Tubes

A report of the evaluation and decision to replace copper-alloy condenser tubes with Type 304 stainless steel, and the performance during the two years since installation.

In July, 1958, the No. 6 Unit surface condenser of the Monongahela Power Company, Rivesville Power Station, was completely retubed with Type 304 stainless-steel tubing, replacing 88-10-2 copper alloy. This condenser now contains 9234 welded stainless-steel tubes $^7/_8$ in. OD × 26 ft. × 0.028 in. wall. The replaced superloy was 16 Bwg with a wall thickness of 0.065 in.

In view of the fact that this condenser has been in service since July, 1958, with a high load factor and subject to all of the variables in operation, it is believed that our experience and collected data will be of interest to many people connected with power-plant operation and design.

Corrosion Data

The Rivesville Unit No. 6 has a capability of 90,000 kw and went in service September 1, 1951. Steam conditions at the throttle are 1250 lb and 950 deg F. Steam exhausts from the low-pressure turbine into a Westinghouse two-pass radial flow condenser. Table 1 gives pertinent condenser and cooling-water characteristics.

The Monongahela River, which furnishes cooling water to the station, is highly corrosive due to coal-mine drainage. Consequently, it is acid in nature with a pH range from less than 3 during dry seasons to 6 during rainy seasons. Due to this condition, we have been faced with a continual problem of fouling, severe corrosion, and a short tube life of our copper-alloy condenser tubes. It is difficult to maintain an acceptable state of cleanliness and adequate cleaning exposes bare metal to the acid attack, which quickly forms new corrosive films. The copper alloys quickly tend to acquire a rough surface coated with a tenacious layer of corrosion products on the water side. The accumulation of mud and slime on top of this can generally be removed with nylon brushes, but, unfortunately, a severe cleaning method is necessary to affect the corroded inner surface. We also noted that the steam side of the copper tubes are coated with a heavy film of iron oxide. The copper-alloy tubes used in Unit No. 6 condenser had a life of about $6^2/_3$ calendar years. A life of about $8^1/_2$ to 9 years could be expected from the same metal installed in the older units with a considerably smaller load factor.

Monongahela Power Company has, over the years, tested a number of copper alloys and several types of stainless steel in attempting to establish the most satisfactory metal for performance and life expectancy. As far back as 1937, a number of pieces of Type 304 were installed in one of the older condensers. This condenser was retubed in 1945, and in view of the fact that the stainless steel did not show any measurable attack, they were not removed. This same condenser was again retubed in 1954, and the Type 304 was carefully re-examined. It was extremely interesting to note that after 17 years' service no pitting or measurable loss of wall thickness was observed. However, we did not seriously consider the use of Type 304 at that time because of its higher cost and reputed poorer heat-transfer characteristics. Stainless Type 304 has been accepted and used for some time in the section under air baffles where tubes may be subject to ammonia attack. Our experience with the stainless tubes has shown that they can be consistently well cleaned by shooting nylon brushes once through the tube, and that the steam side of the stainless tube remains clean and bright.

During May, 1958, a re-examination of the 16 Bwg 88-10-2 copper-alloy tubes in the Unit No. 6 condenser revealed an average wall thickness of slightly over 0.020 in. It was obvious that retubing was necessary in the near future.

Table 1 Rivesville Unit 6 condenser and cooling-water data

Condensing surface	54,997 sf	
Retubed	May, 1958	
Tube material	Welded Type 304 stainless steel	
Number of tubes	9234	
Tube diameter	0.875 in.	
Tube wall thickness	22 Bwg (0.028 in.)	
Length of tubes	26′-$2^5/_8$ in.	
Effective length of tubes	26′	
Water pass area	16.891 sf	
Tube sheet material	Navalbrass	
Tube sheet thickness	$1^1/_4$ in.	
Tubes joined to tube sheet by	Rolled joint	
Number of support sheets	7	
Reference C W flow	49,330 gpm	
Reference C W velocity	6.5 fps	
Reference steam flow to condenser	566,000 lb/hr	
Cooling-water source	Monongahela River	
Maximum water temperature	90 deg F	
Minimum water temperature	32 deg F	
pH (high for July '58–June '59)	7.2	
pH (low for July '58–June '59)	3.6	
pH (average for July '58–June '59)	5.6	
Typical water analyses:		
pH value	3.8	4.1
Free mineral acidity as H_2SO_4	7 ppm	2 ppm
Total acidity as H_2SO_4	26 ppm	20 ppm
Sulfate (SO_4)	130 ppm	120 ppm
Chloride (Cl)	5 ppm	4 ppm
Silica (SiO_2)	6 ppm	8 ppm
Iron (Fe)	4.7 ppm	6.4 ppm
Calcium (Ca)	22 ppm	26 ppm
Magnesium (Mg)	7 ppm	11 ppm
Hardness as $CaCO_3$	84 ppm	109 ppm

Evaluation Data

In view of our experience with stainless-steel tubes over the past several years, we believed it necessary to evaluate and consider their use in the retubing of No. 6 condenser. Since many factors, such as degree of cleanliness, affect over-all heat transfer, we believed that the actual thermal conductivity of the metal may be of lesser importance in the evaluation than we had previously

Contributed by the Joint Research Committee on Boiler Feedwater Studies and presented at the Winter Annual Meeting, New York, N. Y., November 27–December 2, 1960, of The American Society of Mechanical Engineers. Manuscript received at ASME Headquarters, August 23, 1960. Paper No. 60—WA-217.

assigned. It seemed reasonable to consider that, if the stainless was less susceptible to oxidation and fouling, this fact might well offset some of the differences in thermal conductivity. Furthermore, we believed that we could satisfactorily use a welded-seam stainless tube with a much thinner wall to reduce cost and improve heat-transfer capability.

Experience had shown that the average practical cleanliness, which we could expect to reclaim for the copper-alloy tubes, would not be greater than 60 per cent. It was possible, of course, by mechanical or chemical means, to restore cleanliness to a higher level, but the tubes would not retain such cleanliness for a sufficient time to recover the extra cost of cleaning. Furthermore, the bare tube surface would be exposed to direct attack by the acid water, and tube life would be appreciably shorter.

In our evaluation, we chose to consider welded seam 22 Bwg Type 304 stainless-steel tubes. By using the thermal conductivity of Type 304, as recorded by the current HEI standards, our calculations indicated that we should expect almost equal performance with our copper-alloy tubes if we could maintain the stainless tubes 85 per cent clean. Other points of consideration were:

1 We believed we should expect 30 years' life from stainless, compared to seven years for the copper.

2 Welded stainless-steel tubes were within a reasonable price range and appeared to be satisfactory for condenser use.

3 Experimental use of 22 Bwg gave satisfactory results when expanded into the tube sheet.

4 Experience indicated that stainless and the Naval Brass tube sheet could be safely used together without any detrimental effect from galvanic attack.

One debit factor in the evaluation was believed necessary because of the larger water pass area caused by the thinner walled stainless-steel tubes. Consequently, we assumed for calculation purposes, that the 7.0 fps water velocity in the 16 Bwg copper tubes would drop to approximately 6.5 fps in the 22 Bwg steel tubes using the same pumping facilities. However, we believed that if we could maintain 85 per cent or better cleanliness performance, this factor would not be unduly detrimental.

As a result of this evaluation, 22 Bwg Type 304 stainless tubes were purchased and, during July, 1958, installation was made by the Maintenance Department of the Rivesville Power Station. The tubes were expanded into Naval Brass 1¼ in. tube sheets using conventional tools for brass tubing. Of the 9234 tubes, less than 10 leaks were found after they were rolled and tested. We found them easier to handle because of their lighter weight and experienced little trouble in "sticking."

Performance Results

All tests to determine the performance of stainless-steel tubes have been made in the same manner as the routine tests made on the previous 88-10-2 copper-alloy tubes. No special test equipment has been employed and no artificial conditions established at any time during the testing. Cooling-water flow for each test was calculated by heat balance. The average velocity for each test was then calculated from the cooling-water flow and the condenser water pass area. The initial temperature of the cooling water and exhaust pressure were variable but could be recorded, and the cleanliness factor of the tubes could be calculated from each set of test conditions. It should be remembered that, in all of the measurements, the thermal conductivity used for the stainless steel was that given by the HEI standards.

The results of the installation borne out by numerous tests have shown that the actual performance has exceeded our original evaluation and expectation. The improved performance due to improved cleanliness can be graphically seen in Fig. 1. It should be pointed out that in these curves a velocity of 6.5 fps has been

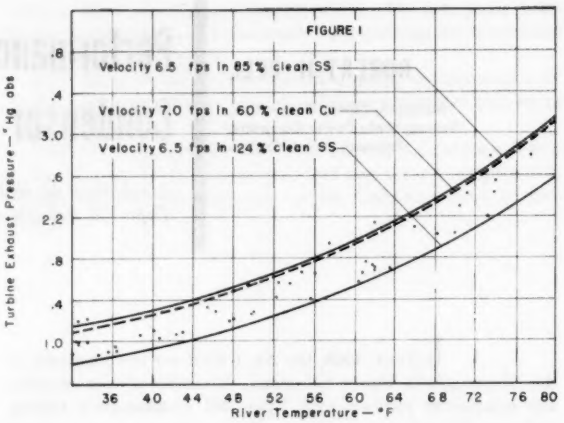
FIGURE 1
Velocity 6.5 fps in 85 % clean SS
Velocity 7.0 fps in 60 % clean Cu
Velocity 6.5 fps in 124 % clean SS
Turbine Exhaust Pressure — "Hg abs
River Temperature — °F

Fig. 1

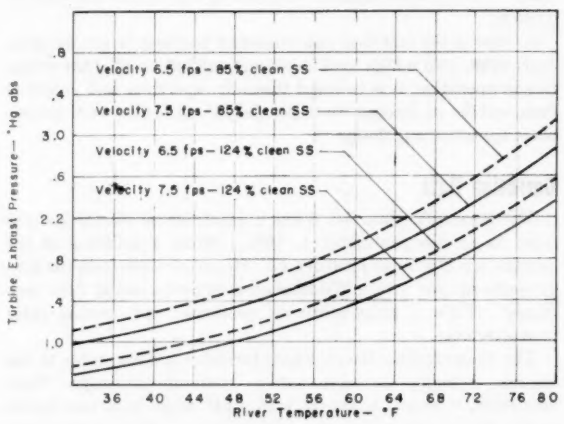
Velocity 6.5 fps – 85 % clean SS
Velocity 7.5 fps – 85% clean SS
Velocity 6.5 fps – 124 % clean SS
Velocity 7.5 fps – 124 % clean SS
Turbine Exhaust Pressure — "Hg abs
River Temperature — °F

Fig. 2

used for stainless steel as a matter of convenience in comparison. The upper solid line represents the calculated anticipated performance of the stainless-steel tubes used in our evaluation and is based on 85 per cent cleanliness factor with 6.5 fps water velocity. The dotted line indicates the best possible performance we could expect with the copper-alloy tubes. These are the two curves which were used in arriving at the decision to install the stainless tubes. The lower solid curve represents the best performance which we have actually attained. In calculating the cleanliness factor, using the actual turbine exhaust pressure and river temperature, together with the HEI thermal conductivity for Type 304 stainless, our answer came to 124 per cent. Obviously, the thermal conductivity of the stainless tubes installed in the Rivesville condenser is considerably better than that indicated by the HEI standard. This good fortune could not have been anticipated since there was no previous experience to indicate that the stainless steel might be better than expected.

The black dots represent actual back pressures obtained by tests since the installation. They were also plotted for the reference water velocity of 6.5 fps. One will observe that the actual performances will lie somewhere between the 85 per cent and 124 per cent clean stainless performance curves. It should be noted again that the copper alloy averaged something less than 60 per cent. Obviously, the over-all turbine heat rate has been appreciably improved by the change to stainless.

As stated in the foregoing, a velocity of 6.5 fps was used because

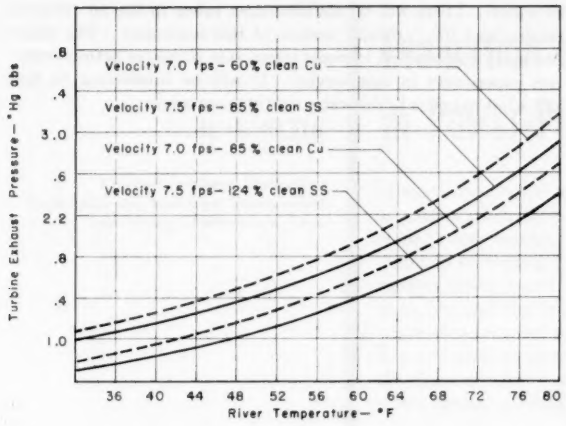
Velocity 7.0 fps – 60% clean Cu
Velocity 7.5 fps – 85% clean SS
Velocity 7.0 fps – 85% clean Cu
Velocity 7.5 fps – 124% clean SS
Turbine Exhaust Pressure – "Hg abs
River Temperature – °F

Fig. 3

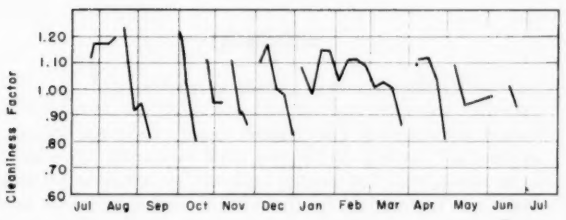

Fig. 4

it was believed that the thinner wall tubes would cause a reduction in velocity. We have been surprised to find that the tests indicate an actual increase in average water velocity to 7.5 fps. This additional benefit is illustrated in Fig. 2. The dashed line curves represent expected performance of 85 per cent and 124 per cent clean stainless-steel tubes with a velocity of 6.5 fps.

The solid line curves represent the actual betterment and performance created by the improvement of water velocity to 7.5 fps. Our performance tests were made under normal existing operating conditions and we have determined that the 7.5 fps velocity is very factual. By examining Figs. 1 and 2, it can be seen that we have gained about as much in back pressure reduction from the unexpected higher velocity as was gained from the equally unexpected betterment in cleanliness factor.

The composite of results including both the velocity and cleanliness factor of stainless steel can be compared with copper-alloy tubes in Fig. 3. At average load, we have had a betterment of from $^1/_2$ to $^3/_4$ in. lower turbine exhaust pressure with the new installation than received from the original copper-alloy tubes.

Since the installation, we have noted that the stainless tubes tend to have the characteristics of self-cleaning, and probably higher water velocity contributes toward this. A certain amount of this higher velocity is apparently due to less resistance inherent in the tubes themselves. This self-cleaning characteristic is illustrated in Fig. 4, showing cleanliness factors versus calendar time. Since a cleaning is expected to restore the cleanliness factor to some higher level, the open spaces were left between the adjacent segments of broken lines to indicate a cleaning was done between the two tests. One will observe that the trend of the cleanliness factor due to river conditions is reflected in the connected segments as time progresses. The rising line indicates the natural self-cleaning ability of the stainless steel due to the presence of suspended abrasive matter. The graph clearly shows the time of year when rains have colored the river with sand and silt.

The frequency of cleaning seems to depend upon the amount (or lack) of suspended solids in the cooling water. Note that from early in January to the last of March no cleanings were attempted. The cleanliness condition during this period remained at such a level that sufficient gain in performance would not justify the cost of cleaning. Toward the end of March it nose-dived to a level where the chances of recovery were sufficient to justify the cost of a cleaning with nylon brushes.

We should point out, however, that, except for prolonged wet-weather periods, we will clean the stainless tubes about as frequently as we will the copper tubes. However, there is a difference—we consistently recover our performance to a high degree, which was not true in the case of the copper-alloy tubes.

Conclusions

In our experience to this time with stainless-steel condenser tubes, we find that they are capable of much better heat transfer than expected. The excellent corrosion resistance insures a long service life in contrast to our former experience. The hard stainless surface resists fouling and corrosion, and cleanliness is more easily maintained. The resistance to wear and errosion permits the use of thinner wall tubes. Additional benefit is received because of its tendency for self-cleaning and natural scouring. Where fouling and corrosion are a problem, as at Rivesville, the thin-walled stainless tubes will produce turbine exhaust pressures equivalent to or better than the thicker-walled copper alloys at any given load and water velocities. In all respects, the differences in performance of stainless-steel tubes from that of copper alloys are definitely in favor of the stainless at Rivesville plant. Some of these advantages were entirely unexpected, it is true, but they exist nevertheless. This, of course, does not mean that stainless-steel tubes are a universal answer. Where cooling-water conditions are such that satisfactory long life is expected by copper alloys the evaluation of stainless steel may become much less attractive. However, where cooling water may result in severe corrosion of copper alloys, the possible use of stainless tubes must be considered.

DISCUSSION

Frank U. Neat[1]

Although Mr. Pell carefully points out that his data apply only to fresh water rivers polluted with mineral acids and further that the water is frequently burdened with abrasive silt, there are more than a few who will rush into a trial of stainless steel under conditions which may be unfavorable. This discusser should like to point out his experience for which he can find no support.

Simply stated the trouble is that if stainless steels are used with water flowing at less than perhaps 10-14 feet per second, at a pH above perhaps 5.5 as a lower limit and this water contains some minimum amount of iron in solution or suspension in possibly colloidal state and some minimum amount of dissolved oxygen, the stainless steel will rapidly assume a tightly bound very thick coating of iron oxide. If the water is sufficiently high in electrical conductivity, the stainless steel is rapidly lost due to oxygen cell pitting. If the water is low in electrical conductivity the tubes will last longer but will eventually hole through. If the water is free of dissolved oxygen, the only difficulty experienced is plugged pipes or tubes. There have been no exceptions to this in this discusser's experience. As may be deduced from the foregoing statements the lower limit of pH, iron content, dissolved oxygen, velocity, and electrical conductivity are unknown.

During 1961, a condenser will be put into service in the Balti-

[1] Senior Engineer, Baltimore Gas & Electric Company, Baltimore, Md.

more Gas and Electric Company system with a quite variably brackish water. Grab samples taken in the vicinity have shown total solids in the range of 400 to 12,000 ppm and pH values from 6.5 to 9.5, such widely varying figures probably resulting from the effects of fresh water flow into the upper reaches of this body of water. There will be stainless-steel tubes in the air removal section and the "erosion" section of this condenser. The stainless steel was selected to resist steam side corrosive action everyone experiences in this service. It will be interesting to find out what happens to the water side of these tubes.

Evaluation of Steam Washers in Power-Plant Boilers

H. A. KLEIN

Research Engineer, Combustion Engineering Inc., Kreisinger Development Laboratory, Chattanooga, Tenn.

A research program was undertaken to study the feasibility of employing steam washers to control silica deposition in high-pressure turbines. Under certain laboratory conditions, steam washing was found to be effective; however, its useful application appears to be limited to a very small number of power stations. Space limitations in modern boiler drums make it difficult to install the bulky equipment without interfering with flow and distribution through the drum. A washer installation can actually be the cause of mechanical carry-over. The use of high-quality make-up water and the prevention of raw-water contamination provide a more economical and trouble-free solution to the silica problem. A steam washer has little practical value in plants where good external control of silica is practiced.

Introduction

THE problem of turbine fouling by silica deposition has existed in the power industry for over 25 years. The exponential increase in power demand and the advances toward higher cycle efficiencies have resulted in a steady increase in operating pressures and the total number of boilers operating at these higher pressures. As a result, virtually all of the larger steam-electric utilities must today consider silica control in their operations. Excellent progress has been made in reducing the frequency and magnitude of the problem. Improved methods of water pretreatment along with a better over-all understanding of the mechanism of volatile carry-over have been largely responsible for this progress. Unfortunately, some utilities are still faced with the necessity to blow down boilers at excessively costly rates in order to prevent serious loss of turbine efficiency.

Straub and Grabowski [1][1] suggested steam washing as a possible solution to silica carry-over in 1945. Coulter [2], in 1956, presented the results of an extensive laboratory investigation which definitely demonstrated that the silica concentration of steam could be reduced by contacting it with relatively pure water. Although the principle of steam washing is simple, there are numerous factors which limit its potential usefulness in actual plant installations. The plant engineer should evaluate steam washing on the basis of his own particular plant conditions before assuming that it is a solution to his carry-over problems.

The Problem

Silica is partially vaporized from high-pressure-boiler water and is carried over in vaporous solution with the steam. As the pressure and temperature are reduced through the turbine, the solubility of silica in the steam is reduced and deposits are formed. Possible mechanisms of volatilization and subsequent deposition are discussed in the literature [1–4]. For a given operating pressure, the amount of silica carried over is primarily a function of the silica concentration in the boiler water although the pH-value does have an effect. Fig. 1 is a plot of the distribution ratio of silica versus the saturation pressure of the boiler. The distribution ratio is defined as the ratio of the concentration of silica in the steam to silica in the boiler water. Data for Fig. 1 were compiled for a boiler water pH-value of 10.3; however, the curve should be reasonably applicable for most normal boiler-water pH-values.

It is difficult to define the maximum concentration of silica which can be tolerated in the steam without deposition. Even if the solubilities of silica in superheated steam were known accurately for all temperature and pressure combinations which exist through the turbine, this might not provide an answer since a supersaturated-steam solution might pass through the unit without detriment. Experience seems to indicate that if the silica concentration in the steam is continuously maintained below 0.020 ppm no serious fouling occurs. For purposes of discussion, we will presume this to be a safe operating limit. From the dis-

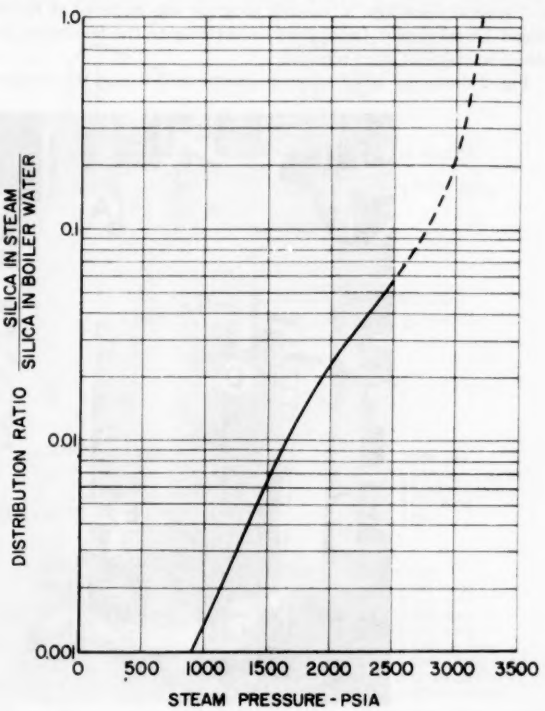

Fig. 1 Distribution ratio of silica

[1] Numbers in brackets designate References at end of paper.

Contributed by the Joint Research Committee on Boiler Feedwater Studies and presented at the Winter Annual Meeting, New York, N. Y., November 27–December 2, 1960, of THE AMERICAN SOCIETY OF MECHANICAL ENGINEERS. Manuscript received at ASME Headquarters, August 24, 1960. Paper No. 60—WA-213.

tribution ratio, it is then possible to estimate the silica level which can be tolerated in a boiler water at a given pressure.

If a steam washer is present in a boiler, the steam in equilibrium with the boiler water is contacted with high-purity feedwater before leaving the drum. This results in a shift in equilibrium, and some of the silica in the steam is transferred to the feedwater. It is, therefore, possible to maintain a higher silica concentration in the boiler water without exceeding the 0.020 ppm limit in the steam than would be possible if the washer were not present. It should be understood that the washer does not discard the excess silica from the system but returns it to the boiler via the feedwater. To eliminate the silica, boiler water must be blown down.

The advantage in having the washer is the fact that the silica concentration in the boiler water can be maintained higher, without exceeding the predetermined limit on the silica concentration in the steam. Since each pound of boiler water contains a greater amount of silica, less blowdown is required to obtain the desired conditions. The dollar value of the washer is represented by the savings in reduced blowdown. This benefit might be realized in a different manner. If the blowdown were held constant, the concentration of silica in the steam might be reduced.

Feasibility of Steam Washing

The concept of steam washing is not a new idea. The author's company employed washers to improve steam purity in their boilers over 25 years ago. At that time, silica deposits were not a major problem, and the equipment was installed primarily for the removal of boiler-water salts from the steam. The major difficulty with these washers was the fact that insoluble sludges caused plugging which interfered with normal operation. As more effective trouble-free steam separators were developed, the use of washers for this application was abandoned. With the advent of the silica problem, however, new interest was aroused, and several years ago, a research program was initiated at Kreisinger Development Laboratory to investigate the feasibility of steam washers for silica removal.

Fig. 2 shows the laboratory equipment used to test the washer models. High-pressure steam was supplied for the tests from a boiler designed to deliver clean dry steam at pressures up to 2000 psi. The test models were contained in a separate drum to permit accurate control and analysis. Models of different types and flow arrangements were evaluated in this installation. Three important conclusions concerning the mechanics of steam washing were derived from the testing program:

1 Silica could be removed effectively from steam in the pressure ranges tested by bringing relatively pure wash water into intimate contact with the steam. Under certain conditions, as much as 80 per cent of the silica in the steam could be removed in laboratory models of matt-type washers.

2 The test results indicated that the flow pattern of the steam and feedwater had little effect on silica-removal efficiency; that is, no significant difference in effectiveness could be noted between the operation of counterflow, parallel-flow, or oblique-flow models.

3 The transfer of silica from steam to water or vice versa appeared to be primarily a function of distribution equilibrium. When the distribution coefficient was low, it was possible to transfer a large amount of silica to a very small quantity of water. If condensation were not completely avoided in the steam line from the auxiliary boiler to the test drum, much of the silica in the steam was absorbed in this condensate. Such condensation greatly improved the apparent performance of the washer, and it was necessary to steam jacket the system completely to obtain reliable results. The effects of precondensation should be recognized in evaluating the results of model washer tests.

Application of Steam Washers in Power Plants

Performance data obtained in laboratory installations similar to the one described can be very misleading. Pressures, flow rates, and silica concentrations of the water and steam entering the washer can be varied independently in the laboratory. Washing efficiencies calculated under these conditions often ignore material-balance limitations which are inherent in boiler operations. In an actual utility cycle, the silica concentrations in the feedwater, the boiler water, and the steam are all interdependent

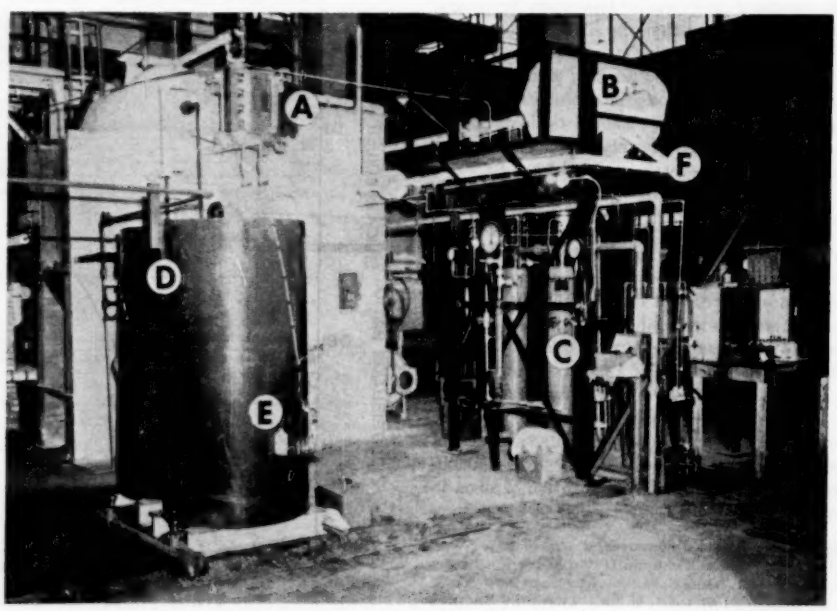

Fig. 2 Arrangement of test equipment showing (A) steam generator, (B) test drum, (C) condensers, (D) collecting tanks, (E) sampling system, (F) feedwater line

during continuous operation. Their relationship is basically a function of boiler pressure and the rate at which silica is introduced and discharged from the system.

Condenser leakage and system make-up water are the two primary sources from which silica enters the cycle. Condenser leakage is an intermittent contamination which is only a problem on brief occasions in most power stations. It is imperative, however, to minimize the occurrence and duration of leaks. Routine analysis of water samples and the use of continuous recording devices offer the best assurance for a quick detection. The use of welded condenser tubes to prevent tube-end leakage is becoming increasingly more popular. Where condenser leakage is a frequent or serious problem, full-flow polishing demineralizers offer an excellent safeguard.

Many plants experience high silica concentrations during initial start-up and following outages. Generally the duration of these conditions is short; however, sometimes siliceous materials initially existing in the cycle are slowly solubilized during operation and constitute a continuous source of contamination. It sometimes requires years for the effects of some complex deposits to disappear completely. Preoperational clean-up of the system is the most effective means of combating this problem.

Even in relatively clean systems, a certain amount of silica can be expected to wash back from the turbine and extraction-steam lines following an outage. Although the amount of material involved may be relatively small, many operators consider it worth while to eliminate this silica before resuming full load and pressure on the boiler. Passage of contaminated condensate through a polishing demineralizer can be beneficial in this regard. Major concern over high silica concentrations following an outage is generally unwarranted since carry-over during this short transient period is seldom responsible for any serious loss of turbine efficiency.

Most serious silica problems are traceable to make-up water. This is true because of the continuous nature of this source of contamination. Even low concentrations of silica in the make-up may represent a sizable quantity of silica in a month's time. Effective pretreatment is the best assurance against silica fouling, and failure to provide good make-up is the most likely cause of trouble. The following are examples of systems which are inherently trouble-free. Turbine deposition will not occur and blowdown is not required. The basic premise is that the concentration of silica in the steam does not exceed 0.020 ppm.

Case 1 If there are no losses of steam or condensate through the cycle and no condenser leakage, no make-up is required and no silica is introduced into the system. Such a cycle operates on 100 per cent condensate returns. Although this is virtually impossible, some plants do approach the condition. If the make-up is sufficiently small, the normal boiler-water-sample flow may provide sufficient blowdown to maintain the desired limits.

Case 2 In the more general case, the loss of a significant percentage of the steam and condensate cannot be avoided, and, therefore, some make-up is required. If the silica concentration of the make-up water is less than that which can be tolerated in the steam and there is no external contamination, blowdown is not necessary for silica control.

Fig. 3 is an example of a 2000-psi system operating under the conditions described in Case 2. The rate at which steam and water are lost from the system is assumed constant and is represented as L lb/hr. It is assumed that this quantity of water is to be replaced with an equal quantity of make-up water containing 0.010 ppm of silica. Regardless of initial conditions, the concentration of silica in the boiler water will inherently adjust until a concentration of approximately 0.454 ppm is reached. At this time the silica concentration in the steam produced will equal 0.010 ppm and this concentration will remain constant through the turbine. The amount of silica leaving the system through steam and condensate losses will then equal the amount introduced with the make-up water, and the system is in equilibrium. All concentrations will remain constant so long as the quantity of silica introduced into the system is unchanged.

Under constant operating conditions, the concentration of silica in the steam will not exceed that in the make-up water in the

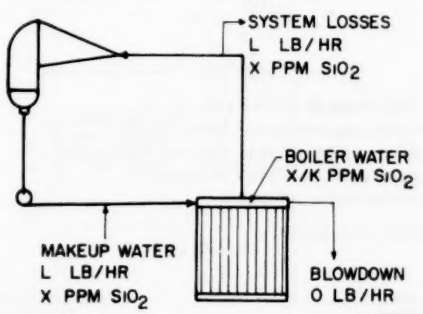

$X < 0.020$

EXAMPLE

IF:

BOILER PRESSURE	=	2000 PSI
STEAM RATE	=	1,000,000 LB/HR
SYSTEM LOSSES	=	20,000 LB/HR
SILICA IN MAKEUP	=	0.010 PPM

THEN:

DISTRIBUTION RATIO - K	=	0.022
SILICA IN STEAM	=	0.010 PPM
SILICA IN CONDENSATE	=	0.010 PPM
SILICA IN FEEDWATER	=	0.010 PPM
SILICA IN BOILER WATER	=	0.454 PPM
SILICA ENTERING BOILER	=	0.240 LB/DAY
SILICA LEAVING BOILER	=	0.240 LB/DAY
SILICA ENTERING SYSTEM	=	0.0048 LB/DAY
SILICA LEAVING SYSTEM	=	0.0048 LB/DAY

Fig. 3 Material balance for silica for system employing high-quality make-up water—no washer

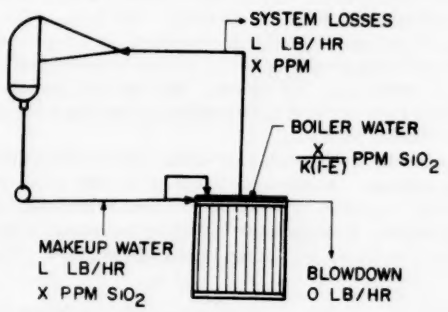

$X < 0.020$

EXAMPLE

IF:

BOILER PRESSURE	=	2000 PSI
STEAM RATE	=	1,000,000 LB/HR
SYSTEM LOSSES	=	20,000 LB/HR
SILICA IN MAKEUP	=	0.010 PPM
WASHER EFFICIENCY	=	0.80

THEN:

DISTRIBUTION RATIO - K	=	0.022
SILICA IN STEAM	=	0.010 PPM
SILICA IN CONDENSATE	=	0.010 PPM
SILICA IN FEEDWATER	=	0.010 PPM
SILICA IN BOILER WATER	=	2.270 PPM
SILICA ENTERING BOILER	=	0.240 LB/DAY
SILICA LEAVING BOILER	=	0.240 LB/DAY
SILICA ENTERING SYSTEM	=	0.0048 LB/DAY
SILICA LEAVING SYSTEM	=	0.0048 LB/DAY

Fig. 4 Material balance for silica for system employing high-quality make-up water—washer

absence of condenser leakage or some other form of contamination. This statement applies to all systems regardless of the specific operating conditions or the quantity of make-up water required. If the silica concentration of the make-up water is less than the value which can be tolerated in the steam, no blowdown will be required.

A silica washer cannot possibly be of any benefit in the case described. Fig. 4 shows the same 2000-psi cycle with a steam washer incorporated in the boiler. Assuming a washing efficiency of 80 per cent, the concentration of silica in the boiler water must equal 2.270 ppm before the system can reach equilibrium. It should be noted that it is not reasonable for the operator to carry the silica concentration at a lower level since it will inherently rise to the value indicated. This is an important fact since it precludes the possible benefit of the washer serving as a "safety element" to prevent surges of silica in the feedwater from carrying over with the steam. The following conclusions can be drawn concerning systems operating on high-purity feedwater, <0.020 ppm SiO_2:

1 In the absence of condenser leakage, system equilibrium will inherently establish a silica concentration in the steam which is no higher than that in the make-up water. Blowdown is not required regardless of boiler pressure or quantity of make-up water.

2 Installation of a washer into this type of system will not reduce the silica concentration in the steam but will raise the silica concentration in the boiler water.

3 In a "zero blowdown" cycle, the presence of a steam washer in the boiler can be a detriment if the effectiveness of washing is temporarily interrupted for any reason. Because the silica concentration in the boiler water is "supersaturated" from the standpoint of the distribution curve, temporary upsets due to "flooding," "plugging," and so on, may cause vaporization of the excess silica in the boiler.

The installation of a steam washer in a boiler can only be beneficial in those systems where boiler blowdown is required to limit the concentration of silica in the steam. The value of the washer is that it will permit higher concentrations of silica to be maintained in the boiler and, therefore, provide more efficient elimination by blowdown. In general, this includes systems where the make-up water used has a higher silica concentration than can be tolerated in the steam.

In a practical unit, washer performance is a definite function of boiler pressure. At pressures in excess of 2000 psi, it becomes virtually impossible to obtain high washer efficiencies. To prevent flooding, it is normally necessary to restrict wash water flow to 5 to 10 per cent of the total feedwater flow. There is a limit to the amount of silica which can be transferred to this small amount of water when the distribution coefficient is high. This limit is a consequence of the silica-holding capacity of the water at the high temperature.

If it is assumed that pure wash water (0.000 ppm silica) is intimately mixed with contaminated steam in the washer until an equilibrium exists, it is possible to calculate a "maximum possible washer efficiency." This theoretical value is a simple function of the percentage feedwater flow employed for washing and the distribution coefficient of silica at the given operating condition. Maximum efficiency may be calculated as follows:

$$E_m = \frac{F}{k + F} \qquad (1)^3$$

where

E_m = maximum possible efficiency
F = ratio of wash water: total feedwater
k = distribution coefficient of silica

Fig. 5 is a plot of maximum washer efficiency as a function of operating pressure and percentage wash-water throughput. It may be noted that efficiency is definitely limited at high pressures when small wash-water flows are employed. It should be understood that the values plotted apply to ideal conditions which cannot be obtained in operation. In an actual washer where contact space is limited and where silica is present in the wash water, even lower efficiencies can be expected.

Figs. 6 and 7 represent cycles in which blowdown is required to limit the silica concentration in the steam to 0.020 ppm. A general material balance is shown to illustrate the effect of a washer on blowdown requirements. From this balance, the following relationships may be derived:

$$B = kL\frac{(x - 0.020)}{0.020 - kx} \quad \text{(No washer)} \qquad (2)^3$$

$$B = kL\frac{(x - 0.020)}{\dfrac{0.020}{1 - E} - kx} \quad \text{(Washer)} \qquad (3)^3$$

where

B = continuous blowdown rate, lb/hr
L = steam and condensate losses, lb/hr
x = silica concentration in make-up water, ppm
k = distribution coefficient of silica
E = actual washer efficiency

[3] Derivation in Appendix.

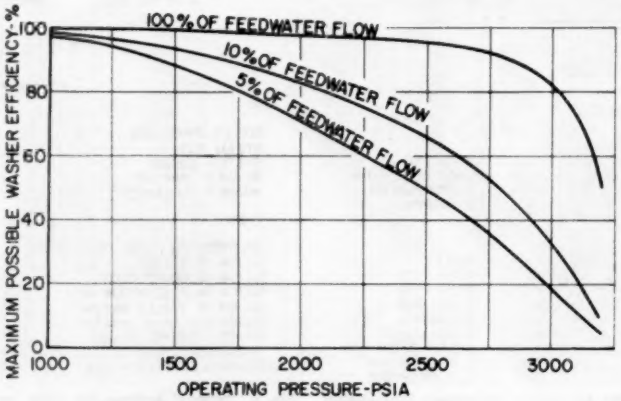

Fig. 5 Maximum possible washer efficiency

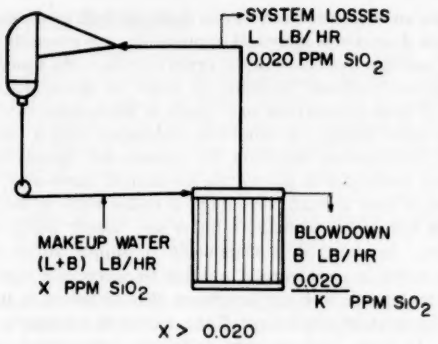

$X > 0.020$

EXAMPLE

IF:

BOILER PRESSURE	=	2000 PSI
STEAM RATE	=	1,000,000 LB/HR
SYSTEM LOSSES	=	20,000 LB/HR
SILICA IN MAKEUP	=	0.100 PPM
SILICA IN STEAM (LIMIT)	=	0.020 PPM

THEN:

DISTRIBUTION COEFFICIENT - K	=	0.022
SILICA IN CONDENSATE	=	0.020 PPM
SILICA IN FEEDWATER	=	0.02175 PPM
SILICA IN BOILER WATER	=	0.909 PPM
CONTINUOUS BLOWDOWN REQUIRED	=	1960 LB/HR
SILICA ENTERING BOILER	=	0.523 LB/DAY
SILICA LEAVING BOILER VIA STEAM	=	0.480 LB/DAY
SILICA ENTERING SYSTEM	=	0.053 LB/DAY
SILICA LEAVING SYSTEM VIA LOSSES	=	0.010 LB/DAY
SILICA DISCHARGED WITH BLOWDOWN	=	0.043 LB/DAY

Fig. 6 Material balance for silica for system employing poor-quality make-up water—no washer

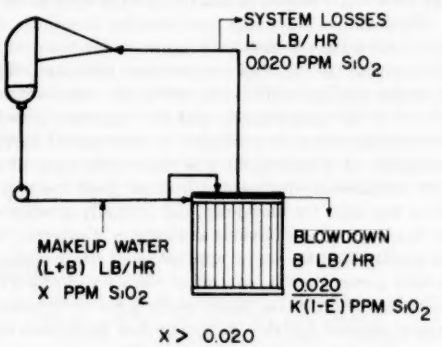

$X > 0.020$

EXAMPLE

IF:

BOILER PRESSURE	=	2000 PSI
STEAM RATE	=	1,000,000 LB/HR
SYSTEM LOSSES	=	20,000 LB/HR
SILICA IN MAKEUP	=	0.100 PPM
SILICA IN STEAM (LIMIT)	=	0.020 PPM
WASHER EFFICIENCY - E	=	0.80

THEN:

DISTRIBUTION COEFFICIENT - K	=	0.022
SILICA IN CONDENSATE	=	0.020 PPM
SILICA IN FEEDWATER	=	0.02163 PPM
SILICA IN BOILER WATER	=	4.545 PPM
CONTINUOUS BLOWDOWN REQUIRED	=	359 LB/HR
SILICA ENTERING BOILER	=	0.519 LB/DAY
SILICA LEAVING BOILER VIA STEAM	=	0.480 LB/DAY
SILICA ENTERING SYSTEM	=	0.049 LB/DAY
SILICA LEAVING SYSTEM VIA LOSSES	=	0.010 LB/DAY
SILICA DISCHARGED WITH BLOWDOWN	=	0.039 LB/DAY

Fig. 7 Material balance for silica for system employing poor-quality make-up water—washer

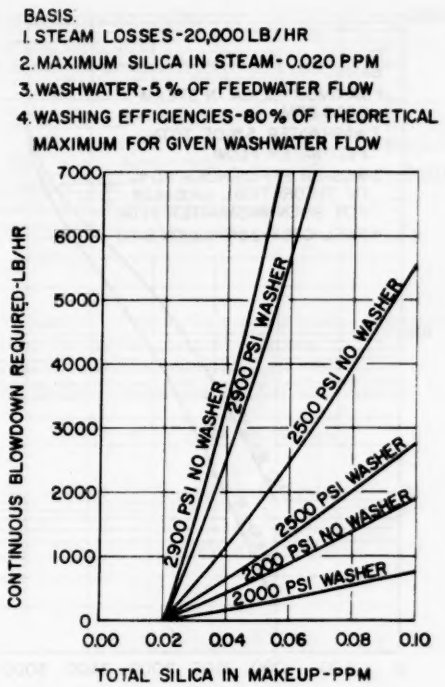

Fig. 8 Effect of steam washing on blowdown requirement

If the unrecoverable steam and water losses from a system are fixed and a washer efficiency is presumed, the comparative blowdown requirement of the cycle then becomes a function of the operating pressure and the silica concentration of the make-up water. Fig. 8 is a plot of equations (2) and (3) for a cycle where 20,000 lb/hr of steam and condensate are lost. This plot illustrates the reduction of blowdown which can be expected as a result of washing the steam. The washer is presumed to utilize 5 per cent of the total feedwater, and the operating efficiency at any pressure is assumed equal to 80 per cent of the maximum attainable value, shown in Fig. 5.

Economics

Although a steam washer can always provide a reduction in blowdown in systems where substandard make-up water is used, generally this is not the most practical solution to the silica problem. The feasibility of a washer installation is dependent on the specific cost of blowdown which is primarily a function of boiler pressure. At very high pressure, it is necessary to limit the concentration of silica in the boiler to a small value even though a washer is employed. Under these conditions, an enormous amount of blowdown may be required to eliminate a small amount of silica from the system. Fig. 9 is a plot of the approximate heat-loss costs of blowdown required to eliminate 1 lb of silica from boilers operating at different pressures. This plot assumes a cost of 25 cents per million Btu and presumes boiler-water concentrations which will limit the silica value in the steam to 0.020 ppm. At high pressure, the cost of controlling silica by blowdown is prohibitive even with washing. Limited washer efficiency and the high heat content of boiler water at the higher pressures contribute to the cost; however, the inherent,

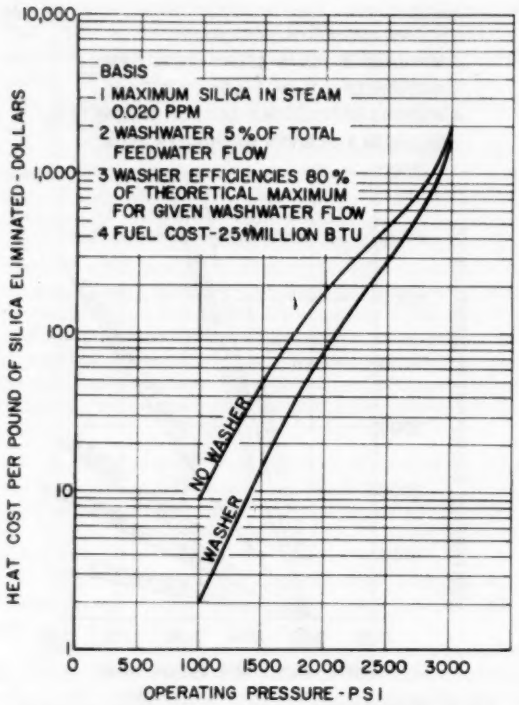

Fig. 9 Estimated heat-loss costs for elimination of silica

poor economy of employing blowdown to control trace constituents is the controlling factor.

In the absence of condenser leakage, silica fouling can virtually always be prevented by utilizing the proper method of treating the make-up water. The equipment and operating costs of such treatment, however, may be high. A steam washer can be economically justified if, and only if, its installation represents a savings in costs over this alternative method of controlling silica. Fig. 9 illustrates why the high-pressure station must always rely on dependable water treatment to prevent turbine deposition.

At pressures below 1500 psi, the economics of washing is somewhat better. At these lower pressures, high washer efficiencies are possible and specific blowdown costs are less. In some cases, the washer might permit the plant to operate with a less expensive method of pretreatment. In order for this to represent any sizable savings, the plant in question must be a high-make-up system. The application of flash tanks or heat exchangers to recover a portion of the blowdown heat would affect the cost picture. Such equipment cannot be readily incorporated into the low-make-up utility cycle where effective feedwater heating by extraction steam is integrated into turbine design. Actually, there are relatively few systems even in the lower pressure range where control of silica with a washer by blowdown is economically competitive to control by optimum pretreatment. The reason is that external removal of trace contaminants is virtually always more practical than internal control.

Potential Problems Related to Steam Washers

If steam washers were trouble-free, it would not be so important to rigidly justify their installation. More is involved, however, than just an increase in the initial cost of the boiler. The steam drum of the modern, high-pressure boiler is already congested with separation and drying equipment, and regardless of design, an effective steam washer is always bulky. Even when the drum diameter is increased appreciably, it is generally necessary to sacrifice free space in the drum or reduce the space occupied by conventional internals in order to accommodate it. Either of these alternatives may result in mechanical carry-over at high boiler rating. It should be understood that a washer is a poor water-steam separator by present-day standards and relatively ineffective in preventing mechanical carry-over. The presence of even a small percentage of boiler water in the steam entering the washer virtually nullifies any benefit which can be obtained. In short, it is mandatory to supply steam to the washer which is mechanically purified to acceptable standards. To guarantee this with any assurance, it is necessary to increase drum diameter greatly or install the washer in a separate steam drum. In large, high-pressure units, the incremental cost involved is sizable.

There are other problems associated with steam washers which should also be considered. Feedwater regulation is complicated by the requirement to proportion flow. The washer may trap insoluble products from the feedwater, and eventual plugging might upset wash-water distribution. Because of the supersaturated silica concentration which inherently exists in the boiler because of the washer, intermittent contamination of the steam can result if performance is inconsistent.

Discussion of Results

Although effective removal of silica by steam washing can be demonstrated in the laboratory, there are very few actual power stations in which this principle can be employed profitably. In operation, the steam washer is not really a silica-removal device since the wash water employed must return the silica to the boiler water. Silica control is actually performed by blowdown, and the function of the washer is merely to improve blowdown efficiency. Unfortunately, at the higher pressures where silica control is most critical, steam washing is inherently inefficient. Space limitations further reduce the performance, and the necessary crowding of the boiler steam drum is conducive to mechanical carry-over. The economics of steam washing is dependent upon blowdown costs. In the absence of condenser leakage, good make-up water eliminates the need for blowdown and virtually guarantees low silica in the steam. The obvious advantages of external removal of silica greatly limit the useful application of steam washers. In the modern power station, control of silica by blowdown is expensive even when effective steam washing can be obtained.

A major premise for this discussion has been that make-up water capable of preventing silica deposition can be produced through practical pretreatment methods. Experience [5] indicates that this assumption is valid. At the time of writing, the author's company had 140 boilers in operation at pressures above 1900 psi including 26 units operating in excess of 2500 psi. To our knowledge, silica fouling has not been a serious problem in any of these plants although none of the boilers is equipped with steam washers. The natural conclusion is that steam washing is unnecessary in the large majority of power stations.

The potential problems associated with steam washers further discourage their use. Although there are specific applications where a steam washer might prove beneficial, the plant engineer should understand clearly the mechanics and economics of steam washing to determine if this approach to silica control is justified.

One of the more common causes of silica deposition is the presence in the make-up water of colloidal silica which will pass through an otherwise effective demineralizer [6]. This contaminant is elusive since it does not generally respond to the normal analytical test used. Although a steam washer might be helpful in these cases, generally it would be more practical to invest in improving the quality of the make-up water.

Summary and Conclusions

A laboratory investigation was performed to study the mechanics of steam washing and to determine the effectiveness of different types of washers for silica removal. On the basis of the information obtained in this investigation, different power-plant cycles were studied to determine how operating conditions and the quality of make-up water affect the applicability of steam washers in actual plant systems. An economic evaluation of steam washing as a solution to the silica-deposition problem was made. The conclusions drawn are as follows:

1 The silica concentration of steam can be reduced effectively by intimately contacting it with relatively pure wash water. The flow pattern of the water and steam through the washer does not significantly affect its efficiency; that is, counterflow, parallel-flow, and oblique-flow models are all equally effective.

2 At the intermediate pressures (800–1500 psi), the silica capacity of the liquid phase is high, and a small quantity of water can absorb appreciable silica. A small amount of condensation in low-pressure steam may absorb a large percentage of the total silica.

3 At the higher pressures (above 2000 psi), the silica-holding capacity of the liquid is quite low. If only a portion of the total feedwater is employed for washing, high silica-removal efficiencies cannot be obtained. The benefits of steam washing in boilers operating above 2000 psi are quite limited.

4 The installation of a steam washer can only be beneficial in those systems where boiler blowdown is required to limit the silica concentration in the steam. If high-quality make-up water is provided to a system, blowdown will not be required to limit the silica concentration of the steam. The presence of a washer in these systems can be of no benefit and may prove to be detrimental.

5 To justify the steam washer economically as a solution to the silica-deposition problem, its installation must constitute a dollar savings over the alternative method of control by proper pretreatment. In general, external removal of silica by pretreatment is more economical and trouble-free. In very high-pressure boilers where washer efficiencies are limited and where the cost of blowdown is prohibitive, the installation of a washer can never be justified.

References

1 F. G. Straub and H. A. Grabowski, "Silica Deposition in Steam Turbines," TRANS. ASME, vol. 67, 1945, pp. 309–316.

2 E. E. Coulter, "Development of Steam Washers for Silica Removal," *Proceedings of the American Power Conference*, vol. 18, 1956, pp. 629–638.

3 F. G. Straub, "Steam Turbine Blade Deposits," University of Illinois, Engineering Experimental Station, Bulletin No. 364, June, 1946.

4 E. E. Coulter, E. A. Pirsh, and E. J. Wagner, Jr., "Selective Silica Carry-Over in Steam," TRANS. ASME, vol. 78, 1956, pp. 869–873.

5 J. D. Williamson and R. F. Andres, "Operation and Water Conditioning of Unit No. 4, Tait Station," *Proceedings of The American Power Conference*, vol. 21, 1959, pp. 265–274.

6 I. B. Dick, "Demineralization by Mixed-Bed Treatment at Waterside Station of Consolidated Edison Company of New York, Inc.," *Proceedings of the American Power Conference*, vol. 18, 1956, pp. 651–660.

APPENDIX

Calculation of Maximum Possible Washer Efficiency

Nomenclature

The nomenclature used in this section of the Appendix is as follows:

W = wash water flow, lb/hr
S = steam flow, lb/hr
x_0 = initial silica concentration of steam, ppm
x_s = final silica concentration of steam, ppm
x_w = final silica concentration of wash water, ppm
F = ratio of wash water : total feedwater
k = distribution coefficient of silica = x_s/x_w

Basis

1 Condensation of steam through the washer is negligible.
2 Steam flow equals total feedwater flow.
3 Wash water is initially free of silica.
4 Distribution equilibrium is reached in the washer.

$$F = W/S \quad \text{(wash-water ratio)} \tag{4}$$

$$k = \frac{x_s}{x_w} \quad \text{(distribution ratio)} \tag{5}$$

$$Sx_0 = Sx_s + Wx_w \quad \text{(material balance for silica)} \tag{6}$$

$$Sx_0 = Sx_s + FSx_w \tag{7}$$

$$Sx_0 = Sx_s + \frac{FSx_s}{k} \tag{8}$$

$$x_0 = x_s + \frac{Fx_s}{k} = x_s(1 + F/k) \tag{9}$$

$$\frac{x_s}{x_0} = \frac{1}{1 + F/k} = \frac{k}{k + F} \tag{10}$$

$$\frac{x_0 - x_s}{x_0} = 1 - \frac{k}{k + F} \tag{11}$$

$$\frac{x_0 - x_s}{x_0} = \frac{F}{k + F} \tag{12}$$

$$E_m = \frac{F}{k + F} \quad \text{(maximum possible washer efficiency)} \tag{1}$$

Calculation of Continuous Blowdown Requirement for System Without a Steam Washer Employing Poor-Quality Make-up Water, Fig 6

Nomenclature

The nomenclature used in subsequent sections of the Appendix is as follows:

M = make-up water requirement, lb/hr
L = system losses of steam and condensate, lb/hr
B = continuous blowdown requirement, lb/hr
x = silica concentration in make-up water, ppm
x_b = silica concentration in boiler water, ppm
k = distribution ratio of silica
F = washer efficiency

Basis

1 No condenser leakage or external contamination.
2 No turbine deposition will occur if the silica concentration in the steam is maintained below 0.020 ppm.
3 The concentration of silica in the make-up water is greater than 0.020 pm.
4 Continuous blowdown requirement is the minimum blow-

down rate necessary to limit the concentration of silica in the steam to 0.020 ppm.

$$Mx = Bx_b + L0.020 \quad \text{(material balance for silica)} \quad (13)$$

$$M = L + B \quad \text{(material balance for water)} \quad (14)$$

$$x_t = \frac{0.020}{k} \quad \text{(distribution relationship)} \quad (15)$$

$$(L + B)x = \frac{0.020B}{k} + 0.020L \quad (16)$$

$$B = kL\frac{(x - 0.020)}{0.020 - kx} \quad \text{(general relationship)} \quad (2)$$

Calculation of Continuous Blowdown Requirement for System With a Steam Washer Employing Poor-Quality Make-up Water, Fig. 7

Basis

1 No condenser leakage or external contamination.

2 No turbine deposition will occur if the silica concentration in the steam is maintained below 0.020 ppm.

3 The concentration of silica in the make-up water is greater than 0.020 ppm.

4 Continuous blowdown requirement is the minimum blowdown rate necessary to limit the concentration of silica in the steam to 0.020 ppm.

$$Mx = Bx_b + L0.020 \quad \text{(material balance for silica)} \quad (17)$$

$$M = L + B \quad \text{(material balance for water)} \quad (18)$$

$$x_b = \frac{0.020}{k(1 - E)} \quad \text{(distribution relationship)} \quad (19)$$

$$(L + B)x = \frac{0.020B}{k(1 - E)} \quad (20)$$

$$B = kL\frac{(x - 0.020)}{\dfrac{0.020}{1 - E} - kx} \quad \text{(general relationship)} \quad (3)$$

DISCUSSION

E. E. Coulter[3]

Although the author has given excellent coverage to various phases of silica removal by steam washing, several of his conclusions are not in agreement with actual measured performance.

First, the author concluded from his tests that counterflow washing has no advantage over parallel-flow or oblique-flow devices. These observations are contrary to the results of similar tests made by the writer's company and are also contrary to theory. A complete theoretical treatment of this subject is impractical here, but the interested reader is referred to the author's reference [2], in which the superiority of counterflow washing is thoroughly illustrated. On this basis, therefore, one must conclude that the "maximum efficiency" values shown in Fig. 5 are valid only for parallel flow washing, and that a counterflow washer can exceed these values by a considerable amount. The most plausible explanation of the author's test results would appear to be that excessive carry-over of wash-water occurred within the washer, thus reducing the silica concentration gradient in the wash-water as it passed through the washer. In this case, the washer would have counterflow in name only, since its net effect would be the same as a parallel-flow washer.

[3] Head, Engineering Physics Section, The Babcock & Wilcox Company, Research Center, Alliance, Ohio. Assoc. Mem. ASME.

The author mentions a similar effect in which excessive carry-over of boiler water into a steam washer will contaminate the wash-water and seriously impair the performance of the washer. This effect emphasizes the need for efficient mechanical separation and illustrates the fact that a steam washer preceded by poorly designed separators or natural separation alone cannot function effectively.

The author points out that a steam washer does not remove silica from the boiler-turbine system, but that it transfers silica from the steam to the boiler water, thus allowing removal of silica from the system by the more efficient use of blowdown. It seems unfortunate, then, that he chose as examples, in Figs. 3 and 4, conditions with no blowdown, the only situation in which a steam washer cannot possibly show an advantage. Furthermore, although a generous two per cent steam and condensate loss from the system is assumed, no boiler water losses are considered—not even a boiler water sample. Figs. 10 and 11 of this discussion illustrate that a continuous boiler water sample of 100 lb/hr (a blowdown of only 0.01 per cent) will effect a 53 per cent reduction of both silica content in the boiler water and the silica concentration in the steam in the boiler equipped with a steam washer. If the steam and condensate losses are reduced to 0.5 per cent, probably a more realistic number, the 100 lb/hr boiler water sample reduces the silica concentration in the steam by 83 per cent. Figs. 10 and 11 also show that a further increase in blowdown to only 0.1 per cent nearly eliminates the difference in boiler water silica concentrations between a boiler equipped with a steam washer and one without. On the other hand, the steam washer drastically reduces the silica content of the steam.

The examples of Figs. 6 and 7, in which a higher silica content of make-up water is assumed, illustrate one advantage of a steam washer, i.e., the reduction in the amount of blowdown required to limit the silica content of the steam to 0.020 ppm. A steam washer is a flexible device and may be operated to provide several beneficial effects, as the operator chooses. If he prefers not to operate on the ragged edge of the turbine deposit problem with 0.020 ppm silica in the steam, he can use the same blowdown as the boiler without the washer (1960 lb/hr) and reduce the silica concentration of the steam to 0.005 ppm. Or he may arbitrarily choose to reduce the blowdown to one half this amount and still obtain a 56 per cent reduction in silica content of the steam.

The cost parameter used in Fig. 9 gives a distorted conception of blowdown cost, for in most circumstances it would take several weeks to eliminate one pound of silica from the system. For example, for the conditions assumed in Figs. 6 and 7, the cost of blowdown is \$7.74 per day and \$3.12 per day, respectively. If the steam losses are reduced from 2 to 0.5 per cent, the blowdown costs are reduced to \$1.73 per day and \$0.78 per day, respectively. If the assumed operating pressure is raised from 2000 psi to 2700 psi, the distribution ratio would increase to 0.084 and the washer efficiency would decrease to 38 per cent for five per cent wash-water flow, according to the author's Figs. 1 and 5. Under these conditions, and with 0.5 per cent steam losses, the cost of blowdown for a boiler without a washer would be \$11.62 per day and \$6.50 per day for a boiler equipped with a washer. These costs are based on the relatively high value of 0.1 ppm silica in the make-up, but even so they can hardly be considered excessive for a plant of 1,000,000 lb/hr capacity.

These costs are also based on the assumption of a silica concentration in the steam of 0.020 ppm. As mentioned previously, it would be prudent to invest a few more dollars per day for increased blowdown to reduce the silica content of the steam below 0.020 ppm. When a steam washer is used, these few extra dollars can quite appropriately be considered low-cost insurance against the much greater loss that can result from turbine deposits.

Finally, the author has considered steam washers only from the standpoint of silica removal. Other boiler-water constituents,

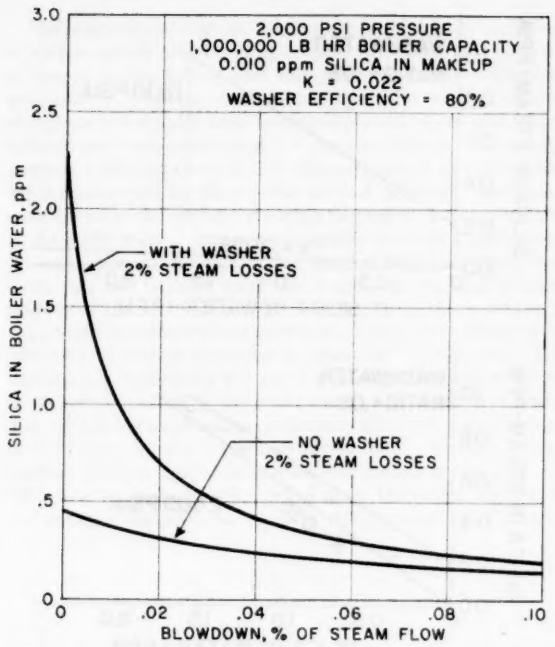

Fig. 10 Effect of blowdown on silica concentration in boiler water

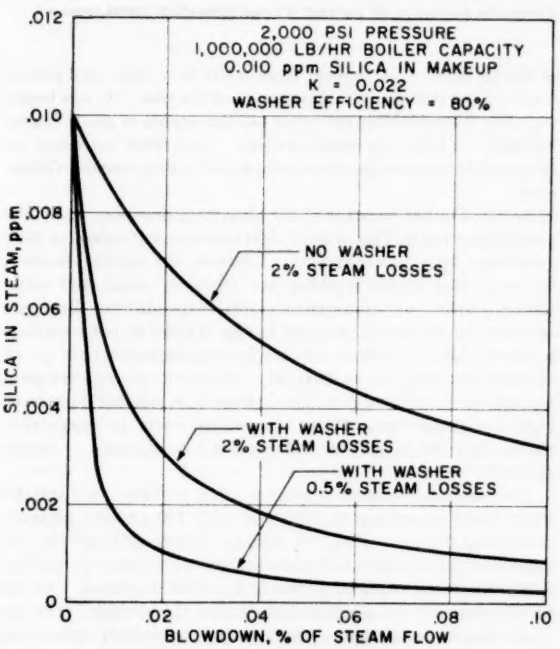

Fig. 11 Effect of blowdown on silica concentration in steam

particularly sodium salts, carry over appreciably in vaporous form above 2000 psi pressure and reach quite significant values above 2500 psi. These impurities can and do form turbine deposits. In ASME Paper No. 57—A-116, "Observed Effects of Deposits on Steam Turbine Efficiency," by J. Angelo and K. C. Cotton, the authors conclude: "These results indicate that about half of the 1.8 per cent gain in the heat rate for increasing initial pressure from 1450 psig to 1800 psig may be lost due to deposits in the steam path." These investigators also found that the deposits were water soluble and contained large percentages of sodium.

During several tests on high-pressure boilers equipped with steam washers, we found that the silica reduction had declined to about 50 per cent, but the washers reduced the sodium content of the steam by 90 to 95 per cent.

The writer must conclude, therefore, that steam washers have a much broader field of application than the author claims. Obviously, under ideal conditions, there is little point in washing steam that is already pure. In practice, however, such ideal conditions are often difficult to obtain and are impossible to maintain during startups and upset conditions, such as condenser leakage and the malfunctioning of the water conditioning equipment. The value of the protection against turbine deposits afforded by a steam washer can easily exceed the initial and operating costs of the washer.

Author's Closure

The author would like to thank Mr. Coulter for his very thorough review of this paper and would like to clarify some of the points discussed.

Mr. Coulter indicates that, on the basis of theory, counterflow washing should show an advantage over other flow patterns. In a strict sense, this is true. Counterflow principles are applied frequently in the chemical industries to obtain just such advantages in processes such as distillation, absorption, and extraction. Silica removal from steam is a liquid-vapor absorption process, so the conclusion is not unreasonable.

However, counterflow characteristics are not obtained merely by passing the liquid and vapor in opposite directions through an absorption column. The advantages of the process are derived from the maintenance of concentration gradients through the column which provide a uniform absorption driving force from inlet to outlet. Thus, the vapor to be purified continuously contacts purer and purer liquid as the contaminant is stripped from it (see Fig. 12). This arrangement provides the greatest absorption efficiency and the purest vaporous effluent. If turbulence causes the pure vapor to contact contaminated liquid prior to leaving the vessel, the advantages of countercurrent absorption are destroyed. To combat this, absorption colums are designed with large height-to-diameter ratios. The dimensions of a boiler drum restrict steam washer design to a very limited depth; and, in view of the turbulence involved, it is difficult to visualize how the concentration gradients necessary for counterflow characteristics could exist. The author will concede that, if steam washing could be performed externally in a properly designed absorption column, counterflow operation might show definite advantages. However, washing in a low-depth, internally installed steam washer is effectively a "continuous batch" process, and the relative direction of the two fluids can be expected to have little or no effect on performance.

Even if countercurrent characteristics could be obtained in a practical washer, the performance limitations at high pressure would still exist. The rate of absorption is dependent upon the mean absorption driving force, which is a function of the distribution ratio. At high pressure, the contact time and contact space necessary for a given performance is greatly increased. The performance of a given washer is thus reduced as pressure is increased. This point is illustrated in Fig. 13, which is a graphical representation of counterflow washing at two different operating pressures. The slope of the equilibrium line (distribution ratio) greatly affects the number of theoretical plates required to provide a given over-all efficiency. At 2500 psia, approximately 7 theoretical plates are required to reduce the silica concentration in the steam 80 per cent while under the same conditions at 1300

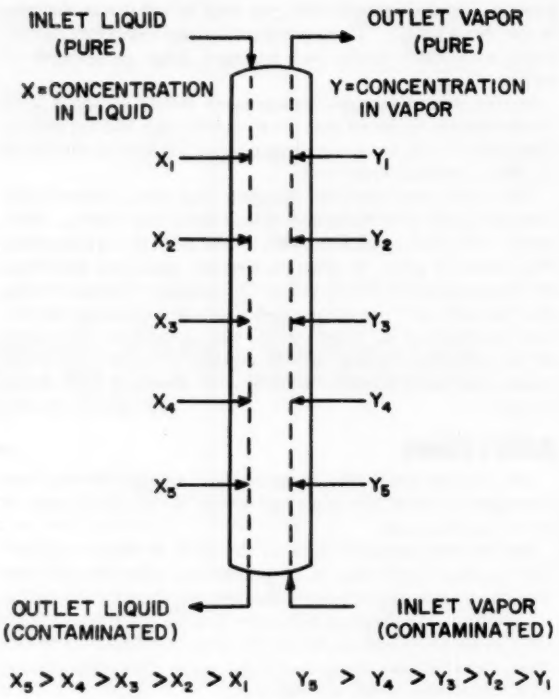

Fig. 12 Illustration of concentration of gradients in counterflow absorption column

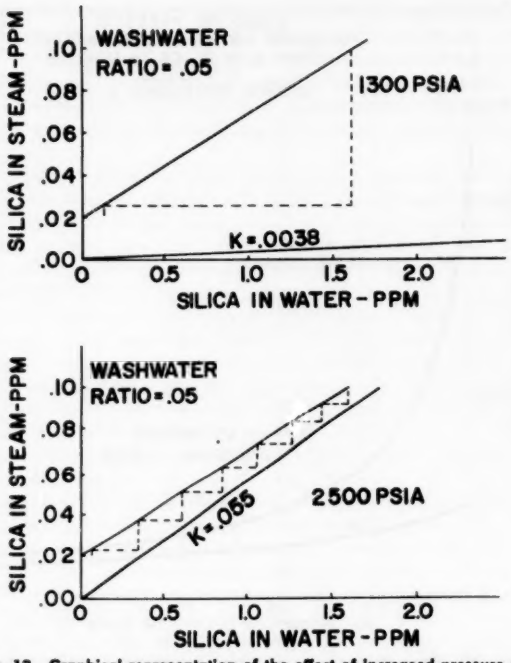

Fig. 13 Graphical representation of the effect of increased pressure on the performance of a counterflow steam washer—the number of steps indicates the number of 80 per cent efficient theoretical plates required

psia, only about 1 theoretical plate is required. Although a truly countercurrent absorption column could exceed the values shown in Fig. 5, there are definite height requirements. Such performance cannot be obtained in a practical steam washer installed in a boiler drum.

Figs. 3 and 4 were included in this paper to correct two rather widespread misconceptions concerning silica control. A belief existed among some operators that objectionably high silica concentrations could be built up in the boiler even though the silica value in the feedwater was tolerably low. Fig. 3 illustrates that the equilibrium concentration of silica in the steam cannot exceed the concentration in the feedwater. Thus, no blowdown is necessary when good feedwater is provided. Fig. 4 was intended to correct the false impression that a system with little or no blowdown was obtaining great benefit from steam washing. Actually, such a system could operate equally well without a washer and with little or no additional blowdown.

In evaluating the advantages of steam washing, it is a fallacy to consider reduced blowdown and reduced silica in the steam as two independent benefits. For a given system, the choice of a silica limit fixes the necessary blowdown rate. For a given specification, the quantity of blowdown necessary will, of course, be less if effective washing is obtained. The installation of a washer must be justified on the basis of the blowdown savings. To make a complete economic evaluation, the operator should estimate the cost of limiting the amount of silica introduced to the system to a point where the need for blowdown is completely eliminated. On this basis, the optimum method of control can be determined.

The purpose of Fig. 9 was to illustrate how the specific cost of controlling silica by blowdown increases with increasing operating pressure. A "pound" basis was used because it is actually the amount of silica deposited in the turbine rather than the concentration in the steam which determines the ultimate cost of the problem. An "ounce" basis could have been used just as well without changing the significance of the plot. It was hoped that Fig. 9 would stress the increased importance of good "housekeeping" in higher pressure systems. Any silica carelessly introduced during outages and startups can be very costly to eliminate.

As Mr. Coulter points out, the blowdown necessary under the conditions cited in Figs. 6 and 7 does not represent excessive daily costs for a large power station. Likewise, the savings obtained by employing steam washing are relatively small and could hardly justify any appreciable capital expenditure. Both are true because the conditions cited in Figs. 6 and 7 do not constitute a serious silica problem. A similar coincidence exists in all systems operating above 2000 psi. Where the savings are great enough to justify washer installation, the residual blowdown costs are prohibitive. When the residual costs are reasonable, the savings resulting from washing are not adequate to justify the initial expense.

For instance, consider a serious silica problem: a 1,000,000 lb/hr boiler, operating at 2000 psig with 100 per cent make-up containing 0.1 ppm silica. A savings of over $200 per day results from the installation of a washer, but a residual cost of about $200/day is still required to obtain the desired control. At still higher pressure, the residual costs exceed the savings. The obvious conclusion is that a plant cannot reasonably operate at pressures above 2000 psi with 0.1 ppm silica in the feedwater.

The economic picture is different at lower pressures where efficient washing can be obtained and where specific blowdown costs are low. In reference [2], Mr. Coulter presented an excellent example when he cited a plant operating at 1325 psi employing 100 per cent make-up containing 0.1 ppm silica. Steam washing can provide a reasonable solution for this type of installation. If this plant were to operate at 2000 psi, however, it would become mandatory to improve the quality of the make-up water. Steam washing could not be justified as a solution at the higher pressure.

The potential use of steam washing to control volatile carryover of sodium salts is an interesting subject. Although it is possible to keep a system free of such salts, some operators consider it advisable to maintain some sodium hydroxide and/or sodium phosphate in the boiler water to control pH and to protect against intermittent condenser leakage. Carryover of treating chemicals presents a different problem than the carryover of an undesirable contaminant such as silica. The amount of volatile carryover must be restricted without reducing the specified concentration in the boiler water. Steam washing may serve as a useful tool for such control. Because of the lower distribution ratios, sodium salts can be more efficiently reduced by washing at high pressures than can silica (see equation 1). The author's company has performed extensive field tests to study the extent of vaporous carryover in boilers operating at pressures of 2600 psig. No significant volatilization was noted in these units with as much as 10 ppm of sodium in the boiler water. However, a problem may exist at higher pressures particularly if the salt concentration in the boiler water is to be maintained high. Whether steam washing finds an application for sodium control in the 2600 to 3000 psig range may well depend upon the water treatment philosophy of the individual operator. If the present trend toward "low solids" and "no solids" boiler water treatment continues, sodium volatilization may never become a problem.

The author agrees with Mr. Coulter that ideal conditions cannot be maintained during startup periods or system upsets. However, the value of a steam washer at such times is doubtful. During startup, the concentrations of silica and corrosion products in the feedwater are generally high. The washing efficiency as a result would be poor, and the possibility of "plugging" the washer with corrosion products would be great. Any entrainment of the wash water with the steam could result in a much greater carryover problem than would exist without washing. If a power station is greatly concerned about silica fouling during startups or during periods of condenser leakage, there is a much more feasible solution. A high-flow, polishing demineralizer can be installed in the cycle to treat all the contaminated drains and condensate which are the source of high silica during startup. The same unit could be used to polish all or part of the condensate during normal operation. The removal of silica by this means is far more economical than steam washing and blowdown. The cost of eliminating silica with such a unit is less than one dollar per pound, regardless of the operating pressure of the boiler.

German Development in Acid Cleaning of High-Pressure Boilers[1]

H. G. HEITMANN
Chief Chemist of Power Plant Department,
Siemens Schuckertwerke AG,
Erlangen, Germany

A new chemical cleaning method for power plants, especially for plants with once-through boilers, is described. In this method chemical cleaning of the loop is accomplished by utilizing temperatures of over 100 C and pH values down to about 4.0. The acid dosing—HCl or H_2SO_4—takes place in the feedwater discharge piping after the boiler feed pump. Before the latter, hydrazine is added to raise the pH value to over five in order to protect the pump. This serves simultaneously as a "transport medium" for the acid through the loop. In addition, hydrofluoric acid can be added to the cleaning solution for the removal of silica, and citric acid for complexing of the dissolved iron. The latter measure will prevent the reprecipitation of dissolved iron. At the time of writing 14 Benson boilers, two Sulzer monotube boilers, and one drum boiler with the associated power-station equipment have been chemically cleaned by the method developed. The cleanings actually carried out are described in part and the information derived from them explained in more detail.

In order to obtain the most trouble-free operation each boiler plant must undergo a thorough cleaning before commissioning. This requirement is valid especially for once-through boilers constructed on the Benson or Sulzer principle. In such cases impurities may easily be carried over into the turbine and may lead to undesirable deposits there. These impurities consist chiefly of rust, mill scale, weld spatter, sand, and other silica compounds. This material not only stems from the boiler but may also come from other parts of the system. By mechanically purging the whole system, particularly at elevated temperatures, most of the impurities may be removed quite easily. This mechanical purging can be improved by firing the boiler and having high-pressure steam escape to the atmosphere at high velocities. These measures, however, do not effect the complete removal of rust, mill scale, and silica compounds. The steam from a purely mechanically cleaned boiler in its initial operational period contains considerable quantities of iron and above all silicic acid. In general it is not possible for the steam to bypass the turbine until necessary purity is obtained. It is thus more or less impossible to prevent high contamination of the turbine blades by iron oxide and silicates during the initial operating period when cleaning is effected by mechanical purging. In addition, particles of rust and mill scale which are not held back by a strainer incorporated in the superheated-steam piping will damage the turbine blades by impingement.

The aim as regards the boiler itself is to build up a thin even protective film of Fe_3O_4 over the internal surfaces. It need not be stressed that this film should only be formed on smooth surfaces. This is, however, only possible if rust and scale deposits have been removed from the boiler surface before commissioning, as otherwise the necessary protective layer will be built up around, or over, any such deposits, the required uniformity then not being obtained. Also, on the one hand large deposits at some places may affect heat transfer and, on the other, the uneven surface may increase the pressure drop. The repeated boiling out of boilers with alkali or phosphate-containing solutions has in the case of once-through boilers only a slight effect, since with this method only loosely clinging rust and scale can be removed. Silica deposits can thereby be partly reduced provided they are not bound in with the iron oxide and that the alkalinity and temperature are high enough. With this treatment water-soluble and thus purgeable alkali compounds may be produced.

Acid Cleaning

Acid cleaning gives excellent results and may be applied to the boiler and, if possible, to the whole boiler-turbine unit with the exception of the turbine itself and the condenser. The suitability of acid cleaning has already been indicated [2 to 4].[2]

In some countries, the acid cleaning of boilers before commissioning has become general practice. In Germany, acid cleaning before commissioning is undertaken less frequently with drum boilers, but with once-through boilers it has gained wide acceptance. In general the acid passed through the boiler will have a concentration of between 5 and 10 per cent at temperatures between 20 and 70 C and will contain inhibitors. For the cleaning itself, HCl is most widely used. In no circumstances will phosphoric acid be used for once-through boilers because with this acid an iron-phosphate film is produced which during subsequent operation without phosphates in the water will redissolve and may result in deposits in the superheater or on the turbine blading [5]. This danger exists with drum-type boilers also due to the phosphate layers formed in the superheater during the cleaning. Occasionally fluoride may be added to the acid to remove the major part of silica deposits. A part of the silicic acid which is bound up with the iron oxide is readily dissolved from the tube surface and purged from the system by the acid cleaning. The procedures followed in such acid cleanings should be generally known [6 to 9]. A circulation loop is established through the boiler incorporating a circulating pump and the cleaning solution is circulated continuously at a rate of approximately 1 m/sec. In most cases HCl (5 to 8 per cent) with an addition of approximately 1 per cent sodium-fluoride, wetting agents and inhibitors is used for cleaning. The cleaning temperature is between 60 and 70 C. The cleaning period is about 5 hr. The major part of the peeled-off mill scale is dissolved completely; a

[1] See Reference [1].[2]
[2] Numbers in brackets designate References at end of paper.

Contributed by the Joint Research Council on Boiler Feedwater Studies of the Power Division and presented at the Winter Annual Meeting, New York, N. Y., November 27–December 2, 1960, of The American Society of Mechanical Engineers. Manuscript received at ASME Headquarters, September 1, 1960. Paper No. 60—WA-227.

small part (<1 per cent) remains in suspension. Subsequent to chemical cleaning, the cleaning solution is expelled by condensate or demineralized water containing hydrazine and then the boiler is stored. If possible, the chemical cleaning is followed by 3 days of boiler operation to establish the formation of a protective film within the boiler tubes.

To enable chemical cleaning to be carried out without large-scale makeshift arrangements, and at the same time to cover the major part of the whole boiler-turbine unit, a method of chemical cleaning[3] has been developed by the author's company, the application of which is described in the following text in more detail.

The cost of this method is less than that of acid-cleaning methods so far used. The procedure may be repeated at any time even after prolonged operating periods without great labor expense. By raising the reaction temperature during the chemical cleaning a considerable acceleration of the rate of reaction is obtained, so that the same result can be achieved in approximately the same time as with the usual chemical-cleaning procedures even with substantially weaker acids. The addition of specific inhibitors was dispensed with for the time being.

Chemical Cleaning With HCl

Table 1 summarizes the attack on iron by hydrochloric acid at different pH values on the basis of the figures established by the company. From this it may be seen that at a pH value of about 4 to 5 (measured at 23 C) there is no stronger attack than with 10 per cent acids with inhibitors added.

Table 1 Iron attack with various pH values and with concentrated acids with inhibitors added

HCl concentration	pH value	Temp, deg	Dissolved-iron quantity, grams Fe/m³/hr
0.000001 n	6.0	100	1.1
0.00001 n	5.0	100	2.0
0.0001 n	4.0	100	2.6
0.001 n	3.0	100	4.3
0.01 n	2.0	100	15.3
0.1 n	1.0	100	122.5
10 pct HCl/inhibitor A		20	2.1
10 pct HCl/inhibitor B		80	1.4

For initial pickling tests carried out in the laboratory, an experimental rig as shown in Fig. 1 was used. In these tests enough acid was added to the circulating water by means of the dosing pump no. 8, Fig. 1, to maintain in the circuit a pH value between 3 and 4. As hydrochloric acid, if it is used alone, is used up completely in the first section of the experimental pipe, in succeeding tests the pH value was at first raised to approximately 8.5 by hydrazine before the acid dosing was begun. Only by this means was it possible to extend the pickling effect over the total length of the experimental pipe. The hydrazine acts, so to speak, as a transporting agent for the acid. For this function, other substances which, with the acid being used, form compounds which may easily be thermally dissociated, such as ammonia, hydroxylamine, and organic amines in particular, may be suitable too.

The tests were carried out under varying conditions. In all cases the experimental pipe, which had been artificially rusted and scaled previously, was completely cleaned. As shown in Fig. 2, the previously rusted experimental pipe has been covered with a completely smooth, fine, black protective film of Fe_3O_4.

Because of the hydrazine treatment, the rust deposits will have been partially changed into Fe_3O_4 and will have loosened in individual cases due to the corresponding increase in volume:

$$6\ Fe_2O_3 + N_2H_4 \rightarrow 4\ Fe_3O_4 + 2\ H_2O + N_2 \qquad (1)$$

By the subsequent HCl addition hydrazine monochloride is produced or, respectively, -dichloride:

$$N_2H_4 + HCl \rightarrow N_2H_4 \cdot HCl,$$
$$\text{or } N_2H_4 + 2\ HCl \rightarrow N_2H_4 \cdot 2\ HCl \qquad (2)$$

Both salts are acidic, and the HCl, being easily split off especially by thermal dissociation, reacts with both the produced Fe_3O_4 and that already present:

$$Fe_3O_4 + 8\ HCl \rightarrow FeCl_2 + 2\ FeCl_3 + 4\ H_2O \qquad (3)$$

The simultaneously existing hydrazine reduces the $FeCl_3$ produced:

$$4\ FeCl_3 + N_2H_4 \rightarrow 4\ FeCl_2 + 4\ HCl + N_2 \qquad (4)$$

Due to the acid being used up according to equation (3) there is a local rise in the pH value. Hence the $FeCl_2$ produced is hydrolized:

$$FeCl_2 + 2\ H_2O \rightarrow Fe(OH)_2 + 2\ HCl \qquad (5)$$

The sum of the reactions in equations (1), (3), (4), and (5) gives

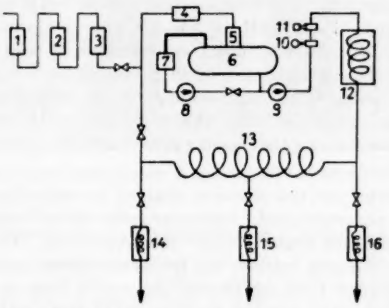

Fig. 1 Arrangement of experimental rig

1 Cation filter
2 Anion filter
3 Mix bed filter
4 Preheater
5 Deaerator
6 Feedwater tank
7 Dosing tank
8 Dosing pump
9 Feed pump
10 Conductivity meter
11 pH meter
12 Furnace
13 Experimental tube
14 Cooler
15 Sampling cooler

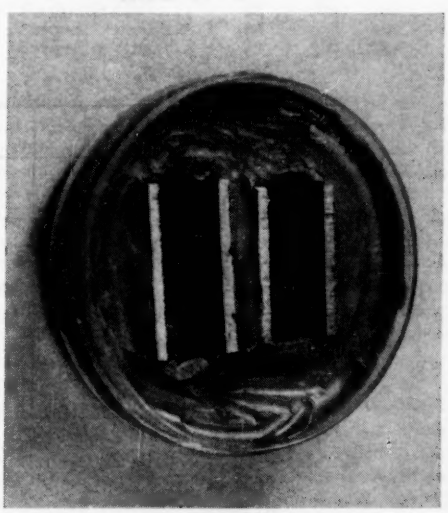

Fig. 2 Experimental tube treated with HCl/N_2H_4. Left, before; right, after cleaning.

[3] DBP (German Federal Patent), U. S., and other foreign patents pending.

$$6\,Fe_2O_3 + 3\,N_2H_4 + 22\,H_2O \xrightarrow{HCl} 12\,Fe(OH)_2 + 8\,H_2 + 3\,N_2 \quad (6)$$

Theoretically the acid used up at the start of the reaction is always regenerated. Only the hydrazine must be consumed slowly, as was confirmed by the investigations. On the whole a certain state of equilibrium will arise between all these possible reactions. As ultimately a part of the dissolved iron remains in the solution a low consumption of acid will take place.

Shortly after the conclusion of the initial laboratory experiments there arose at a power station with a Benson boiler (plant A) the opportunity and necessity to prove the method in a large-scale experiment. In this boiler the hydraulic test had been undertaken with corrosive well water. As a result large rust deposits were formed in the tubes. As the boiler was not fully drainable, normal cleaning with strong acid could not be risked.

The essence of the method developed is that the circulation of the cleaning solution is accomplished by means of the boiler feed pump and that the pickling acid is dosed only downstream of the boiler feed pump, the pH value of the cleaning solution being thereby lowered to 3.5 to 4.5. Upstream of the boiler feed pump it is possible to raise the pH value to 5.0, which is permissible for the pump, by adding ammonia or hydrazine, if need be. An advantage of circulating the cleaning solution by means of the boiler feed pump is that the cleaning may be carried up to the working pressure of the boiler, thus keeping down the volume of gases produced during the cleaning process and, as a result, avoiding trouble.

For carrying out this chemical cleaning the following circulation cycle was established: Feedwater tank—boiler feed pump—high-pressure feed heater—boiler—feedwater tank. Provisional piping was required only for the connection of the boiler outlet to the feedwater tank, for heating the system from an existing boiler-turbine unit, and for draining away waste water. The suction pipe exit inside the feedwater tank was fastened within the tank to minimize entrainment of any undissolved rust and scale particles and to separate them in the tank. The boiler consisted of two halves completely separated from each other, which were to be cleaned consecutively. The total volume of the system to be cleaned was approximately 130 cu m. The boiler has a maximum continuous output of 240 tons/hr.

Prior to chemical cleaning, each half of the boiler was washed out for $^1/_2$ hr with 70 ton/hr of condensate originating from previous operation, until almost clear water (slightly opalescent) drained out at the boiler outlet. During the washing, 10 milligrams/liter of hydrazine were added to the condensate (50 C) by means of a dosing pump. After refilling the feedwater tank (80 cu m) with condensate, 120 liters of 25 per cent solution of hydrazine hydrate were added and the charge was heated to 100 C with steam. During circulation the whole system was heated slowly to 100 C by means of auxiliary steam. The pH value of the system was initially 8.6. After about 1 hr, the dosing of hydrochloric acid (20 per cent solution) was commenced at the rate of 44 liters/hr. The pH value dropped within 2 hr to 4.3 and sank on further circulation to about 4.1. During the cleaning operation the hydrazine content was between 10 and 20 milligrams/liter. The acid dosage was continued until the pH value at the boiler outlet remained almost constant and the iron content at this point rose only slightly. Details are given in Fig. 3. During the chemical cleaning the feedwater tank was partly drained periodically and the water loss was made up with condensate. It is difficult to determine quantitatively the amount of iron oxide going into the solution. A rough estimate gives about 135 kg of iron. The acid consumption amounted to 420 liters of 32 per cent HCl. After cleaning the first half of the boiler the second half was cleaned in a similar way. The quantity of rust removed amounted to about 100 kg calculated as iron; the acid consumption was 420 liters of 32 per cent HCl, as before.

In the case of the second half of the boiler there was a pH drop before the boiler inlet to 3.6. This was probably due to smaller quantities of impurities being present, since the rest of the boiler and feed system had already been cleaned of rust and scale during the cleaning of the first half of the boiler.

Following the acid cleaning of both halves of the boiler, each half was washed out separately from the feedwater tank with hot condensate dosed with hydrazine at a rate of 100 tons/hr until

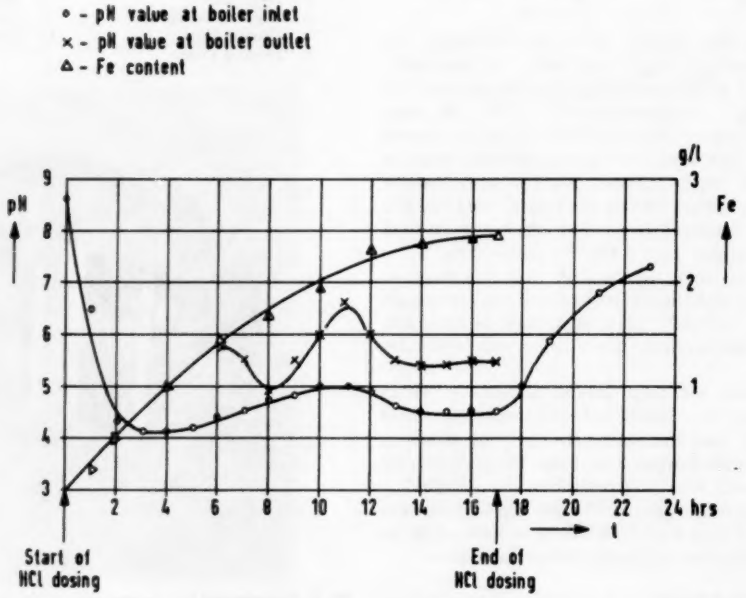

Fig. 3 pH and Fe values measured during cleaning of plant A

the pH at the outlet had risen to 7 and the draining wash water was perfectly clear.

The entire system in cleaned condition was then stored, until commissioning, with condensate containing hydrazine (8 ppm N_2H_4). The total hydrazine requirements from the start of cleaning until storage amounted to 800 liters of 25 per cent hydrazine hydrate.

From this first large-scale application of the new cleaning method various conclusions can be drawn which are considered below. In the first unit it became apparent that the part of the flow drained off and washed out during the cleaning contained large quantities of oil. The oil results from the tube-manufacturing process. Because of this the danger arises that the acidic feedwater is not carried uniformly to all parts of the system and that the effect of the cleaning process is thereby impaired. To prevent this, the second unit of plant A was treated with a solution of P 3 zix, a powerful alkaline wetting agent of the Henkel Company, prior to the acid treatment. Two hundred kilograms of P 3 zix were injected into the feedwater tank filled with demineralized water. The feedwater treated with this solution was circulated in the loop at a rate of 200 tons/hr for 25 hr at 100 C. Then the solution was drained out from the loop and the latter thoroughly washed with demineralized water until the effluent was clear. After this, there was a chemical cleaning similar to that of the first unit except that at 2-hr intervals the acid dosing was shut off, and for 30 min the boiler was circulated at 180-tons/hr output and 24-kg/cm² gage pressure. The temporarily increased circulation velocity served the purpose of loosening sludge deposits that might have occurred and of washing them into the feedwater tank where a certain amount of settling took place.

Experience has shown that, if the circulation velocity is too low, tube blockages can occur due to sedimentation, resulting in tube failures during subsequent operation. However, the hazard of tube blockages due to sedimentation may be reduced to a minimum if the procedure described is adhered to. A powerful blowing out of the boiler prior to commissioning should in any event be carried out. The tube specimens cut out before and after chemical cleaning showed complete success. As Fig. 4 shows, rust and scale were completely removed. Unlike the original rough surface consisting of rust deposits, the tubes had a thin uniform layer of Fe_3O_4, which—as later investigations showed—is to be regarded as a protective layer. The success of the chemical cleaning is demonstrated by the analysis obtained during the first operational period. The iron as well as the silicic-acid content range within reasonable limits, in contrast to the results obtained with uncleaned Benson-boiler plants, where the silica content especially is substantially higher during the initial operating period. Admittedly, at each new start-up the levels of iron and silicic acid are at first somewhat higher, but they fall off to reasonable levels in a relatively short time.

Chemical Cleaning With Sulfuric Acid

In further laboratory experiments the feasibility of using sulfuric acid was examined in order to enable the cleaning method also to be applied to boilers featuring secondary superheaters made from austenitic material. As is generally known, chloride ions may lead to stress corrosion of austenitic steels at elevated temperatures. At the same time the capability of fluorides to dissolve silicic acid was investigated to combine, if possible, removal of silica from the loop with the acid treatment. The experiments, which were repeated several times, extended in each case over 24-hr periods. The values measured during the experiments are shown in Table 2 as average values. The reason for the high iron content of the water at the end of the experiments was mainly that the experimental tube became completely derusted and descaled during the experiment. The quantity of

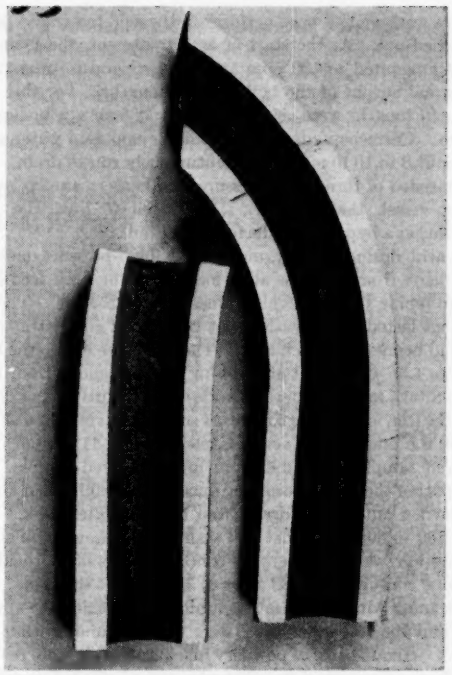

Fig. 4 Superheater tube of plant A before (left) and after (right) cleaning

Table 2 Cleaning experiments with a mixture of sulfuric and fluoric acid

Hours	Sampling location	pH value	N_2H_4, ppm	F′, ppm	Fe, ppm	SiO_2, ppm
0.00	Feedwater pump	7.8	2.5	0	0.08	0.04
0.00	Feedwater tank	7.6	2.0	0	0.08	0.04
1.00	Feedwater pump	3.0	23	168	0.65	0.07
1.00	Feedwater tank	3.4	21	155	0.68	0.08
2.00	Feedwater pump	3.6	20	175	0.95	0.09
2.00	Feedwater tank	3.2	19	171	1.02	0.09
4.30	Feedwater pump	3.1	18	215	2.4	0.35
4.30	Feedwater tank	3.1	18	210	2.6	0.38
12.00	Feedwater pump	3.1	20	230	10.5	0.7
12.00	Feedwater tank	3.2	19	227	11.0	0.7
20.00	Feedwater pump	3.0	21	225	188	2 5
20.00	Feedwater tank	3.2	21	224	210	2.6
24.00	Feedwater pump	2.8	20	252	198	2.7
24.00	Feedwater tank	3.0	20	250	240	2.8

silica dissolved, which during the experiments occurred in the form of quartz, is relatively small. However, it must be considered that even in pure fluoric acid the solubility of fused silica is only very small. In power plants, silica is present partially in the form of more or less soluble silicates. Pure quartz sand, however, can be attacked only slightly. The experiments as well as the experience gained later in large-scale plants make it clear that at least partial success may be achieved by a fluoride treatment of the system. That this removal of silicates within the system is to a large extent dependent on the kind of silicate impurities present is shown by the experience which was gained in two large-scale installations, where the same treatment gave widely different results.

In the case of another plant with an austenitic secondary superheater a sulfuric acid cleaning was carried out, and it was considered of utmost importance to pickle the whole high-pressure system including the reheater and the reheater piping, if possible. In order to establish a loop for circulation it was necessary to provide the system with some temporary connecting lines. After a treatment with a powerful alkaline wetting agent followed by

intensive washing had been performed, the acid treatment proper was carried out. At the start of acid treatment, the hydrazine content amounted to 120 ppm and the temperature was 120 C. The normal output of the boiler is 120 tons/hr. For this cycle 140 to 150 tons/hr were circulated at 14 kg/cm² abs boiler inlet pressure. Corresponding to the available make-up water quantity, about 8 to 10 tons/hr were continuously run to drain. The loop consisted of three high-pressure feed heaters, the boiler, the starting vessel, the reheater, the hot-reheat line, the cold-reheat line as a bypass, and the feedwater tank.

The acid dosing was by means of a high-pressure metering pump made from stainless steel located in the high feedwater-pressure piping before the high-pressure feed heaters. The acid treatment lasted 17 hr, with about 20 liters of concentrated sulfuric acid being dosed each hour. The pH value before the boiler inlet was 4.5. Overnight acid dosing was suspended from 10:00 p.m. to 8:00 a.m. A material alteration of the pH values did not occur, the iron level in the circulated solution having risen slightly and, at the end of the acid treatment, being 1120 ppm in the unfiltered sample, and 1090 ppm in the filtered sample. The major part of the sludge occurring during the cleaning had already been carried out by the drain from the feedwater tank. Altogether 450 to 500 kg of rust and scale were removed. The acid consumption was 310 liters of concentrated sulfuric acid, the hydrazine consumption 380 liters of 15 per cent solution. After final cleaning with condensate containing hydrazine the start-up vessel and the feedwater tank were emptied and mechanically cleaned. About 10 kg of powdery black iron oxide were removed from the start-up vessel together with some included particles of scale, and from the feedwater tank about 1 kg of weld spatter and scale. About 3 kg of iron-oxide particles had accumulated in the dismantled strainer of the feed-pump suction line. The iron-oxide sludge arising from the hydrolysis of $FeCl_2$ was not collected by the strainer. These particles also passed through a 0.09-mm mesh test strainer. As experience has shown, these impurities are completely harmless for the boiler feed pump during the comparatively short cleaning period.

Tube specimens cut out after washing with two feed pumps (210 tons/hr) showed a completely smooth surface with a very thin black protective layer of Fe_3O_4. As a further check for any pockets of sludge deposits that might have remained in the headers, one header under the ash hopper and the reheater-inlet header were cut open. These headers were likewise in perfect condition and completely free from iron oxide and scale.

In further investigations carried out with the experimental Benson test rig, various boiler materials were tested for their behavior with the cleaning solution. Of the greatest interest were possible alterations in the structure of the material. For this purpose, the following materials were welded together as an experimental tube.

(1) (2) (3) (4) (5)
AN 15 – 13 CrMo 44 – 10 CrMo 910 – 15 Mo 3 – St 45.8

where

(1) = austenitic steel; (2) = 1 Cr 0.5 Mo alloy steel;
(3) = 2.25 CrMo alloy steel; (4) = 0.3 Mo alloy steel;
(5) = carbon steel

One hundred and twenty liters/hr of acid cleaning solution at 140 C were pumped for 100 hr through this experimental tube. The hydrazine content was maintained at between 40 and 80 ppm. An adjustment of the pH value was achieved by adding a mixture of 50 per cent sulfuric acid and 40 per cent fluoric acid in the proportion 5:1. During the experiment 20 liters/hr of demineralized water were continuously drained out through the deaerator. The pH value of the solution was adjusted to between 3.5 and 4.0.

After completion of the experiment the boiler tubes in new condition, as delivered, were compared by means of photomicrographs with those exposed to corrosion. The inside surfaces of the treated pieces of tube showed an essentially smoother and cleaner finish than those of the untreated material. The tubes, as delivered, already exhibit certain surface defects. This can influence negatively the formation of protective layers during the operation of untreated boilers. It is still possible that with un-

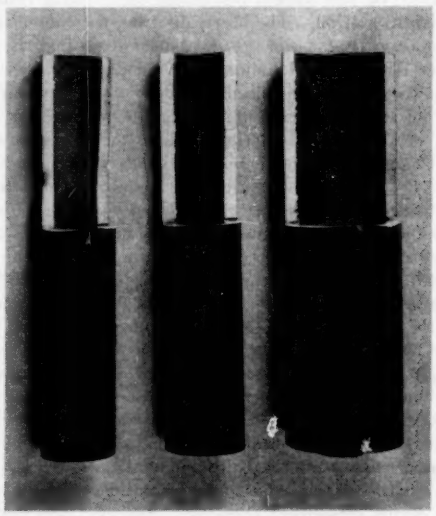

Fig. 5(a) Tube specimens, left to right: 13 CrMo 44, 15 Mo 3, St 45.8, as delivered (before cleaning)

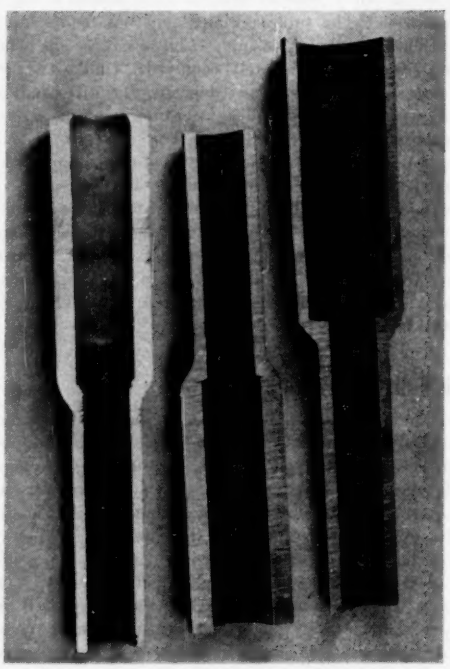

Fig. 5(b) Tube specimens after chemical cleaning with H_2SO_4/HF

13CrMo 44	10 CrMo	St 45.8
AN 15	15 Mo 3	15 Mo 3

treated materials break-away particles from surface defects will dissolve into the water only during subsequent operation. With all specimens the most important fact to be recorded is that after the chemical removal of the oxide skin there is no local attack such as grain-boundary or similar corrosion. This demonstrates that, with the cleaning method developed, slight though not measurable corrosion of the material may take place, but that no local corrosion occurs in the process. Figs. 5(*a* and *b*) show the external change in the inside surface of the tube. While the original specimens show in part strong rust deposits, the inside surfaces of the treated tubes were covered completely with a thin uniform protective coating.

Chemical Cleaning With Acids and Iron-Complex-Forming Agents

Further experiments concern the question of how the formation of sediment arising from the hydrolysis of $FeCl_2$ may be prevented and thus how deposits and tube blockages may be avoided from the outset. The most promising appeared to be organic materials which form complex compounds with iron ions so that the iron at high pH values is held in a solution. The most suitable complexing agents for iron are organic acids containing hydroxyl groups or their respective salts. For instance, tartaric acid, citric acid, grape sugar, and cane sugar were investigated. These substances form complexes with iron salts which are not destroyed even if the pH value is raised with ammonia. The best results were achieved with citric acid. Laboratory experiments carried out under the conditions prevailing during acid cleaning—presence of hydrazine and bi and trivalent iron—showed that at an iron:citric-acid molar ratio of up to 2 no iron precipitation is to be feared. Although, according to the data given in the relevant literature [10], citric acid can bind iron as a complex at the ratio of 1:1, it is essential for this type of acid cleaning that the iron is not precipitated up to a pH value of approximately 7. The citric acid also may be used directly as a cleaning acid, but then it must be used in a higher concentration up to approximately 3 per cent [11]. However, this increases the cleaning costs on the one hand and, on the other hand, a separate circulating pump with all associated piping and connections is needed for circulating the cleaning solution. In later acid-cleaning experiments, citric acid was therefore used only as a complex former. The acid cleaning proper was carried out in this case, too, with a mixture of sulfuric acid and fluoric acid. The experiments by means of the Benson test rig were conducted in a way similar to the previous ones. An H_2SO_4/HF mixture was dosed into the cleaning solution with citric acid, ammonia, and hydrazine being added at a circulation rate of 120 liters/hr and 100 C temperature. The pH value was maintained at between 3.5 and 4.0, the cleaning time amounting to 20 hr. The cleaning solution, colorless at the start of the experiment, changed to a pale yellow color, then became deep yellow, and finally turned into a greenish brown color. No iron-hydroxide precipitation could be observed even at the end of the experiment.

In this case rough spots due to rust deposits existing prior to cleaning were entirely removed, a completely smooth inside tube surface being produced. Admittedly there was not the original deep black appearance, but a light gray sheen. The formation of a straight protective layer does not take place in the presence of citric acid.

The question arises as to the quantities required for a full-scale use of citric acid as a complex former. Since no quantitative statements can be made on the degree of contamination of a boiler-turbine unit, it is only possible to estimate roughly the amount of rust and scale to be dissolved. On the basis of past experience the cleaning solution does not contain more than 5 kg of iron per m^3. The amount of citric acid required would then be approximately 1 per cent of the water volume. In practice it has been observed that this amount of citric acid is sufficient to prevent the precipitation of iron.

Additional Chemical Cleaning Methods for Power Plants

Finally, some large-scale methods of chemical cleaning will be discussed which make clear the possibilities of the process. If sufficient cleaning water is available and if there is the possibility of attaining high circulating velocities, then the cleaning may be carried out without complexing compounds. This was the case with plant C, where there existed a "larger" and a "smaller" loop. The large loop consisted of feedwater tank—boiler feed pump—hp feed heater—boiler (two boilers in parallel, each of 160 tons/hr output)—start-up vessel—cold storage tank—condensate pump—feedwater tank. By connecting the start-up vessel directly to the feedwater tank an additional smaller loop resulted. The cleaning itself was carried out in a similar way as with plant B. Due to the change-over facilities from the large to the small loop, it was possible to proceed with chemical cleaning and subsequent washing without interrupting circulation, so that the hazard of sludge deposition in the boiler was minimized. During circulation in the small loop the cold storage tank could be emptied, mechanically cleaned, and refilled with condensate. Since this tank had a storage capacity of 240 cu m of water, the system could be intensively washed out after changing over to the larger loop from which the return flow was discharged before reaching the cold storage tank. In this way the whole system could be cleaned completely and then stored with hydrazine without a break. About 730 kg of iron were removed in the dissolved condition during cleaning, as well as the rust and scale separated in the form of sediment. The cleaning was carried out separately for each boiler at a pH value between 3.9 and 4.5. The total acid consumption amounted to 1620 kg of concentrated sulfuric acid, the hydrazine consumption, including storing, to 1000 kg of 15 per cent solution.

Perfect tube specimens cut from the feed-heater outlet header and from the superheater proved the success of the cleaning. The tubes and also the vessels included in the cleaning showed a completely even surface covered with a very thin protective layer of Fe_3O_4.

It may be concluded from hydrogen measurements taken on commissioning the boiler-turbine unit [12] that this layer has really the character of a protective layer. These measurements were taken by means of a gas chromatograph. The gases contained in samples of condensed steam are continuously washed out by means of argon. Of this gas mixture, a sample is fed into the chromatograph every 15 min and split up into its individual components by an adsorption column. The fractionized gases are fed into a cell measuring their thermal conductivity. In this process, from the difference between the thermal conductivity of pure argon and that of the argon contaminated by the individual gas components, it is possible to determine the quantity of the gases contained in the steam. This quantity is registered by a recorder—compensograph (range 0 — 1 mv). Fig. 6 shows that the hydrogen concentrations recorded are essentially lower than for boilers not cleaned by the method described in the foregoing. It is also significant that boilers cleaned this way are not so prone to corrosion between cleaning and commissioning as boilers cleaned by the conventional method, since the latter method produces a highly

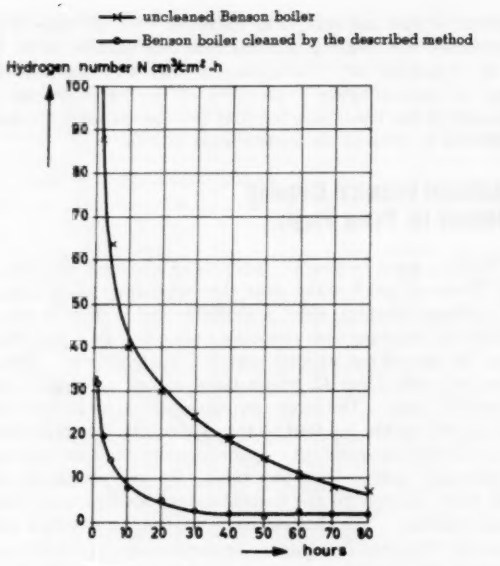

Fig. 6 Hydrogen values during first hours of operation

active clean metallic surface. This is also shown by the stability of tube specimens in temporarily corrosive wet laboratory air.

In the case of plant D only a small amount of condensate was available for chemical cleaning, which had become necessary due to the poor condition of the boiler tubes. This was a new power plant of two boiler-turbine units each of 36 mw and boiler ratings of 118 ton/hr. Air condensers were used for the exhaust steam from the turbine. Condensate had to be either produced in an oil-heated auxiliary boiler with a rating of 4 tons/hr or supplied by truck. It was only on commissioning the second unit that the demineralizing plant which had been ordered later became available. The system to be cleaned consisted of feedwater tank—boiler feed pump—high-pressure feed heater—boiler—starting vessel—start-up tank—start-up recirculation tank—start-up recirculation pump—main deaerator—feedwater tank. No provisional piping was required for the system. The chemical cleaning itself was to be carried out with complex-forming agents.

After treatment with P3 and precleaning the system, the feedwater-tank contents were dosed at first with 350 liters of 28 per cent ammonia solution and 100 liters of 15 per cent hydrazine solution. Subsequently 750 kg of citric acid were introduced through a dissolving tank. Such quantities were put in that some diammonium citrate was produced as an end product to protect the boiler feed pump by preventing the pH value from falling too low. For direct introduction of the citric acid during cleaning a dosing pump of too great a capacity was required, and this was not available. After intimate mixing by introducing steam, the feedwater-tank charge had a pH value of 6.1; the hydrazine content was at 100 ppm. This solution was first pumped through the system several times to attain a uniform distribution, but it was warmed at the same time to 100 C with the steam from the auxiliary boiler. During circulation a slowly deepening yellow coloration of the cleaning solution could be observed which signified that the iron oxide was already going into a complex solution. Dosing was performed from an iron dosing tank by means of a fine dosing pump of Hasteloy. The acid was injected into the feedwater pressure piping after the high-pressure feed heater. A mixture of 80 per cent (by volume) concentrated sulfuric acid and 20 per cent of 60 per cent solution fluoric acid was used for the acid treatment. Because of the acidic vapors being formed, the mixing of these two acids is not completely safe. Therefore it is more practical to dose the sulfuric acid and the fluoric acid directly from the delivery vessel intermittently. The sediment was not removed during cleaning to prevent citric-acid losses. The circulation rate was limited by the capacity of the start-up recirculation pump to 80 tons/hr.

The acid treatment took 20 hr. The cleaning solution, colored yellow at the beginning of the acid dosing, changed during the cleaning process through light brown into deep dark brown. It remained, however, absolutely clear and free from iron-hydroxide precipitates. Despite an acid dosage of 54 liters/hr the pH value fell only to a minimum of 4.7, or, in the case of the second boiler, to 4.1. As ammonium citrates were present, the water was strongly buffered, so that the acid dosing only produced a relatively small lowering of the pH value. For the same reason dosing with ammonia/hydrazine raised the pH value only slowly. After this had risen again to 6.8, the unit was washed out and stored. The cleaning solution was drained out through the start-up tank. As no water was drained off during cleaning, the dissolved iron-oxide and silica quantities could be determined with fair accuracy.

The water volume amounted to about 100 cu m. About 600 kg of iron and 6.5 kg of silica were dissolved. Altogether 520 liters of concentrated sulfuric acid and 70 liters of 60 per cent fluoric acid were consumed. It should be noted that the hydrazine requirement at the start of cleaning was very high, then, however, it remained for practically the whole duration of the cleaning process at around 50 ppm. In contrast to other power plants, the hydrazine consumption was extremely small. It amounted to 225 liters of 15 per cent solution including storage. This low consumption was probably due to the presence of citric acid, which complexes the dissolved trivalent iron so that it cannot be reduced further by the hydrazine. The somewhat higher cost of cleaning by using citric acid—100 kg cost about DM 250 ($60.00) may be compensated somewhat by the lower consumption of hydrazine. Tube specimens cut out from the final evaporator and the superheater before and after cleaning prove the success of this cleaning method.

In addition to the first unit of plant D the uncleaned live-steam piping and reheat piping were blown out together with the boiler. This completed the cleaning, the weld spatter and dissolved-scale particles still remaining in the boiler being blown out in the process. Steam samples taken at the boiler outlet at the end of two 3-hr blowdowns were absolutely clear and free from undissolved particles. During commissioning of the boiler-turbine unit and subsequent operation, no tube failures occurred through tube blockages or through acid retained from the cleaning operation. The latter had been removed completely by washing and blowing down. The second boiler-turbine unit was cleaned in the same way with good results. The first operational values for iron and silica are compared in Figs. 7 and 8 with those for uncleaned boilers. The advantage of cleaning a power plant before commissioning is clearly demonstrated.

The cleaning of plant E was carried out in a similar manner to plant D, so that a detailed description is unnecessary here. After extensive experience had been gained from cleaning ten Benson boilers, further cleaning of boiler plants and entire unit-type power plants was entrusted to a firm of specialists who already had gained wide experience in the chemical cleaning of power plants by conventional methods.

Up to the time of writing, this firm has cleaned several power plants; among others one plant with two Sulzer monotube boilers and one plant with a drum-type boiler. Drum-type boilers are

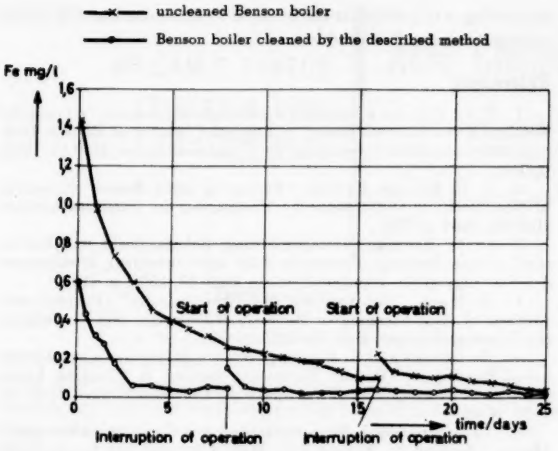

Fig. 7 Fe values during first time of operation

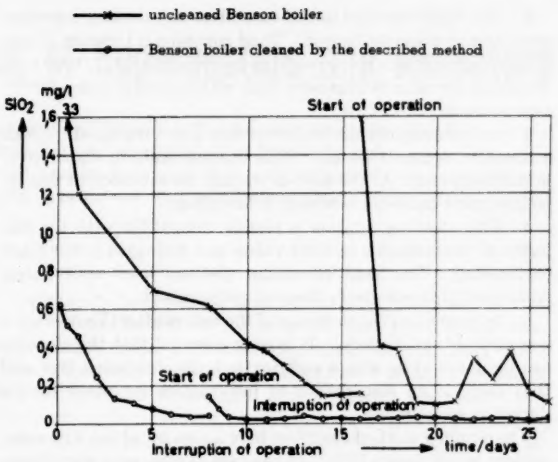

Fig. 8 SiO_2 values during the first period of operation

also cleaned by the once-through process, using the boiler feed pump for circulation. To achieve once-through circulation of the cleaning solution in the riser-downcomer system, the boiler drains installed in this part were interconnected and returned to the feedwater tank. Under certain circumstances it may be more practical to clean the whole main circulation system by the method described here, while cleaning the boiler drum and the riser-downcomer system by the method employing 5 to 10 per cent acids which has hitherto been used.

Conclusion

In conclusion, a description will be given of one acid-cleaning operation of a power plant with once-through boilers undertaken by this specialist firm. The loop to be cleaned is shown in Fig. 9. To establish the loop required, the high-pressure and low-pressure casings of the turbine were bypassed by temporary piping. The hot reheat line was connected to the low-pressure system and thus the loop was established. Ahead of the low-pressure system a draining facility was retained. First the whole system was filled with water and brought to approximately 100 C temperature by a small oil fire in the boiler. Then the temperature was maintained by introducing steam into the feedwater tank. Simultaneously, dosing of a caustic solution containing a wetting agent was commenced. The alkaline treatment took 12 hr. Its purpose was principally to remove oil and grease residues from the system. Proportionate to the approximately 200 cu m total volume of the system to be cleaned, 4000 kg of 50 per cent NaOH and 400 kg of wetting agent were injected into the feedwater tank by centrifugal pumps. The temperature was raised to 125 C. Subsequent to the alkaline treatment the entire system was flushed with softened water and the alkaline solution expelled. Feedwater tank 2 was cleaned mechanically prior to the chemical-cleaning operation, while the loop continued to operate through feedwater tank 1.

At the beginning of the acid treatment the temperature in the loop was first raised to approximately 80 C. By means of a dosing pump, the following amounts of chemicals were introduced into the feedwater tank:

200 kg of inhibitor
80 kg of wetting agent
100 kg of hydrazine (15 per cent)
1800 kg of citric acid
500 kg of sodium fluoride

This mixture was circulated by means of the boiler feed pump and at the same time the temperature was raised to about 110 C by introducing auxiliary steam. The pH value mounted rapidly to 5. After 7 hr the content of dissolved iron amounted to 3700 ppm and the hydrazine content to 70 ppm. By adding concentrated sulfuric acid after the boiler feed pump the pH value before the boiler inlet was lowered to 4.0. After the pH value dropped below 5.0 in the feedwater tank, ammonia was injected ahead of the feed pump to protect it. In about 12 hr, after the content of dissolved iron had reached a nearly constant value of 4600 ppm, the cleaning was terminated. Without any interruption of circulation, the whole system was flushed with demineralized water. Due to the presence of a condensate demineralizer plant 100 cu m of demineralized water per hr were available, so that the whole system could be flushed until the conductivity at the flushing drain attained 3 mhos. To check flow and to recognize possible tube blockages in the boiler, the tubes of the platen superheater and of the reheater were monitored during flushing. All tubes had the same temperature and consequently were passed by the flushing water.

Subsequent to acid cleaning and flushing, the boiler was operated for 3 days to form a protective film of Fe_3O_4 in the cleaned tubes. After this short-term operation the boiler was stored with deionized water containing hydrazine until final commissioning. Altogether approximately 1000 kg of iron (in the form of Fe_3O_4) and 17 kg of silica were removed from the system.

The following conclusions may be derived from the experience gained in acid-cleaning operations carried out so far:

1 With two exceptions, no damage has occurred to the boiler feed pumps used for circulation. During the cleaning process pumps are operated at as low a speed as possible; in general, at no more than 2500 rpm, at which speed wear is negligible. In one dismantled feedwater pump the clearance at the balancing device was measured, this being the most sensitive part of the pump. This tolerance was 0.32 mm before cleaning and 0.35 mm afterward. In the case of a feed pump whose speed could not be lowered to less than 6000 rpm a small amount of wear had arisen due to considerable amounts of sand in the feedwater and condensate lines, so that after cleaning the discharge plate had to be ground and the bushing had to be replaced. To avoid such mechanical damage to the feedwater pumps it is practical to lengthen the suction flange in the feedwater tank and to provide it with a horizontally mounted strainer tube to enlarge the filtering surface.

2 The inhibitors used in this case effect an extensive corrosion protection of the metallic iron. Total corrosion is between 15 and 30 gram/m² and thus corresponds at its worst to a few 1/1000 mm. Therefore corrosion is no greater than with a normal hydrochloric-acid cleaning.

3 Acid dosing into the feedwater line is accomplished through a specially designed nozzle. This ensures uniform distribution in the feedwater. At the time of writing, no corrosion at this injection point has been observed in any plant.

4 This cleaning solution is readily compatible with the majority of the materials used for valves and fittings in power-plant engineering. The hard chromium platings used with Sulzer boilers and Sulzer control valves are not attacked.

5 In most cases the cleanness of the boilers after this operation was entirely satisfactory. It is only essential that the cleaning can be undertaken with a sufficiently large circulating flow and that there is no disturbance or interruption by other factors during its performance.

The cleaning method described here is also suitable for cleaning nuclear power plants [13]. In the case of nuclear power plants, cleaning the reactor and the whole piping system prior to commissioning is of particular importance to minimize the difficulties arising from corrosion products.

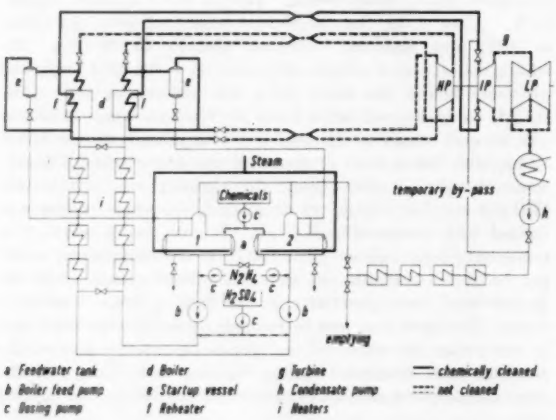

Fig. 9 Scheme for chemical cleaning of a power plant

References

1 H. G. Heitmann, excerpts with supplements from "Chemische Reinigung von Bensonkesseln" (Chemical Cleaning of Benson Boilers), *Mitteilungen der Vereinigung der Grosskesselbesitzer*, Heft 62, 1959, p. 319.

2 H. E. Hoemig, Richter, "Reinigung neuer Kessel" (Cleaning of New Boilers), *Mitteilungen der Vereinigung der Grosskesselbesitzer*, Heft 32, 1954, p. 386.

3 H. E. Hoemig, "Dampfspaltung, Schutzschicht und Korrosion" (Steam Split-up, Protective Film and Corrosion), *Mitteilungen der Vereinigung der Grosskesselbesitzer*, Heft 33, 1955, p. 416.

4 G. Resch, "Ziel und Art der Kesselbeizung" (Purpose and Method of Acid Cleaning of Boilers), *Mitteilungen der Vereinigung der Grosskesselbesitzer*, Heft 53, 1955, p. 27.

5 H. Dörsam and R. Kretzer, "Neuere Erfahrungen mit Grosskessel-Beizungen" (Recent Experience Gained in Cleaning Large Boilers), *Mitteilungen der Vereinigung der Grosskesselbesitzer*, Heft 53, 1958, p. 92.

6 "Kesselreinigung durch Auskochen mit Chemikalienlösungen" (Boiler Cleaning by Boiling Out With Chemical Solutions), VGB Pamphlet No. 1, Vereinigung der Grosskesselbesitzer, 1954.

7 S. T. Powell, "Acid Cleaning: Power-Plant Maintenance Tool," *Power*, vol. 95, 1951, pp. 89–91.

8 K. Rummel, "Über das Beizen neuer Hochdruckkessel" (On Acid-Cleaning New High-Pressure Boilers), *Mitteilungen der Vereinigung der Grosskesselbesitzer*, Heft 53, 1958, p. 89.

9 R. E. Novak, "Preparatory Measures for First Start-Up of Steam Generators" (title retranslated from German, as original source was not available), *Combustion*, vol. 24, 1953, p. 45.

10 (*a*) M. Bobtelsky and J. Jordan, "The Structure and Behavior of Ferric Tartrate and Citrate Complexes in Dilute Solutions," *Journal of The American Chemical Society*, vol. 69, 1947, p. 2286. (*b*) O. E. Lanford and J. R. Quinan, "A Spectrophotometric Study of the Reaction of Ferric Iron and Citric Acid," *Journal of The American Chemical Society*, vol. 70, 1948, p. 2900. (*c*) R. C. Warner and J. Weber, "The Cupric and Ferric Citrate Complexes," *Journal of The American Chemical Society*, vol. 75, 1953, p. 5086. (*d*) R. E. Hamm, C. M. Shull, Jr., and D. M. Grant, "Citrate Complexes With Iron(II) and Iron(III)," *Journal of The American Chemical Society*, vol. 76, 1954, p. 2111.

11 E. B. Morris and E. Q. Pirsh, "Organic Acids for Cleaning Power-Plant Equipment," ASME Paper No. 58—A-282, 1958.

12 E. Ulrich, "Ziele und Grenzen der Wasserstoffmessung im Hochdruckkesselbetrieb" (Purpose and Limits of Hydrogen Measurement in High-Pressure Boiler Operation), *Mitteilungen der Vereinigung der Grosskesselbesitzer*, Heft 49, 1957, p. 252.

13 K. R. Schmidt, "Nutzenergie aus Atomkernen" (Utilizable Energy From Atomic Nuclei), Walter de Gruyter Publishers, Berlin, Germany, first edition, 1960 (general reference).

WILLIAM F. ASHTON
STANLEY M. ROSE
Sumco Engineering, Inc.,
Caldwell, N. J.

Acid Cleaning of Superheaters and Reheaters

The object of this paper is to present both laboratory and field experience in the chemical cleaning of drainable and nondrainable superheaters and reheaters.

It will be limited to the general discussion of flow characteristics, types of solvents, equipment used, and methods employed, with emphasis on actual results obtained in the field.

Introduction

From the time that solvent cleaning proved to be an effective and economical method of removing deposits from internal boiler heating surfaces, there has remained the problem of cleaning any unit that contained various parallel circuits that are either nondrainable or nonventable. The problem of cleaning superheater and reheater elements has concerned the entire power industry, as well as the chemical cleaning contractor.

There have been many cases where nondrainable superheater elements have been cleaned using the conventional "fill-and-soak" method, but these cleaning jobs were confined to low pressure units and entailed the removal of all handhole caps in the headers and individual flushing of each tube. This procedure was time-consuming and, in many cases, effective cleaning was not accomplished due to the stagnation of spent solvents in tubes that were heavily fouled. As steam-generator design advanced, superheaters and reheaters were fabricated in an all-welded construction, thus eliminating any possibility of individual flushing of elements.

Scope of Problem—Preliminary Laboratory and Field Work

It is generally recognized that due to the high temperatures and pressures associated with the modern steam-generating units, a clean superheater and reheater will tend to alleviate the problems associated with foreign materials entering the turbine. Erosion of steam ports and impingement on turbine blading by mill scale will be kept to a minimum if the superheater and reheater are cleaned after erection and prior to initial operation.

Another phase of the problem was the build-up of dense iron oxide deposits during operation due to various reasons. It is not the intent of this paper to discuss the reasons for this deposition but rather to recognize the existence of the problem and the methods of cleaning that had to be evolved in order to cope with it.

The preliminary investigation centered on the following points:

1 Characteristics of flow in parallel elements.

2 Effects of corrosion and erosion with various solvents and inhibitors.

3 Possibility of a single method to remove both mill scale prior to initial operation and to remove deposits after extended operational use.

4 Actual field application in the preliminary stage.

Flow Characteristics. The investigation of flow characteristics proceeded from the theory that the solvent flow should, as nearly as possible, approximate the operational flow through the unit to be cleaned. For example, a million pph boiler would require a flow of approximately 2000 gpm with approximately 1½ to 2 feet per second through the parallel elements.

Contributed by the Joint Research Committee on Boiler Feedwater Studies and presented at the Winter Annual Meeting, New York, N. Y., November 27–December 2, 1960, of The American Society of Mechanical Engineers. Manuscript received at ASME Headquarters, August 26, 1960. Paper No. 60—WA-219.

Laboratory tests proved that velocities of the order of 1 to 2 fps were effective in sweeping air and other gases from nonventable loops and entraining them in the fluid flow. These gases could be then vented at a point of decreased pressure. It was found that distribution of flow through the parallel elements was uniform enough to anticipate favorable field results.

Corrosion and Erosion Data. Due to the velocities involved in supply piping to the various superheater and reheater elements, considerable laboratory time was devoted to extensive evaluation with the use of inhibited citric and other organic acids, coupled with a re-evaluation of inhibited hydrochloric at high velocities. The results of these tests are presented in Table 1.

Table 1 Corrosion inhibition[a]

Coupon	Solvent	Temperature	Exposure time	Corrosion rate, lb/ft²/day
1	5% Inhibited citric	200° F	8 hr	0.0014
2	5% Inhibited citric	200° F	8 hr	0.0011
3	5% Inhibited citric	200° F	8 hr	0.0012
4	5% Inhibited HCl	165° F	8 hr	0.0040
5	5% Inhibited HCl	165° F	8 hr	0.0039
6	5% Inhibited HCl	165° F	8 hr	0.0040

[a] All tests were conducted on mild steel at a velocity of 20 fps.

As the results indicated, satisfactory inhibition was obtained with all solvents, although cleaning effectiveness with some solvents tested were found to be both a function of high-steady temperature, high flow, and concentration. Emphasis was placed on the use of economical and readily available solvents, although work is being continued with other solvents that give indication of practicality in field work.

Single Method for Removal of Both Mill Scale and Operational Deposits. Both the removal of mill scale and the removal of operational deposits pose several common problems and several distinctly opposite problems. The study was designed to reconcile any disadvantages in order to provide for one single method, which would be economical with regard to the type equipment utilized, methods, and procedures.

The first area investigated was the problem of preheating and draining nondrainable elements. Preheating could be accomplished easily by forcing condensate from the boiler into the superheater elements. This accomplished the preheating of the elements, but no method was found to completely eliminate the condensate in all tubes except by evaporation. Various methods such as bumping with air or inert gas were found to be inadequate. Hence it was felt that any method evolved would have to include uniform displacement in all elements rather than any attempt to preheat and displace the condensate with a gas before acid blending. It was concluded that with high flow through the units, with steam applied to the solvent externally to the boiler, preheating could be accomplished regardless of what mill scale or operational deposits were present.

The next area of discussion was the type of solvent to be used and the feasibility of its use with the Hi-Flo method. The choice

of acid narrowed to two solvents, inhibited hydrochloric and inhibited citric acid. The results in Table 1 show that both acids could be used safely with regard to corrosion and erosion.

The next problem posed was their compatibility with the materials of construction and their ability to remove both mill scale and operational deposits. While it is not within the scope of this paper to discuss the relative properties of the two acids, it was concluded that hydrochloric acid could be used for both type deposits, being limited in its use to units containing only carbon steel, due to the problem of chloride corrosion cracking in stainless steel at boiler operating temperatures. It was also concluded that, generally speaking, citric acid could be used for both type of deposits but particular emphasis had to be placed on flow, higher temperature, and time of retention in the units. In addition, the chelating ability of citrate would prevent deposition in nondrainable areas.

The final area to be investigated was the displacement of the acid solvents, neutralization and its displacements, and the final water flushes. If high flow provided uniform mixing in the initial stages, there would be no additional problems in the subsequent stages. It was, therefore, concluded that a single method, utilizing a Hi-Flo technique, could be applicable for removal of both mill scale and operational deposits except for the following: Use of any solvent would depend upon material of construction, type of deposit, and modified method of high flow with the use of hydrochloric acid.

Actual Field Application in the Preliminary Phase. The first field application was conducted at an eastern refinery for the removal of a soluble deposit in a vertical furnace consisting of twenty-four 2-in. U-type parallel elements. Connections were provided for a flow of approximately 800 gpm, which approached the operational flow of 925 gpm. The unit was preheated by circulating water and adding steam. Temperatures were checked on each individual element and were found to be similar within a 10-deg range. Acid was then blended into the stream and circulated until no change in concentration was noted. Circulation was stopped and restarted every hour for ten minutes during the retention time in order to displace partially spent solvent and add heat to the solution.

After the unit was cleaned and neutralized, inspection was made at three points which visibly showed the removal of all deposits in both the nonventable and nondrainable loops. The conclusions from this experience led to several subsequent jobs using the Hi-Flo method that are not pertinent to this discussion, but gave the Project Engineers invaluable data with regard to the peculiarities encountered in high flow operation with regard to equipment, solvent application and other related problems.

Field Experience in Cleaning of Superheaters and Reheaters

There were two basic types of design that were encountered in the cleaning of superheaters and reheaters. One was the drainable type unit with nonventable loops, the other design was the conventional pendant type with both nondrainable and nonventable elements. The following describes our field experience.

Cleaning of Drainable-Type Units With Nonventable Loops. A large scale operation in the cleaning of a nonventable but drainable type superheater and reheater took place in a large eastern public utility. Steam flow through the convection superheater was in the range of 2,000,000 pph and 1,600,000 pph in the reheater. The holding capacity of the superheater and reheater, respectively, was 15,000 gallons and 35,000 gallons, including main steam, cold and hot reheat lines.

The superheater contained 260 parallel elements and the reheater 315 parallel elements. Materials of construction included both carbon steel and stainless steel. Due to the presence of austenitic steel, the use of inhibited citric acid was considered above any other organic acid. Temporary piping was erected in order to accommodate flows up to 4000 gpm. Fig. 2 shows a typical layout for the cleaning. It may be noted that, where practical, the main steam line cold and hot reheat lines should be included in the cleaning circuit.

Due to low ambient temperatures (below freezing), certain precautions were taken in the field in order to maintain a solvent temperature of not less than 180 deg F. (Note: Laboratory results with 3 per cent inhibited citric acid above 180 deg F indicated an effective fast cleaning job in less than 4 hr.) The precautions taken were to lag all temporary piping, install space heaters in reheater and superheater gas passes, and to circulate water for several hours on a trial run to insure that temperatures could be maintained.

During the initial water circulation some pertinent observations were noted. An existing 400-gpm pump had been hooked up in parallel with the Hi-Flo pump and the water recirculated at 400 gpm. During this circulation period, the temperature was raised to 220 deg F by injection of steam at the blending station. After equilibrium has been reached, the Hi-Flo pump was cut in the circuit. In a short period of time the temperature dropped approximately 60 deg F, and it was found necessary to add water to the system that was apparently full when circulated at a much lower rate.

The immediate conclusions drawn from these two observations were that there was short circuiting of various elements at the lower flow rate in addition to entrapped air in the various loops. These conclusions were verified by other data during the introduction of the solvent stage.

After the temperature was stabilized at the Hi-Flo rates, recirculation was reduced to 400 gpm during the introduction of the acid. A calculated amount of concentrated citric acid, equivalent to 3 per cent of the total holding capacity, including overflow, was blended into the circulating stream. After approximately one half the acid was pumped in, the system had reached equilibrium at 3 per cent. Verification checks were made at that point, and it was decided to pump in the remaining concentrate. The percentage acid doubled to 6 per cent where it remained during the period of low circulation. When the Hi-Flo pump was started, the concentration of acid immediately started to drop at a rate faster than would be expected for a normal cleaning curve until it reached approximately 3 per cent. Again, it was concluded that short circuiting through the elements was indicated verifying the previous observation during the initial water phase.

Due to the prevailing optimum conditions of high temperature and high flow, cleaning was virtually completed within $2^1/_2$ hr after the solvent had been added. The iron removal from both the reheater and superheater sections were in the range of 0.4 per cent as Fe, a figure that was expected as probable for this type system. Visual inspection of both units was limited, however, in all cases where tubes were cut; complete removal of all oxidation products was indicated.

It is noteworthy that, during the flushing and neutralizing stages, only volatile alkaline materials were introduced, in order to minimize precipitation of salts.

All stages were drained under nitrogen. Flushing consisted of filling the unit several times with heated condensate and recirculation until turbidity and iron concentration remained constant, then draining. The second large scale operation was performed on a similar unit for the same utility. Other than the fact that larger-sized lines were used in the temporary piping allowing greater flow, no significant changes were made in procedure or method. The results were equivalent to that obtained on the first units cleaned.

Cleaning of Pendant-Type Units. The cleaning of pendant-type superheater and reheater was performed for a Southern utility.

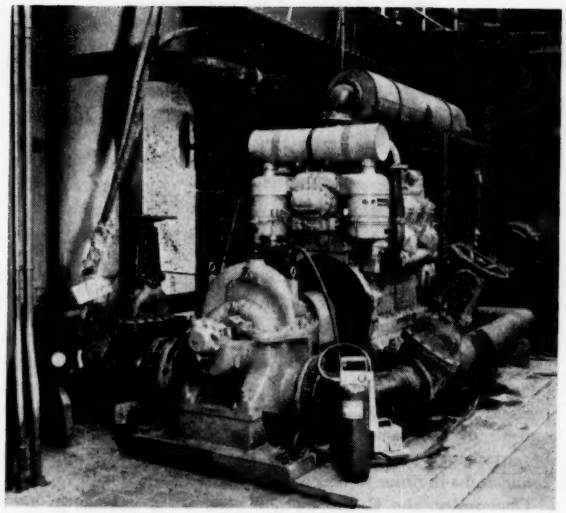

Fig. 1 Hi-Flo pump and engine rated at 5000 gpm

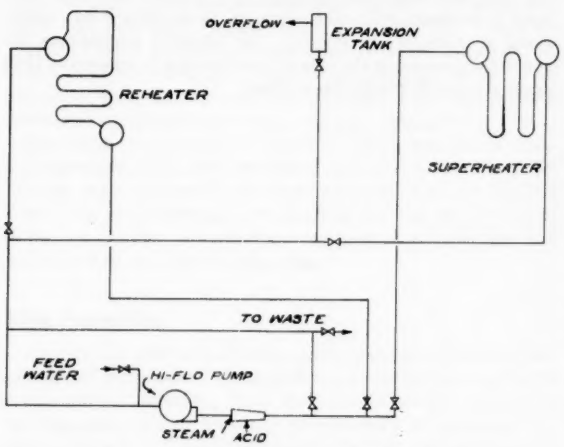

Fig. 2 Typical arrangement for Hi-Flo cleaning

Fig. 1 illustrates the type equipment used. This job was dissimilar from the previous application inasmuch as these units were to be cleaned for operational deposits rather than mill-scale removal and, second, the units were nondrainable.

A survey of the job showed fairly heavy deposits of dense iron oxide in both secondary superheater and reheater elements. The superheater contained 48 elements and the reheater 72 elements with both systems holding approximately 5000 gallons each. Due to other operational problems, the reheater contained austenitic steel in addition to carbon steel, while the secondary superheater contained only carbon steel. However, the use of hydrochloric acid was not considered in the preliminary plan to clean the secondary superheater due to the possibility of incomplete flushing.

Laboratory tests conducted under optimum conditions indicated the removal of the deposit within a 24-hr retention time, using ammoniated citric acid. Although it is not the purpose of this paper to discuss the relative merits of various solvents, a note must be made with regard to this solvent, particularly in the area of field operation where heavy operational deposits exist. A 3 per cent ammoniated acid solution will sequester approximately 0.062 lb of iron per gallon, which represents a four-to-one ratio of citric acid to iron. Ammonia must be added to the citric acid in order to prevent the precipitation of insoluble iron salts.

Cleaning of the secondary superheater was preceded by the cleaning of the drainable primary superheater, which was cleaned using the conventional fill-and-soak method with hydrochloric acid. The circuit through the secondary superheater was accomplished by pumping through the main steam line to the outlet header, through the secondary superheater and inlet header, then through the outlet header of the primary superheater where temporary connections and piping were provided to return to the pump suction.

The reheater circuit was accomplished by pumping into the hot reheat line to the outlet header through the reheater elements and return through the same temporary piping used in the secondary superheater circuit. The steam-generating unit was designed for 600,000 pph. Actual solvent flow was over double this flow rate through the pendant units. The unit was particularly suited to field evaluation as every single element was fitted with a thermocouple and, moreover, temperature tests could be made with the use of a portable pyrocon on every element.

The cleaning of the secondary superheater and reheater with ammoniated citric acid proceeded at a rate slower than was anticipated from the laboratory results. After a period of time, certain tubes were cut open and found to be less clean than expected. In an effort to evaluate this condition, a tube sample was inserted in a side stream and exposed to the same recirculation time and temperature as the individual elements. However, the flow rate through this sample tube was approximately three to four times as great as the flow rate through each individual element. When the sample tube was virtually clean, inspection was made in the unit and the cleaning was not as complete as in the sample tube. In addition, the deposit in the secondary superheater, although of the same chemical constituency, was much denser and more impervious to the solvent than that of the reheater. It was therefore concluded that a high flow rate, in addition to maintaining a temperature over 200 deg F with an unsaturated solvent, was necessary to complete the dissolving of the deposit. Accordingly, steps were taken to increase the rate of flow during the reheater cleaning. Results of the reheater cleaning were in the range of 95 per cent.

In the interest of economics and time, a decision was made to complete the cleaning of the secondary superheater, using inhibited hydrochloric acid. The decision was based on two major points: 1, All results of temperature readings indicated that flow through all tubes were virtually equivalent; and 2, inspection results of tubes after water flushing showed little or no insolubles. Therefore we anticipated no short circuiting of solvent during the acid stage and complete removal of the hydrochloric acid during the flushing stage. Adequate facilities were provided for flushing.

Prior to the introduction of the inhibited hydrochloric acid, the secondary superheater was recirculated with water at 175 deg F, at which time the acid was blended into the system. After the acid had reached equilibrium, recirculation was halted and resumed at intervals in order to purge system of generated gas and to maintain a maximum temperature of 165 per cent F. Concentrations leveled off after 8 hr at which time the unit was prepared for a once-through flushing operation.

Arrangements had been made to provide for a source of clear water to the hot well of the condenser. During flushing, two condensate pumps were started to supply the boiler feed pump, which in turn delivered 600,000 lb per hr to the boiler. Flow was through the primary superheater to the secondary superheater and out the temporary piping to waste. Flushing was conducted for a period of 3 hr.

When the chloride content of the effluent water equalled that of the influent to the secondary superheater, flushing was discontinued and the system recirculated at a high flow rate. It is noteworthy that there was no rise in chlorides during this period, which indicated that the hydrochloric acid had been purged from the system. A volatile alkaline material was introduced for neutralization and also displaced during the final flush with condensate. Inspection of the secondary superheater showed almost 100 per cent cleanliness of all the sections of tubes removed. A probe of the tube bends indicated no deposits present in the adherent or loose state in either the nonventable or nondrainable bands. Prior to going on the line, both the secondary and reheater sections were steam blown. Results during the steam blow showed much less material removed than would normally be expected from a unit going on steam initially. In addition, the turbine strainers were examined after a month of operation and were found to be virtually free of deposits.

Results

On units numbered 1, 2, 4, and 5 in Table 2, inspection was made in the headers and a total of five individual tube samples were removed. The results showed the metal in a clean condition with no apparent corrosion or pitting. Inspection on units 3 and 6 showed the removal of heavy iron-oxide deposits.

Conclusions

The data presented in this paper indicate that engineering-wise, cleaning of nonventable and pendant type superheaters and reheaters is practical. However, additional field work must be accomplished before definitive statements can be made with regard to the minimum flow required to clean nonventable loops and to displace acid solvents in nondrainable elements. An important concept is designing the elements with adequate connections in order to accommodate the required solvent flows.

Chemically, the Hi-Flo method of cleaning has shown itself to be effective, although the use of solvents has been limited to a few that have been used extensively. Without question, more work is necessary with other solvents, particularly where operational deposits are concerned. Our research laboratories are continually exploring the uses of new solvents in relation to their application with the Hi-Flo method.

Table 2 Amounts of iron oxide removed

	Type unit	Reason for cleaning	Approximate holding capacity	Amount of oxide removed
1	Nonventable superheater	Mill scale	25000 gal	870 lb
2	Nonventable superheater	Mill scale	25000 gal	830 lb
3	Pendant superheater	Operational deposits	5000 gal	2280 lb
4	Nonventable reheater	Mill scale	40000 gal	1660 lb
5	Nonventable reheater	Mill scale	40000 gal	1710 lb
6	Pendant reheater	Operational deposits	5000 gal	2480 lb

E. B. MORRIS
Chemical Engineering Section
Head, American Electric Power
Service Corporation, New York, N. Y.

Precautions in the Use of Citric Acid for Chemical Cleaning

Introduction

Following extensive laboratory investigation and pilot-scale testing in 1956, inhibited citric acid was employed for preoperational mill-scale removal from the Philo Unit 6 supercritical-pressure steam generator [1–3].[1] Citric acid has since been used three times for operational deposit removal from the Philo Unit. It was also utilized three consecutive times for the Indiana & Michigan Electric Company's Breed Plant supercritical-pressure steam generator. This 450-mw unit was placed in commercial operation in 1960.

Since the first use of this acid on a large commercial scale in 1956, the interest in citric acid has greatly increased, particularly where certain specific requirements must be met. Its characteristics were especially desirable where austenitic alloys were involved in order to avoid chloride stress-corrosion cracking. It would meet the conditions found in once-through boilers, nondrainable components, such as reheaters and superheaters, nuclear power systems, and many piping arrangements.

Literature references do not disclose exactly how many cleaning operations have been performed with this acid. For once-through units, successful cleanings have been reported for Tait Unit 4 [4], for Eddystone Units 1 and 2 [5], and for Avon Unit 8 [6]. A number of comparable preoperational cleanings are understood to be in the planning stage.

Basic Precautions

As with any new tool, effective techniques must be developed by use and experience. Citric acid as a chemical cleaning tool is no exception. Resulting from the initial laboratory and pilot investigations, certain necessary precautions and techniques became apparent. Although somewhat obvious and elementary, they deserve repetition because of their fundamental importance and in the way they differ from conventionally used hydrochloric acid. These basic considerations are:

1 Sufficient reactant must be used to dissolve the iron oxide present. Ordinarily, this presents no problem, except in the case of an extremely low ratio of volume to surface, which might occur where very small-diameter tubes are involved in a boiler, heat exchanger, or superheater.

2 Positive circulation of the citric-acid solvent is required to avoid local depletion. Thermal circulation in the "fill-and-soak" procedure is insufficient for citric acid. Thus this acid lends itself to the once-through boiler, superheaters, and the like. It is not suited for the conventional natural-circulation boiler where forced circulation is impractical from design considerations.

3 A velocity of 2 fps for forced circulation is considered satisfactory in most cases to fulfill the requirement of item (2), as well as assuring flow distribution in parallel circuits. Excessive velocity should be avoided because of increased corrosion rates, the upper practical limit perhaps being 4 to 6 fps for properly inhibited acid.

4 The optimum temperature level of 200 to 220 F should be maintained to assure a rapid reaction rate and complete removal of iron-oxide deposits. The upper limit may be increased perhaps 20 deg F without increasing the corrosion rate excessively. However, a lower limit of 180 F should be considered the absolute minimum because of the drastically reduced reaction rate.

5 A 3 per cent concentration of citric acid usually has been employed where otherwise 5 per cent hydrochloric would be used. This concentration was originally selected for economic and other reasons [1] and has proved satisfactory in most instances. Considerations of acid strength must be related not only to amount of deposit, but the criterion of item (1) as well.

6 The use of citric acid should be restricted to iron-oxide deposits as mill scale, rust, and operational magnetic oxide. It is ineffective on silicates, copper, and is of limited effectiveness on calcium deposits, such as hydroxyapatite.

Further experience with citric acid has demonstrated that two adverse conditions can occur. These are:

1 Precipitation of an iron citrate from the solvent.

2 Formation of a colored colloidal iron complex if rinsing and flushing are deferred.

This paper explores these two problems and means for their prevention.

Precipitation of Iron Citrate

In 1959 the work at one laboratory disclosed that under certain conditions a precipitate would form in citric-acid solutions and that this precipitate could be redissolved by additional citric acid [7]. At about the same time, the American Electric Power System Laboratory encountered a similar effect, which was studied further. Two months later, the Avon Unit 8 cycle was cleaned with citric acid, as reported by Vyhnalek [6]. This is the only reported instance of precipitation occurring during a full-scale, citric-acid cleaning operation.

The earliest work on citric acid showed extremely low solubilities for various iron oxides agitated with the acid solvent in glass. Accordingly, the apparatus shown in Fig. 1 was used for all subsequent work. It features simple temperature and flow-rate controls, and the tubular specimen can be a boiler-tube section, or a pipe or tube specimen oxidized in the laboratory to simulate actual service conditions. Most of the work described has been carried out with $^1/_2$-in. black-iron pipe which was pickled, then reoxidized to a heavy mill-scaled condition in a furnace. Moist air was used as the oxidizing atmosphere.

Preliminary results indicated that much greater solubilities for iron in 3 per cent citric acid than the theoretical could be obtained, indicating the probability of supersaturated solutions. The literature lists numerous citrate complexes with iron, but with considerable disagreement as to their composition. For example, Bobtelsky and Jordan [8] assign molar ratios of ferric iron to citrate of 1:1, 2:3, and 3:2. For these ratios, the saturation iron content for 3 per cent citric acid would be 0.87, 0.58, and

[1] Numbers in brackets designate References at end of paper.

Contributed by the Joint Research Council on Boiler Feedwater Studies of the Power Division and presented at the Winter Annual Meeting, New York, N. Y., November 27–December 2, 1960, of The American Society of Mechanical Engineers. Manuscript received at ASME Headquarters, August 29, 1960. Paper No. 60—WA-221.

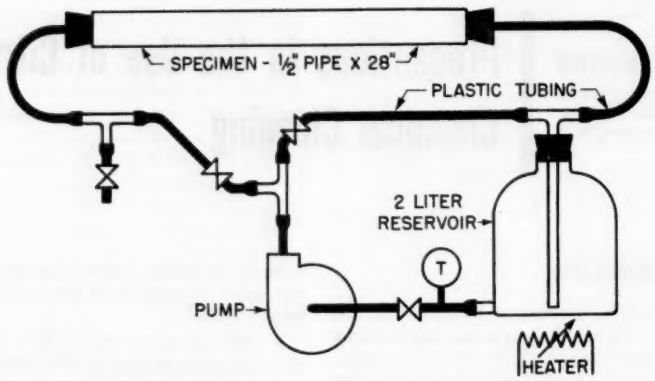

Fig. 1 Schematic of apparatus for citric-acid cleaning tests

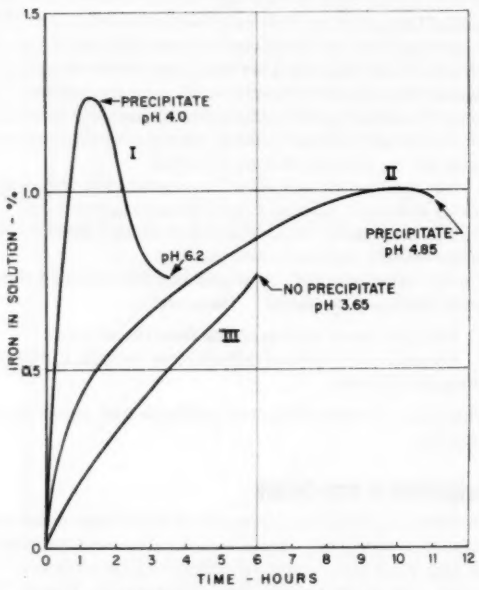

Fig. 2 Solubility of Fe_3O_4 in 3 per cent citric acid

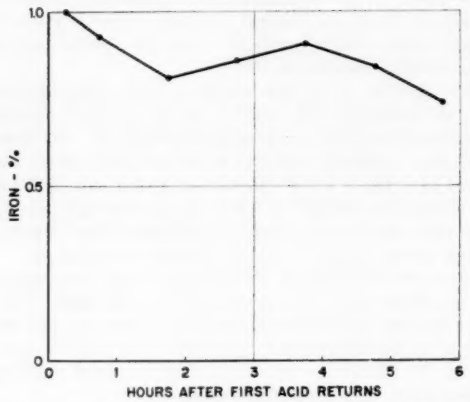

Fig. 3 Iron concentrations during citric-acid treatment of Breed steam generator

1:30 per cent, respectively. Bell and Shaw [9] report that the most stable complex exists where the citric-acid concentration is four times the concentration of iron. By extrapolation, one might conclude that 0.75 per cent is the upper solubility limit for iron in 3 per cent citric acid. Values as high as 1.4 per cent have been obtained in the laboratory and slightly more than 1 per cent in actual cleaning operations.

Fig. 2 illustrates the results of three laboratory tests with 3 per cent citric acid on tubular specimens containing magnetic iron-oxide scale. Curve I shows precipitation occurring at 1.35 per cent Fe and a pH-value of 4.0 after 1 1/3 hr. The iron concentration then decreased and the pH-value increased to 6.2 [7]. Similarly conducted tests by the AEP Laboratory show that for Curve II, precipitation occurred at a pH-value of 4.85 and an iron concentration of 1.0 per cent after 10 hr. Curve III shows no precipitation at a pH-level of 3.65 after 6 hr with an iron concentration of nearly 0.8 per cent.

Laboratory data illustrate a wide variation in results which so far cannot be accounted for definitely. Precipitation has been demonstrated at iron concentrations as low as 0.44 per cent and as high as 1.22 per cent with as nearly identical test conditions as could be established. In general, when precipitation does occur, it is evident at the end of 4 to 6 hr contact time, at a pH-value of 4.0 to 5.0, and an iron concentration of 0.5 per cent or higher. No specific reasons can as yet account for the erratic results obtained in the laboratory where precipitation may occur only once out of six tests on the average. There does appear, however, definite indications of sensitivity to time, temperature, and pH, the first two factors seemingly having the greatest effect.

On the other hand, commercial cleaning experience has shown the absence of precipitation [1, 4, 5], except in one instance [6]. Fig. 3 shows the iron concentration for the initial citric-acid cleaning of the Breed Plant steam generator during which precipitation did not occur.

The grayish precipitate found in practice [10] and in laboratory tests appears to be a form of iron citrate with similar compositions reported as:

	Avon Unit 8	*AEP Laboratory*
Fe, per cent	21	37
Organic, per cent	79	48
Citrate ion, per cent	—	50

This precipitate was found in both instances to be essentially insoluble in citric acid, but soluble in hot water. Ammonia water dissolves the precipitate, but with precipitation of ferrous hydroxide. Specific identity of the iron-citrate complex has not been established, but it has been determined as a ferrous, rather than a ferric complex. This perhaps parallels experience with hydrochloric-acid cleanings where the ferric ion is absent from the acid solutions due to a reduction mechanism.

Based on both laboratory and industrial experience, there is a possibility of sudden precipitation and settling out of an iron-citrate complex when citric acid is employed for cleaning operations. However, the probability of this occurrence is fairly low even though the solutions are supersaturated with iron.

What then are the precautions to be taken to prevent precipitation occurring? If it does occur, what then can be done to compensate for any adverse effects? As yet there are insufficient data to define exactly the conditions of precipitation. However, certain precautions are essential. These in some degree relate to the basic precautions initially listed and are:

1 Do not permit temperatures to decrease.

2 Maintain constant forced circulation at the highest velocity consistent with tolerable corrosion rates.

3 Use the minimum contact time which will assure removal of the iron-oxide deposits. Normally 3 to 4 hr should suffice for the average cleaning.

4 Do not add fresh citric acid to the partially or completely depleted solvent.

5 If the iron concentration in the solvent rapidly decreases and the pH increases, especially if it reaches 4.5, displace the citric-acid solvent promptly with hot water. Displacement should be made using the maximum practical velocity. Following this, hot water should be recirculated, and repeated if necessary, until pH and iron levels indicate that any deposited precipitate is redissolved.

Formation of Colored Colloidal Complex

As distinct from precipitation, the second effect that can be experienced is the formation of an iron-citrate complex on metal surfaces. This complex is only slightly soluble in water and is removed very slowly as a highly colored colloid. Formation of this complex apparently occurs when citric acid is drained and the residual film is permitted to dry or "bake" on the metal surfaces due to the contained heat.

Since the Breed Unit 1 steam generator is fully drainable, the original chemical-cleaning plans included drainage disposal of the used citric-acid solution at the end of the recirculation period. This was to be followed by refilling and draining for repeated rinses in order to conserve time and demineralized water. Because of delays encountered due to freezing of drain valves, the schedule was modified to eliminate the repeated rinse-drainings planned. Following is an outline of the procedure:

1 Recirculated 3 per cent citric acid for 6 hr (70,000 gal volume).

2 Drained citric acid to waste under nitrogen (24 hr required).

3 Filled with Zeolite-softened water.

4 Displaced rinse fill with Zeolite-treated water until pH 6.5 (4 hr).

5 Displaced Zeolite-softened water with demineralized water containing 200 ppm hydrazine and 10 ppm ammonia (3 hr).

6 Recirculated chemically treated water at 200 F (5 hr); final pH 8.3.

7 Flushed to waste at high velocity (1 hr).

8 Drained under nitrogen for dry storage.

About 2 weeks later, recirculation was begun through the entire cycle and steam generator for the preoperational water clean-up phase. Immediately the water became highly colored and also showed some turbidity. This apparent iron complex and/or colloid was nonremovable by the condensate-polishing filters and demineralizers, nor was it removable by filtering through a membrane having a pore size of 0.45 micron.

During the next week, 4 cycles of recirculation, followed by draining the entire cycle, were carried out with little decrease in the colored complex. Meanwhile, it had been determined by laboratory bomb tests that temperatures of 500 to 600 F would "break" the complex and flocculate the iron to make it readily filterable. During these tests, it was observed that the pH-value decreased on heating as the complex apparently was decomposed.

Because of other considerations, recirculation clean-up was deferred and advantage taken of the opportunity to acid-clean the steam generator again. This second operation was modified specifically to displace the acid with water at a velocity of 6 to 7 fps, then to recirculate ammonia and hydrazine-treated demineralized water at 200 F, followed by an 8 fps flush to waste. During these operations, as well as subsequent recirculation clean-up, no adverse effects were noted. There was complete absence of any nonfilterable iron complex or color.

Several tube sections removed for examination after the first cleaning showed yellow-red to reddish-brown deposit films. These contained magnetite as the principal constituent and had a varying ignition loss. Values of carbon ranged from 1 to 7 per cent and hydrogen from 0.7 to 3 per cent. Residue from evaporation of the highly colored condensate showed 12 per cent carbon and 2 per cent hydrogen. Infrared spectrophotometric analysis [11] of an ether extract of the water residue gave principal absorption bands that indicated the presence of: CH_2; CH_3; acid-carbonyl group; evidence of ester. The specific presence of citric acid was not confirmed since the absorption spectra did not indicate the specific wave lengths for this constituent. However, the color substance most likely was present originally as an iron-citrate complex and/or colloid.

The formation of this color complex has been demonstrated in the laboratory by using a slight modification of the apparatus shown in Fig. 1. In this case, a 3-ft section of $^1/_2$-in. pipe packed with nails to secure more surface area was used. The pipe was kinked slightly so that about 20 ml of solution would be retained when the specimen was drained in the horizontal position.

After recirculating 2 liters of inhibited 3 per cent citric acid through each oxidized test specimen at 200 F for 6 hr, the specimens were drained, then dried in an oven for 16 hr at 210 F. Three successive rinses of distilled water or solution were then made by recirculating 2 liters for 30 min each.

Fig. 4 shows the APHA color and iron content for three rinses of cold water for one specimen and three rinses of 180 F water for a second. The blank for comparison represents similar treatment of a test specimen except that the citric acid was displaced with water before the specimen was oven-dried and then given three water rinses.

Fig. 5 shows similar data for hot and cold rinses containing 50 ppm hydrazine and ammonia to a pH-value of 9.2 compared with the same blank. The rinses in every case were free of turbidity and colored yellow to yellow-orange. None, however, were as deep in color as the Breed water during the initial recirculation. In these tests, there was little correlation between color and iron content of the rinses. The data indicate more effective rinsing with hot water than with cold, and a more effective rinse with either hot or cold hydrazine-ammonia-treated water than with cold water alone.

Table 1 compares data for the first rinse of two of the test series with a water sample from the Breed Plant. It is of particular interest that in each case color removal could only be obtained with charcoal. Also, the carbon/hydrogen ratios are approximately half that of citrate ion.

One other case [12] having a common drainage factor involved a natural-circulation boiler from which the spent citric acid was drained hot. There was a 10-hr delay in rinsing and a red-oxide deposit over the surfaces was reported. This deposit was removed by a dilute ammonium-citrate solution. It is possible there are other instances where citric acid was drained hot and

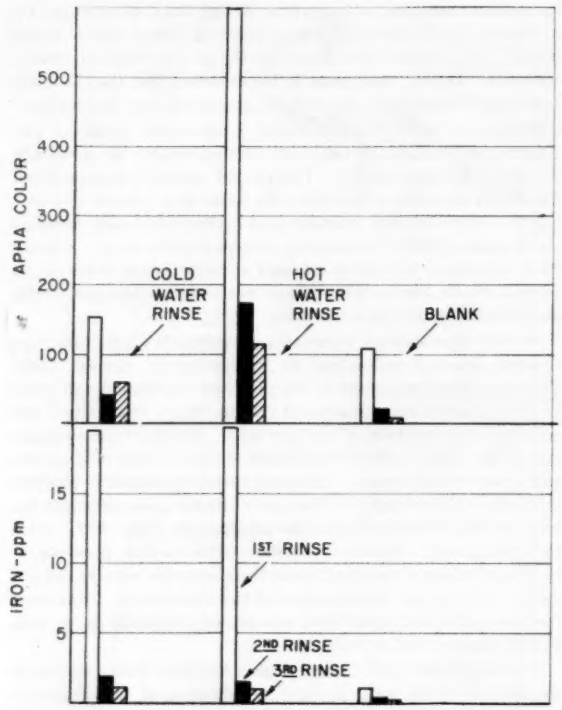

Fig. 4 Laboratory simulation of colored complex formation from citric acid using water rinses

Table 1 Comparison Breed water with laboratory specimen rinses

	Breed water	Laboratory rinse Test A	Test B
APHA color	2000+	265	510
pH	7.2	5.0	4.8
Evaporated solids, ppm	323	292	270
Color removal:			
By filtration	No	No	No
By demineralizer	No	No	No
By charcoal	Yes	Yes	Yes
By ammonia	No	No	No
Analysis of Solids, Per Cent			
Iron oxide, Fe_2O_3	79.8	40.6	50.6
Carbon, C	6.3	29.7	23.3
Hydrogen, H	1.2	3.9	2.8
Oxygen, O_2 (difference)	12.7	25.8	23.5
Ratio C/H[a]	5.2	7.7	8.2

[a] Ratio for citrate ion is 14.2.

similar reactions occurred, but went unrecognized by reason of other circumstances.

As to precautions, we add the following:

Do not drain hot citric acid from equipment. It is necessary to displace the solvent with water to avoid the possibility of continued reaction of residual films and formation of a colored colloidal complex. Such material will be expected to be especially troublesome in once-through cycles.

Conclusion

Citric acid is an extremely useful chemical cleaning tool for special purpose applications. However, like any other tool, its effectiveness depends on the techniques used. Certain precautions must be observed, many of which differ from those employed for conventional hydrochloric-acid techniques. These are:

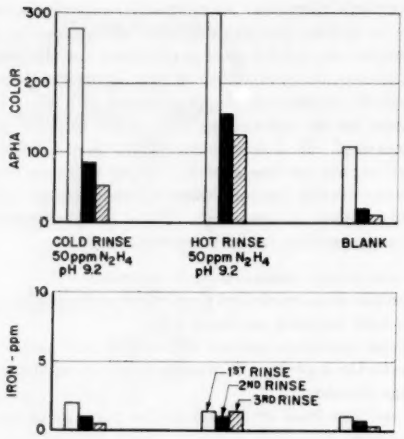

Fig. 5 Laboratory simulation of colored complex formation from citric acid using N_2H_4 and NH_3 rinses

1 Sufficient reactant.
2 Positive circulation.
3 Optimum temperature.
4 Nature of scale and deposits.

To this summary, additional experience adds two more:

5 Prevention of precipitation:
(*a*) Temperature.
(*b*) Time.
(*c*) Circulation and velocity.
(*d*) pH and iron concentration.
6 Prevention of residual deposits by avoiding hot drainage.

References

1 C. M. Loucks, E. B. Morris, and E. A. Pirsh, "Organic Acids for Cleaning Power Plant Equipment," ASME Paper No. 58—A-282, 1958.

2 T. T. Frankenberg, A. G. Lloyd, and E. B. Morris, "Operating Experience With the First Commercial Supercritical-Pressure Steam-Electric Generating Unit at the Philo Plant," *Proceedings of The American Power Conference*, vol. 20, 1958, p. 144.

3 J. D. Andrew, Jr., P. H. Koch, and E. A. Pirsh, "Operating Experience With the First Commercial Supercritical-Pressure Steam Generator at Philo," *Proceedings of The American Power Conference*, vol. 20, 1958, p. 161.

4 J. D. Williamson and R. F. Andres, "Operation and Water Conditioning of Unit No. 4 Tait Station," *Proceedings of the 21st Annual Water Conference*, 1959.

5 Private communication, W. B. Willsey, Philadelphia Electric Company.

6 H. J. Vyhnalek and C. D. Banks, "Water Treatment Experience During the Startup and Initial Operation of the Avon Supercritical Unit," 22nd Annual Water Conference, 1960.

7 Private communication, Dow Industrial Service.

8 M. Bobtelsky and J. Jordan, "The Structure and Behavior of Ferric Tartrate and Citrate Complexes in Dilute Solutions," *Journal of The American Chemical Society*, vol. 69, 1947, pp. 2286–2290.

9 W. E. Bell and J. K. Shaw, "Evaluation of Iron Sequestering Agents in Water Flooding," *Producers Monthly*, vol. 22, 1958, pp. 20–23.

10 Private communication, H. J. Vyhnalek, Cleveland Electric Illuminating Company.

11 Research Report No. 7299, The Babcock & Wilcox Company Research Center.

12 Private communication, S. Alfano, Houston Lighting and Power Company.

A. J. STEPANOFF
Ingersoll-Rand Company,
Phillipsburg, N. J. Mem. ASME

Inlet Guide Vane Performance of Centrifugal Blowers

The function and effectiveness of the inlet guide vanes to control the blower output and power requirements are examined. Calculated and experimental results of the power reduction by means of guide vanes are presented. The concept of the "Inlet Specific Speed" widely used in centrifugal pump field is discussed in application to the blowers. A method of estimating the performance of single-stage blowers for any position of the guide vanes is suggested. A "casing characteristic" is introduced for this purpose and its utility for the calculation of the impeller diameter for a reduction of the output is demonstrated. The performance of the inlet vanes of multistage blowers is reviewed.

Introduction

To meet variable head-capacity requirements single and multistage blowers are frequently equipped with guide vanes at the impeller approach. At a constant speed and at a fixed capacity, say at best efficiency point (bep), the effect of the guide vanes appears as a reduction of head and power input to the blower. At a constant head or discharge pressure guide vanes permit a reduction of the rate of flow and a reduction of the minimum or pumping capacity, accompanied with a reduction of consumed power. The same results can be accomplished with throttling the discharge pipe without any power reduction. Throttling the blower inlet pipe can produce the same effects with a noticeable saving in bhp. The inlet guide vanes can perform the same function with a greater saving than the simple throttling alone of the inlet pipe. This phase of the guide vane performance (power saving) is the main subject of this article. It is convenient for discussion to assume the blower operated at its rated inlet cfm, or at bep rate of flow, and consider the effects of guide vanes on the head, efficiency, and bhp. Except when specifically stated the discussion will refer to a single stage blower such as shown in Fig. 1. The typical performance is shown in Figs. 2(*a*), (*b*), and (*c*) at constant speed.

Head Reduction With Inlet Guide Vanes

The head reduction caused by the guide vanes is accomplished in three phases:

1 Head reduction due to gas deflection in the direction of the impeller rotation expressed by the subtractive term of the Euler's equation for the theoretical head produced by the impeller, given below:

$$H_e = \frac{u_2 c_{u2} - u_1 c_{u1}}{g} \qquad (1)$$

where

H_e is the theoretical head (Euler's head)
u_2 is the peripheral velocity at the impeller discharge
u_1 the same at impeller entrance or impeller eye
c_{u2} is the tangential component of the absolute velocity at impeller exit
c_{u1} ditto at inlet
g is gravitational constant

Contributed by the Compressor Subcommittee of the Hydraulic Division and presented at the Winter Annual Meeting, New York, N. Y., November 27–December 2, 1960, of The American Society of Mechanical Engineers. Manuscript received at ASME Headquarters, July 28, 1960. Paper No. 60—WA-130.

Figs. 3 and 4 show the above velocities on the velocity triangles.

2 Reduction of head due to prerotation alone can take place only at a small angle of deflection of the radial velocity δ, Fig. 3. Since the free area between the two adjacent guide vanes is reduced directly as cos δ for a fixed rate of flow in inlet pipe throttling effects appear. The flow is accelerated through the vanes and then suddenly decelerated incurring loss of head and efficiency. In the case of pure throttling efficiency is reduced in the same ratio as the head.

$$H_a/H = e_a/e \qquad (2)$$

Here H is the blower head and e hydraulic efficiency with vanes in

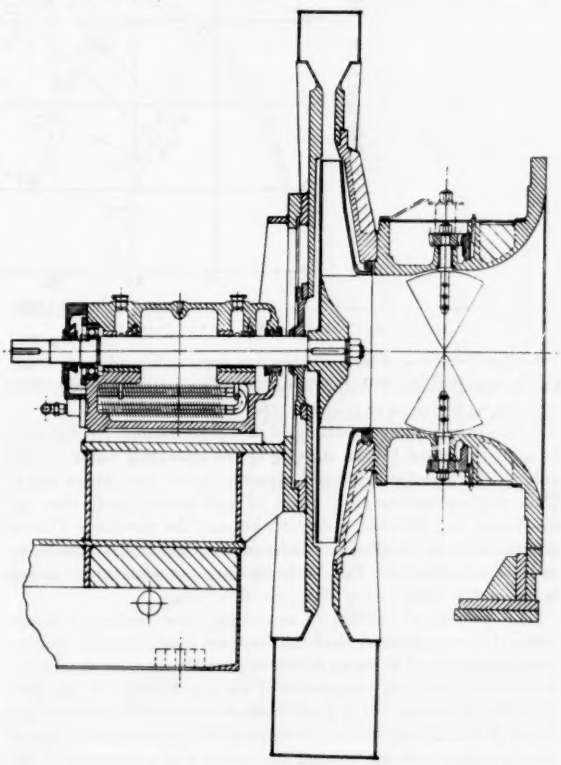

Fig. 1 Blower with inlet guide vanes

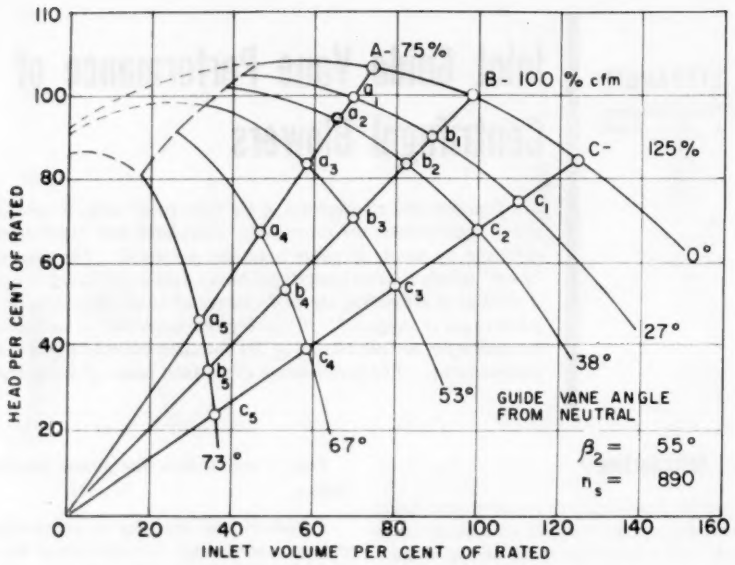

Fig. 2(a) Inlet guide vane performance head-capacity at constant speed

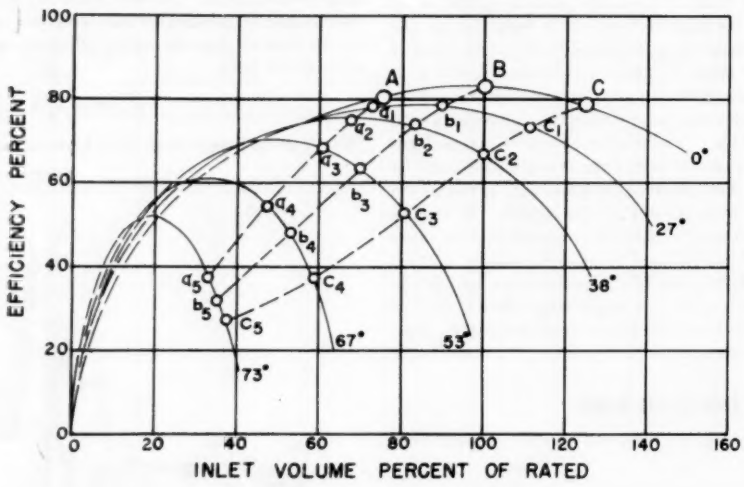

Fig. 2(b) Efficiency

the neutral position. With the subscript a are the same variables with vanes active or in position other than neutral.

3 In practice pure throttling of the inlet cannot be realized. It is accompanied by the shifting of the operating point on the volumetric impeller exit head-capacity curve to a lower head. This shifting occurs as a result of gas density reduction by throttling, i.e., pressure reduction beyond the throttle. This is accompanied by an efficiency reduction but not in the same ratio as the head reduction, Fig. 5. In this manner some power saving is realized by comparison with pure throttling.

This process of shifting of operating point becomes evident when it is remembered that the impeller head-capacity characteristics expressed in terms of the volumetric capacity at impeller exit remain the same irrespective of the gas density. If the inlet pipe cfm up-stream of the guide vanes is maintained constant and equal to that at bep with vanes neutral with guide vanes in operation a greater volume beyond the vanes will correspond to the same weight of flow through the machine, Fig. 5.

This phase of the head reduction plays an important role in multistage blowers; where only the first stage is equipped with guide vanes the rest of the stages operate at constant weight of flow but at progressively increased volumetric capacities and reduced heads. The stages become thus mismatched in an increasing measure toward the high pressure end of the machine.

To summarize: (1) When the head is reduced by prerotation alone efficiency essentially remains constant

$$e = \text{constant}$$

(2) Pure throttling is characterized by that

$$H_a/H = e_a/e$$

(3) Reduction of head as a result of gas density reduction occurs in such a manner that

$$H_a/H < e_a/e$$

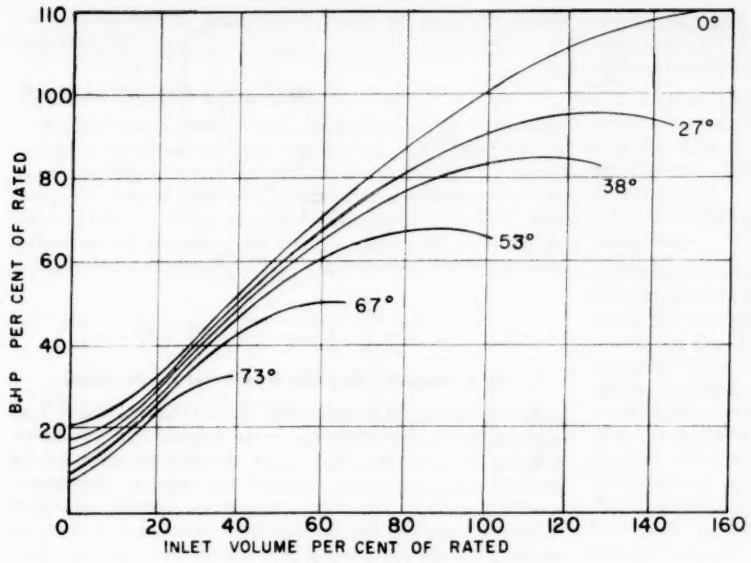

Fig. 2(c) Brake horsepower

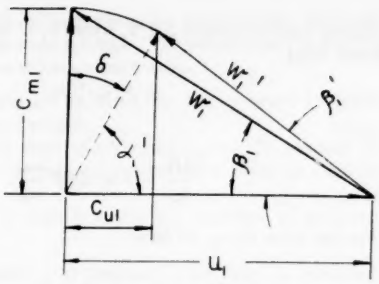

Fig. 3 Inlet velocity triangle

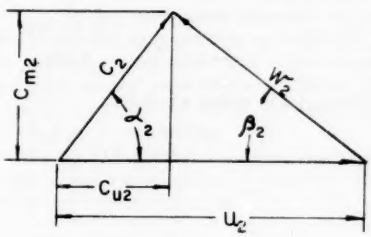

Fig. 4 Discharge velocity triangle

In practice all three effects appear simultaneously so that

$$(\text{bhp})_a/\text{bhp} < 1$$

in every case.

Prerotation

Under this heading calculations will be made of the head reductions due to prerotation caused by the guide vanes for six blowers of different specific speeds given in Table 1. All blowers operate at the same speed of 4800 rpm and capacity, 10,000 cfm at bep at impeller exit. Different heads were assigned to each blower to obtain the desired range of specific speeds. Table 2 gives several design elements common for all specific speeds for three values of the impeller discharge angles $\beta_2 = 25$, 40, and 55 degrees compiled from the design data given in reference [1],[1] Fig. 6.12. The impeller inlet velocity c_{m1} is taken as 1.30 c_{m2} in every case. The head reductions in feet are tabulated for the guide vane angle setting 15, 30, 45, 60, and 75 degrees from neutral. Assuming that the same rate of flow at bep is maintained for all guide vane positions the results of vane action will appear as a flow deflection such that

$$c_{u1} = c_{m1} \sin \delta$$

Table 1 Heads and specific speeds of six blowers

4800 rpm	10,000 cfm at impeller exit bep					
Head, ft	15,000	8800	6000	4500	3500	2300
Specific speed based on cfm	350	525	700	875	1050	1460

Table 2 Common design elements to all specific speeds at best efficiency points

				Symbol
Impeller discharge vane angle, deg	25	40	55	β_2
Radial velocity at impeller discharge, ft	100	127	143	c_{m2}
Ditto at entrance	130	165	186	c_{m1}
Inlet velocity head, ft	263	423	537	h_v
Head reduction ft at guide vane setting				ΔH
Angle degrees $\delta = 15$	165	182	193	
$\delta = 30$	317	364	375	
$\delta = 45$	450	500	530	
$\delta = 60$	550	610	650	
$\delta = 75$	615	683	725	

[1] Numbers in brackets designate References at end of paper.

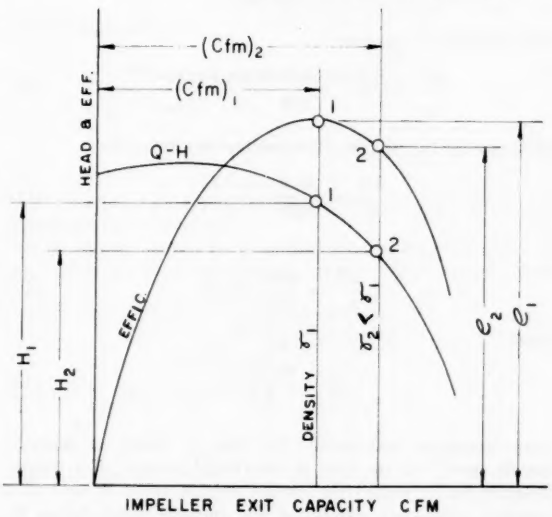

Fig. 5 Impeller performance with vanes neutral (subscript 1) and vanes active (subscript 2) at constant inlet cfm and weight of flow

Then, for the head reduction due to prerotation we obtain an expression

$$\Delta H = \frac{u_{m1} c_{m1} \sin \delta e_{va}}{g} \tag{3}$$

where u_{m1} is the peripheral velocity at the mean effective diameter at the impeller entrance without a hub obstruction defined as

$$D_{m1}^2 = \frac{D_1^2 - 0^2}{2}$$

D_1 being the impeller eye diameter, e_{va} is the vane effectiveness in deflecting the flow, taken as equal to 0.70. The exact value of it is not known and is not important for the purpose of this discussion.

It is convenient to express the head reduction ΔH in dimen-

sionless form as a ratio $\Delta H/h_v$ where h_v is the impeller inlet velocity head.

$$h_v = c_{m1}^2/2g \tag{4}$$

then

$$\frac{\Delta H}{h_v} = 1.40 \sin \delta \frac{u_{m1}}{c_{m1}} \tag{5}$$

For the value of u_{m1} we have

$$u_{m1} = \frac{D_1 n}{\sqrt{2} \times 229} = \frac{D_1 n}{324} \tag{6}$$

Value of D_1 we obtain from

$$c_{m1} = \frac{4 \times 2.4 \text{ cfm}}{\pi D_1^2} \tag{7}$$

where D_1 is in inches, n is in rpm

$$D_1 = 1.74 \frac{(\text{cfm})^{1/2}}{(c_{m1})^{1/2}} \tag{8}$$

and

$$u_{m1} = \frac{1.74 n (\text{cfm})^{1/2}}{324 (c_{m1})^{1/2}} \tag{9}$$

Then equation (5) becomes

$$\frac{\Delta H}{h_v} = \frac{1.74 \times 1.40 \times \sin \delta}{324} \frac{n(\text{cfm})^{1/2}}{(c_{m1})^{3/2}} \tag{10}$$

Substitute for $c_{m1} = (2gh_v)^{1/2}$ equation (10) becomes

$$\frac{\Delta H}{h_v} = \frac{\sin \delta}{3060} \cdot \frac{n(\text{cfm})^{1/2}}{h_v^{3/4}} \tag{11}$$

or

$$\frac{\Delta H}{h_v} = \frac{\sin \delta}{3060} \times S_1 \tag{12}$$

where

$$S_1 = \frac{n(\text{cfm})^{1/2}}{h_v^{3/4}} \tag{13}$$

is an expression very similar to what is known as "suction specific speed" in the field of centrifugal pumps. For incompressible fluids (water) the suction specific speed is used as a criterion completely describing the impeller inlet design irrespective of the head, specific speed, and size. For centrifugal pumps, the suction specific speed has the form

$$S_1 = \frac{n(\text{gpm})^{1/2}}{(\text{NPSH})^{3/4}} \tag{13a}$$

where gpm is gallons per minute, NPSH is net positive suction head above the vapor pressure. This can be expressed as

$$\text{NPSH} = h_v \times \text{constant}$$

Although the suction specific speed does not give any new relation between the variables entering into the impeller inlet design, it is widely used for centrifugal pump classification as to the suction conditions. It so happened that for a continuous and consistent row of impeller types the suction specific speed is essentially constant and equal to $S_1 = 8000$. For the impeller approach without prerotation the suction specific speed is associated with a fixed value of the impeller inlet angle β_1.

For compressible fluids (gases) the utility of concept of the suction specific speed is impaired by the fact that the affinity laws apply to the volume of the gas at the impeller exit, but do not hold for the inlet cfm. As a result, the inlet specific speed for blowers does not remain constant for different performance specific speeds n_s. Thus for the blowers and conditions listed in Table 1 operated on air, the maximum variation of S_1 from the average is 6 per cent, and β, $1^1/_2$ degrees at a constant value of β_2.

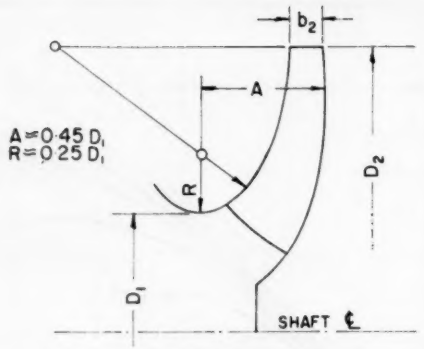

Fig. 6 Impeller inlet profile for different specific speeds

Remark 1. It should be noted that impeller geometrical proportions as they appear on the impeller profile (Fig. 6) are closely associated with the hydraulic type or specific speed n_s of the blower. The ratios b_2/D_2 and D_1/D_2 have been used for impeller classification prior to the universal adoption of specific speed n_s. At the same time, for single stage blowers of a wide range of specific speeds and $\beta_2 = 25$ deg it has been found that the leading impeller inlet proportions, such as the ratio A/D_1 in Fig. 6 are approximately constant and equal to 0.45. This may serve as a graphical illustration of the fact that the impeller inlet design is essentially independent of the head or impeller outside diameter.

This observation is not inconsistent with the concept that impellers of different specific speeds can be thought of (but never are) as obtained from one impeller by cutting the outside diameter. Thus the main geometrical proportions of the impeller inlet profile such as A/D_1 are common to several specific speeds.

Remark 2. To summarize: For incompressible fluids impellers of different specific speeds using the same discharge angle β_2 have the same inlet velocity triangles (dimensionless) or simply have the same value of the inlet angle β_1. This is approximately true for blowers.

Impellers of different specific speeds designed for the same capacity and speed, such as those listed in Tables 1 and 2, have in the discharge velocity triangles identical part ABC (Fig. 7) referring to the relative flow through the impellers. The parts containing the absolute velocities at impeller discharge BCE_1, BCE_2, etc., are different for each specific speed, depending on heads and

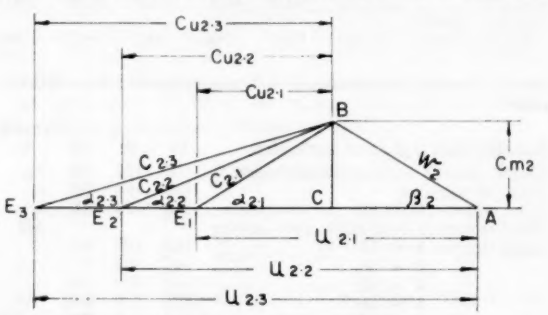

Fig. 7 Discharge velocity triangles for impellers of different diameters (Euler's theoretical)

impeller diameters. This applies equally to centrifugal pumps and blowers.

Power Saving With Guide Vanes

The last item in Table 2 shows calculated head reductions in feet at bep for impellers with discharge angles $\beta_2 = 25$, 40, and 55 degrees and at guide vane settings 15, 30, 45, 60, and 75 degrees from the neutral position. Expressed as percentages of the blower heads for different specific speeds (given in Table 1) these reductions will express power saving as compared with head reduction by the simple throttling. Fig. 8 shows a plot of the calculated percentages of head reductions for three impeller discharge angles and four guide vane settings. The actual power saving by this means will be lower for several reasons:

1 Impeller efficiency is impaired by the presence of guide vanes in the impeller approach.

2 The value of the vane effectiveness $e_{va} = 0.70$ assumed in equation (5) cannot be realized by the crude vanes as used for this purpose.

3 The throttling is unavoidable when the flow is deflected with vanes.

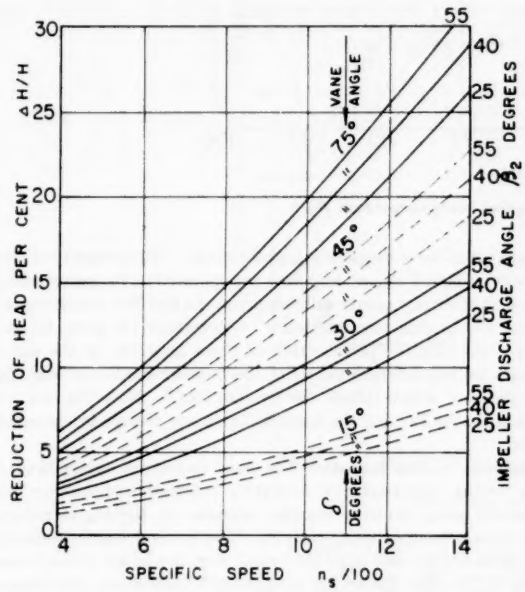

Fig. 8 Calculated power reduction due to prerotation at rated cfm

The actual power saving by the use of guide vanes as compared with simple throttling can be seen from Figs. 9 and 10 based on numerous observations on several blowers of different specific speed. In Fig. 9 are plotted in per cent efficiency ratios with the guide vanes active (e_a) to that with guide vane neutral (e) against the head ratios in per cent with vanes in operation (H_a) to the head at normal performance test with vanes at zero angle (H). Both ratios are taken at the same capacity. Points of blowers of the same specific speed tend to fall on the same line irrespective of capacity and guide vane setting.

The ratio of the power input to the blower with guide vanes active $(\text{bhp})_a$ to that with vanes neutral (bhp) is equal to the ratio of heads divided by the ratio of efficiencies.

$$\frac{(\text{bhp})_a}{\text{bhp}} = \frac{H_a}{H} \cdot \frac{e}{e_a} \tag{14}$$

This is evident from:

$$\text{vanes neutral bhp} = \frac{WH}{33000\,e} \tag{15}$$

$$\text{vanes operative } (\text{bhp})_a = \frac{WH_a}{33000\,e_a} \tag{16}$$

For the same weight of flow W dividing equation (16) by (15) equation (14) is obtained.

Fig. 10 was plotted from the test data in Fig. 9 to show the bhp ratio versus the head ratios for blowers of several specific

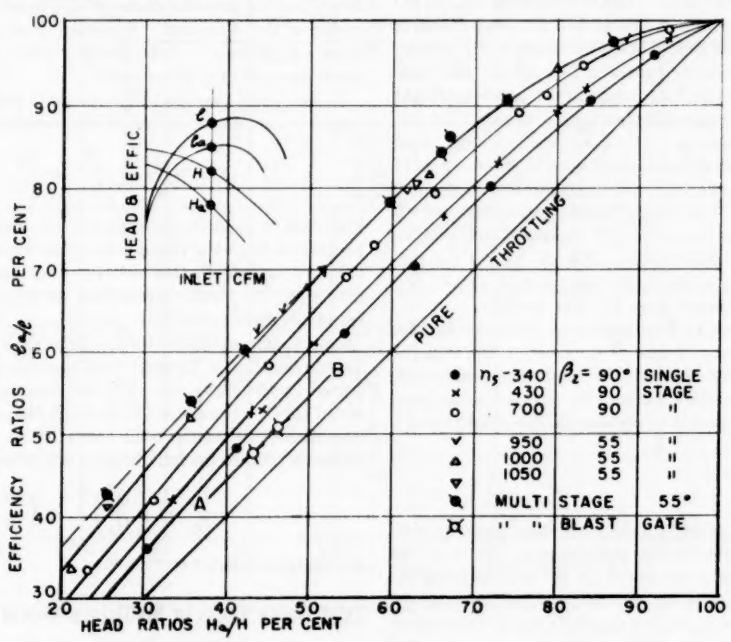

Fig. 9 Head and efficiency reduction with guide vanes

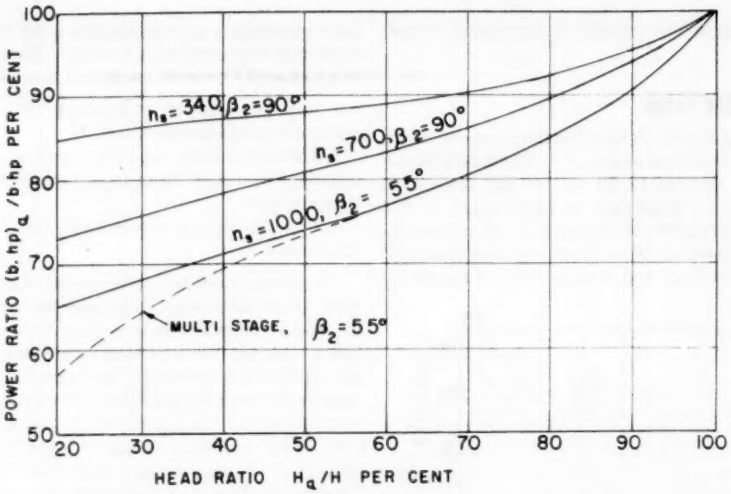

Fig. 10 Power reduction with inlet guide vanes based on test data, Fig. 9

speeds calculated following the equation (14), and thus represents the measured combined effect of prerotation, throttling, and density reduction.

Estimation of Blower Performance for Different Position of Guide Vanes

Below is presented a method of estimation of the head capacity and efficiency for three points on the blower characteristics for any position of the guide vanes. The points are selected as intersections of lines AO, BO, and CO in Fig. 2(*a*) and the head-capacity curves for several vane positions 1, 2, 3, 4, and 5, corresponding to the δ = 27, 38, 53, 67, and 73 degrees from neutral. Line BO is drawn through the rated point with vanes neutral [100 per cent cfm Fig. 2(*a*)] and the origin of the head and capacity scales. Line AO is drawn similarly through 75 per cent capacity point and line CO through the 125 per cent point. The intersections for line AO are marked a_1, a_2 . . . for vane positions 1, 2 . . . . and similarly for lines BO and CO. The points of intersections a_1, b_1, c_1, etc., are transferred on the efficiency curves in Fig. 2(*b*) at the same capacity. Note that the lines A-a_5, B-b_5, and C-c_5 are not straight lines in Fig. 2(*b*). It so happened that for a given impeller discharge angle β_2 the points a_1, a_2 . . . b_1, b_2 . . . c_1, c_2 . . ., etc., tend to plot on a common curve irrespective of specific speed. Fig. 11 shows a collection of such experimental points for β_2 = 55 deg and Fig. 12 the same for β_2 = 90 deg. Heads, capacities, and efficiencies are expressed as percentages of the same variables for the points A, B, and C, respectively. For all points the percentages of heads and capacities are equal for each point—this being a property of the straight lines AO, BO, and CO.

Using charts Figs. 11 and 12 three points can be established for head, capacity, and efficiency for any vane position and impeller discharge angles 55 and 90 degrees. For any other values of β_2 interpolation and extrapolation have to be resorted to as presently no test data are available to prepare similar charts for different values of β_2.

Casing Characteristics

The line BO in Fig. 2(*a*) has a definite physical meaning intimately connected with the blower performance. Thus, if the head-capacity characteristics are drawn on the dimensionless coordinates such as $\phi = c_{m2}/u_2$ for capacity and the pressure coefficient $\psi = H/(u_2^2/g) = c_{u2}/u_2$, the line BO (Fig. 13) will represent in dimensionless form the absolute velocity at the impeller discharge c_2'/u_2 in magnitude and direction. The property of the line BO is that if several impellers are operated in the same casing the best efficiency points will remain on the line BO, which represents the "casing characteristics." Reference [2] gives an example showing the performance of three impellers of the same profile having different values of the impeller discharge angle β_2 the bep's of which fall on the "volute line." Note that for all points on the BO line the head and capacity change in the same ratio.

Reducing Impeller Diameter. The most important application of the "casing characteristics" is that for calculation of the impeller diameter when reducing impeller diameter by turning to reduce the blower head-capacity output. The method was introduced by Bergeron [3] and later has found wide use in the other countries [4, 5]. The rule widely used in the United States (Reference [1], p. 71) states that with the cut impeller the capacity varies directly as the impeller diameter and head varies, directly as the square of the diameter. However, it was found necessary to allow a slight excess of the impeller diameter to compensate for the more rapid drop of capacity.

In Bergeron's method it is assumed that both the head and capacity vary as the square of the impeller diameter.

$$\frac{Q_1}{Q_2} = \frac{H_1}{H_2} = \frac{D_1^2}{D_2^2} \tag{17}$$

Variation of capacity as square of the impeller diameter can be justified as both the radial velocity at impeller discharge c_{m2} and the area normal to this velocity vary directly as the impeller diameter. No further corrections are required with this method for moderate impeller cuts.

Application of this method in practice is very simple. In Fig. 14 suppose the full diameter head-capacity characteristic is represented by the curve AB. The required operating point is designated by C. Draw line OC through the origin of head-capacity co-ordinates to intersect the curve AB at D. Then the reduced diameter ratio to the full diameter will be represented by

$$\frac{D_e}{D_d} = \left(\frac{Q_e}{Q_d}\right)^{1/2} = \left(\frac{H_e}{H_d}\right)^{1/2} \tag{18}$$

requiring no further corrections.

Inlet Guide Vanes in Multistage Blowers

Since in a multistage blower only the first stage is equipped

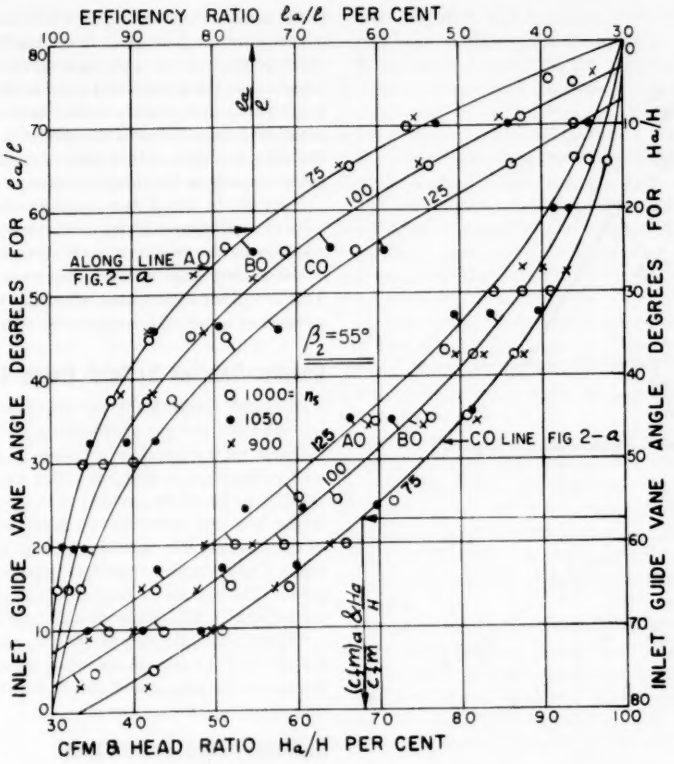

Fig. 11 Guide vane performance, single stage blowers

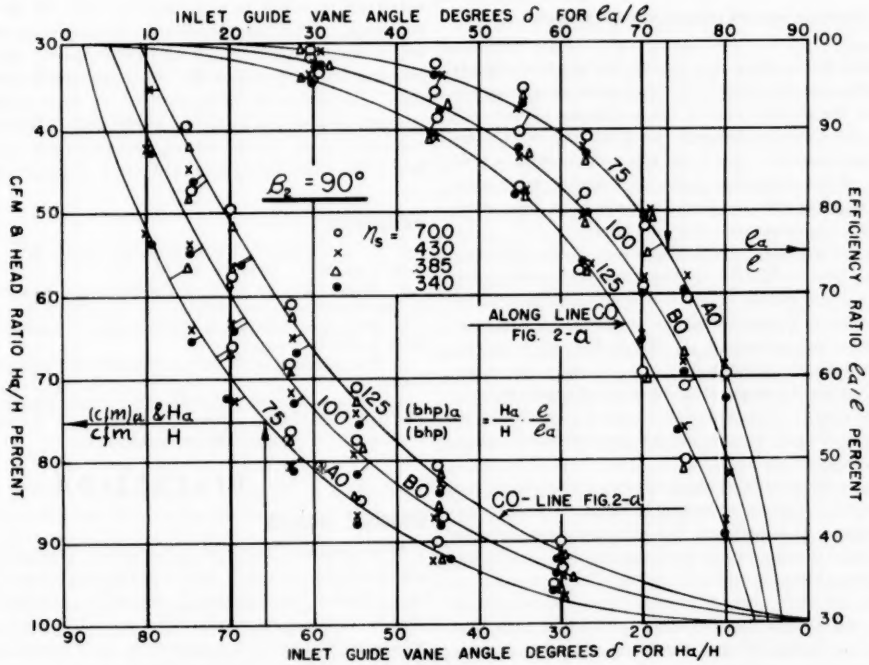

Fig. 12 Guide vane performance, single stage blowers

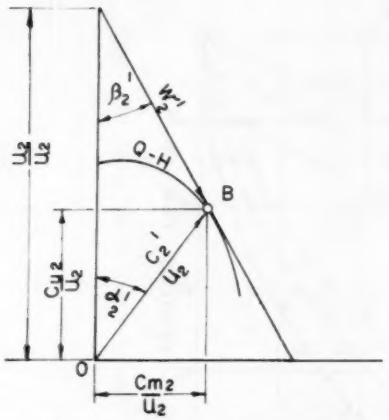

Fig. 13 Dimensionless characteristics of impeller

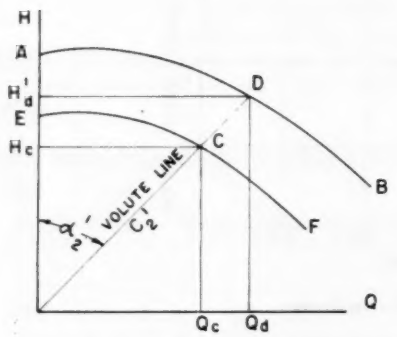

Fig. 14 Performance with reduced impeller diameter

with the inlet guide vanes, the power saving due to prerotation is only a small fraction of the total power reduction of a complete machine. By far the greatest part of the multistage blower output reduction is accomplished through the throttling and the reduction of the gas density. The latter effect appears as a progressive shifting of the operating point to a higher volumetric capacity at the impeller exit and hence a lower head from stage to stage toward the high pressure end of the blower.

Fig. 9, among other things, shows also a plot of the efficiency ratios against the head ratios for multistage blowers with guide vanes in operation and points taken at several capacities. The effect of the number of stages could not be discerned. In fact, the power reduction for multistage blowers in Fig. 10, based on test data in Fig. 9 for the greater part of the head ratio range, coincides with that for the single stage blowers of approximately the same specific speed. It is only for the head ratios below 50 per cent that the multistage blowers show a greater power reduction than the single stage blowers.

Fig. 9 also shows the results of the inlet pipe throttling with a gate valve (line AB). A power reduction of 7.5 per cent was realized in this manner. It is believed that the power saving could be further increased if some means were provided to restore the uniform flow beyond the gate valve in the impeller approach.

In view of the fact that power reduction due to prerotation in the first stage is only a small fraction of the total power reduction of the complete multistage blower the head and efficiency reductions do not lend themselves to be simply expressed in terms of the guide vane angular position. The movement of the guide vanes operating mechanism in practice is governed by the direct observation of the desired effect on the blower output very much in the same manner as is done when the head-capacity of a blower is varied by the blast gate throttling the inlet or discharge. The exact position of the gate disk or the valve stem is of little interest. For the purposes of records the blower performance with guide vanes in operation is tied to the relative angular or linear position of the member of the actuating mechanism which controls the vane position, rather than the angular displacement of the guide vanes from the neutral position.

It should be noted that a considerable variation in the test results of multistage blowers with inlet guide vanes in operation in addition to the reasons already discussed is caused by the degree of the original stage mismatching when impeller selection is made. This is further aggravated when the test is made on a different gas and at a reduced compression ratio.

Counter-Rotation by Inlet Guide Vanes

Although theoretically the impeller output could be increased by deflecting the gas approaching the impeller inlet in direction opposite to the impeller rotation in practice the ability of the inlet guide vanes to perform such a function is very limited. The throttling cannot be avoided with vanes set for counter-rotation as the free area between two adjacent vanes is reduced directly as cos δ, where δ is the vane setting angle from the neutral position. The maximum impeller output is obtained with $\delta \approx 20$ degrees. The maximum head increase at the bep is of the order of 7.5 per cent. The efficiency as a rule is lower by 1.0–1.5 points.

With a constant speed driver if a greater increase of the impeller output over the normal operating conditions is required—the latter should be placed sufficiently below the maximum output to make such an increase possible.

Stationary Inlet Guide Vanes

Occasionally multistage blowers are provided with stationary inlet guide vanes in front of impeller inlet of each stage. The vanes are arranged as a replaceable part of the return channel vanes. They are attached to the interstage packing ring or seal, known also as impeller inlet guide vanes. As a means of increasing impeller output the stationary guide vanes are ineffective. Reduction of head-capacity by this method is always accompanied with a reduction in efficiency, thus indicating that reduction of the output results primarily from the throttling effect of the guide vanes and a reduction of gas density.

References

1 A. J. Stepanoff, "Turboblowers," John Wiley & Sons, Inc., New York, N. Y., 1955, pp. 86–90.

2 Blom, "Development of the Hydraulic Design for the Grand Coulee Pumps," TRANS. ASME, vol. 72, 1950, p. 53.

3 Bergeron, "Machines Hydrauliques," Dunod, Paris, France, 1928, p. 237 (in French).

4 Klein-Schanzlin & Becker Handbook, "Pumpen," p. 106 (in German).

5 Susuma Terada, "Variation of Characteristics of Centrifugal Pumps by Reduction of Impeller Diameters," Library of Congress, Number 621-67-01, p. 1456 (in Japanese).

DISCUSSION

Robert J. Jackson[2]

It is certainly worth while to have a paper by Dr. Stepanoff which records so much basic information about compressor design. One of the continually occurring problems in all fields is that of obtaining a ready reference on specific subjects by a recognized authority to supplement the more general texts which frequently become obsolete before a replacement is available.

I would like to comment on two sections of this paper which I

[2] Compressor Engineer, De Laval Steam Turbine Company, Trenton, N. J.

feel could use some further clarification. The first matter is the use of the term "Pure Throttling" with respect to the inlet of a compressor. The type of throttling referred to as pure throttling is in reality the same as the effect achieved with discharge throttling and would be more clearly referred to as such.

For the user, and in most cases the designer, to best consider the effects of suction throttling, pressure ratio and horsepower curves drawn for the conditions existing upstream of the throttle valve are more useful than any other type of data.

If a given pressure ratio is assumed across a throttle valve, downstream pressure divided by upstream, the true volume of gas flowing to the compressor is increased by the reciprocal of this ratio. With this new volume the true compression ratio of the blower can be read directly from the curve in Fig. 15. The over-all ratio is found by multiplying the compression ratio of the blower and the expansion ratio across the throttle.

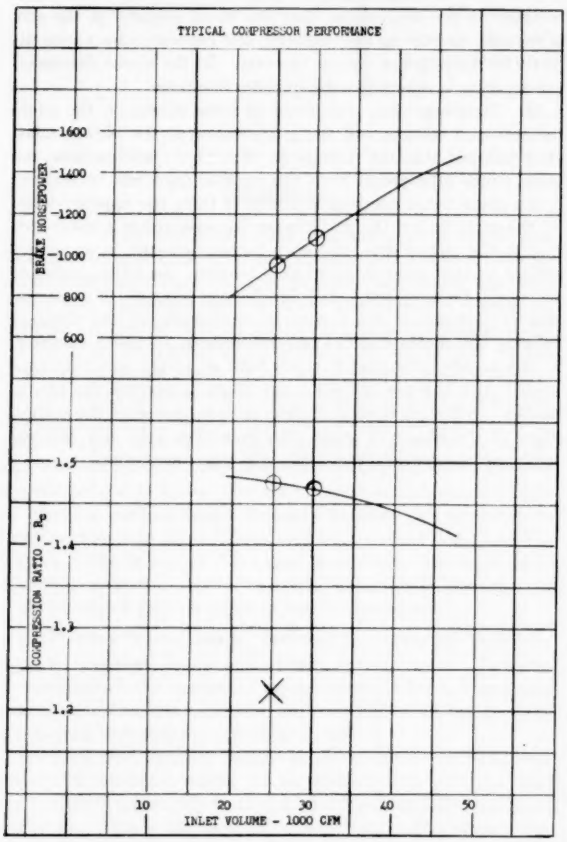

Fig. 15 Typical compressor performance

The horsepower is found by reading the value off the curve at the true inlet volume and multiplying by the throttle valve pressure ratio. This will compensate for the density change.

It is true that this type of throttling, as pointed out by Dr. Stepanoff, will be more efficient than discharge throttling. For discharge throttling the horsepower would be read directly off the curve using the process volume flow at the compressor inlet.

For an example of this type of a problem the following performance would be obtained from the set of curves shown.

If we have 25,000 cfm flowing to this compressor at a given set of inlet conditions, the pressure ratio would be 1.476:1 and the horsepower required would be 955. If the throttling were done on the discharge side to reduce the over-all ratio to 1.224:1 the horsepower would remain the same.

With suction throttling the throttle ratio would be 0.833:1 and the compressor inlet volume 30,000 cfm where the compressor pressure ratio is 1.469:1 and the horsepower read from the curve is 1085. For the over-all ratio of 1.224:1, the horsepower is the 1085 multiplied by 0.833 or 903. The power saving by throttling the inlet instead of the discharge would be 52 horsepower.

The second point in this paper which I feel should be further clarified is suggested method of determining the performance of a compressor wheel when the diameter is reduced. I would like to point out that there are circumstances when none of the relationships given will be satisfactory.

In some cases it is desirable to cut the vanes only and leave the two disks the full diameter. In this case the disks, which extend beyond the vanes, add considerably to the head developed by the wheel. This effect was determined in tests made at De Laval several years ago.

Even where wheels are cut uniformly across the periphery, the shape of vanes and gas passages can cause considerable deviation from the theoretical relationships. In fact, we have been quite surprised to see one wheel which had very good performance that had a head rise when the diameter was reduced with no change in efficiency. A thorough analysis showed that the tests were correct and that the strange behavior was due to the wheel geometry.

Our conclusion from this background is that wheel cutting is a matter which must be handled carefully in order to decide what must be done to reach the desired end performance.

I wish to repeat that these comments should in no way detract from the value of Dr. Stepanoff's paper but are intended to show that any general rule is only as good as the situation to which it is applied.

E. W. Tanzberger[3]

The author made a commendable contribution by presenting the subject matter in a comprehensive manner, thereby clarifying in detail a "device" which has been applied in an increasing number of compressor applications, particularly those where constant speed operation is indicated.

Referring to Fig. 3 and the statement concerning the effectiveness of the vanes in deflecting the flow, it is possible to define, and therefore predict somewhat more accurately, the "vane effectiveness." By sizing the flow areas at the downstream side of the inlet vanes in such a manner that a continuous acceleration of the gas is maintained to the inlet edges of the impeller blades, loss of efficiency is minimized considerably. The c_m at the guide vane is thereby accelerated and for constant c_u the angle δ will be decreased. However, the c_u at the guide vane is reduced due to space conversion which is particularly pronounced at the large radius stream line extending from the geometric center of the inlet piping radially outward to the impeller blade; this affects a further reduction of the angle δ. Based on these two considerations and their effective application, a closer correlation can be established between the *actual* inlet vane angle and the *actual* approach angle at the inlet edges of the impeller blade.

Assuming a constant weight flow (Fig. 3), the component c_{m_1} will remain essentially unchanged; this would establish a relationship $c_{u_1} = c_{m_1} \tan \delta$ rather than $c_{u_1} = c_{m_1} \sin \delta$. For small inlet vane angles the difference in most cases is negligible.

If an increase or decrease of weight flow at constant head is desirable or necessary, it can be accomplished by the utilization of movable or stationary inlet vanes; however, the characteristic curves will thereby be displaced for the best efficiency point,

[3] Manager, Centrifugal Research and Engineering Department, Clark Bros. Company, Division of Dresser Industries, Olean, N. Y. Mem. ASME.

corresponding to the radial (neutral) guide vane position. The effectiveness of this arrangement has been repeatedly demonstrated by realizing an inlet capacity increase of 12 per cent and a decrease of 17 per cent with a reduction of efficiency of only 0.7 and 0.5 points, respectively. The shift away from the bep relative to the stated conditions underlines the importance of proper initial matching of impeller and volute (casing) design which the author has clearly treated and emphasized in his paper.

The effect on head and capacity when reducing the impeller diameter may well be investigated in more detail in order to correlate the theory with actual experimental data. It appears that the geometry of the impeller profiles, and particularly the discharge blades angles, have a significant influence on the anticipated performance.

It is most encouraging that the author has presented the material in such detail; future studies and evaluations may well be worth while to clarify and correlate the presented theory with the actual performance of inlet guide vanes.

Author's Closure

Contributions by Messrs. Jackson and Tanzberger are greatly appreciated. Mr. Jackson presented a method of estimation of power reduction by means of the throttle valve in the inlet pipe when the pressure ratio across the throttle valve is assumed, and a constant weight of flow is maintained. The method is equally applicable to the case, more common in practice, when the reduced compressing ratio of the machine is specified. This would require two approximations to locate the point on the head-capacity (inlet volume upstream of the throttle valve) and bhp curves of the blower.

The author is in complete agreement with Mr. Jackson that the "pure throttling" effect of the guide vanes is not any different from the throttling of the blower discharge. This becomes evident from equation (14) when the ratio of $(\text{bhp})_a/\text{bhp}$ is set equal to unity. Then $H_a/H = e_a/e$, which is the definition of the pure throttling (equation 2).

Both discussers have pointed out the inaccuracy of the rules for head-capacity determination of a blower with impeller diameter reduced by turning. There seems no disagreement that head is reduced as square of the impeller diameter. But to estimate the capacity two methods are in use. The first one states that capacity where that head will occur is reduced as the impeller diameter. For many years the author was leaning toward this rule. However, the past few years the author joined the advocates of the rule that capacity also varies as a square of the head, as presented in this paper. It is believed that a greater accuracy for capacity calculation is given by the expression

$$\frac{Q_1}{Q_2} = \frac{D_1^2\, b_1}{D_2^2\, b_2}$$

where b_1 and b_2 are the impeller widths at the exit with the original and reduced diameters, respectively. This relationship is based on the assumption that the radial velocity at the exit is reduced directly as the diameter and capacity also varies directly as the impeller area at the exit. In the above discussion the capacity is referred to the impeller discharge.

Mr. Tanzberger has elaborated to some extent on the effectiveness and efficiency of the guide vanes at the blower inlet. It is believed that the damage to efficiency, resulting from the guide vanes' interference with the impeller inlet, can be reduced if the guide vanes are removed farther from the impeller inlet. At the same time if the guide vanes are arranged in a plane normal to the blower axis, and on a larger diameter, in a manner similar to that used in multistage blowers, the effectiveness of vanes will be increased. As following the principle of conservation of momentum the tangential component of the absolute velocity will increase as the flow proceeds to a smaller diameter.

This article attempted to throw light on several prol lems connected with the use of inlet guide vanes to control the blower output. Solutions to some of them were suggested by the author. Some of the phases of guide vane operation were only touched upon and require a further study and experimentation.

A. J. STEPANOFF
Development Engineer,
Ingersoll-Rand Company,
Phillipsburg, N. J. Mem. ASME

H. A. STAHL
Engineer, Ingersoll-Rand Company,
Phillipsburg, N. J. Mem. ASME

Dissimilarity Laws in Centrifugal Pumps and Blowers

Two kinds of dissimilarities are discussed: (a) Planned dissimilarities between the different hydraulic types as expressed by the performance specific speed; (b) deviation from geometrical similarity which is "forced" to accommodate some special condition at the same performance specific speed. Experience has shown that irrespective of a continuous variation of the design element of a consistent row of hydraulic types of impellers, there are certain factors or criteria which remain constant for different specific speeds. The best known of these is the suction specific speed. From the second group of dissimilarities the most common examples are mismatched impellers and cases. In solving such problems the designer's judgment is based on a knowledge of causes and effects in selecting certain design elements to meet the desired performance, because these follow certain rules which are "laws" of Nature. The object of this paper is to review the most common of these laws as applied to dissimilar pumps and blowers.

Introduction

The well-known laws of dynamic similarity of flow through hydraulic centrifugal machines form the basis of a design system for centrifugal pumps, blowers, and water turbines. These laws, frequently referred to as "affinity laws," permit one to predict the performance of a machine if tests of a geometrically similar model are available. Experience has shown that the behavior of machines which are not geometrically similar also follows certain laws which permit the designer to predict their performance, sometimes by interpolation or extrapolation of data of existing types, sometimes by estimating the effects of certain design elements which differ from the existing models. The designer's judgment is based on a knowledge of causes and effects in selecting certain design elements to meet the desired performance, because these follow certain rules which are "laws" of Nature. The object of this paper is to review the most common of these laws as applied to dissimilar pumps or blowers.

Two kinds of dissimilarities should be recognized:

1 Planned dissimilarities between the different hydraulic types as expressed by the performance specific speed. The laws of variation of the important design elements for a continuous row of specific-speed types are well established in the form of charts such as appear in references [1] and [2].[1]

Identical head-capacity design conditions can be met at a given speed with machines which are not geometrically similar. The major variation results from the use of different impeller discharge angles β_2. This is the most important independent design element of centrifugal impellers. Even for a given value of β_2 the same specific speed may be met with dissimilar designs by employing a "tight" impeller in a "loose" casing and vice-versa. The objective of each designer is to select those design constants which will realize optimum efficiency.

Experience also has shown that irrespective of a continuous variation of the design elements of a consistent row of hydraulic types of impellers, there are certain factors or "criteria" which remain constant for different specific speeds. The best known of these is the "suction specific speed." This will be elaborated upon later and several others will be discussed.

2 The second class of dissimilarity applies to a given performance specific speed and comprises a great number of cases which can be subdivided into two groups (*a*) where a deviation from the geometrical similarity is "forced" to accommodate some special conditions and (*b*) where, for geometrically similar pumps, deviation from the affinity laws is caused by special operating conditions or fluid properties, such as Reynolds number, or effects of speed, size, or viscosity; cavitation for pumps or effect of Mach number for blowers; effect of the impeller approach, as for example sump design for vertical pumps, or inlet guide vanes in blowers.

The latter subgroup (*b*) will not be discussed in this paper. Of the first group (*a*) only the most common problems will be presented with the intention of tracing the laws which govern the behavior of the pumps or blowers when geometrical similarity is impaired.

Suction Specific Speed

The hydraulic design of an impeller is completely defined by the inlet and discharge-velocity triangles. To make these applicable to all similar impellers, irrespective of speed or size of the machine, it is convenient to draw the velocity triangles on dimensionless scales, expressing all velocities as ratios to their respective peripheral velocities. Thus it becomes apparent that angles in the velocity triangles really determine the characteristics of the impeller. Figs. 1 and 2 show the inlet and discharge-velocity triangles with the notations of several components as used in this discussion.

For an inlet-velocity triangle having radial inlet, it is evident that

$$\alpha_1 = 90°; \text{ and } \tan \beta_1 = c_{m1}/u_1$$

or

$$c_{m1} = u_1 \tan \beta_1 = nD_1 \tan \beta_1/229 \qquad (1)$$

where c_{m1} is the true radial velocity based on the measured capacity plus the estimated leakage loss with allowance made for the reduction of the free area normal to c_{m1} by the vane thickness; u_1 is the inlet peripheral velocity at the impeller-eye diameter D_1.

[1] Numbers in brackets designate References at end of paper.

Contributed by the Pumping Machinery Subcommittee of the Hydraulic Division and presented at the Winter Annual Meeting, New York, N. Y., November 27–December 2, 1960, of The American Society of Mechanical Engineers. Manuscript received at ASME Headquarters, August 1, 1960. Paper No. 60—WA-145.

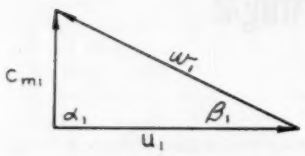

Fig. 1(a) Inlet-velocity triangle, radial inlet

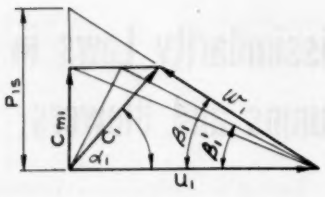

Fig. 1(b) Inlet-velocity triangle, prerotation allowed

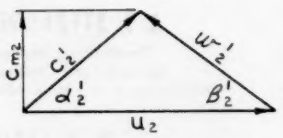

Fig. 2 Input-velocity triangle at discharge

In addition to equation (1), the following relation should also be satisfied:

$$c_{m1} = \frac{Q}{0.785 D_1^2} \times 0.321 \tag{2}$$

Equating (1) and (2) and rearranging, we obtain

$$\frac{Q}{nD_1^3} = \tan \beta_1 \left(\frac{0.785}{229}\right) \frac{1}{0.321} \tag{3}$$

where n is rotative speed.

The expression

$$Q/nD_1^3 = q_{1s} \tag{4}$$

may be termed the "inlet specific capacity," representing capacity in the dimensionless form.

Still another form of the criterion of the suction conditions can be obtained from equations (1) and (2) by solving equation (1) for D_1 and substituting its value into equation (2) and rearranging the terms as follows:

$$D_1 = \frac{c_{m1} \times 229}{n \tan \beta_1} \tag{5}$$

$$Q = \frac{0.785 (229)^2 c_{m1}^3}{n^2 (\tan \beta_1)^2 0.321} \tag{6}$$

hence

$$\frac{0.785^{1/3} \times 229}{0.321^{1/3} \tan \beta_1} = \frac{nQ^{1/3}}{c_{m1}^{1/3}} \tag{7}$$

If we denote $c_{m1}^2/2g = h_{s1}$, the velocity head through the impeller eye, the NPSH value can be expressed through h_{s1} and a numerical constant K_1 as follows:

$$\text{NPSH} = K_1 h_{s1} \tag{8}$$

Substitution of c_{m1} in terms of h_{s1} in equation (7) results in

$$\frac{0.785^{1/3} \times 229 \times (2g)^{3/4}}{0.321^{1/3} \tan \beta_1} = \frac{nQ^{1/2}}{h_{s1}^{3/4}} \tag{9}$$

and finally

$$\frac{8147}{K_1^{3/4} \tan \beta_1} = \frac{nQ^{1/2}}{(\text{NPSH})^{3/4}} = S_1 \tag{10}$$

The expression S_1 is well known under the name of suction specific speed. For the radial inlet, this is directly connected to the inlet angle β_1 as follows:

$$\tan \beta_1 = 8147/K_1^{3/4} S_1 \tag{11}$$

where $K_1 > 1$ is a constant for a given design of impellers. Note that, although equations (3) and (9) are quite different in form, they are identities and when solved for $\tan \beta_1$ give exactly the same answer. From the appearance of the equation (10), it can be stated that high suction specific speed is associated with a low value of the vane entrance angle β_1. This leads to a low radial velocity c_{m1} and a large impeller-eye diameter. In a general way, a low angle β_1 leads to a low NPSH requirement at the capacities lower than the best efficiency point (bep). However, the NPSH values increase rapidly above the bep. To reduce the NPSH values at the bep and higher capacities, c_{m1} is reduced further. This means that some prerotation is allowed at the bep, Fig. 1(*b*). It is convenient to express the degree of prerotation by the ratio

$$R_1 = \frac{P_{1s}}{c_{m1}} \tag{12}$$

which determines the values of the absolute inlet angle α_1. Under these conditions, equation (10) takes the form

$$\frac{8147 R_1}{\tan \beta_1} = \frac{nQ^{1/2}}{h_{s1}^{3/4}} \tag{13}$$

Thus it may seem that a higher suction specific speed can be realized by allowing prerotation at impeller approach. However, in practice, this cannot be realized since without special inlet guide vanes the flow cannot be given the prerotation required for a shockless entrance at an angle β_1 exactly equal to the vane entrance angle. The liquid will enter the vanes at an angle β_1' lower than β_1, causing separation on the low-pressure side, obstructing the flow, and possibly reducing the efficiency at bep.

The physical meaning of the diagram in Fig. 1(*b*) is that the impeller inlet is designed for a shockless entrance corresponding to the radial velocity P_{1s}. The design capacity based on the c_{m1} corresponds to a partial capacity in respect to the foregoing capacity at shockless entrance.

Specific speed S_1 is widely used in the centrifugal-pump field for classification of the impellers as to their NPSH requirements. Within the limit where the affinity laws hold, the suction specific speed remains constant, irrespective of the head or speed of the pump. However, recent investigations have demonstrated that the affinity laws as applied to impeller-inlet conditions do not hold and that the suction specific speed increases with speed, specific speed, and efficiency of pumps as discussed in reference [3].

For compressible fluids (gases), the utility of the concept of suction specific speed is impaired by the fact that the affinity laws apply to the volume of the gas at the impeller exit, but do not hold for the inlet volumetric capacity. As a result, the inlet specific speed for blowers does not remain constant for different performance specific speeds n_s. For that reason, the suction specific speed, is not used in the blower field.

Impeller-Discharge Specific Speed

Under this designation will be introduced a criterion of the impeller performance represented by the following formula:

$$S_2 = \frac{nQ^{1/2}}{h_{s2}^{3/4}} \tag{14}$$

where

$$h_{s2} = c_{m2}^2/2g$$

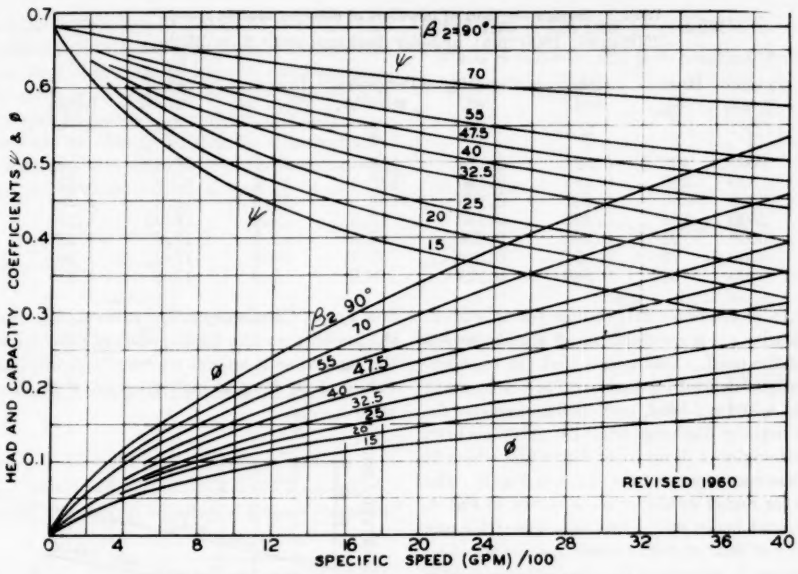

Fig. 3 Head and capacity coefficients versus specific speed

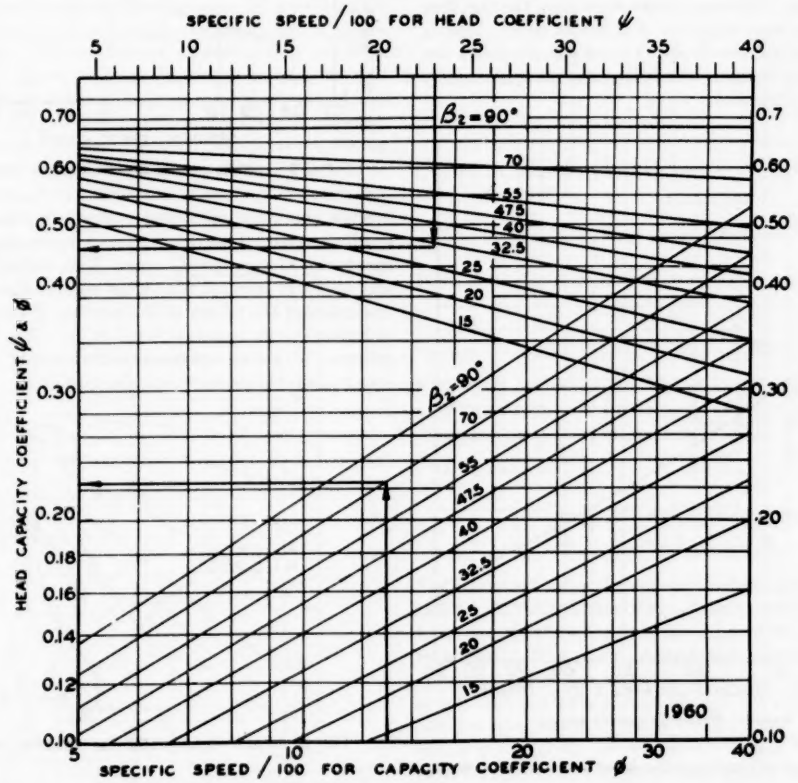

Fig. 3(a) Head and capacity coefficients versus specific speed

and c_{m2} is the meridional velocity at impeller discharge. In Table 1 are listed several design elements of impellers of different performance specific speed:

$$n_s = \frac{nQ^{1/2}}{H^{3/4}} \tag{15}$$

The capacity of 2500 gpm is the same for all seven impellers The speed is also constant (1800 rpm) and the impeller-discharge angle $\beta_2 = 25$ deg. The heads were selected to obtain the desired range of specific speeds. The peripheral velocity u_2, the impeller outside diameter D_2, and the impeller-exit radial velocity c_{m2} were calculated from the head and capacity coefficients ψ and

Table 1 Design elements of impellers of different specific speeds

(2500 gpm; 1800 rpm; impeller discharge angle $\beta_2 = 25$ deg)

Specific speed, n_s	Head, ft, H	Head coef, ψ	Capacity coef, ϕ	Peripheral velocity, u_2	Impeller diam, in., D_2	Exit radial vel, ft c_{m2}	Ratio, c_{m1}/c_{m2}
1	2	3	4	5	6	7	8
1000	400	0.528	0.114	156	20.0	17.8	1.35
1500	240	0.480	0.140	127	16.2	17.8	1.31
2000	100	0.440	0.165	109	13.9	18.0	1.28
2500	159	0.407	0.185	97.5	12.4	18.05	1.25
3000	95	0.380	0.200	89.5	11.4	17.9	1.22
3500	76	0.357	0.216	82.7	10.5	17.9	1.20
4000	64	0.340	0.228	78.0	9.9	17.8	1.17

ϕ taken from Fig. 9.15 of reference [1], reproduced in Fig. 3. Note that the exit velocity c_{m2} is constant for all specific speeds and is independent of the head. This means that the impeller-discharge specific speed S_2, defined by equation (14), is constant irrespective of specific speed n_s, head, or impeller diameter for the same value of the impeller discharge angle β_2. This has been found to be true for all angles of β_2 up to 90 deg, a fact which in itself tends to prove the consistency of the chart in Fig. 3. The value of S_2 decreases for higher values of β_2 as shown in Fig. 4. Thus the value of S_2 and hence of c_{m2} can be selected for any value of β_2 irrespective of head or performance specific speed n_s. Like suction specific speed S_1, equation (10), the discharge specific speed S_2 does not add any new or independent relation between the variables involved. However, at the same time, the fact that S_2 is constant shows that impellers of different specific speeds form a continuous and consistent row of types which follow a law of dissimilarity, i.e., $S_2 = \text{const}$. Thus the value of c_{m2} is uniquely determined for each value of β_2.

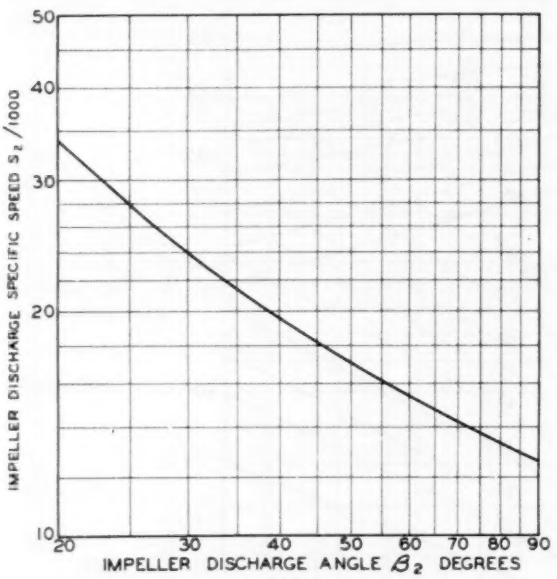

Fig. 4 Impeller discharge specific speed

Note that selection of the impeller-inlet meridional velocity c_{m1} is rather arbitrary. Thus to realize the lowest possible NPSH requirements (higher suction specific speed S_1), the lowest practical values of c_{m1} are used. The minimum impeller-inlet angle β_1 (about 15 deg) sets the low limit for c_{m1}. For a normal design aiming at an optimum peak efficiency it is customary to express c_{m1} in terms of c_{m2} or a ratio c_{m1}/c_{m2}. In column 8 of Table 1 are given such ratios for several specific speeds. This ratio approaches unity for high-specific-speed pumps of axial-flow type. Continuity of the ratio c_{m1}/c_{m2} leads to continuity of the impeller profiles for impellers of different specific speeds. At the same time it assures continuity in the vane shape, as higher values of β_2 demand higher values of β_1 to maintain the same ratio c_{m1}/c_{m2}.

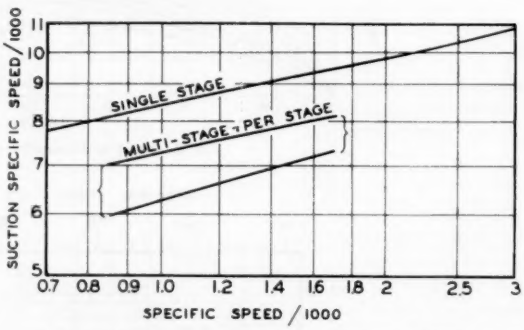

Fig. 5 Suction specific speed variation versus n_s (Esman)

Since the value of S_2 and c_{m2} remain constant for different specific speeds and the ratio c_{m1}/c_{m2} is decreasing for higher specific speeds the suction specific speed S_1 as defined by equations (9) and (10) will increase for higher specific speeds n_s. A further discussion of the causes of the increase of suction specific speed at higher specific speeds is found in [3]. Fig. 5 reproduced from reference [4] shows experimental variation of the suction specific speed versus the performance specific speed.

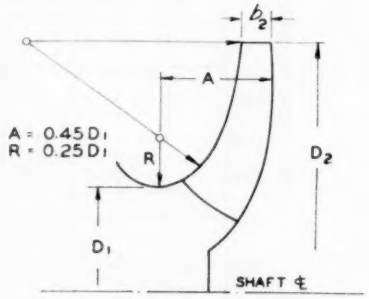

Fig. 6 Impeller-inlet profile for different specific speeds

Remark 1. It should be noted that impeller geometrical proportions as they appear on the impeller profile, Fig. 6, are closely associated in the hydraulic type or performance specific speed n_s of the pump. The ratios b_2/D_2 and D_1/D_2 have been used for impeller classification prior to the universal adoption of specific speed. At the same time, for the single-stage pumps and blowers of a wide range of specific speeds and $\beta_2 = 25$ deg, it has been found that the leading impeller proportions, such as the ratio

A/D_1 in Fig. 6, are essentially constant and equal to 0.45. This may serve as a graphical illustration of the fact that the impeller-inlet design is independent of the head or impeller outside diameter. This observation is not inconsistent with the concept that impellers of different specific speeds can be thought of (but never are) as obtained from one impeller by cutting the outside diameters. Thus the main geometrical proportions of the impeller-inlet profile, such as A/D_1, are common to several specific speeds

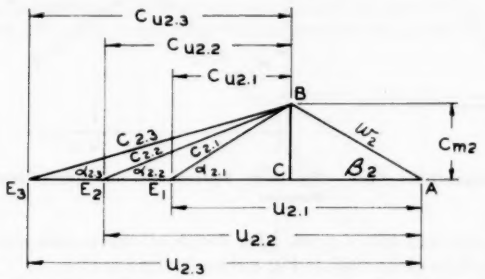

Fig. 7 Discharge velocity triangles for impellers of different diameters (Euler's theoretical)

Remark 2. To summarize: Impellers of different specific speeds using the same discharge angle β_2 have the same inlet-velocity triangles (dimensionless) or simply have the same value of the inlet angle β_1. For pumps of normal design, the inlet angle β_1 at impeller-eye diameter D_1 is most frequently equal to β_2. Impellers of different specific speeds designed for the same capacity and speed, such as listed in Table 1, have in the Euler's theoretical discharge-velocity triangles identical parts ABC, Fig. 7, referring to the relative flow through the impellers. The parts containing the absolute velocities at impeller discharge BCE_1, BCE_2, and so on, are different for each specific speed depending on heads and impeller diameters. This applies equally to centrifugal pumps and blowers.

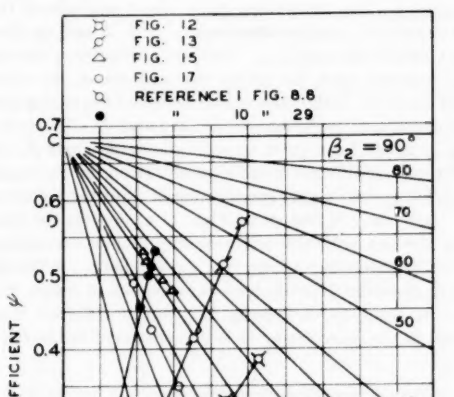

Fig. 8 Universal chart of head and capacity coefficients

Application of the Law S_2 = Constant

For n = constant and Q = constant the ratio of performance specific speeds yields

$$\frac{n_{s1}}{n_{s2}} = \left[\frac{H_2}{H_1}\right]^{3/4} = \left[\frac{u_2}{u_1}\right]^{3/2}\left[\frac{\psi_2}{\psi_1}\right]^{3/4} \tag{16}$$

Introducing

$$\phi_1 = c_{m1}u_1 \quad \text{and} \quad \phi_2 = c_{m2}u_2 \tag{17}$$

and

$$c_{m1} = c_{m2} = \text{const} \tag{18}$$

and solving for ϕ_1/ϕ_2 gives

$$\frac{\phi_1}{\phi_2} = \left[\frac{n_{s1}}{n_{s2}}\right]^{2/3}\left[\frac{\psi_1}{\psi_2}\right]^{1/2} \tag{19}$$

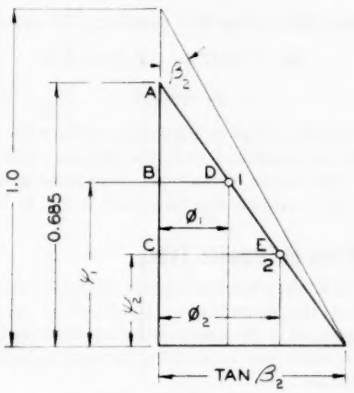

Fig. 9 $\phi - \psi$ diagram

From geometry in Fig. 9 we obtain

$$\frac{\psi_1}{\psi_2} = \frac{\tan\beta_2 - \phi_1}{\tan\beta_2 - \phi_2} \tag{20}$$

Combining (19) and (20) leads to

$$\frac{\phi_1}{\phi_2} = \left[\frac{n_{s1}}{n_{s2}}\right]^{2/3}\left[\frac{\tan\beta_2 - \phi_1}{\tan\beta_2 - \phi_2}\right]^{1/2} \tag{21}$$

hence

$$\left[\frac{\phi_2}{\phi_1}\right]^2 = \left[\frac{n_{s2}}{n_{s1}}\right]^{4/3}\left[\frac{\tan\beta_2 - \phi_2}{\tan\beta_2 - \phi_1}\right] \tag{22}$$

For a selected value of the impeller-discharge angle β_2 this equation permits calculation of the capacity coefficient ϕ for any performance specific speed n_s if the value of ϕ for one specific speed is known. This point, determined experimentally, fixes the "normal" design for a continuous row of consistent hydraulic types. Several such normal designs are possible, depending on whether the design is based on a "tight" impeller and more liberal volute areas, or vice-versa. This is characterized by the ratio b_2/D_2. Values in Fig. 3 represent ϕ and ψ-values for the normal design for the optimum efficiency. Note that the chart in Fig. 8 is "universal" in the sense that values of ϕ and ψ for all possible designs fall in their respective β_2-lines sliding up or down for different values of b_2/D_2. Or conversely, each point on a given β_2-line may represent different specific speeds n_s depending on b_2/D_2-values.

Example. For $\beta_2 = 25$ deg, $\tan\beta_2 = 0.466$, determine value of ϕ_2 for $n_s = 4000$ if $\phi_1 = 0.162$ for $n_s = 2000$.

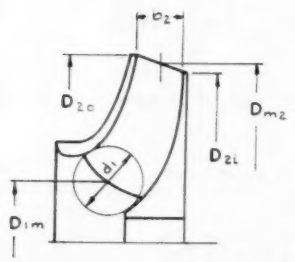

Fig. 10 Definition of mean effective diameter

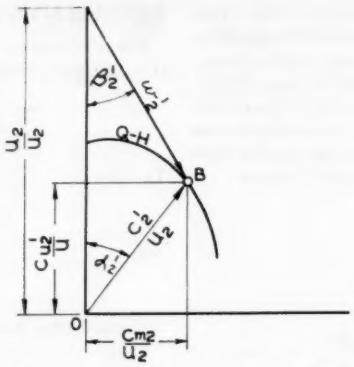

Fig. 11(a) Dimensionless characteristics of impeller

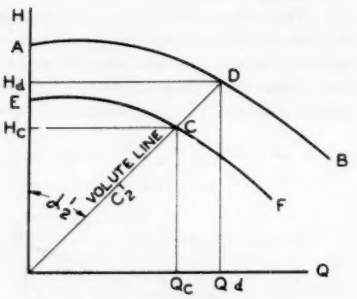

Fig. 11(b) Performance with reduced impeller diameter

Substituting these values into equation (22) we obtain

$$\phi_2^2 + 0.217\,\phi_2 - 0.1012 = 0$$
$$\phi_2 = 0.228 \tag{23}$$

The chart in Fig. 3 was checked and corrected to comply with equation (22) as compared with the original chart previously published. The values of the head coefficients ψ were revised at the same time to satisfy the basic chart in Fig. 8.

Universal Chart of Impeller Types

(*a*) As a third law of the dissimilarity of impeller types, it can be observed that the shutoff head H_s (head at zero measured capacity) expressed in dimensionless form is the same for impellers of different specific speeds and using different impeller-discharge angles β_2. Thus

$$H_s/(u_2^2/g) = 0.585 = \text{const} \tag{24}$$

where u_2 is the impeller-discharge peripheral velocity based on the mean effective diameters D_{m2} defined as (Fig. 10)

$$D_{m2}^2 = \frac{D_{2o}^2 + D_{2i}^2}{2} \tag{25}$$

This holds for the whole range of specific speeds including axial-flow impellers. Minor deviations from equation (24) are caused by the fact that the impeller zero capacity falls to the left of the measured test zero-capacity point. Also, the same impeller may show a different shutoff head in different pump casings. Thus "tight" volute casing tends to raise the shutoff head and vice-versa, Fig. 17.

(*b*) If the head coefficients

$$\psi = \frac{H}{u_2^2/g}$$

at bep of impellers of different specific speeds having the same value of β_2 are plotted against the capacity coefficient

$$\phi = c_{m2}/u_2$$

the points tend to line up along a straight line intersecting the axis of ϕ at the point $\phi = \tan \beta_2$ and the axis of ψ at a point $C = 0.685$ common to all values of β_2. Fig. 8 is based on such a plot for single-stage pumps and blowers of 85 per cent or better efficiency at bep. The mean effective diameter D_{m2}, equation (25), was used for u_2 calculations. The chart contains several controlling design factors for impellers of different specific speeds and using different values of the impeller-discharge angle β_2 and thus represents the law of construction of dissimilar impellers to form a continuous row of types. For details of construction and the properties of the chart in Fig. 8 consult reference [1].

Note that there is no way to enter the chart in Fig. 8 to pick out values of ψ and ϕ to design an impeller of a given specific speed. The chart in Fig. 3, based on the chart in Fig. 8, gives ψ and ϕ-values plotted against performance specific speed. Since the location of the bep is affected by the casing, the chart in Fig. 3 fixes the impeller proportions (b_2/D_2) for different specific speeds. In this manner, different charts of the type shown in Fig. 3 can be constructed from the same chart, Fig. 8, which is more universal. The points representing impellers of different proportions (b_2/D_2) will slide up or down their respective β_2-lines depending upon the casing design—to meet the same head-capacity and speed conditions.

Casing Characteristics

The hydraulic design of centrifugal-pump and blower casings is determined by two elements, namely, the magnitude of the absolute velocity at impeller discharge c_2', Fig. 2, and its direction or the value of the angle α_2'. But since velocity c_2' for similar pumps depends upon the pump size and speed, the absolute-velocity angle α_2' is then the only criterion of the casing type for pumps of different performance specific speed n_s. This is evident in Fig. 8, where for a given impeller-discharge angle β_2 (say 25 deg) the bep for different specific speeds fall on the corresponding line labeled 25 deg, higher specific speeds requiring higher values of α_2'. On the *Q-H* test curve Figs. 11(*a*) and (*b*) the line connecting the bep with the origin of co-ordinates corresponds to the line representing c_2' on the (ψ-ϕ)-chart. Although its length or direction depends upon the selection of scales, this line retains its property of locating the bep of different impellers operated in the same casing as is demonstrated in the following text:

(*a*) Fig. 12 shows the performance of a 12-in. mixed-flow pump with a vaned diffuser casing of specific speed $n_s = 5700$. The three impellers have identical profiles but have different values of β_2 (and hence β_1). The best efficiency points fall on the "casing" line *OA*. The same points are marked in Fig. 8.

(*b*) Fig. 13 shows a test of a 24-in. blower of the volute type with three impellers of the same profile and different values of the impeller-discharge angle $\beta_2 = 25$, 40, and 55 deg. The best efficiency points fall again on the casing-characteristic line *OA*.

(*c*) When the same impeller is tested in the same casing with impeller-diameter cut, it so happens that the bep falls on the casing-characteristic line, Fig. 11(*b*). This means that both capacity and head are reduced in the same ratio, namely,

$$\frac{Q_1}{Q_2} = \frac{H_1}{H_2} = \frac{D_1^2}{D_2^2} \tag{26}$$

Variation of capacity as the square of the impeller-diameter ratio can be justified as both the radial velocity at impeller discharge c_{m2} and the area normal to this velocity vary directly as the impeller diameter.

Application of this method in practice for calculation of the impeller-diameter cut is very simple. In Fig. 11(*b*), suppose the full diameter head-capacity characteristic is represented by the curve *AB*. The required operating point is designated by *C*. Draw line *OC* through the origin of head-capacity co-ordinates to intersect the curve *AB* at *D*. Then the reduced diameter ratio to the full diameter will be represented by

$$\frac{D_c}{D_d} = \left(\frac{Q_c}{Q_d}\right)^{1/3} = \left(\frac{H_c}{H_d}\right)^{1/2} \tag{27}$$

The method was introduced by Bergeron [5] in France and later found wide use in the other countries [6, 7]. The widely used rule states that, with the cut, impeller capacity varies directly as the impeller diameter, and head varies directly as the square of

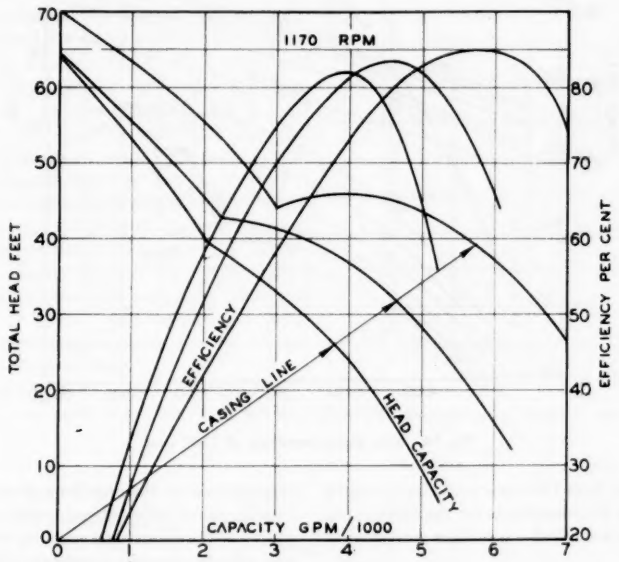

Fig. 12 12-in. vertical propeller pump n_s = 5700 with 3 impellers same profile and different β_2

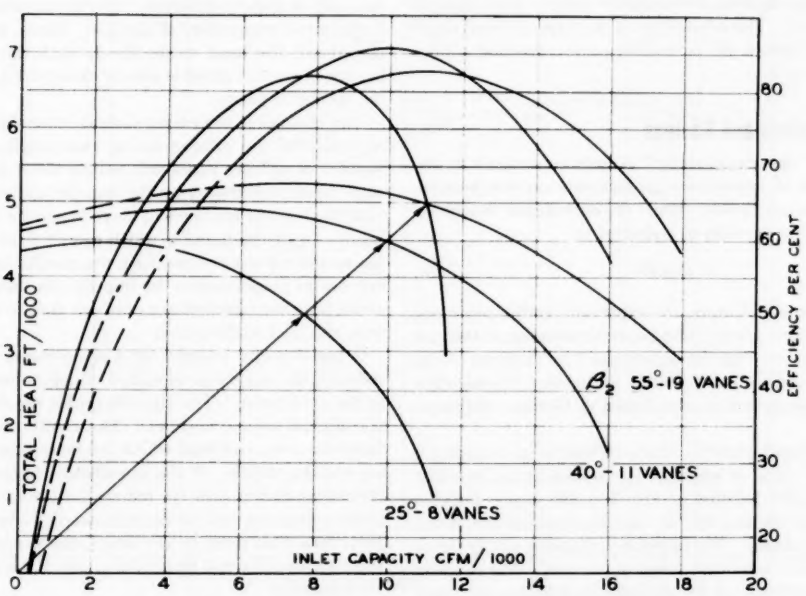

Fig. 13 24-in. single stage blower 3 impellers in the same volute; 3550 rpm

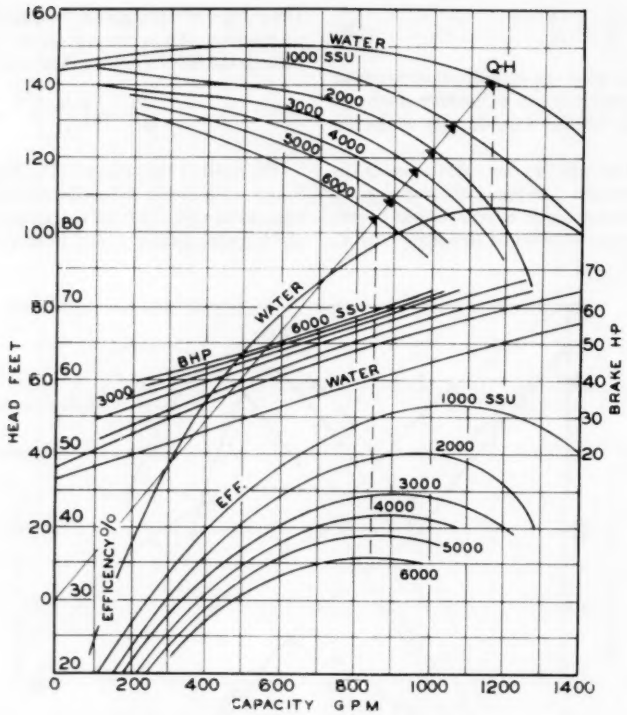

Fig. 14 6-in. pump handling oil 1750 rpm

the diameter. However, it was found necessary to allow a slight excess of the impeller diameter to compensate for the more rapid drop of capacity. In Bergeron's method, no further correction is necessary.

(*d*) Fig. 14 shows a test of a single-stage pump handling oil of different viscosities. Note that the bep at different viscosities fall satisfactorily on the casing-characteristic line *AO*. In fact, they fit better on this line than on the constant specific-speed line, as was suggested in [1]. The advantage of the first method, originally proposed by Grabow [8], is that the same correction applies to the head and capacity.

Mismatched Impellers and Casings

The concept of "specific capacity" is very convenient in discussing the effects of several design elements on the location of the best efficiency point (bep) of centrifugal machines. Algebraically, specific capacity q_s is defined as

$$q_s = Q/nD^3 \tag{28}$$

Expressed in fundamental units, the expression is dimensionless, representing a number 1/rps. The physical meaning of the q_s is capacity per revolution with an impeller of 1 ft diameter. The number serves as an index of pump or blower "throughflow ability" as a complete unit (a translation of German "Schluckfähigkeit").

The theoretical head-capacity characteristic of an impeller is a straight line, the slope of which is determined by the impeller-discharge angle. The location of the bep and hence impeller specific speed is determined by the combined restrictive action of the impeller and casing. The impeller and casing jointly locate the point of minimum combined losses of the unit. The shape of the *Q-H*-curve is determined by the combined hydraulic losses. The restrictive action of the complete unit can be differently divided between the impeller and the casing, i.e., "tight" (narrow) impeller and a rather liberal casing or vice-versa. The restrictive ability of the centrifugal machine should not be connected in any way with the combined resistance to the flow which causes loss of head, but should be thought of as an efficient nozzle that determines the rate of flow. Thus two pumps or blowers of different specific speeds may be equally efficient, but their specific capacities may be greatly different. Specific capacity of similar pumps is the same irrespective of the size. Since, for a given diameter and speed, the head varies slowly with the specific speed, the change in specific speed is mostly determined by the variation of the specific capacity.

Any changes in the casing such as reduction of the volute area, reduction of the diffuser-casing vane angle, or increase of the number of diffuser vanes will reduce the specific capacity. But since head is produced by the impeller alone, it will not change near the bep but the bep will move to a lower capacity and higher head. Or, if the impeller width or eye diameter is increased, or the number of vanes is reduced, the specific capacity will increase but not in proportion to the impeller-discharge-area increase because impeller passages are only one link in a series of passages from the inlet to the outlet.

A low-capacity impeller for a given casing can be obtained by reducing the normal or standard impeller-discharge and eye area in the same ratio. The impeller profile should be kept similar to the original normal impeller. As a result, the bep will move to a lower capacity and head which can be estimated from the following considerations: If the impeller-discharge and eye area and the volute-throat area are reduced in the same ratio $f < 1$, then the bep capacity will be approximately f-fraction of the normal. But when the casing is left intact, the bep capacity of the low-capacity impeller will be not f-fraction, but a greater fraction f_e of the normal, or

$$f < f_e < 1$$

Assuming that the restrictive ability of the complete unit is equally divided between the impeller and the casing, the capacity factor f_c can be approximately equal to the average

$$f_c = (f + 1)/2$$

This is approximately equal to the formula suggested by Esman [4]

$$f_c = f^{1/2} \tag{29}$$

The latter being slightly lower and perhaps safer. For instance, if $f = 2/3$, $f_c = 1.667/2 = 0.833$, and $f_c^{1/2} = 0.816$.

Fig. 15 showing the performance of four impellers in the same casing indicates that the location of bep follows equation (29) approximately [9]. The bep head can be estimated in the following manner: For low-capacity impellers (A, B, C) at capacities $f \times$ (bep capacity) of the normal impeller, the head is the same as that at the bep of the normal impeller (points $\dot{B}$ and $\dot{C}$). At zero capacity the Q-H-curves tend to come to a common point slightly to the left of the zero-capacity point. Thus the head-capacity curve of the low-capacity impellers can be drawn by eye through one point and a common zero-capacity point. The foregoing procedure for estimating the head of the low-capacity impeller does not apply to high-capacity impellers. Due to the casing-area limitation (volute throat), the Q-H-curve of the high-capacity impeller does not develop normally enough to locate the $f \times$ (bep capacity) capacity ($f > 1$). An alternate and more direct method of bep head determination with the aid of the chart in Fig. 8 is suggested in the following.

Note that, although the specific speed of the low-capacity impeller is lower, the bep heads are lower than the normal head. Due to the pump casing being too large for the low-capacity impellers, the bep is moved to the higher capacity and hence lower head than the impeller dimensions would indicate.

This also is evident from Fig. 8 where the bep of four impellers are plotted, the lower-capacity impellers moving to a lower head coefficient ψ and higher capacity coefficient ϕ. All four points fall on a constant $\beta_2 = 27$-deg line. Fig. 8 (enlarged) also can be used for determination of head (ψ) when capacity is estimated with the aid of equation (29).

Fig. 16 reproduced from reference [4] shows the decrease of shutoff head for low-capacity impellers in terms of the ratio of the impeller-discharge area of low capacity to that of the normal

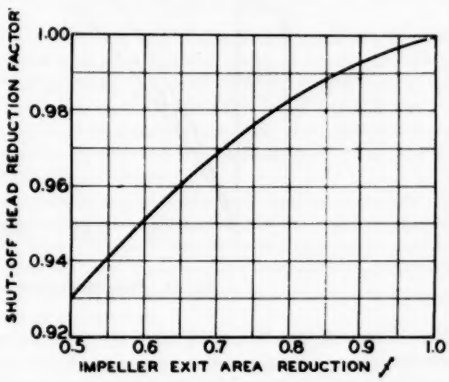

Fig. 16 Shutoff head reduction for low-capacity impellers (Esman)

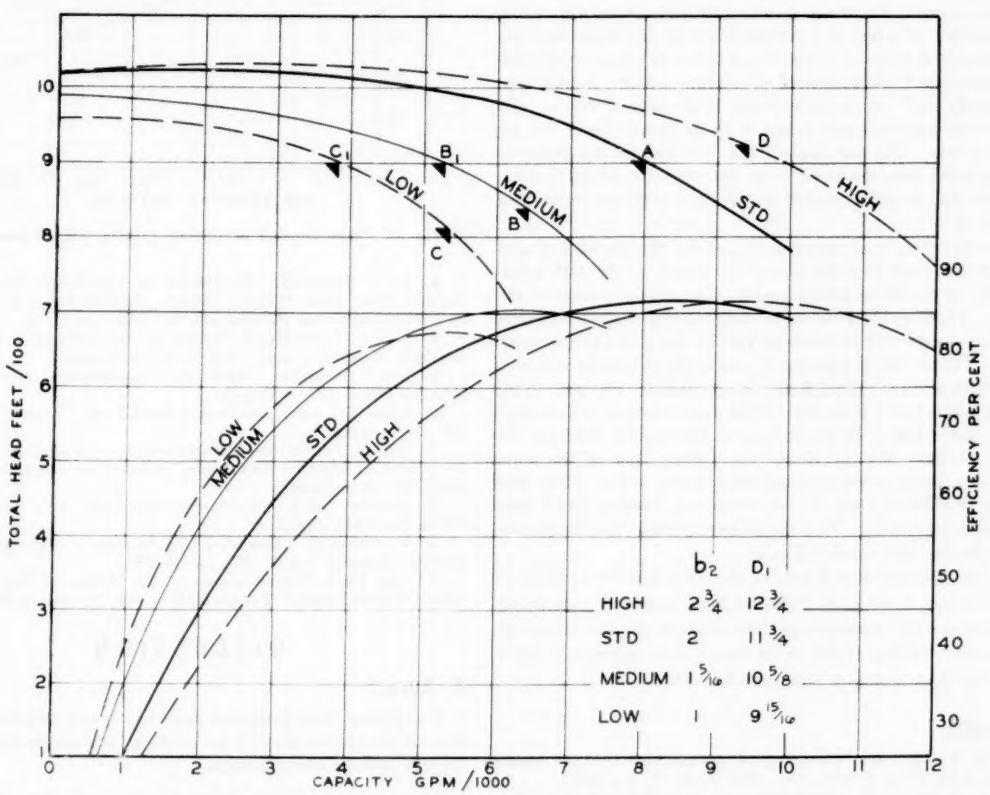

Fig. 15 14-in. 2-stage pump; 1780 rpm; $D_2 = 21\frac{1}{2}$ in., $\beta_2 = 27$ deg; 8 vanes (Lobanoff)

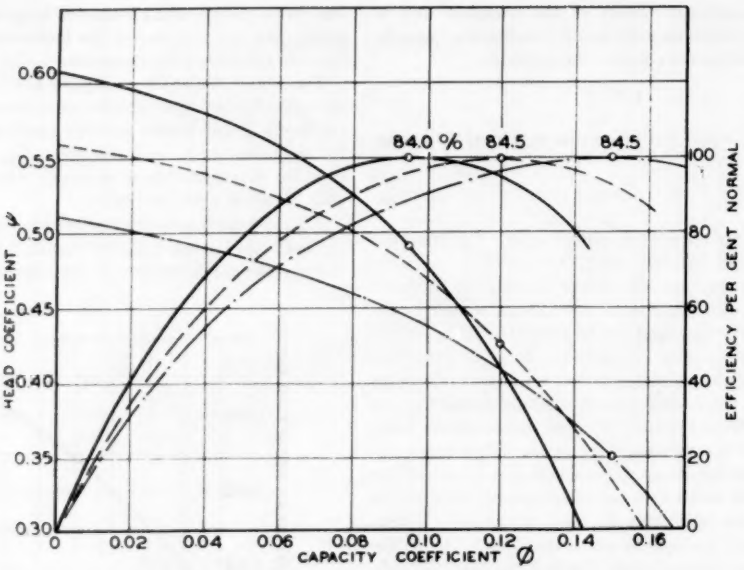

Fig. 17 Performance same impeller in three different volute cases (Krisam)

impeller. The test data in Fig. 15 agree satisfactorily with the curve in Fig. 16.

To estimate performance of the same impeller in two different casings of the same type (volutes) the same reasoning as the foregoing is applied. It is assumed that the restrictive ability of the complete pump or blower is equally divided between the casing and impeller. If a test in a normal volute is available, then the bep capacity of the same impeller in a different volute, which has the throat area f times that of the normal volute, is equal approximately to $f^{1/3}$ times bep capacity in the normal volute. To estimate the bep head plot ϕ and ψ on the chart, Fig. 8, for the normal volute. The new bep will fall on a straight line connecting this point with the point C on the chart (constant β_2-line). Then the head ψ can be read off on this line for the new estimated capacity ϕ.

Since the theoretical head produced by the impeller (input head) is the same in both cases, the shape of the test head-capacity curve will be determined by the hydraulic losses in the volute. These will be lower in the large volute at capacities over the normal and will be lower at partial capacities in the small volute. Hence the head-capacity curve in the large volute is flatter with a lower shutoff head. In general, the bep head in the large volute is lower than that of the same impeller in the small volute, but is higher than the head in the smaller volute at the same capacity. Fig. 17 shows the performance of the same impeller in three volutes of different throat areas. Note that the bep in different cases lie on a common tangent to all three head-capacity curves. This should be expected from the properties of the universal chart in Fig. 8.

Fig. 18 shows the shutoff head of the same impeller in different volute casings in per cent of shutoff head in the normal casing, plotted against the ratio of capacities at bep in per cent of normal. The points from Fig. 17 fall on the same line irrespective of which one out of three casings is taken as a normal.

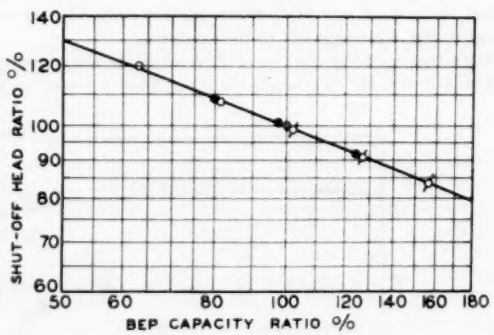

Fig. 18 Same impeller in different volutes; shutoff head ratio

References

1 A. J. Stepanoff, "Centrifugal and Axial Flow Pumps," second edition, John Wiley & Sons, Inc., New York, N. Y., 1957.

2 A. J. Stepanoff, "Turboblowers," John Wiley & Sons, Inc., New York, N. Y., 1955.

3 A. J. Stepanoff, "Cavitation in Centrifugal Pumps With Liquids Other Than Water," TRANS. ASME, Series A, JOURNAL OF ENGINEERING FOR POWER, vol. 83, 1961, pp. 77–79.

4 Esman, "Centrifugal Pumps for the Petroleum Industry," Machgis, Moscow, Russia, 1951, p. 90 (in Russian).

5 Lewis Bergeron, "Machines Hydrauliques," Dunod, Paris, France, 1928, p. 237 (in French).

6 Klein, Schanzlin, and Becker Hand Book, "Pumpen," 1959, p. 106 (in German).

7 Terada, "Variation of Characteristics of Centrifugal Pumps by Reduction of Impeller Diameters," Library of Congress Number 621.67.01 (in Japanese).

8 Grabow, "ZEK Pumpen und Verdichter," vol. 1, 1959, Halle, DDR, East Germany, p. 12.

9 V. Lobanoff, "Designing the Modern Centrifugal Pump," *Pipeline Industry*, vol. 6, 1957, pp. 36–40.

10 Carl Blom, "Development of the Hydraulic Design for the Grand Coulee Pumps," TRANS. ASME, vol. 72, 1950, p. 53.

DISCUSSION

A. Kovats[2]

The authors have presented again a new and notable contribution to the knowledge of rules existing between design elements and the performance of pumps.

[2] Chief-Engineer-Pumps, Foster Wheeler Corp., New York, N. Y. Mem. ASME.

There is only one point where I cannot completely agree with the authors. This is equation (24), wherein the shutoff head in dimensionless form is constant = 0.585 for pumps and blowers with an 85 per cent or better efficiency.

Even if the shutoff head of the most common pumps is close to 0.585, there is no relation between this value and the best efficiency. Many high specific speed pumps (N_s = 4000 to 6000) have 10 to 15 per cent lower shutoff heads and have over-all efficiencies as high as 90 per cent.

One of the recent improvements in the field of high specific speed pumps was the lowering of the shutoff head, because it also decreases the shutoff horsepower without affecting the efficiency.

Also, Fig. 17 of the paper shows performance curves of an impeller in three different casings and the combination with the highest efficiency values have shutoff heads of 0.51 and 0.56.

There are other design elements which affect the shutoff head. Guide vanes or ribs close to the impeller eye raise the shutoff head and they are commonly used with very low specific speed impellers, to assure a constantly rising characteristic. On the other hand, removing ribs from the impeller entrance of axial flow pumps decreases the shutoff head and horsepower considerably without changing the head, capacity, and efficiency at the design point.

Regarding the dimensionless value of the shutoff head I would rather say that in addition to the impeller-casing relationship it also depends on the ratio of the impeller-blade inlet and outlet diameters and on the inlet guidance of the fluid.

Authors' Closure

Mr. Kovats has expressed some doubts as to the validity of the equation (24) of the paper, which gives the value of the shutoff head in the dimensionless form as equal to 0.585 irrespective of specific speed and the impeller discharge angle. He quotes a few examples of deviations from the above value caused by changes in one or more parts comprising a pump. In this connection it should be borne in mind that in a study of pump performance covering a wide range of specific speeds it is usually assumed that all pumps belong to one consistent and continuous row of hydraulic types. By this is meant that the controlling design elements and their effects, such as shutoff head, are continuous. To minimize the effect of scale it is desirable to have all pumps of good efficiency. Efficiency otherwise has no direct connection with the observed variation of the design constants or their effect.

Equation (24) was one of the first generalized relationships that evolved from such a study. This demonstrated the utility of the concept of the "mean effective impeller diameter" used in this article. It is on the basis of this concept that it was possible to organize the design and performance information of the charts similar to Fig. 8, covering the whole field of centrifugal pumps including axial flow pumps.

The authors were aware of the numerous exceptions to the rules suggested by such charts, but in every case it was possible to trace the reason for such results to the change in one or more design elements from those which constituted a continuous and consistent line. Such deviations and exceptions were expected and were well understood.

Cases quoted by Mr. Kovats are of such nature. It depends upon the skill of the designer to recognize the deviations from the normal design and estimate their effect on the pump performance.

The Significance of the Hall Effect for Three MHD Generator Configurations

L. P. HARRIS
J. D. COBINE
General Electric Research Laboratory, Schenectady, N. Y.

Analyses are presented for the influence of the Hall effect on electrical terminal characteristics, generated power per unit volume, pressure gradient, and generator efficiency in three configurations for MHD generators. The results indicate that desirable generator characteristics can be attained when the Hall effect is either negligible or dominant.

Introduction

Because most published treatments of MHD generators have dealt with only one generator configuration, the impression is widespread that the Hall effect in gaseous conductors imposes severe limits on the power density attainable in such generators. We show here, after a preliminary review of the origins of the Hall effect, that there are generator configurations suited for use at high values of B/p, the ratio of magnetic flux density to pressure, where the Hall effect is dominant, as well as at low values of B/p, where the Hall effect can be neglected.

Conductivities and the Hall Effect

The Hall effect is a phenomenon arising when electric currents flow in a conductor subjected to a magnetic field. Then the components of electric field and electric current density in the plane perpendicular to the magnetic field are not parallel, but are displaced from parallelism by a definite angle characteristic of the magnetic flux density and the properties of the conductor. This effect is found in all types of conductors, solids, liquids, and gases, and occurs because the magnetic field exerts forces on moving charged particles in addition to the electrostatic forces caused by electric fields.

Because the Hall effect is so basic a physical phenomenon, it can be found even in the most simple models of electric conduction. Here we review the origins of this effect in terms of the model sketched in Fig. 1, in which the conduction electrons move in response to the constant applied vector force $\underline{F}_e$ with a steady-state vector drift velocity $\underline{v}_e$ given by

$$\underline{v} = \frac{\mu_e}{e}\,\underline{F}_e \qquad (1)$$

The quantity e is the magnitude of the electronic charge, and μ_e a constant (for sufficiently small values of F_e) called the electronic mobility. Equation (1) indicates that the conduction electrons are treated as particles subject to the applied force $\underline{F}_e$ and to an internal damping force provided by interactions between the electrons and the other particles they encounter as they drift through the conductor.

The results obtained from this model agree qualitatively with those derived from all the more sophisticated models of electric conduction and are identical to those gained from the "constant collision frequency" model, in which the electronic mobility is assumed independent of electron energy [1].[1]

Fig. 2 illustrates the situation when only an electric field $\underline{E}'$,

[1] Numbers in brackets designate References at end of paper.

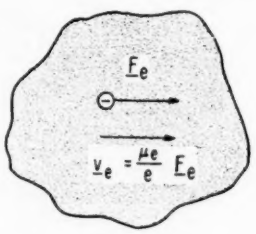

Fig. 1 Basic model for steady-state electronic mobility

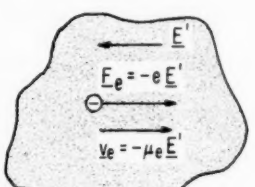

Fig. 2 Electron drift caused by electric fields only

Contributed by the Fuels Division and presented at the Winter Annual Meeting, New York, N. Y., November 27–December 2, 1960, of The American Society of Mechanical Engineers. Manuscript received at ASME Headquarters, October 27, 1960. Paper No. 60—WA-329.

Nomenclature

B = magnetic-flux density
E' = electric field in fluid reference frame
E = electric field in stationary reference frame
e = {electronic charge; electrons (subscript)}
F = force
h = specific enthalpy of gas
i = ions (subscript)
J = electric current density
L = load (subscript)
M = gas molecular weight
N = particle density
n = load-resistance parameter, equation (18)
oc = open-circuit conditions (subscript)
P = electric power output per unit volume
p = gas pressure
R = universal gas constant
ss = short-circuit conditions (subscript)
T = gas temperature
u = gas flow velocity
v = particle drift velocity
x, y, z = {rectangular co-ordinates; rectangular components (subscript)}
β = Hall-effect parameter, equations (10, 13)
γ = specific-heats ratio
η = local conversion efficiency, equation (25)
μ = particle mobility
ρ = gas density
σ_0 = electronic conductivity of gas
$\perp$ = perpendicular to magnetic field (subscript)

measured by an observer stationary with respect to the conductor, acts on the conduction electrons. Now the force $\underline{F}_e$ is

$$\underline{F}_e = -e\underline{E}'$$

and, from Eq. (1), the drift velocity is

$$\underline{v}_e = -\mu_e\underline{E}'. \tag{2}$$

If there are N_e conduction electrons per unit volume, the electronic current density $\underline{J}_e$ is

$$\underline{J}_e = -N_e e\underline{v}_e, \tag{3}$$

which, by use of Eq. (2), can be expressed as

$$\underline{J}_e = N_e e\mu_e\underline{E}'. \tag{4}$$

Equation (4) has the form of Ohm's law

$$\underline{J}_e = \sigma_0\underline{E}' \tag{5}$$

with the conductivity σ_0 given by the well-known formula

$$\sigma_0 = N_e e\mu_e. \tag{6}$$

When both an electric field $\underline{E}'$ and a magnetic flux $\underline{B}$ are present, the force on the electron is

$$\underline{F}_e = -e(\underline{E}' + v_e \times \underline{B})$$

and, from Eq. (1), the drift velocity is

$$\underline{v}_e = -\mu_e(\underline{E}' + \underline{v}_e \times B). \tag{7}$$

Equation (7) can be split into components parallel to and perpendicular to the magnetic flux density B. The equation for drift velocities parallel to the magnetic field has the form of Eq. (2), and currents and electric fields parallel to B are related by equations like Eqs. (5) and (6). The geometry for the drift velocity and electric field components in the plane perpendicular to $\underline{B}$ is sketched in Fig. 3; the y-axis of the co-ordinate system is chosen parallel to $\underline{B}$. Equation (7) then yields two simultaneous algebraic equations relating the x and z-components of $\underline{E}'$ and $\underline{v}_e$:

$$\left.\begin{aligned} v_{ex} - \mu_e B v_{ez} &= -\mu_e E_x' \\ \mu_e B v_{ex} + v_{ez} &= -\mu_e E_z' \end{aligned}\right\}. \tag{8}$$

and

These have the solutions

$$\left.\begin{aligned} v_{ex} &= -\frac{\mu_e}{1 + (\mu_e B)^2}(E_x' + \mu_e B E_z') \\ v_{ez} &= -\frac{\mu_e}{1 + (\mu_e B)^2}(E_z' - \mu_e B E_x') \end{aligned}\right\}. \tag{9}$$

and

If β_e is defined by

$$\beta_e = \mu_e B, \tag{10}$$

then the electric current densities for the co-ordinates of Fig. 3 can be written as

$$\left.\begin{aligned} J_{ex} &= \frac{\sigma_0}{1 + \beta_e^2}(E_x' + \beta_e E_z') \\ J_{ey} &= \sigma_0 E_y' \\ J_{ez} &= \frac{\sigma_0}{1 + \beta_e^2}(-\beta_e E_x' + E_z') \end{aligned}\right\} \tag{11}$$

where σ_0 is given by Eq. (6). The physical content of Eqs. (11) can be expressed by three rules: (1) The relation between currents and electric fields parallel to the magnetic field $\underline{B}$ is not affected by the presence of $\underline{B}$; (2) the current density component

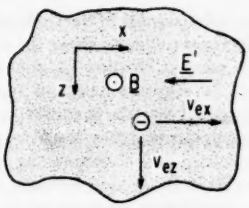

Fig. 3 Geometry for electron drift in crossed electric and magnetic fields

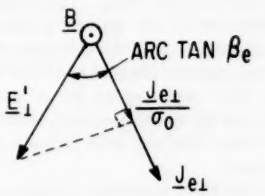

Fig. 4 Relations between current and electric field components perpendicular to the magnetic field

$\underline{J}_{e\perp}$ perpendicular to $\underline{B}$ is displaced in angle clockwise about $\underline{B}$ from the electric field component $E'_\perp$ perpendicular to $\underline{B}$ by an amount arctan β_e; (3) the projection of $E'_\perp$ on $J_{e\perp}$ has the magnitude $J_{e\perp}/\sigma_0$ (Tonk's theorem) [1]. The last two rules are illustrated in Fig. 4.

For conduction in gases under conditions where β_e takes very large values, greater than 10 or 15, Eqs. (11) must be corrected for the currents carried by positive ions, whose mobility we denote by μ_i. This correction is simple because the inequalities

$$\mu_i \ll \mu_e \tag{12}$$

and

$$\mu_i B \triangleq \beta_i \ll 1 \tag{13}$$

always hold for the operating conditions in MHD generators. That is, the ionic mobilities are much less than electronic mobilities and the Hall effect within the ion system is negligible. Thus the ion current density $\underline{J}_i$ can be written as

$$\underline{J}_i = N_i e\mu_i\underline{E}'. \tag{14}$$

The addition of the ion current of Eq. (14) to the electron current of Eq. (11) yields for the approximate components of the total current density $\underline{J}$

$$\left.\begin{aligned} J_x &= \frac{\sigma_0}{1 + \beta_e^2}[(1 + \beta_i\beta_e)E_x' + \beta_e E_z'] \\ J_y &= \sigma_0 E_y' \\ J_z &= \frac{\sigma_0}{1 + \beta_e^2}[-\beta_e E_x' + (1 + \beta_i\beta_e)E_z'] \end{aligned}\right\}. \tag{15}$$

Here we have used Eq. (12) and the neutrality condition, $N_e = N_i$. The rules relating the components $\underline{J}_\perp$ and $\underline{E}_\perp$ differ little from those given before for the electronic currents. The angle between $\underline{J}_\perp$ and $\underline{E}_\perp$ is the arctan $(\beta_e/1 + \beta_i\beta_e)$, and the projection of $\underline{E}_\perp$ on $\underline{J}_\perp$ has the magnitude $(1 + \beta_i\beta_e)J_\perp/\sigma_0$.

Three Generator Configurations

Figs. 5 and 6 contain schematic drawings of the two MHD generator configurations that have received greatest attention to date. Both these schemes use the transverse currents and voltages generated to extract electric power from the enclosed flow. Fig. 5 illustrates the generator [2] in which the electrodes

are broken up into isolated pairs of electrode segments, each with its own isolated electrical subload. Since the purpose of electrode segmentation is to prevent the flow of axial currents, the axial length occupied by a segment pair and its insulating spacer should be small compared with the channel span in the z-direction. Thus a practical generator probably would require 20 to 50 pairs of electrode segments. The corresponding subdivision of the electrical load into 20 to 50 isolated subloads represents a severe handicap to this configuration for many applications.

Fig. 6 shows the generator [3] with continuous electrodes. In this generator there should be no electric field parallel to the flow, but large axial currents can exist. This design might be considered a modification of the preceding one, in which short-circuiting connectors join all the electrode segments on each side of the channel, thereby paralleling all the electrical subloads and permitting their replacement by a single load resistor. This scheme removes the major objection to the preceding design, but suffers itself from relatively poor performance when the Hall effect is pronounced.

Fig. 7 illustrates a third generator configuration that has been developed recently. In appearance it too seems a modification of the first design. Here the previous electric subloads are replaced by short-circuiting connections and the total electrical load is connected between the electrode-segment pairs nearest the generator entrance and exit. Its principle of operation differs from that of the two preceding configurations, for electric power extraction is accomplished here by use of axial currents and voltages. The transverse currents serve here only to provide the necessary mechanical resistance to the flow. In these respects this configuration resembles the Karlovitz generator [4]. This new design provides a two-terminal electrical output and, because its operation depends on the existence of the Hall effect, a performance that is good when the Hall effect is pronounced.

In many respects, such as requirements on structural design, gas conductivity, gas-electrode electrical contact, and mechanical flow characteristics, these three types of generators are substantially equivalent. There are interesting differences, however, in the electrical terminal characteristics and in variations with operating conditions of the generated power per unit volume, pressure gradient, and generator efficiency. To permit a simple analysis of these differences we neglect any distortion in the currents and voltages within the channel caused by finite size of electrode segments or the variation in area of the channel along its flow axis. Then the constraints on the current densities $\underline{J}$ and the electric fields $\underline{E}$ (measured in stationary co-ordinates) imposed by the construction of each generator are:

$$\left.\begin{aligned} &\text{generator (1): } J_y = 0, \quad J_z = 0 \\ &\text{generator (2): } J_y = 0, \quad E_z = 0 \\ &\text{generator (3): } J_y = 0, \quad E_z = 0 \end{aligned}\right\}. \tag{16}$$

Equations (15), (16), and the transformation

$$\underline{E}' = \underline{E} + \underline{v} \times \underline{B} \tag{17}$$

determine the fields and currents in the generators. Here $\underline{v}$ is the fluid velocity in the generator. These solutions are tabulated in Table 1 in terms of σ_0, β_i, β_e, B, u, and the parameter n defined as

$$n \triangleq \frac{\text{load resistance}}{\text{load resistance} + \text{internal resistance}}. \tag{18}$$

Equations (12) and (13) have been used in deriving these results.

The electric field E_{Loc} between the load terminals at open-circuit conditions and the short-circuit load-current density J_{Lss} for the three generators are:

$$\left.\begin{aligned} &\text{generator (1): } E_{Loc} = uB, \quad J_{Lss} = \frac{1}{1+\beta_i\beta_e}\,\sigma_0\,uB \\ &\text{generator (2): } E_{Loc} = uB, \quad J_{Lss} = \frac{1+\beta_i\beta_e}{1+\beta_e^2}\,\sigma_0\,uB \\ &\text{generator (3): } E_{Loc} = \frac{\beta_e}{1+\beta_i\beta_e}\,uB, \\ &\qquad\qquad\qquad\qquad J_{Lss} = \frac{\beta_e}{1+\beta_e^2}\,\sigma_0\,uB \end{aligned}\right\} \tag{19}$$

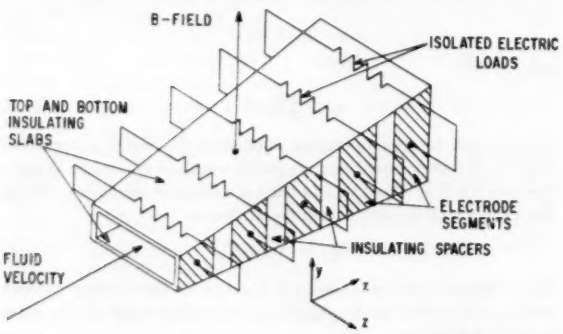

Fig. 5 Generator (1)—transverse power extraction, segmented electrodes

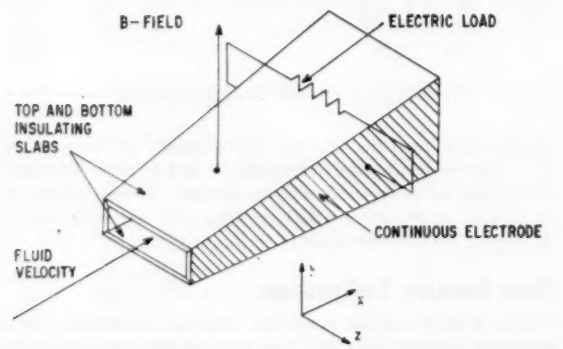

Fig. 6 Generator (2)—transverse power extraction, continuous electrodes

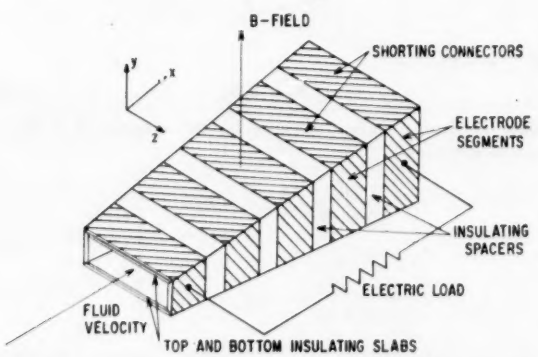

Fig. 7 Generator (3)—axial power extraction

The output powers P per unit channel volume are:

$$\left.\begin{aligned}
&\text{generator (1):}\quad P = \frac{1}{1+\beta_i\beta_e}\,\sigma_0 u^2B^2n(1-n)\\
&\text{generator (2):}\quad P = \frac{1+\beta_i\beta_e}{1+\beta_e^2}\,\sigma_0 u^2B^2n(1-n)\\
&\text{generator (3):}\quad P = \frac{\beta_e^2}{(1+\beta_e^2)(1+\beta_i\beta_e)}\,\sigma_0 u^2B^2n(1-n)
\end{aligned}\right\} \tag{20}$$

In addition to the indications of impedance levels and densities of generated power, we need measures of the efficiencies of energy conversion in the three generators. A high power density has little value in large power systems unless it is accompanied by a high conversion efficiency. Estimates of efficiencies are obtained from the momentum and energy balances for the flow.

When we neglect inertial forces (constant-velocity generator) and friction forces, the momentum balance reduces to an equality between pressure forces and electromagnetic forces:

$$\frac{dp}{dx} = -J_yB. \tag{21}$$

Use of Table 1 then gives, for $\beta_i\beta_e \ll 1$;

$$\left.\begin{aligned}
&\text{generator (1):}\quad \frac{dp}{dx} = -\sigma_0\, uB^2(1-n)\\
&\text{generator (2):}\quad \frac{dp}{dx} = -\sigma_0\, uB^2\,\frac{1-n}{1+\beta_e^2}\\
&\text{generator (3):}\quad \frac{dp}{dx} = -\sigma_0 uB^2\,\frac{1+n\beta_e^2}{1+\beta_e^2}
\end{aligned}\right\} \tag{22}$$

If we neglect heat transfer to the outside and changes in gas kinetic energy in the generator, the energy balance for the generators can be written

$$\rho u\frac{dh}{dx} = \underline{E}\cdot\underline{J} \tag{23}$$

where ρ and h are the mass density and specific enthalpy of the gas flow. Use of the ideal-gas relations

$$p = \rho\frac{R}{M}\,T,$$

$$h = \frac{\gamma}{\gamma-1}\,\frac{R}{M}\,T,$$

where R, M, T, and γ are the universal gas constant, the gas molecular weight, gas temperature, and specific-heats ratio, transforms Eq. (23) to the form

$$\frac{\gamma}{\gamma-1}\,\frac{pu}{T}\,\frac{dT}{dx} = \underline{E}\cdot\underline{J},$$

which combines with Eq. (21) to yield

$$\frac{\gamma}{\gamma-1}\,\frac{d(\ln T)}{d(\ln p)} = -\frac{\underline{E}\cdot\underline{J}}{uJ_yB} \tag{24}$$

The right side of Eq. (24) is the ratio of the electrical power output per unit volume to the mechanical power per unit volume expended by the flow in pushing against the electromagnetic forces. This ratio is approximately equal to the effective generator efficiency defined, by analogy with turbine practice, as the ratio of the power output of an actual generator to that of an adiabatic, reversible machine operating with the same inlet temperature and inlet and outlet pressures. (This approximation is close to the correct result when the percentage change in pressure through the generator is small. For finite pressure drops the right side of Eq. (24) is somewhat less than the generator efficiency.) If we represent the right side of Eq. (24) by the symbol η, this equation can be integrated to yield

$$\frac{T}{T_0} = \left(\frac{p}{p_0}\right)^{\eta\frac{\gamma-1}{\gamma}}$$

when η is a constant. When $\eta = 1$, this result reduces to the familiar form for a reversible adiabatic process.

Use of Eq. (24) and Table 1 yields

$$\left.\begin{aligned}
&\text{generators (1) and (2):}\quad \frac{\gamma}{\gamma-1}\,\frac{d(\ln T)}{d(\ln p)}\,\underline{\Delta}\eta = n\\
&\text{generator (3):}\quad \frac{\gamma}{\gamma-1}\,\frac{d\,(\ln T)}{d\,(\ln p)}\,\underline{\Delta}\eta = (1-n)\,\frac{n\beta_e^2}{1+n\beta_e^2}
\end{aligned}\right\} \tag{25}$$

for the efficiencies of the three configurations when $\beta_i\beta_e \ll 1$.

Table 1 Solutions for currents and electric fields

Generator (1)

$$J_x = 0$$

$$J_z = \frac{1}{1+\beta_i\beta_e}(1-n)\sigma_0 uB$$

$$E_x = E_x' = -\frac{\beta_e}{1+\beta_i\beta_e}(1-n)uB$$

$$E_z = -nuB,\ E_z' = (1-n)uB$$

Generator (2)

$$J_x = \frac{\beta_e}{1+\beta_e^2}\,\sigma_0 uB(1-n)$$

$$J_z = \frac{1+\beta_i\beta_e}{1+\beta_e^2}\,\sigma_0 uB(1-n)$$

$$E_x = E_x' = 0$$

$$E_z = -nuB,\ E_z' = (1-n)uB$$

Generator (3)

$$J_x = \frac{\beta_e}{1+\beta_e^2}(1-n)\sigma_0 uB$$

$$J_z = \frac{n\beta_e^2 + (1+\beta_i\beta_e)^2}{(1+\beta_e^2)(1+\beta_i\beta_e)}\,\sigma_0\, uB$$

$$E_x = E_x' = -\frac{\beta_e}{1+\beta_i\beta_e}\,nuB$$

$$E_z = 0,\ E_z' = uB$$

Discussion of Results

Equations (19) and (20) indicate that the performance of each of the generators is poor if $\beta_i\beta_e > 1$. In this range, the positive ions no longer are tied effectively by collision processes to the neutral gas atoms, and one link in the chain of processes transferring the thermal energy of the gas to an external electrical load is weakened seriously. The range $\beta_i\beta_e < 1$, which allows values

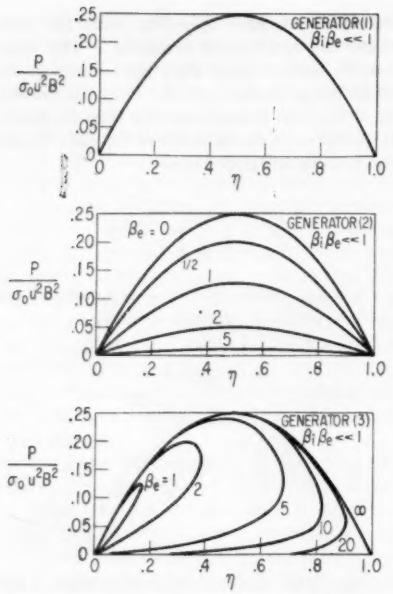

Fig. 8 Relations between power and efficiency for the three generators

of β_e as large as 30 to 50, includes all conditions of interest for MHD power generation. Within this range of interest, Eqs. (19), (20), (22), and (25) indicate that the performance of generator (1) is independent of β_e. Generator (2) tends to approximate the performance of (1) when $\beta_e \ll 1$; but it deteriorates in power density as β_e increases. Generator (3) provides power densities and efficiencies comparable to those of (1) when $B_e \gg 1$, but is poor in both these factors when β_e is small.

Fig. 8 contains plots of the ratio $P/(\sigma_0 u^2 B^2)$ versus the efficiency factor η. The plot for generator (1) is the parabola

$$\frac{P}{\sigma_0 u^2 B^2} = \eta(1 - \eta).$$

For generator (2), it is a series of similar parabolas that are increasingly confined to the low-power-density region as β_e increases. The curves for generator (3) are more complex and vary from the single point (0, 0) for zero β_e to the parabola of generator (1) for infinite β_e. For small β_e these curves are confined entirely to the low-efficiency region. From these graphs we can conclude that, for operation at high power densities and efficiencies exceeding eighty per cent, generator (1) can be used for all values of β_e, generator (2) for values $\beta_e < 1$, and generator (3) for $\beta_e > 10$.

The practical significance of these results depends on the variation of β_e with the operating parameters of the generator. For all working gases we can express β_e as

$$\beta_e = K\frac{B}{p}$$

where K depends on the operating temperature and gas composition. For air-like gases, such as nitrogen or combustion gases, seeded with a few per cent of alkali vapor, K is about 1.5 or 2 in the 1500 to 2500 K temperatures of interest for MHD generators, if B is expressed in webers/meters^2 and p in atmospheres. For an alkali-seeded helium gas K is between 2 and 3, and for seeded argon somewhere in the range 20 to 50. Then for operating pressures between 1 and 10 atmospheres and magnetic flux densities between 0.5 and 5.0 webers/m^2 (5000–50,000 gauss), it appears that generators (1) and (2) are the designs best suited for use with air-like body gases or helium, and generators (1) and (3) for the high-electron-mobility gases such as argon.

Conclusions

The generator configurations described here can provide high power density, high efficiency, and two-terminal electrical outputs either when the Hall effect is moderate, $\beta_e < 1$, or when it is dominant, $\beta_e > 10$. In the intermediate range, $1 < \beta_e < 10$ operations suffer from low power density or low efficiency unless a multiterminal electrical output can be used.

References

1 W. P. Allis, "Motion of Ions and Electrons," *Handbuch der Physik*, vol. 21, 1956.

2 L. Steg and G. W. Sutton, "Prospects of MHD Power Generation," *Astronautics*, vol. 5, No. 8, August, 1959.

3 R. J. Rosa and A. Kantrowitz, "Magnetohydrodynamic Energy Conversion Techniques," in book "Direct Conversion of Heat to Electricity," J. Kaye and J. A. Welsh, Editors, John Wiley & Sons, Inc., New York, N. Y., 1960.

4 B. Karlovitz, et al., "Process for the Conversion of Energy and Apparatus for Carrying Out the Process," U. S. Patent 2,210,918, August 13, 1940.

S. WAY
Mem. ASME

S. M. DeCORSO
Mem. ASME

R. L. HUNDSTAD

G. A. KEMENY
Mem. ASME

W. STEWART

W. E. YOUNG
Mem. ASME

Westinghouse Research Laboratories, Pittsburgh, Pa.

Experiments With MHD Power Generation

This paper is a report on the development of an experimental MHD electrical generator which derives its energy from the combustion of a liquid fuel and oxygen. The fuel burned is a number 2 distillate oil in which a soluble potassium octoate is mixed to increase the degree of thermal ionization in the product gas. The actual generating volume is approximately 125 cubic inches and the rating of 10 KW has been exceeded.

The paper describes some of the broad construction features of the generator and problems arising during its operation. Other sections deal with the fuel and combustion systems, fuel characteristics, and the electrical and magnetic aspects. The theory of MHD power generation in a uniform duct is presented. Results of the experiments are presented and actual performance compared with theory. The paper is illustrated with photographs and sketches of the various components and curves of power and voltage.

1 Introduction

The conventional process of generating electrical power consists of moving metallic conductors in the presence of a magnetic field. The idea of using fluid conductors is quite old and was considered, in fact, by Faraday [1][1] in 1831; he experimented with mercury flowing in a glass tube between the poles of a magnet, and proposed use of tidal currents in the terrestrial magnetic field for power generation.

These devices would convert mechanical power to electrical power. If one is interested in conversion of thermal to electrical power it is necessary to use a gas instead of a liquid conductor in order to realize a volume change. Numerous references in this connection appear in the patent literature [2, 3, 4, 5]. Experiments were made with a gaseous magnetohydrodynamic (MHD) generator in the period 1938–1944 by B. Karlovitz [5]. The Karlovitz device used an axial electric field. Because of the particular field arrangement chosen and because of the low gaseous conductivity realized, this generator did not develop appreciable power.

Employing the original crossed field arrangement used by Faraday in the mercury experiments, and proposed for a gaseous generator by Rudenberg [2], one can set up an operable MHD generator that puts out appreciable amounts of power. Experiments with such generators have recently been reported. In contrast to some earlier investigations [6, 7, 8, 12] in which the gas was heated by an electric arc, the present work deals with a combustion gas system [9, 10]. The use of combustion products for direct MHD generation of power is of considerable practical interest as it circumvents development of an elaborate nuclear reactor.

Thermal cycle studies have shown that if an MHD generator is operated at a temperature above 2500 deg K very attractive cycle efficiencies can be realized. Discussion of such thermal cycles is beyond the scope of this paper. The reader is referred to references [9] and [11]. It should be emphasized that the realization in working power plants of the anticipated high efficiencies is some years away, and hinges upon the solution of

[1] Numbers in brackets designate References at end of paper.

Contributed by the Fuels Division and presented at the Winter Annual Meeting, New York, N. Y., November 27–December 2, 1960, of The American Society of Mechanical Engineers. Manuscript received at ASME Headquarters, October 27, 1960. Paper No. 60—WA-328.

Nomenclature

x, y, z = rectangular co-ordinates
L, b, d = generator length, breadth, and depth, meters
$\vec{u}$ = velocity, meters/second
$\vec{B}$ = magnetic induction, webers/meter²
$\vec{E}$ = electric intensity, volts/meter
$\vec{F}$ = electromagnetic body face, newtons/meter³
$\vec{j}$ = current density, amperes/meter²
σ = gas conductivity, mhos/meter
u_x, u = x-component of velocity
B_y, B = y-component of magnetic induction
E_z, E = z-component of electric intensity
j_z, j = z-component of current density
F_x = x-component of body force
V = potential difference between electrodes, volts
δV = combined electrode drop, volts
ρ = gas density, kg/meter³
p = pressure, newtons/meters²
h = specific enthalpy, joules/kg
R_g = gas constant, joules/kg deg K
T = gas temperature, degrees Kelvin
γ = ratio of specific heats of gas
T_t = total temperature of gas, deg K
M = flow Mach number at any point
w = mass flow rate, kg/sec
C_1, C_2, C_3, C_4 = constants defined in Eq. (14)
δ = ratio defined in Eq. (14)
ϕ = a function of u/u_0 defined by Eq. (17)
λ_1, λ_2 = functions of u/u_0, C_3, and C_4
K_1, K_2, K_3 = functions of C_1, C_2, C_3, C_4
ϕ_1 = value of ϕ for $u = u_1$ and $x = L$
V^* = theoretical open circuit voltage
$F(\bar{T})$ = temperature dependent part of σ
$\bar{p}, \bar{T}$ = mean values of p and T in generator
R = load resistance, ohms
P = generated power, watts
R_i = internal (gas) resistance of generator, ohms
I = current, amperes
I_a = approximate current, $u_1/u_0 \approx 1$
P_a = approximate power, $u_1/u_0 \approx 1$

(*Continued on next page*)

many technical problems of development and application of high temperature resisting materials. To make a start, the problems of the generator itself are being investigated first. Experiments made with a small generator of about 10-kw capacity, fed by combustion products, are discussed in the present paper. This generator was first run on load in February, 1960, and testing has continued to the present time.

2 Theory of the MHD Generator

We deal with the arrangement shown in Fig. 1. Gas enters a duct of uniform area with speed u_0, pressure p_0, and temperature T_0. The gas is assumed to have a certain concentration of alkali metal atoms to enhance the conductivity.

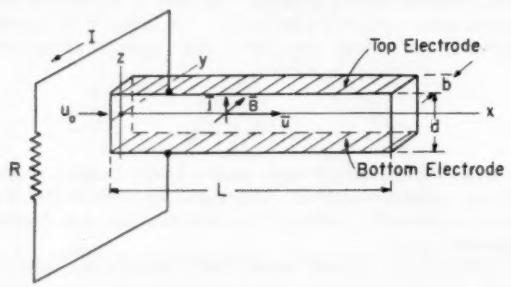

Fig. 1 MHD generator scheme

A uniform magnetic field with magnetic induction $\vec{B}$ is assumed, with $\vec{B}$ in the y-direction. Walls $y = \pm b/2$ are insulators and walls $z = \pm d/2$ are conductors, which serve as electrodes, and are connected to the external circuit of resistance R.

Flow velocity $\vec{u}$ in conjunction with $\vec{B}$ gives rise to the electric field relative to the moving gas

$$\vec{E}' = \vec{E} + \vec{u} \times \vec{B} \tag{1}$$

where field $\vec{E}$ is that due to the difference of potential between the electrodes, as modified by any drop δV at the electrode-gas interfaces. The current density is

$$\vec{j} = \sigma(\vec{E} + \vec{u} \times \vec{B}) \tag{2}$$

A body force $\vec{F}$ will be present in the gas of amount

$$\vec{F} = \vec{j} \times \vec{B} \tag{3}$$

The components of the several vectors may now be summarized

Vector	x-component	y-component	z-component
$\vec{u}$	u_x	0	0
$\vec{B}$	0	B_y	0
$\vec{E}$	0	0	E_z
$\vec{j}$	0	0	j_z
$\vec{F}$	F_x	0	0

We have for E_z, j_z, and F_x:

$$E_z = -\frac{V + \delta V}{d} \tag{4}$$

$$j_z = \sigma(u_x B_y + E_z) \tag{5}$$

$$F_x = -j_z B_y \tag{6}$$

In the following treatment the subscripts will be dropped. Assumptions will be made as follows:

(*a*) State properties and flow speed are uniform over any section.

(*b*) The fluid is a frictionless, compressible perfect gas.

(*c*) Perturbation of the applied magnetic field by the current is neglected.

(*d*) Leakage currents are neglected.[2]

(*e*) Electric conductivity is a scalar quantity, with a value determined by the mean temperature and pressure in the generator duct.

(*f*) Heat losses are neglected.

The governing equations for flow in the MHD duct may then be written as follows: (See Reference [13].)

conservation of mass:

$$\rho u = \rho_0 u_0 \tag{7}$$

[2] Magnetic field overlap tends to reduce such currents. Effects of end leakage in several configurations have been discussed by Steg and Sutton [11].

Nomenclature

h_t = total specific enthalpy, joules/kg
h'_{ti} = enthalpy at inlet entropy and outlet total pressure
η_i = internal generator efficiency
η_e = generator electrical efficiency
η = generator combined efficiency
η' = approximate efficiency by Eq. (36)
μ = electron mobility, meters^2 sec^{-1} volts^{-1}
q_e = electronic charge, 1.6×10^{-19} coulombs
n_e = number of free electrons per cubic meter
ϵ_1, ϵ_2 = concentrations of K atoms and OH particles
α_1, α_2 = fractions ionized of K and OH
n = number of particles per unit volume
V_i = ionization potential, volts
k = Boltzmann constant, 1.38×10^{-23} joules/deg K
m_e = electron mass, kg
v = electron velocity in gas
$f(v)$ = distribution function of velocities
ν = collision frequency, electrons and various species, sec^{-1}
A = duct area, or $b \cdot d$, meters^2
w' = fictitious mass flow rate, Eq. (43)
$V_{obs}{}^*$ = observed value of V^*
V^* = theoretical apparent value of open circuit voltage with leakage currents present
I_{ss} = short circuit current, amperes
R' = external applied resistance, ohms
R^* = leakage resistance, ohms
I' = current to R', amperes
I^* = current to R^*, amperes
$C_2{}^*$ = value of C_2 at condition $I' = 0, I = I^*$
J_B = current from battery in battery test, amperes
V_B = battery voltage
σ_{oth} = conductivity at inlet by theory (Fig. 3)
σ_0 = conductivity at inlet inferred from generator tests

Inlet state indicated by subscript 0 on flow quantities

Outlet state indicated by subscript 1 on flow quantities

Total state indicated by subscript t on flow quantities

conservation of momentum:

$$\frac{d}{dx}(\rho_0 u_0 u + p) = -jB \tag{8}$$

conservation of energy:

$$\rho_0 u_0 \frac{d}{dx}\left(h + \frac{u}{2}\right)^2 = jE \tag{9}$$

gas equations:

$$p = \rho R_g T;\ h = \frac{\gamma}{\gamma - 1},\ \frac{p}{\rho} \tag{10}$$

total temperature ratio:

$$\frac{T_t}{T} = 1 + \frac{\gamma - 1}{2} M^2 \tag{11}$$

Mach number:

$$M = u\sqrt{\frac{\rho}{p\gamma}} \tag{12}$$

mass flow rate:

$$w = \rho_0 u_0 bd \tag{13}$$

It is convenient to introduce the following dimensionless parameters:

$$C_1 = C_4 + \frac{C_3}{2} + C_2(1 + C_3);\ C_2 = \frac{E}{Bu_0};$$

$$C_3 = \gamma M_0^2;\ C_4 = \frac{\gamma}{\gamma - 1};\ \delta = \frac{\delta V}{u_0 Bd} \tag{14}$$

From (7), (8), (9), and (10) one finds a relation of pressure ratio and velocity ratio:

$$\frac{p}{p_0} = \frac{C_1 - C_2 C_3 \frac{u}{u_0} - \frac{C_3}{2}\left(\frac{u}{u_0}\right)^2}{C_2 + C_4 \frac{u}{u_0}} \tag{15}$$

Equations (8) and (5) with substitution for p from (15) then give a relation between x and u:

$$\frac{\sigma B^2 x}{\rho_0 u_0} = \phi\left(\frac{u}{u_0}\right) \tag{16}$$

where

$$\phi\left(\frac{u}{u_0}\right) = K_1 \ln \lambda_1 + K_2 \ln \lambda_2 + \frac{1 - \frac{p}{p_0}\lambda_1 - K_3 C_3(1 - \lambda_1)}{C_3(C_2 + 1)} \tag{17}$$

$$\lambda_1 = \frac{C_2 + 1}{C_2 + \frac{u}{u_0}};\ \lambda_2 = \frac{C_2 + C_4}{C_2 + C_4 \frac{u}{u_0}}$$

$$K_1 = 1 - \frac{K_3 C_4}{C_2(1 - C_4)};\ K_2 = 1 - K_1 - \frac{1}{2C_4};$$

$$K_3 = \frac{2C_1 + C_2^2 C_3}{2C_2 C_3(1 + C_4)}$$

In particular, when $x = L$ we have $u = u_1$, $p = p_1$, and $\phi = \phi_1$:

$$\frac{\sigma B^2 L}{\rho_0 u_0} = \phi_1 \tag{18}$$

Selection of supersonic inlet flow to the generator is inadvisable because of high leaving losses that would result (exit flow would be supersonic or choked) and because of the lower temperature and conductivity that would accompany the high Mach number.

Parameter C_2 is a loading parameter and measures the ratio of voltage to open circuit voltage. Thus, from (4) and (5) the open circuit voltage is

$$V^* = u_0 Bd(1 - \delta) \tag{19}$$

while the voltage, in general, is, by (14)

$$V = u_0 Bd(-C_2 - \delta) \tag{20}$$

so that

$$\frac{V}{V^*} = \frac{-C_2 - \delta}{1 - \delta} \tag{21}$$

For the case $\delta = 0$ we see that $-C_2$ is simply V/V^*. At short circuit conditions C_2 is $-\delta$ if we have electrode drops, or zero if $\delta = 0$. At open circuit $C_2 = -1$.

For subsonic flow in the MHD constant area generator the velocity increases (Reference [17]) and hence we would have $u_1/u_0 > 1$. The greater one takes u_1/u_0 the greater will be length L. A limit for u_1/u_0 is set by choking. Choking is most prone to occur at the short circuit condition, and at that condition it can be avoided[3] if (for $\delta = 0$)

$$\frac{u_1}{u_0} < \sqrt{\frac{2C_1}{2C_3C_4 - C_3}} \tag{22}$$

For MHD generator design u_1/u_0 might be chosen and L calculated by (18). For analysis of a particular generator L is fixed, and the u_1/u_0 value must be found which satisfies (18), with the assigned values of C_1, C_2, C_3, C_4.

The temperature ratio for the generator is given by

$$\frac{T_1}{T_0} = \frac{u_1}{u_0} \cdot \frac{p_1}{p_0} \tag{23}$$

For a given gas composition the conductivity will be a function of mean temperature $\bar{T}$ and mean pressure $\bar{p}$:

$$\sigma = \frac{F(\bar{T})}{\sqrt{\bar{p}}} \tag{24}$$

$$\bar{T} = \frac{1}{2}(T_0 + T_1);\ \bar{p} = \frac{1}{2}(p_0 + p_1)$$

By use of relations (15), (18), (23), and (24) the gas-dynamic solution of the generator problem can be obtained.

We come next to consideration of the electrical characteristics. The open circuit voltage and operating voltage have already been mentioned. The current from the generator is obtained by integration of jb, using (8):

$$\mathrm{I} = \frac{\sigma u_0 BLb}{\phi_1}\left[1 - \frac{u_1}{u_0} + \frac{1}{C_3}\left(1 - \frac{p_1}{p_0}\right)\right] \tag{25}$$

The power, which is VI is given by

[3] Outlet Mach number is given by $M_1^2 = M_0^2(u_1/u_0)(p_0/p_1)$. We place $M_1 = 1$ and solve for u_1/u_0 using (15) with $C_2 = 0$.

$$P = \frac{\sigma u_0^2 B^2 (Lbd)}{\phi_1} (-C_2 - \delta) \times \left[1 - \frac{u_1}{u_0} + \frac{1}{C_2}\left(1 - \frac{p_1}{p_0}\right)\right] \quad (26)$$

Ratio of internal to external resistance is

$$\frac{R_i}{R} = \frac{1 - \frac{u_1}{u_0} + \frac{1}{C_2}\left(1 - \frac{p_1}{p_0}\right)}{\phi_1(-C_2 - \delta)} \quad (27)$$

At short circuit conditions the foregoing relations apply with ϕ_1 evaluated for $C_2 = -\delta$. In case $\delta = 0$ we have

$$(\phi_1)_{C_2=0} = \left(1 - \frac{1}{2C_4}\right) \ln \frac{u_0}{u_1} + \frac{1}{C_2}\left(1 - \frac{p_1 u_0}{p_0 u_1}\right) - \frac{C_1}{2C_4 C_2}\left(1 - \frac{u_0^2}{u_1^2}\right) \quad (28)$$

The nature of the dependence of current on C_2 can be seen if we examine the case for u_1/u_0 close to unity. In this case the approximate values I_s and P_s are

$$I_s = \sigma u_0 BLb(1 + C_2) \quad (29)$$

$$P_s = \sigma u_0^2 B^2 (bLd)(1 + C_2)(-C_2 - \delta) \quad (30)$$

We see that P_s depends parabolically on C_2 or I_s.

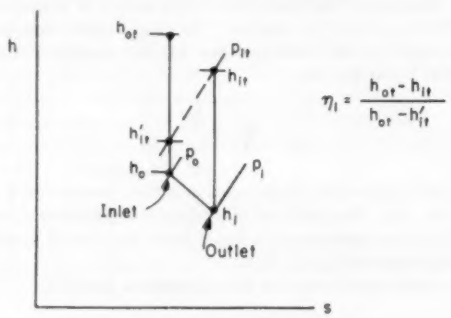

Fig. 2 MHD generator efficiency

The MHD generator will have, inevitably, a certain internal loss when power is drawn. An entropy rise occurs, and an internal efficiency can be defined as the ratio of total enthalpy drop to isentropic enthalpy drop for fixed outlet total pressure as illustrated in Fig. 2:

$$\eta_i = \frac{h_{0t} - h_{1t}}{h_{0t} - h_{1t}'} \quad (31)$$

Thermodynamic considerations lead to

$$\eta_i = \frac{\left(1 + \frac{\gamma - 1}{2} M_0^2\right) - \left(1 + \frac{\gamma - 1}{2} M_1^2\right)\frac{T_1}{T_0}}{\left(1 + \frac{\gamma - 1}{2} M_0^2\right) - \left(1 + \frac{\gamma - 1}{2} M_1^2\right)\left(\frac{p_1}{p_0}\right)^{\frac{\gamma - 1}{\gamma}}} \quad (32)$$

$$M_1^2 = M_0^2 \left(\frac{u_1}{u_0}\right)^2 \frac{T_0}{T_1}$$

Total power output is related to total enthalpy drop as follows, by integration of (9)

$$P = w(h_{0t} - h_{1t}) - I \cdot \delta V \quad (33)$$

If we let η_e stand for an electrical efficiency defined by

$$\eta_e = \frac{P}{P + I \cdot \delta V} \quad (34)$$

then the combined generator efficiency would be

$$\eta = \eta_e \cdot \eta_i \quad (35)$$

An alternate formulation of efficiency is the ratio of power to ideal power for $R_i = 0$, for given current. This efficiency η' would be

$$\eta' = \frac{V}{V^*} \quad (36)$$

In case the outlet pressure of the generator is specified, along with mass flow and inlet total temperature, the inlet state and velocity will depend on loading. The relations that have been given can be used to deal with problems of this type, but one must keep in mind that u_0 depends on generator load. This form of the problem is presented by the experimental generator described in this paper.

3 Conductivity of the Gas

Free electrons will be the principal charge carriers in the conducting gas. These electrons will be provided by the formation of positive ions. The gas tends to remain electrically neutral, except under special circumstances, and we therefore have, in general, the same number of negative and positive charges per unit volume. The formation of positive ions is therefore essential in rendering the gas electrically conducting. If we depend on the thermal equilibrium state of ionization it is important to have atoms present of a variety that are easily ionized, that is, they must have low ionization potential. The ionization potentials for several elements are listed below [14]

cesium	3.87 electron volts
rubidium	4.16 electron volts
potassium	4.32 electron volts
sodium	5.12 electron volts
barium	5.19 electron volts

For economic reasons, potassium is an attractive additive to supply ions and render the gas electrically conducting.

The conductivity may be formulated in terms of electron density, electron mobility, and electronic charge:

$$\sigma = n_e \mu q_e \quad (37)$$

The number of free electrons per cubic meter, n_e, depends on the number of positive ions and negative ions. The latter may be formed in moderate degree by electron attachment to certain species. It appears that in combustion product gases OH is the principal attaching species. Thus, if ϵ_1 and ϵ_2 are the concentrations of potassium atoms and OH particles, respectively, and if α_1 and α_2 are the respective fractions ionized, and if n is the total number of particles per unit volume

$$n_e = n(\alpha_1 \epsilon_1 - \alpha_2 \epsilon_2) \quad (38)$$

The fractions α_1, α_2 may be computed by equations of the Saha type governing thermal equilibrium ionization [15]. For example, for α_1 we have (for $\alpha_1 \ll 1$)

$$\alpha_1 = \frac{0.183 T^{3/4}}{\sqrt{p\epsilon_1}} \exp(-q_e V_i / 2kT)$$

where

q_e = electronic charge, 1.60×10^{-19} coulombs
V_i = ionization potential, volts
k = Boltzmann constant, 1.38×10^{-23} joules/deg
p = gas pressure, newtons/m^2
T = gas temperature, deg K

The mobility μ measures the drift velocity of electrons in the gas under the action of unit electric field. In MKS units its dimensions are meters$^2 \cdot$ sec$^{-1} \cdot$ volts^{-1}. Since electron displacement by the field depends on electron speed it is proper to evaluate μ by appropriate integration over the (assumed) Maxwell velocity distribution.

$$\mu = \frac{4\pi q_e}{3m_e} \int_0^\infty f(v) \frac{d}{dv}\left(\frac{v^3}{\nu}\right) dv \qquad (39)$$

where

v = electron velocity, meters/sec
$f(v)$ = velocity distribution function
ν = collision frequency of electrons and various species

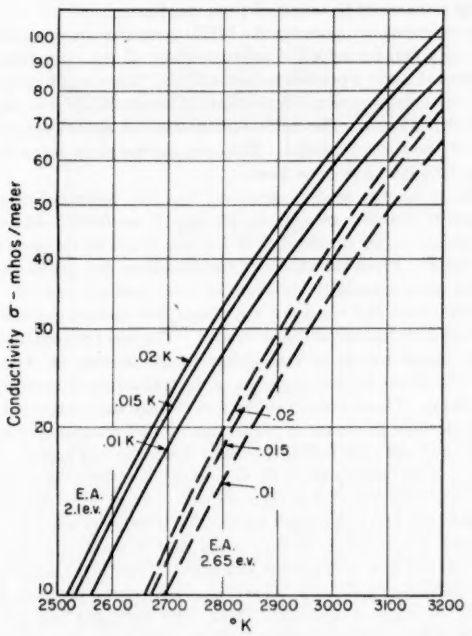

Fig. 3 Conductivity of gaseous reaction products from $CH_2 + 3/2\ O_2 + n_K K$ at equilibrium at 1 atm. Effects of ion scattering, electron attachment to OH, and KOH association considered.

m_e = electron mass, kg
q_e = electron charge, coulombs

Calculations using most reliable data for collision cross sections and frequencies were carried out by Frost and Phelps [16]. The gas of interest consisted of the products of combustion, in equilibrium, of ethylene, C_2H_4, in stoichiometric mixture with oxygen, with a certain amount of potassium addition. Electron-ion interactions were considered, and electron attachment to OH. Calculated conductivity values are given in Fig. 3.

The conductivity as given in Fig. 3 is at 1 atm pressure. The effect of a pressure other than 1 atm is that σ varies approximately inversely at $\sqrt{p}$. (This would be most nearly correct if the resistivity due to electron scattering by ions were negligible; it is in fact relatively small.) Two sets of curves are given, one set for 2.1 e.v. electron affinity of OH and one set for 2.65 e.v.

4 MHD Experimental Arrangement

An assembly diagram of the device is shown in Fig. 4, and a photo in Fig. 5. The model consists of three major component parts, the combustion chamber, the mixer, and the generator. The metal walls of both the mixer and generator are water cooled on the outside and lined with ceramic. The mixer serves to provide space and time for completion of combustion and acts as a plenum chamber from which the hot gases can be discharged into the generator. The magnet is mounted on jacks and is shown in the lowered position in Fig. 5.

The generator consists of three distinct stages—each with its own pair of electrodes. The magnetic field is horizontal and

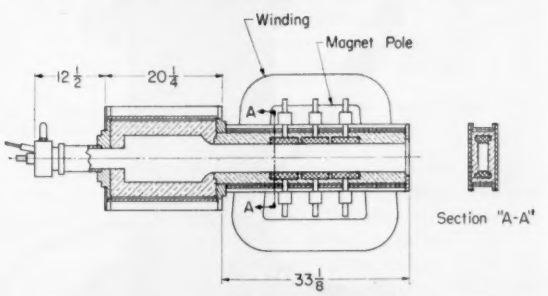

Fig. 4 Schematic diagram of combustor and generator assembly

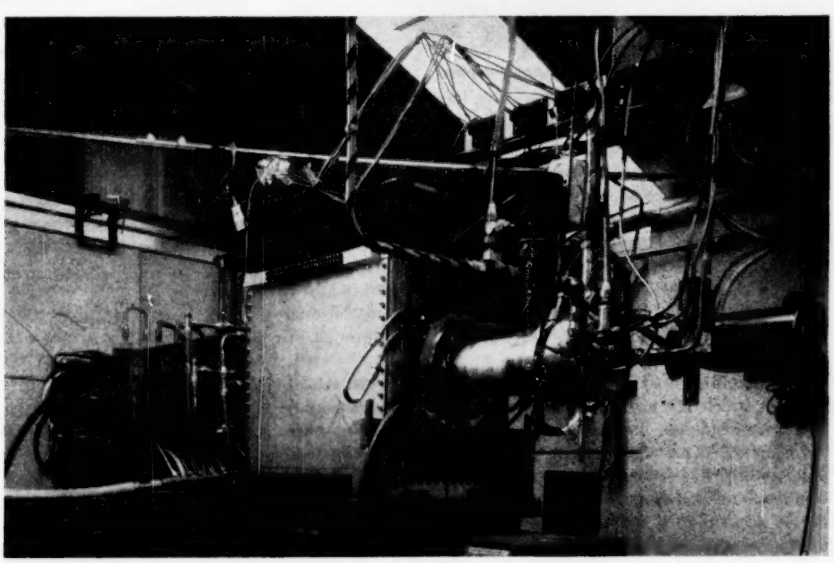

Fig. 5 MHD generator assembly. Magnet in lowered position.

transverse to the flow direction, and magnetic induction values up to 14,000 gauss have been used. The flow channel through the generator is a rectangular duct of nominal dimensions, $1^3/_8$ inches in the magnetic field (transverse) direction, $4^7/_8$ inches in the direction between electrodes, and 16 inches in the gas flow direction. Since the walls were lined with ceramic, a variation of $\pm^1/_{32}$ inch (or more, in case of damage) from nominal dimensions could be expected.

A photo of the combustion chamber which is used to produce the high temperature gases for the generator is shown in Fig. 6. This burner is constructed of four main component parts; the upstream end plate with the fuel nozzle, the ignitor, the oxygen manifold, and the water cooled combustion section.

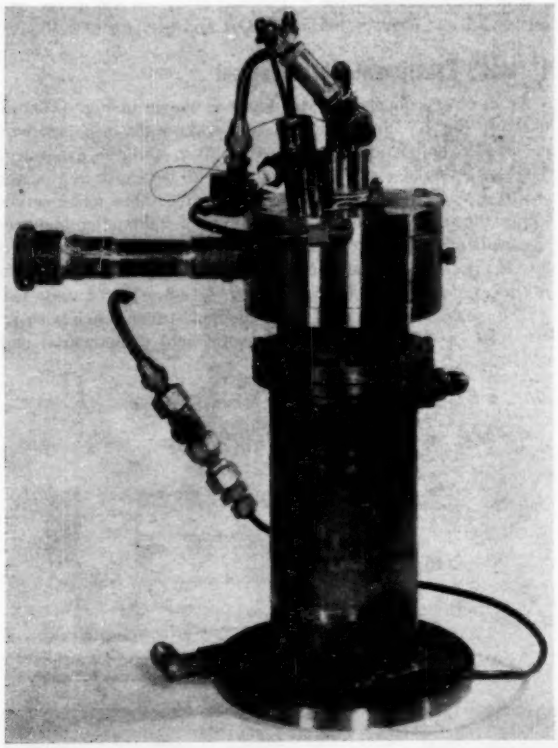

Fig. 6 Combustion chamber

The fuel nozzle is of the dual orifice type of nominal 60 deg spray angle. It is surrounded by a gas-assist swirl element through which a portion of the main oxygen flow is metered to provide assistance for atomization of the fuel. A simplified line diagram of the fuel and oxygen system is shown in Fig. 7.

Any of three fuels may be passed through the nozzle; propane, diesel oil, or potassium-seeded diesel oil. The propane is used for preheating the generator apparatus, and may be brought in through both the primary and secondary elements of the dual-orifice nozzle. The liquid fuels are injected solely through the secondary (larger) orifice.

A manifold is used to distribute the oxygen to several slots through which it flows into the burner. When operating the generator at design conditions, the pressure drop across these swirl slots is many times greater than critical. The two main objectives of this strong swirl are to provide wall cooling of the combustion chamber and stability of combustion. The wall cooling is accomplished by the high velocity blanketing layer of oxygen which sweeps the inner wall of the burner. This blanketing layer persists for approximately four diameters downstream from the oxygen manifold. The extreme stability of this type of burner as regards air-fuel operational limits and heat release limits stems from the reverse flow in the center of the chamber. The strong reverse flow of hot gases is induced by the low pressure region in the core of the vortex arising from the tangential flow of oxygen. The back flow serves as a constant source of ignition for the incoming fuel and oxygen, and also aids in vaporizing the fuel.

The combustion chamber proper is $3^1/_2$ inches in diameter and 12 inches long. The heat release at the design operating condition for the MHD generator is approximately 15×10^6 Btu/hr with a pressure level of 1.6 atm. If it were desired, much greater heat release rates could be obtained from this burner.

The required hot gases for the MHD generator are produced by burning a fuel consisting of approximately 43 per cent diesel oil, 45 per cent 2-ethyl-potassium hexoate, and 12 per cent butyl cellosolve in an oxygen-nitrogen mixture, at about 95 per cent oxygen equivalence ratio. The potassium in the fuel constitutes 10 per cent of the fuel by weight. Nitrogen-oxygen mass ratios in the range 0 to 0.5 have been used.

The potassium-seeded diesel oil has the following physical property: specific gravity at 60 deg F = 0.956; kinematic viscosities = 300 centistokes at 100 deg F and 65 centistokes at 160 deg F. From the aspect of fuel handling, the problems presented were essentially the same as for a residual fuel oil. The opacity of the fuel ruled out any visual flow-metering device and the fuel lines had to be heater-traced. The fuel temperature had to be monitored at several points in the system as shown in Fig. 7 to assure proper operation of the fuel nozzle, flowrator, and fuel pump. Checks made at the fuel storage tank indicated that no noticeable time-rate of separation of fuel components exists Safety devices were installed to shut down the fuel system in the case of either overpressure or abnormal under-pressure fuel conditions. The fuel and oxygen control systems were interlocked so that both fuel and oxygen are shut off if either is shut off. This provides a convenient simultaneous shut down at the end of a test, as well as a malfunction safeguard. The fuel control panel also contained generator, mixer, and combustor pressure gages, as well as magnet controls. These, with pertinent fuel pressure and flow indications were recorded by camera at short intervals. Another camera recorded electrical data simultaneously, and a single clock, common to both photo sets, provided data synchronization.

From the standpoint of producing maximum generator power output, it would be desirable for the gases to be at the highest temperature in order to realize the highest conductivity. However, it was found desirable to limit the top temperature by dilution of the gases with nitrogen to avoid damage to the internal surfaces.

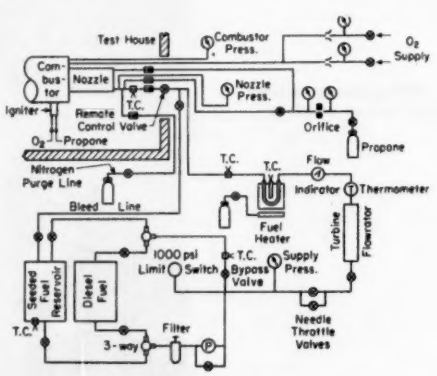

Fig. 7 MHD fuel and oxygen system

The ignitor, which is only used during lightup of the main combustion chamber, has essentially the same swirl design features as the main chamber. However, it burns propane and oxygen and has a conventional spark plug for ignition.

It has been found necessary to gradually warm the mixer and generator to avoid excessive breakage of the ceramic bricks by thermal stresses. Warm-up periods of approximately one hour are used. During this time propane and oxygen are burned at 1 to 4 per cent design heat rate.

When the warm-up is completed the magnetic field is applied, and the liquid fuel mixture and the main oxygen supply are turned on.

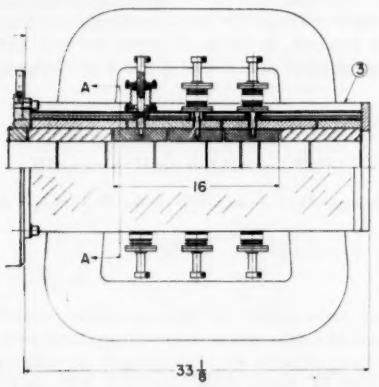

Fig. 8 MHD generator

We come now to the description of the generator itself. In a device of this type, formidable problems are presented in holding a 5000 deg F gas stream at high velocity and insulating the electrodes. The model, as pictured in Fig. 8, features a water cooled metal enclosure fitting closely between magnet poles. This envelope is lined with electrically and thermally insulating ceramic brick, interlocked so as to be self-supporting and presenting a smooth internal surface to the gas stream. The three pairs of electrodes are shown mounted in opposite walls, connected to terminal pieces which pass through insulated bellows, the bellows providing the necessary flexibility for thermal expansion. As in the case of the ceramic side brick, the electrodes are interlocked so that with no external support they cannot be dislodged and swept downstream.

There are only a few materials, insulators or conductors, that possesses the high melting points required in this application. Additionally they must be chemically and physically inert to the high gas stream and resistant to thermal shock. Several promising families of refractories may be listed as follows:

Electrical insulators	Electrical conductors
oxides	refractory metals
some nitrides	most nitrides
most zirconates	borides
	carbides

Specificially, the properties of borides, nitrides, and zirconates have not been well established but several are under investigation. Oxides, of which magnesia and stabilized zirconia are the more readily obtainable, were considered for electric insulators. However, the resistivity of zirconia is relatively low at high temperatures, and magnesia decomposes well below its melting point. Beryllia has excellent thermal shock resistance but its melting point is lower than that of zirconia. Hafnia and thoria are too rare and costly for large scale application.

As to the electrical conductors, many of the carbides are quite unstable and burn readily when oxygen is present. On the other hand, silicon carbide bonded graphite shows evidence of having oxidation resistance superior to the commercial grade graphite, which has been used in most of the tests. Tungsten and W-Ta alloy, although expensive, have been considered as electrode materials and used in the experimental program. Rhenium is so rare as to have possible application in MHD devices only as a thermocouple material.

The electrical properties of several of these materials as a function of temperature are shown in Fig. 9. It will be seen that data in the present range of interest is available for only graphite and tungsten. The melting point for each material is listed in the figure.

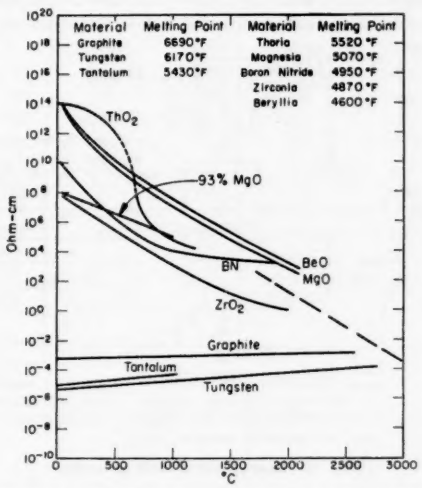

Fig. 9 Electrical resistivity of several conductors and insulators (from Kingery, Norton, Campbell, reference [18, 19, 20])

Although little high temperature data exist for the insulators, a rough extrapolation suggests that many normally insulating materials might become the equivalent of graphite in resistivity around 2800 deg C, as shown by the dashed curve.

Preliminary evaluations have been made with stabilized Zirconia and MgO as sidewall insulators and graphite, tungsten, and W-Ta alloy as electrodes. The problem is still under investigation. A moderate degree of side wall cooling would alleviate the insulation problem.

The magnetic field was obtained using an electromagnet with a "C" shaped iron core. Exciting coils were fourteen "pies" of 176 turns each wound on detachable iron pole pieces. Copper fins having the form of washers and with water cooling tubes fixed at the edges were interposed to cool the pies. A uniform field of 14000 gauss was produced within a five inch gap of a seventeen and one half by twenty inch section of the MHD generator. At that field the exciting coils dissipated forty-four kilowatts. Direct current power was obtained from a motor-generator set supplying two hundred twenty volts and two hundred amperes. Field of the magnet was controlled by employing a variable voltage source for excitation of the DC generator. The eight ton magnet assembly could be lowered away from the MHD generator using an elevator made from four coupled screw jacks driven by a motor. The magnet can be seen in Fig. 5, and the position of the pole faces in relation to the generator is seen in Fig. 8.

We give a description next of the electrical system. Initial system calculations indicated that an electrical power output of about 5 to 10 kw would have to be dissipated and measured. An important requirement of the instrumentation was to allow for rapid load adjustment and for continuous recording of the test meter readings. During most of the tests the attempt was made

to obtain the variation of the electrical power output with respect to the value of the load current and with respect to time.

Fig. 10 shows how the load current was adjusted by varying the external load resistance by means of suitable switches and rheostats. Resistance in each of the three individual circuits could be adjusted over the range of 0.1 to 5 ohms. The currents indicated next to the resistances in Fig. 10 are maximum steady-state currents, and operation at double these values proved satisfactory for short periods. For most of the test runs it was attempted to obtain data near the maximum power output level of the MHD generator. This was accomplished by presetting the series resistance at the top of the figure to such a value that a 0 to 1 ohm resistance variation with the tandem rheostats would yield total circuit resistances both above and below the optimum value.

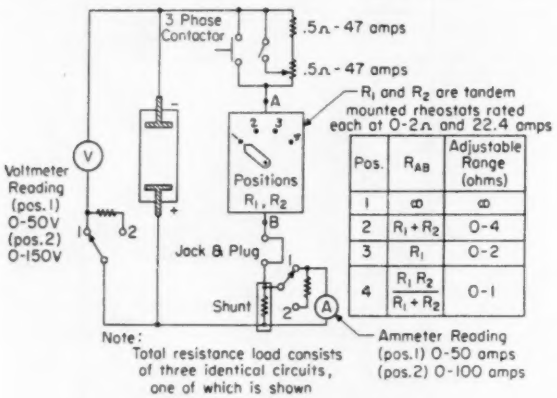
3 Phase Contactor
.5Ω - 47 amps
.5Ω - 47 amps
R1 and R2 are tandem mounted rheostats rated each at 0-2Ω and 22.4 amps
Voltmeter Reading (pos.1) 0-50V (pos.2) 0-150V
Positions R1, R2
Jack & Plug
Shunt
Note: Total resistance load consists of three identical circuits, one of which is shown
Ammeter Reading (pos.1) 0-50 amps (pos.2) 0-100 amps
Pos. | RAB | Adjustable Range (ohms)
1 | ∞ | ∞
2 | R1 + R2 | 0-4
3 | R1 | 0-2
4 | R1R2/(R1 + R2) | 0-1

Fig. 10 Load circuit of MHD generator

During the run, the three sets of tandem rheostats were geared together so as to give identical resistances in each circuit. Electrical output data were obtained by slowly and continuously adjusting the resistance between points A and B from the maximum value at positions 4, that is, one ohm, to the resistances which resulted in about a 100 ampere current in the circuit having the highest current. At this point, the rheostat movement was reversed and resistances were again increased to one ohm. The time interval required for decreasing and increasing the resistance to the initial value was about one minute for most tests. For each test, data were also obtained at open circuit condition and, if time permitted, at some of the higher resistance settings. The range switches on the voltmeters and ammeters were connected to actuate each set of three meters together and, whenever possible, the range switches were adjusted to read the meters on the scale yielding the greater accuracy.

During the test run, the meters on the electrical output panel and an electric timer were photographed at about one half second intervals. Measurements were obtained by reading the projected film image on a screen.

The jack and plug arrangement shown in Fig. 10 was only used when it was desired to introduce an external voltage to measure generator internal electric resistance at no power generation. For this measurement, a battery was plugged into the jack and resistances were obtained from the voltmeter and ammeter readings. Leads of either the voltmeters or ammeters had to be reversed for these measurements.

5 Test Conditions

Gas was supplied to the experimental MHD generator by combustion of oxygen and a fuel mixture containing No. 2 furnace oil, butyl cellosolve, and 2-ethyl potassium hexoate. Various amounts of nitrogen were added as diluent.

The fuel analysis was as follows:

	Mass fraction	Atoms/C atom
carbon	0.6500	1.000
hydrogen	0.1092	2.000
potassium	0.1000	0.0473
oxygen (by difference)	0.1408	0.1628

The stoichiometric over-all reaction with oxygen can be expressed as follows:

$$CH_2(0.04735K)(0.08140_2) + 1.4304O_2 \rightarrow CO_2 + H_2O + 0.02367K_2O$$

This leads to the stoichiometric O_2/fuel mass ratio of 2.48.

In the experiments a little less than stoichiometric oxygen was used. The reaction, in terms of actual product species for 95 per cent oxygen and addition of θ moles of nitrogen, would be written:

$$CH_2(0.04735\ K)(0.0814O_2) + 1.3589O_2 + \theta N_2 \rightarrow n_O \cdot O + n_H \cdot H + n_{OH} \cdot OH + n_{H_2O} \cdot H_2O + n_{NO} \cdot NO + n_N \cdot N + n_{CO_2} \cdot CO_2 + n_{CO} \cdot CO + n_{H_2} \cdot H_2 + n_{O_2} \cdot O_2 + n_{N_2} \cdot N_2 + 0.04735\ K$$

The O_2/fuel mass ratio is in this case 2.355. The equilibrium compositions at 1 atm and several temperatures were evaluated and flame temperatures were determined by enthalpy balance. This was done for N_2/O_2 mass ratio of 0, 0.25, and 0.50. The higher heating value of the fuel had been measured and found to be 14829 Btu/lb. The equilibrium flame temperature and gas compositions at flame temperature are given in Table 1.

For the flow into and through the generator "frozen" composition was assumed. Enthalpy of the gas mixtures listed in Table 1 can be evaluated at various temperatures, and the enthalpy drop from the value at flame temperature determined. Enthalpies are given in Table 2. The velocity, density, and mass flow can be calculated by the following equations:

$$u_0 = \sqrt{2(h_{0t} - h_0)} \qquad (40)$$

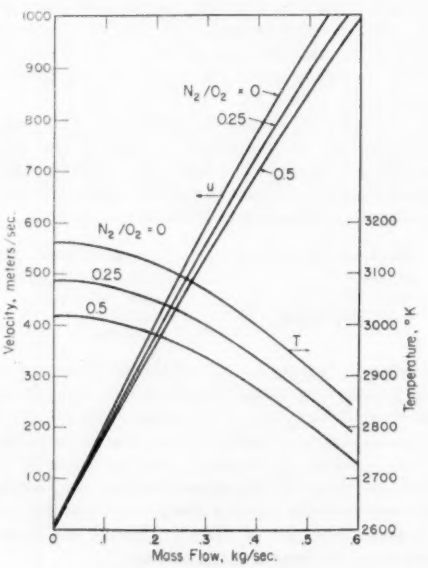

Fig. 11 Velocity and temperature of gases in generator. Fixed composition flow. 95 per cent O_2 equivalence.

O_2: Fuel ratio 2.355
Fuel: CH_2 (0.0814 O_2)(0.04735 K)
1.5 atm. assumed pressure

Table 1 Equilibrium compositions at adiabatic flame temperature

N_2/O_2 (mass ratio)	0		0.25		0.50	
Flame Temp. °K	3162		3086		3018	
Species	Moles / kg mole fuel	Mole fraction	Moles / kg mole fuel	Mole fraction	Moles / kg mole fuel	Mole fraction
O	.125	.049	.100	.035	.082	.025
H	.124	.048	.106	.037	.087	.027
OH	.213	.083	.188	.065	.166	.051
H_2O	.675	.263	.711	.245	.746	.230
NO	0	0	.038	.013	.047	.015
N	0	0	.0018	.0006	.0019	.0006
CO_2	.387	.151	.419	.144	.453	.139
CO	.613	.239	.581	.200	.547	.168
H_2	.148	.058	.138	.047	.126	.039
O_2	.234	.091	.208	.072	.192	.059
N_2	0	0	.368	.127	.751	.231
K	.0473	.0184	.0473	.0163	.0473	.0146
Total moles	2.567	1.000	2.906	1.002	3.248	1.000
Mass/kg mole fuel	61.97		72.84		83.248	
Molecular wt	24.14		25.06		25.77	
Gas constant; Joules/kg °K	344.4		331.8		322.6	

Table 2 Enthalpy h_0 of combustion product gases, joules/kg × 10^{-6}

O_2: Fuel Ratio 2.355
Fuel: CH_2 (0.0814O_2)(0.04735 K)
1.5 atm assumed pressure

N_2/O_2	0	0.25	0.50
Temp.			
2500	3.504	3.378	3.285
2750	3.952	3.808	3.703
3000	4.404	4.244	4.126
3250	4.860	4.682	4.551
3162	4.700	-----	-----
3086	-----	4.405	-----
3018	-----	-----	4.160

$$\rho_0 = \frac{p_0}{R_g T_0} \tag{41}$$

$$w = \rho_0 u_0 A \tag{42}$$

Molecular weights were determined for the several gas compositions, and gas constants determined. Any assumed u_0 leads to a particular value of h_0 and T_0, for a given gas mixture, and to a given ρ_0 and w if p_0 is assumed. It is convenient to plot values against mass flow w. Such curves are shown in Fig. 11. Pressure p_0 has been taken at 104,300 newtons/m² (1.03 atm) and the generator cross section at 0.00511 m² for construction of Fig. 11.

When pressure and section area are different from the nominal values of 104,300 newtons/m² and 0.00511 m² the curves of Fig. 11 may still be used, provided one enters the abscissa at a fictitious flow rate w' defined by

$$w' = \frac{0.00511}{A} \cdot \frac{104{,}300}{p} \cdot w \tag{43}$$

In Table 3 are given operating parameters for tests made in the spring of 1960. The velocity u_0 at the inlet was determined using Fig. 11 and the fictitious flow rate w' obtained from (43). Interpolation was made between the curves for various N_2/O_2 ratios. The pressures listed in Table 3 are mean values of inlet pressure p_0, that is, they represent the mean inlet pressures obtained over a range of loads. We must keep in mind that p_0 and also u_0 will change slightly as more current is drawn from the generator, owing to the retarding effect of the integrated body force jB. The precision of certain of the measurements at the stage of development that existed when these tests were made was such that recording the changes in the u_0 and p_0 values for various loads was not justified.

Table 3 Generator test conditions

Date	3/4/60	3/25/60	4/14/60	5/6/60	5/26/60	6/29/60
P_o newt./m²	103200	114500	112400	118400	119000	116000
P_o atm	1.02	1.13	1.11	1.17	1.18	1.24
A meters²	0.00511	0.00693	0.00511	0.00511	0.00511	0.00511
Fuel rate kg/sec	0.0694	0.118	0.111	0.118	0.143	0.1056
O_2 rate kg/sec	0.169	0.287	0.270	0.277	0.3375	0.250
N_2 rate kg/sec	0	0	0.0272	0.091	0	0.1251
w kg/sec	0.239	0.405	0.408	0.486	0.481	0.481
O_2/fuel	2.44	2.43	2.43	2.35	2.36	2.365
O_2 equiv.	0.98	0.98	0.98	0.946	0.951	0.953
N_2/O_2 by mass	0	0	0.101	0.328	0	0.500
u_o m/sec	483	542	719	763	812	693
B webers/m²	1.00	1.40	1.40	1.40	1.40	1.40
d meters	0.124	0.124	0.124	0.124	0.124	0.124
b meters	0.0413	0.0559	0.0413	0.0413	0.0413	0.0413
L meters	0.406	0.406	0.406	0.406	0.406	0.406
T_{ot} °K	3162	3162	3129	3064	3162	3018
T_o °K	3098	3082	2983	2895	2981	2877
w' kg/sec	0.241	.2722	0.3786	0.428	0.422	0.398
K mole fraction	0.0184	0.0184	0.0175	0.0158	0.0184	0.0146

6 Results and Discussion

In Table 4 we summarize results of the six tests previously

Table 4 MHD generator test results

(MKS units)

Date	3/4/60	3/25/60	4/14/60	5/6/60	5/26/60	6/29/60
u_0Bd	59.9	94	125	132.5	141	120
$V^*_{obs.}$	27	45	48	101	100	75
I_{ss}	214	360	450	540	400	244
P_{max}	1500	3800	6100	9400	10400	4650
$(P_{max}/bdL)10^{-6}$	0.72	1.35	2.93	4.52	5.00	2.24
I_{ss} (1st sect.)	----	----	152	122	143	101
R_i (1st sect.)	----	----	0.925	1.06	0.965	1.158
σ_0	----	----	24	21	23.1	19.1
$\sigma_{0\ th}$	----	----	37	25.4	35.5	22.5
R''	----	----	0.18	1.35	0.91	0.86

Note: $\sigma_{0\ th}$ based on 2.65 e.v. electron affinity of OH in Figure 5. R'' is for entire generator length, from Equation 47 with $V'' = V^*_{obs.}$

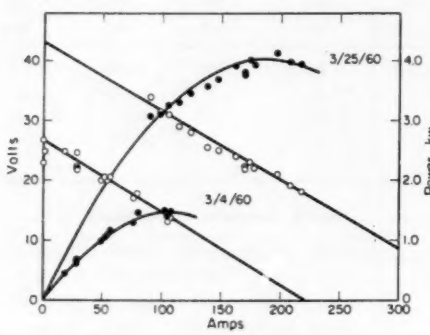

Fig. 12 Test results on MHD generator

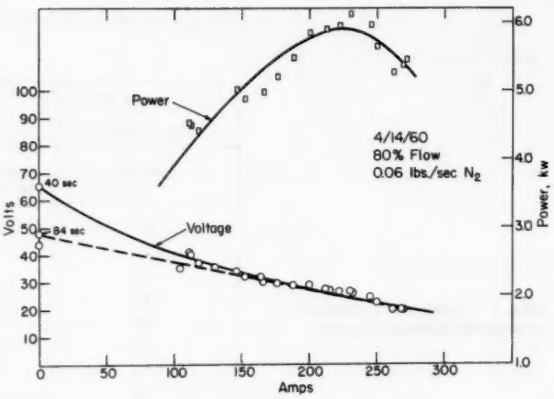

Fig. 13 Test results in MHD generator

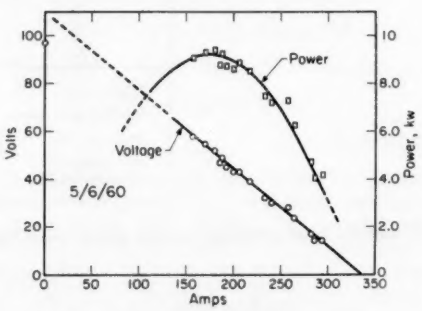

Fig. 14 Test results on MHD generator

mentioned. Voltage and power data points for several tests are given in Figs. 12, 13, and 14. The power is the sum of the power generated in the three generator sections and the current is the sum of the currents. The voltage points represent the average of the values obtained from the three stages at any one load setting.

Variation in generated power from one test to another arises from the various flow velocities, gas temperatures, and wall leakage resistance conditions. Maximum power generated was 10.4 KW.

The first line in Table 4 gives the Faraday voltage u_0Bd, which would be the theoretical open circuit voltage (Eq. (19)) neglecting electrode drops and leakage currents. This value is based on the mean inlet velocity u_0 during a test. The observed open circuit voltage $V_{obs}{}^*$ is seen to be somewhat less than u_0Bd.

The short circuit current I_{ss} in Table 4 is obtained by extrapolation of the voltage curve to zero voltage, as I_{ss} was not measured directly.

If there were leakage conduction paths there would be a theoretical apparent open circuit voltage V'', less than the value V^* given by (19). In this case the leakage path resistance might be regarded as part of the general load resistance R and equations (25), (26), (27) would still apply. To see the extent to which leakage conductance might cause V'' to be lower than V^* we might consider a generator length L having external (applied) resistance R' and leakage resistance R''. Let I' and I'' be the corresponding currents. Then

$$I = I' + I''; \quad \frac{1}{R} = \frac{1}{R'} + \frac{1}{R''} \tag{44}$$

The current I' is the one that would normally be measured as it flows through the applied load. The apparent open circuit voltage would be obtained when $I' = 0$ and $I = I''$ and $R = R''$. At this condition there would be a C_2 value we could designate C_2'', and it would be related (approximately) to the resistance ratio by[4]

$$\frac{R_i}{R''} = \frac{1 + C_2''}{-C_2'' - \delta}; \quad C_2'' = -\frac{1 + \dfrac{R_i}{R''}\,\delta}{1 + \dfrac{R_i}{R''}} \tag{45}$$

and the ratio of V'' to V^* would be (by 21)

$$\frac{V''}{V^*} = \frac{-C_2'' - \delta}{1 - \delta} \tag{46}$$

Continuing a step further, C_2'' may be eliminated from (45) and (46) to give (47)

$$\frac{V^*}{V''} = \frac{R_i}{R''} + 1 \tag{47}$$

We see, therefore, that if R'' were $2R_i$ then V'' would be only $^2/_3$ of V^*.

Certain tests were made April 19, 1960, that shed light on the value of δV in the generator experiments and the value of R'' for zirconia side walls. A battery was connected to the generator terminals and B was set at zero. A test was made burning fuel oil containing no potassium; the product gas was then presumably nonconducting, or in any case a very poor conductor. The current J_B supplied by the battery at voltage V_B would then

[4] Note that for u_1/u_0 close to unity, as is the case here, $\left[1 - \dfrac{u_1}{u_0} + \dfrac{1}{C_i}\left(1 - \dfrac{p_1}{p_0}\right)\right] \Big/ \phi_1$ approaches $(1 + C_2)$.

be the leakage current, and R'' would be the quotient V_B/J_B. Seeded fuel was also burned with the battery connected, still with $B = 0$. In this case voltage $V_B - \delta V$ would drive current $J_B - V_B/R''$ through the gas. The internal resistance R_i would then be the ratio

$$R_i = \frac{V_B - \delta V}{J_B - V_B/R''} \tag{48}$$

in which R'' is from the unseeded fuel run and the other quantities are for the seeded fuel run. Since we are satisfied with an approximate result for δV we may write for R_i the alternate expression based on a power generation test at conditions similar to those of the April 19 tests:

$$R_i = \frac{V^*}{I_{ss}} = \frac{u_0\, Bd - \delta V}{I_{ss}} \tag{49}$$

The test of April 14 had such similar conditions. We may now equate the values of R_i from (49) and (48) and solve for δV:

$$\delta V = V_B \left[\frac{1 - \dfrac{u_0\, Bd}{I_{ss}} \left(\dfrac{J_B}{V_B} - \dfrac{1}{R''} \right)}{1 - \dfrac{V_B}{I_{ss}} \left(\dfrac{J_B}{V_B} - \dfrac{1}{R''} \right)} \right] \tag{50}$$

The tests of April 14 and April 19, 1960, gave

$$u_0 Bd = 125 \text{ volts} \qquad \frac{J_B}{V_B} - \frac{1}{R''} = 2.5 \text{ mhos}$$

$$I_{ss} = 450 \text{ amps} \qquad V_B = 9 \text{ volts}$$

$$\therefore \delta V = 2.9 \text{ volts}$$

A considerable variation in the observed quantities could have occurred without materially increasing δV. It is significant that δV is only of the order of 3 volts.

Quantities J_B/V_B and R'' varied with time due to gradual heating of the ceramic in the battery test, but the difference $J_B/V_B - 1/R''$ remained fairly constant at about 2.5 mhos. The value of R'' varied from 0.20 ohms at 30 seconds after starting to 0.13 ohms after 60 seconds; the value was then leveling out.

Returning now to Equation (47) we can ask how much leakage resistance would have to be present to cause the ratio V^*/V'' to be the same as $V^*/V_{obs}{}^*$. In this calculation we may use again the approximate relation $R_i = V^*/I_{ss}$, with $\delta V = 3$ volts in the expression for V^*. Values of R'' giving the afore-mentioned agreement of $V_{obs}{}^*$ and V'' are given in Table 4. These are the leakage resistance values that would have to be present if the entire open circuit voltage defect were to be accounted for by wall leakage. We see that for the test of 4/14/60 the R'' value obtained in this way agrees fairly well with the range of values measured, 0.13 to 0.20 ohms, in the test of 4/19/60. The R'' values in other tests are higher, principally because side walls of magnesia were used, rather than zirconia.

A comparison may also be made of theoretical and experimental values of σ at conditions near the generator inlet. Taking the T_0 and p_0 values in Table 3, which fairly well represent the inlet conditions, values of σ which we denote σ_{0th} may be determined from Fig. 3, with appropriate pressure correction. Next, examining the data for the upstream generator section only, we would have in Equation (49) (with $\delta V = 3$ volts) an estimate of R_i for the gas in the upstream generator zone. From this a value σ_0 can be calculated:

$$\sigma_0 = \frac{3d}{R_i b L} \tag{51}$$

The factor 3 comes in since the length is $L/3$. These values of σ_0, based on the tests, are also given in Table 4.

Finally, a comparison may be made between experimentally generated power and theoretical power. Since the calculation of theoretical power over a range of loads is a rather involved procedure it was done for the test of 5/6/60 only. The outlet static pressure was assumed fixed at 1 atm, and the mass flow, inlet total temperature, and gas composition were taken at the values mentioned previously for this test. An analysis was then made on the basis of Equations (15), (17), (18), and (26) taking account of the effect of change in C_2 on inlet conditions. A conductivity value was used based on the experimental value of 21 mhos/meter with appropriate alteration for changes in T_0 and p_0 with loading. The 21 mhos/meter value was assumed to correspond to the state 2895 deg K, 1.17 atm. Leakage currents and friction were assumed zero. In this way the theoretical curve in Fig. 15 was obtained; along side it are plotted the experimental points.

A large part of the discrepancy in Fig. 15 can probably be accounted for by leakage currents. Other contributing factors would be wall friction, which would give lower flow velocities than the theoretical values with no friction, and temperature defect, due either to heat loss or incomplete combustion. A temperature defect would reduce both u_0 and σ.

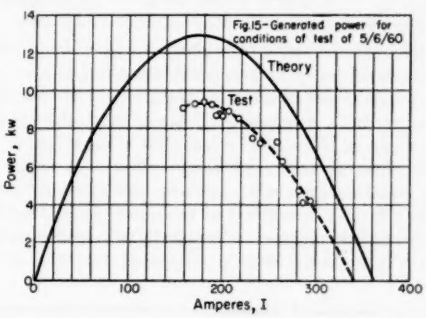

Fig. 15

7 Conclusions

Appreciable amounts of power can be generated by flowing an ionized gas stream through a transverse magnetic field with a mutually perpendicular electric field arrangement. The observed performance of such a device agrees fairly well with theoretical predictions. However, to realize the full potential of the MHD generator it is necessary that leakage currents, heat losses, and friction be reduced to a minimum.

The observed gaseous conductivity, based on ratio V^*/I_{ss} agrees reasonably well with theoretical values. Seeding with potassium, of the order of 1 to 2 per cent in the gas, is sufficient to realize conductivities in the 10 to 40 mho/meter range at temperatures 2700 K to 3000 K.

Deviations of observed and theoretical open circuit voltage could be explained largely by leakage currents. Electrode drops do not appear to amount to more than 3 to 5 volts.

The type of gas generator, and the flow system generally used in these experiments can serve as a starting point for design of larger combustion gas fired MHD generators.

The side wall construction problem is still an outstanding one. The tests have shown that care must be taken to avoid leakage currents through the side walls and to avoid uneven thermal expansions causing cracking and spalling.

The electrode problem can be solved only with materials which are highly resistant to oxidation, which have low vapor pressure, and which are good conductors. Some of the refractory metals appear promising but their application should be combined with constructional features which ease the operating conditions.

References

1 M. Faraday, "Experimental Researches in Electricity," First Series, London, England, 1839.

2 R. Rudenberg, "Thermoelectric Apparatus," U. S. Patent 1,717,413, June 18, 1929.

3 C. Petersen, "Method for Transforming the Kinetic Energy of Gases Into Electrical Energy," U. S. Patent 1,443,091, January 23, 1923.

4 E. Rupp, "Method of and Apparatus for Generating Electrical Energy," U. S. Patent 1,916,076, June 27, 1933.

5 B. Karlovitz, "Process for the Conversion of Energy," U. S. Patent 2,210,918, August 13, 1940.

6 M. Camac and G. S. Janes, "Applied Magnetohydrodynamics at Avco-Everett Research Laboratory," Dynamics of Conducting Gases, Northwestern University Press, 1960.

7 R. J. Rosa, "Experimental Magnetohydrodynamic Power Generation," *Journal of Applied Physics*, April, 1960, p. 735.

8 *Wall Street Journal*, October 29, 1959.

9 S. Way, "Magnetohydrodynamic Generators," *Westinghouse Engineer*, July, 1960.

10 S. Way and R. L. Hundstad, "Direct Generation of Power From a Combustion Gas Stream," VIII Combustion Symposium, Pasadena, Calif., August 30, 1960.

11 L. Steg and G. W. Sutton, "Prospects of MHD Power Generation," *Astronautics*, July, 1960.

12 P. Sporn and A. Kantrowitz, "Magnetohydrodynamics," *Power*, November, 1959.

13 S. Way, "Design Considerations in MHD Generators," Conference on Engineering Aspects of Magnetohydrodynamics, AIEE, Philadelphia, Pa., 1960.

14 "Handbook of Chemistry and Physics," Chemical Rubber Publishing Company, 31st edition, p. 1975.

15 Maxfield and Benedict, "Theory of Gaseous Conduction and Electronics," McGraw-Hill Book Company, Inc., New York, N. Y., 1941, p. 264.

16 L. S. Frost and A. V. Phelps, private communication, Westinghouse Research Laboratories.

17 E. L. Resler, Jr., and W. R. Sears, "Prospects for Magnetohydrodynamics," *Journal of the Aeronautical Sciences*, April, 1958.

18 W. D. Kingery, "Property Measurements at High Temperature," John Wiley & Sons, Inc., New York, N. Y., 1959.

19 F. H. Norton, "Refractories," third edition, McGraw-Hill Book Company, Inc., New York, N. Y., 1949.

20 J. E. Campbell, "High Temperature Technology," John Wiley & Sons, Inc., New York, N. Y., 1956.

J. KENNETH SALISBURY
Consulting Engineer,
Atherton, Calif. Fellow ASME

Power-Plant Performance Monitoring

Introduction

THE thermal performance of any steam power plant depends only on the *thermodynamic cycle* in which it operates and the *effectiveness of the components* that implement this cycle. By usage the term "cycle" has come to mean far more than a repetitive series of thermodynamic processes. It includes within its connotation items such as initial and exhaust conditions, whether or not reheat is employed, the number and arrangement of feedwater heaters, and the location and number of boiler feed pumps. The term "effectiveness of components" includes elements such as efficiencies of turbines and pumps, terminal differences of feedwater heaters, pressure drops in extraction piping, condenser temperature difference, and mechanical and electrical efficiency. Thus any monitoring concept must embody means for determining the effect on heat rate of changes in the environmental conditions (e.g., steam conditions), as well as means for detecting the effect of change in component effectiveness. We shall consider the criteria for component effectiveness first, assuming design steam conditions to exist, then the effect on heat rate of changes in environment, and finally the translation of the basic environmental relationships into criteria for monitoring component effectiveness.

Maintaining the effectiveness of components is basically an operating problem, rather than a design problem. Normally it is achieved by spot checks of the equipment through efficiency tests, analysis of operating data, and so on. However, the performance of complex modern plants often may vary from expected performance by as much as 2 to 3 per cent, due to deterioration of the effectiveness of the components. The sudden appearance of a fault in any element of the system frequently goes undetected.

From these facts it seems likely that a considerable margin of improvement in over-all performance of the plant exists, provided a method can be devised that will conveniently, economically, and continuously monitor the effectiveness of the plant components. It is the intent of this paper to outline the theory upon which can be built a process of continuous-performance monitoring by means of automatic instrumentation.

One of the advantages of the system proposed herein is that the magnitude of the investment in performance-monitoring equipment may be tailored to suit the economics. The proposed system is adaptable to the installation of a very large number or of a small number of transducers and computing elements, each self-sufficient within its own province. For smaller plants, only the most important of these need be purchased. For the extremely large plant, where even a few tenths of one per cent change in performance may cost thousands of dollars per year, it may be

[1] Numbers in brackets designate References at end of paper.

Contributed by the Power Division and presented at the Winter Annual Meeting, New York, N. Y., November 27–December 2, 1960, of THE AMERICAN SOCIETY OF MECHANICAL ENGINEERS. Manuscript received at ASME Headquarters, July 28, 1960. Paper No. 60—WA-222.

Nomenclature

A = approximate fractional increase in heat rate due to ΔH_e, dimensionless

B = approximate fractional increase in heat rate due to Δh_f, dimensionless

C = ratio of output above reheat point to output of low-pressure system, equation (35), dimensionless

G_r = fractional reduction in heat rate achieved by the addition of reheat, dimensionless

H_1 = inlet enthalpy to low-pressure turbine, Btu/lb

H_2 = inlet enthalpy to high-pressure turbine, Btu/lb

H_c = enthalpy of exhaust steam at entrance to condenser, Btu/lb

H_e = effective extraction enthalpy of steam leaving all low-pressure turbine-extraction openings [2],[1] Btu/lb

H_E = effective extraction enthalpy from high-pressure turbine, Btu/lb

H_l = extraction enthalpy of steam leaving lowest pressure extraction opening, Btu/lb

H_x = exhaust enthalpy of high-pressure turbine, Btu/lb

h_{bf} = enthalpy of condensate leaving top heater, Btu/lb

h_c = enthalpy of condensate entering lowest pressure heater, Btu/lb

h_f = enthalpy of feedwater leaving top heater of low-pressure system, Btu/lb

$\Delta h = h_{bf} - h_f$ = rise in enthalpy through highest pressure heater (above reheat point), Btu/lb

n = ratio of total low-pressure-heater duty to heat supplied by low-pressure extraction steam, dimensionless

ΔP_c = increase in power output of condenser flow due to increase in low-pressure turbine efficiency, Btu/lb

P_t = total power output of low-pressure turbine, Btu/lb

Q = heat supplied to the cycle, Btu/lb

ΔQ = increase in heat supplied caused by addition of reheat, Btu/lb

q = heat rejected from the cycle, Btu/lb

Δq = increase in heat rejected from the cycle, Btu/lb

R_l = enthalpy rise across lowest pressure heater, Btu/lb

r = dimensionless heat rate, Btu/Btu

S = fractional increase in $(\Delta Q/Q)$ caused by any change in reheat system, dimensionless

U = used energy of high-pressure turbine $(H_2 - H_x)$, Btu/lb

u = used energy of low-pressure turbine $(H_1 - H_c)$, Btu/lb

w = extraction flow per pound of condenser flow, dimensionless

w_l = extraction for lowest heater per lb condenser flow, dimensionless

w_r = extraction for top heater of reheat system, lb per lb of entering flow, dimensionless

Subscripts and Greek

c = pertaining to nonextraction low-pressure cycle or condenser

n = pertaining to low-pressure "nonreheat" portion of reheat cycle

r = pertaining to complete reheat cycle

η = efficiency or realization ratio

Δ_i = fractional change in reheat heat rate due to change in parameter i, dimensionless

economical to monitor all possible faults, to facilitate immediate detection and correction.

This paper, covering the "Deviation-Monitoring Concept," outlines the theory and fundamental analytical concepts that compromise the basis of automatic performance monitoring equipment currently under development by the Bailey Meter Company. The application of this theory through use of a computer programmed to simulate a reheat power system is discussed in a companion paper.[2]

The author has long been completely convinced that performance monitoring is an extremely complex subject, some of the intricacies of which may elude us for years. At the same time the reader is forewarned that the solutions to such problems cannot be comprehended completely on the first reading. Even though the analytical developments are straightforward, and an effort has been made to present them lucidly, understanding of the true import of the results comes only after considerable effort. Extensive examples are presented later to facilitate understanding.

The Deviation-Monitoring Concept

This concept is predicated on the simple and axiomatic fact that the heat rate of a turbine cycle will be identical with the design heat rate unless one or more deviations from design conditions exist. Such deviations may lie either in effectiveness of a component, or in steam conditions imposed upon the cycle. The method analyzes each component of the over-all plant heat rate by means of a simple criterion, compares this criterion with the standard value (which may be either design conditions or the acceptance test), and interprets any variation of this criterion from the standard as a fractional change in heat rate from the standard, that is, as a "deviation." The algebraic summation of the deviations in heat rate, when applied to the standard heat rate, yields the operating heat rate. In other words, expressed algebraically

$$r' = r(1 + \Delta_1 + \Delta_2 + \ldots\ldots) \qquad (1)$$

In this equation each of the Δ's will be determined by a computer, the input to which is the criterion of performance of the given component, and the output of which is the fractional heat-rate deviation Δ_n.

The detection of faults in a piece of power-plant equipment and evaluation of the loss caused by such a fault is a time-honored routine. The philosophy proposed herein extends this approach to the ultimate limit, in which *all* deviations from standard performance are identified, and the algebraic total added to the reference performance, as in equation (1), to find the operating heat rate. Thus the favorable and unfavorable deviations are identifiable, and the contribution of each to the total is placed in proper perspective.

It is emphasized that the reference heat rate, the first factor of the right-hand member of equation (1), need not be *test* performance. It may, in fact, be *any* arbitrary level of performance for which all relevant data are known, e.g., design performance, guarantee performance, acceptance test performance, provided only that the value of each of the Δ-values is referred to this standard level of performance. It is preferable that the standard performance be a reasonably close approximation of operating performance, because under this condition the magnitude of the Δ's is small, and second-order effects are minimized. In most cases it is desirable to use guarantee data as the standard performance level, because all relevant data for the performance criteria are known on a consistent basis, or can be determined analytically. It is well known that in modern power plants the guarantees almost invariably are an extremely close approximation of actual performance; thus guarantees constitute the most convenient reference.

Returning to the axiom that the operating heat rate will be equal to the design or standard heat rate unless deviations occur, the only qualifications that must be applied are, obviously, that:

1 All deviations must be considered.

2 The rate of change of heat rate with the performance criterion of a particular component must be known accurately.

It clearly would be desirable to find linear relations between variations of the criteria and deviations in heat rate. In most situations, particularly for small variations of the criteria, a linear relationship is adequate for our purposes, as will be demonstrated.

The entire concept of deviation monitoring is predicted on the same philosophy as that which permits the use of "correction factors" in power-plant testing [1]. In any physical system the rate of change of one variable with respect to another is more accurately known than the absolute values of the variable itself. That is, for example, while the absolute value of a turbine efficiency may not be known accurately, the *rate of change* of this efficiency with exhaust pressure is quite well known, because it is amenable to analytical solution. Similarly, the effect of change in turbine-inlet temperature on turbine efficiency is known more accurately than the turbine efficiency itself.

Specifically, suppose it is found by test that the basic criterion of heater-system performance H_s varies appreciably from the expected value of this criterion.[3] When the magnitude of this variation is known, the effect on heat rate ΔH_s may be found immediately either by manual methods or by means of a computer, using the applicable relationship. If it is found that ΔH_s is 0.3 per cent, there is presumptive evidence that the actual heat rate of the plant is 0.3 per cent poorer than the standard, unless other offsetting deviations exist. Similarly, it may be found by measurement, for example, that the efficiency of the low-pressure turbine is higher than guaranteed. Such a deviation would cause the heat rate to be lower than the standard by a predictable amount. When such deviations as these are applied to the reference heat rate, as in equation (1), the operating heat rate is found as a net result.

The entire philosophy of the deviation-monitoring method embodies four steps; that is, one must:

1 Find the departure of any performance parameter from the "standard" value.

2 Find the relationship between changes in each parameter and heat rate, preferably in linearized form.

3 Apply the relationship to the change in the performance parameter to find the net deviation in heat rate.

4 Add up the individual deviations to find the total change in heat rate.

Thus the operating heat rate is found by quantitative evaluation of a number of individual determinants. The virtues of this approach are:

1 The deviation-monitoring concept, by considering separately the individual effects, eliminates the possibility that a fault in one component may be masked by superior performance of another, preventing improvement of the over-all performance.

2 Any Δ known to be small or uncontrollable may be omitted from consideration or, alternatively, may be approximated in accordance with the results of manual testing, or other available information.

3 The source and magnitude of any deviation from standard performance may be identified, and the cost of this deviation in terms of fuel readily determined. This cost may be balanced against the cost of repairing the fault, and a logical decision as to the best course of action made.

[2] H. T. Hoffman and C. P. Welch, "The Application of the Deviation Concept of Turbine Cycle Monitoring," published in this issue, pp. 423–432.

[3] Reference [2], p. 389.

4 The deviation of over-all plant performance from the standard at loads other than the operating condition under which the test is made frequently may be predicted, because of the predictability of the respective individual deviations.

5 Deviation from the standard performance depends only on rates of change of physical quantities, like correction factors, rather than absolute values. For this reason the results should be more accurate. There are some exceptions to this principle, such as the turbine efficiency, which obviously must be measured in absolute magnitude.

6 Any component of the performance-monitoring equipment may be omitted or may become inoperative without introducing major error in the final result. The error will be limited to the magnitude of the deviation normally indicated by the component in question.

Determinants of Reheat-Cycle Heat Rate

We are concerned primarily with the turbine reheat cycle. Reheat-cycle heat rate is defined as the total energy input to the working fluid in the boiler and reheater, between final feedwater temperature and high-pressure turbine inlet and, in the reheater, per unit of net energy output. To simplify the explanation we will consider, for the moment, that the reheat cycle is operating at design inlet pressure and temperature, reheat pressure and temperature, and exhaust pressure. The focus of our interest will include turbine efficiency, heater cleanliness, and other such factors within the province of the turbine cycle. Since mechanical and electrical losses are always essentially equal to guarantee values, they will not be considered further in this paper. Heat rates, as used, are those that would obtain with no mechanical or electrical losses.

It is convenient to consider the complete reheat cycle in two separate portions, a viewpoint that has been presented by the author in earlier work [3]. Under this approach the heat rate of the complete reheat cycle is considered to be equal to the heat rate of the low-pressure portion, adjusted for the gain that arises as a result of reheat. Thus for monitoring purposes the task is broken down into two major portions; namely, monitoring of the low-pressure cycle and monitoring of the fractional gain due to reheat G_r. Algebraically,

$$r_r = r_n(1 - G_r) \tag{2}$$

Low-Pressure System. Considering first the low-pressure portion, it previously has been demonstrated [1] that the heat rate of a simple regenerative cycle, such as that represented by the low-pressure portion of a reheat plant, may be found from the theoretical non-extraction heat rate corresponding to the design steam conditions, by dividing it by the turbine efficiency and reducing the result to allow for the gain that results from regenerative feedwater heating. Obviously a separate correction must be made for mechanical and electrical losses. Expressed algebraically,

$$r_e = \frac{\text{Th SR}(H_1 - h_c)}{\eta_{tb}} = \frac{\text{nonext Th heat rate}}{\eta_{tb}} = \frac{\text{const}}{\eta_{tb}} \tag{3}$$

$$r_n = r_e(1 - G_f) \tag{4}$$

in which η_{tb} is the over-all turbine "shaft efficiency" (frequently known as "wheel efficiency"), and G_f is the fractional gain due to the use of regenerative feedwater heating.[4]

Under our hypothesis that cycle conditions, including feedwater enthalpy, are equal to standard conditions, the theoretical nonextraction heat rate is a known and fixed quantity. Thus for purposes of monitoring the low-pressure system it is necessary only that we monitor (*a*) the turbine efficiency and (*b*) the gain due to feedwater heating.

High-Pressure System. The relationship by which the gain due to reheat, G_r, may be monitored has been given previously[5] and is repeated herewith using the nomenclature in Fig. 1.

$$G_r = [r_n(1 - G_r) - 1]\left\{\frac{H_2 - H_x}{H_1 - h_f}\left[\left(1 + \frac{\Delta h}{H_E - h_{bf}}\right)\left(1 - \Delta h\,\frac{H_E - H_x}{(H_E - h_f)(H_2 - H_x)}\right)\right]\right\} \tag{5}$$

so that when $H_E = H_x$, as when the high-pressure heater is connected to the high-pressure turbine exhaust

$$G_r = (r_r - 1)\left(\frac{H_2 - H_x}{H_1 - h_f}\right)\left(\frac{H_x - h_f}{H_x - h_{bf}}\right) \tag{6}$$

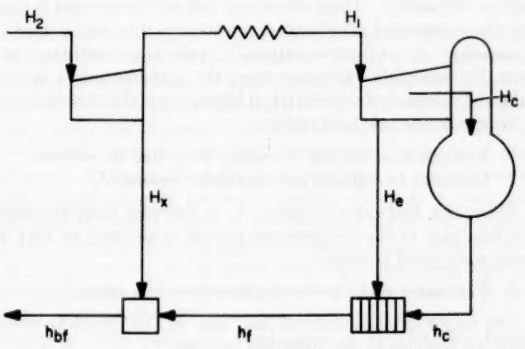

Fig. 1 Nomenclature

This equation specifies the factors that affect the theoretical gain due to reheat. As outlined in a previous paper [3] the theoretical gain invariably is reduced, in an actual reheat cycle, by a "realization factor," designated as η_i. This realization factor arises because of the degradation of energy that flows between the high-pressure and low-pressure portions of the cycle. The loss due to this effect invariably is small. We eliminate it from consideration herein by using a pumped heater to avoid flashed drains. It may be handled, where desirable, by other means.

The loss that results from interconnections between the high and low-pressure portions of the cycle frequently is made up of several components, each involving a relatively small flow, such as gland leakage or valve-stem leakage. Monitoring of all elements of the interconnection loss would require an investment in equipment that may be unjustified by the improvements which occasionally might be made. As a consequence, it is suggested, as an alternative, that the loss due to the interconnections be determined for each of the individual interconnections by analytical means. Then, on the assumption that the enthalpy values will probably vary but slightly from the design values, the flow quantities may be measured (by either manual or automatic instrumentation) and the calculated losses under design conditions prorated in accordance with the flow. By this means an excellent first approximation to the deviation in heat rate that arises from a fault in the interconnections is obtained at low cost.

Alternatively, it is not at all unreasonable to ignore completely

[4] Note that reference [1] used PG ("percentage gain") to designate the fractional gain due to regeneration. To match the nomenclature for the gain due to reheat, G_r, this regeneration gain is designated herein as G_f; that is, G_f = PG. A method for evaluating it for any cycle is given by eq. (7), p. 391, of reference [2].

[5] See reference [3], equations (17) and (18) combined.

possible faults in the interconnections, and to eliminate them from consideration in performance monitoring. Ignoring *variations* of the realization factor η_i does not introduce an error in heat rate of an amount equal to the loss. Instead, the interconnection loss is regarded as constant and equal to the *design loss* by such an approach. If a change in the interconnection loss occurs, due to some fault in the system, it obviously is not detected.

By inspection of equation (5) it is observed that the variables most likely to affect the gain due to reheat are $(H_2 - H_x)$ and Δh. The former is used energy in the high-pressure turbine, an important element, obviously, in determining the gain due to reheat. The latter is the enthalpy rise across the high-pressure heater system, and determines, in large measure, the quantity of extraction taken from the high-pressure system, hence the extra flow to which heat may be added in the boiler, thus increasing the gain due to reheat. Both of these factors may be monitored, and the results compared with design values. Increase in either factor will increase the gain due to reheat. However, a change in $(H_2 - H_x)$ may result from change in either H_2 or high-pressure turbine efficiency. Thus sometimes the environmental factors and the component effectiveness are inextricably intertwined.

Summary. Apart from variations in cycle steam conditions and normally negligible variations from the manufacturer's quoted values of mechanical and electrical losses, the major determinants of low-pressure-cycle heat rate are:

1 Low-pressure turbine efficiency from line to exhaust.
2 Gain due to regenerative feedwater heating G_f.

When the feedwater enthalpy h_f is different from standard, the heat rate of the low-pressure system is affected, so that we must add a third criterion.

3 Feedwater enthalpy leaving low-pressure system h_f.

The major determinants of heat rate of the complete reheat plant, in addition to the foregoing, include:

4 High-pressure turbine used energy $(H_2 - H_x)$.
5 Rise in feedwater enthalpy in high-pressure heaters Δh.
6 Realization factor η_i (not considered further herein).

Thus we now are aware of the major criteria that delineate the effectiveness of the components of a reheat system under *design steam conditions*. It is not adequate, however, to devise a system that does not consider changes in design conditions. To do so we must consider the possibility of changes in *any* parameter that affects heat rate, including steam conditions. Shown in Fig. 1 is the nomenclature used in this paper. All of the variables shown thereon affect the heat rate r_r but, most importantly, *no other variable than those shown* has an effect on the reheat heat rate; that is,

$$r_r = f(H_c, h_c, H_s, h_f, H_1, H_x, h_{bf}, H_2) \quad (7)$$

If we are able to relate changes in each of these variables to change in heat rate, we may find the total change in heat rate by summing up the individual changes. This will be a major objective of the remainder of this paper. Furthermore, by using various combinations of the parameter changes we may monitor individual components, which is the ultimate objective, according to the effectiveness criteria outlined in the foregoing. For example, change in the high-pressure turbine used energy appears as $\Delta(H_2 - H_x) = \Delta H_2 - \Delta H_x$. Similarly, a change in high pressure heater rise is $\Delta(h_{bf} - h_f) = \Delta h_{bf} - \Delta h_f$.

Thus the fundamental attack is to find the effect of each variable in equation (7), and later to combine them as required for monitoring. To accomplish this objective it is necessary to establish a heat-rate relationship that recognizes changes in the two major portions of the system separately, in accordance with the viewpoint of equation (2).

The General Monitoring Equation

It is evident from equation (2) that

$$\frac{\Delta r_r}{r_r} = \left(1 + \frac{\Delta r_n}{r_n}\right)\left(1 - \frac{G_r}{1 - G_r}\left(\frac{\Delta G_r}{G_r}\right)\right) - 1 \quad (8)$$

hence

$$\frac{\Delta r_r}{r_r} \approx \frac{\Delta r_n}{r_n} - \frac{G_r}{1 - G_r}\left(\frac{\Delta G_r}{G_r}\right) \quad (9)$$

By equation (9) we see that we need to find $\Delta r_n/r_n$ and $\Delta G_r/G_r$ as the first step. From Fig. 1 it is seen that

$$r_n = f(H_c, h_c, H_s, h_f, H_1) \quad (10)$$

Furthermore, G_r is dependent on r_n because, by equation (5)

$$G_r = f(r_n, \text{etc.}) \quad (11)$$

In other words, to find the fractional change in reheat heat rate, $\Delta r_r/r_r$, we must first find the effect of any changes in the low-pressure system on r_n. The resulting change in r_n will, of itself, cause a change in G_r, which must be evaluated for use in equation (8) or (9). Having found the net effect of Δr_n on r_r, there remains the problem of changes in the high-pressure system, which affect G_r. That is, changes in H_x, h_{bf}, and H_2 will affect G_r. These effects must be evaluated as $\Delta G_r/G_r$, and applied to find the additional effect on r_r. Our problem thus reduces to finding analytical expressions relating the change in each parameter to the resulting change in heat rate.

Monitoring the Low-Pressure Cycle

Effect of ΔH_s on Heat Rate of Low-Pressure System, r_n. A method by which the effect of ΔH_s on r_n may be found already has been developed.[6] If all operating conditions, including turbine-exhaust pressure, turbine efficiency, turbine initial conditions, and final feedwater temperature are standard, the determination of the effect of ΔH_s on r_n is given by equation (12) [2] in first approximation. The first approximation, designated as A for convenience, is linear in ΔH_s:

$$\left.\frac{\Delta r_n}{r_n}\right]_{H_s} \approx (r_n - 1)w\frac{\Delta H_s}{H_s - h_c} \; (\equiv A, \text{ by definition}) \quad (12)$$

As later demonstrated in an example, the first approximation is adequate in all normal situations. The exact relationship is given herewith, however, for convenience

$$\left.\frac{\Delta r_n}{r_n}\right]_{H_s} = \frac{A\Big/\left(1 + \dfrac{\Delta H_s}{H_s - h_f}\right)}{1 - \left[\left(\dfrac{r_n}{r_n - 1}A\right)\Big/\left(1 + \dfrac{\Delta H_s}{H_s - h_f}\right)\right]} \quad (13)$$

It must be borne in mind that H_s is the flow-weighted enthalpy of steam taken from the extraction openings of the low-pressure turbine for feedwater heating. Methods for determining H_s are given in reference [2].

Only rarely are environmental conditions identical with standard conditions, so that normally it will be necessary to make corrections for the changes in H_s caused by change in these conditions if we wish to evaluate the effectiveness of the heater system (of which H_s is a measure), and compare it with the standard; that is, we must restore the measured value of H_s to the value that would exist if the environmental conditions were standard. Comparison of the corrected value with the standard will yield a dif-

[6] Reference [2], equation (7), p. 391.

ference, ΔH_s, in general. This difference is a measure of the faults that exist in the heater system. The effect of these faults on heat rate of the low-pressure system is given by equations (12) and (13).

To correct a measured value of H_s to standard conditions, corrections must be made for

1 Change in exhaust pressure from standard.
2 Change in turbine efficiency from standard.
3 Change in inlet pressure from standard.
4 Change in inlet temperature from standard.

Consider first the correction for exhaust pressure. This is discussed at length in reference [2]. It is there shown that, if we neglect secondary effects, the change in H_s with condensate enthalpy is given by [2]

$$\Delta H_s = n \frac{w_l}{w} \left(\frac{H_s - H_l}{R_l} \right) \tag{14}$$

If a fault exists within the turbine it will increase the enthalpy of the extracted steam. The manner in which this enthalpy is affected, and the extraction openings for which the enthalpy is affected, depend on where the fault lies. It is obvious that the heater system should not be charged for faults that lie within the turbine. Thus if it is found in monitoring turbine efficiency that it is lower than the standard value, a correction (decrease) must be made in the measured value of H_s, to restore it to the value that would exist with the standard stateline.

The determination of the location of a fault in turbine efficiency is difficult. It has been proposed [2] that in the absence of better information the fault in turbine efficiency be considered to be distributed uniformly throughout the machine. Under this convention the value of H_s will be changed by a fraction of the change in exhaust enthalpy, as a result of the fault in turbine efficiency. This fraction will be the ratio of the used energy between inlet and H_s and the total used energy on the machine; that is,

$$\Delta H_s = \frac{H_1 - H_s}{H_1 - H_e} (\Delta H_e) \tag{15}$$

Equation (15) expresses a ΔH_s that results from a change in H_e. If H_e is higher than standard, H_s will also be higher, and a subtractive correction must be made to the measured value of H_s.

The correction of measured H_s for inlet pressure and temperature has been discussed at length in reference [2], p. 394. While methods for estimating the change in H_s with inlet pressure and temperature are available, these are approximate at best. It is recommended that for greatest accuracy the manufacturer be requested to provide correction curves for H_s as a function of inlet pressure, temperature, and throttle flow. The corrections to H_s are linear within the useful range, so that calculation of a single off-design heat balance should suffice for each, at any given flow.

The foregoing discussion relates entirely to the problem of comparing the *effectiveness of the heater system* with the design performance, to discover a possible fault. It is emphasized strongly, however, that where this is not the objective, it is *not necessary* to make the corrections outlined to find a change in heat rate from some known condition. In other words, using methods developed later, it is perfectly possible to find the change in r_n from the change in each of its determinants, that is,

$$\Delta r_n = f(\Delta H_e, \Delta h_c, \Delta H_s, \Delta h_f, \Delta H_1) \tag{16}$$

whether or not the respective components are operating at design effectiveness.

In finding an influence coefficient for each of these, all of the others are assumed to remain constant. For small changes, the total effect on heat rate is the sum of the separate individual effects, to a close approximation. Expressed algebraically

$$\frac{\Delta r_n}{r_n} \approx \frac{1}{r_n} \left[\left(\frac{\partial r_n}{\partial H_e} \right) \Delta H_e + \left(\frac{\partial r_n}{\partial h_c} \right) \Delta h_c + \left(\frac{\partial r_n}{\partial H_s} \right) \Delta H_s + \left(\frac{\partial r_n}{\partial h_f} \right) \Delta h_f + \left(\frac{\partial r_n}{\partial H_1} \right) \Delta H_1 \right] \tag{16a}$$

in which the parenthetical quantities are the influence coefficients that are derived later.

It must be noted that in the complex modern plant the measurement of H_s is not without problems. Accuracy in flow measurement is essential, and extraneous heat inputs to the heater system must be accounted for. Nevertheless, since the entire contribution of the heater system to heat rate is determined exclusively by H_s and environmental factors, either H_s must be measured or an alternative must be devised. The alternative might consist of measurement of all data for all heaters, and calculation of extractions by heat balance, with subsequent analysis by well-known methods. It would seem that the cost of extensive instrumentation and manual analysis might well exceed that of direct measurement of H_s, despite the requirement for accuracy in the latter.

It also is to be noted that H_s provides an *over-all* measurement of the effectiveness of the *heater system*. Faults in the heater system taken as a whole are identified as to effect on heat rate, but not as to location within the system. Further work, not presented herein, has indicated a method by which, with additional development, faults in individual heaters may be detected and evaluated. At the moment it is considered that an over-all check of the effectiveness of the heater string, taken as a unit, accomplishes the broad objective of monitoring major components. Whether identification of a particular heater as the offender in a faulty heater system can be automated economically will depend, obviously, on the complexity of the relationship that will be developed, and the cost of the necessary instrumentation.

Change in Final Feedwater Temperature of Low-Pressure Cycle. The foregoing discussion provides a method by which the effectiveness of the heater system may be measured, and the effect on heat rate of any change in effectiveness evaluated through the use of equation (12), using a corrected measured value of H_s. It has been assumed that changes in H_s occur as a result of fouling of certain heaters, but that the final feedwater temperature leaving the top low-pressure heater h_f remains unchanged.

It is possible under certain circumstances for the final feedwater temperature to change, without change in H_s. For example, if the top heater is fouled the feedwater temperature will be reduced, as well as the extraction quantity taken from the highest opening in the low-pressure turbine. This would tend to reduce the value of H_s. A simultaneous fault in one or more of the lower heaters would have the effect of raising H_s, so that no net change would be apparent. To isolate the effect of final feedwater temperature alone on heat rate one must assume H_s to remain unchanged, and proceed directly to an analysis of the effect of change in h_f.

Using the methods developed by the author [2], it may be shown that to a first approximation the change in heat rate of the low-pressure system caused by change in feedwater temperature leaving the low-pressure system is given by a relationship that is linear in Δh_f

$$\left. \frac{\Delta r_n}{r_n} \right]_{hf} \approx -(r_n - 1)(1 + w) \left(\frac{H_1 - H_s}{H_1 - h_f} \right) \left(\frac{\Delta h_f}{H_s - h_s} \right) \quad (\equiv B, \text{ by definition}) \tag{17}$$

By analogy with equation (12) this linear approximation of the change in heat rate is designated by B. It is sufficiently accurate for most purposes. However, the exact relationship, corresponding to equation (13) is

$$\left.\frac{\Delta r_n}{r_n}\right]_{h_f} = \frac{B\Big/\left(1 - \dfrac{\Delta h_f}{H_s - h_f}\right)}{1 - \left[\left(\dfrac{r_n}{r_n - 1}B\right)\Big/\left(1 - \dfrac{\Delta h_f}{H_s - h_f}\right)\right]} \tag{18}$$

Equations (12) and (17) represent approximate forms corresponding to changes in H_s and changes in h_f, respectively. The corresponding exact relationships are given by equations (13) and (18).

It must be borne in mind that equations (13) and (18) are predicated on constant h_f and constant H_s, respectively. If changes in both take place, the losses may be found by using the applicable equations and adding the results. Where changes are small, the result is quite accurate. However, the interaction of H_s and h_f, each on the other, introduces small second-order effects when the results are added.

In summary, we now have means for finding the effect on heat rate of the low-pressure cycle due to changes in the primary criterion of heater-system effectiveness H_s and changes in feedwater temperature leaving the top low-pressure heater. To find the total change in r_n at design steam conditions, we need only to evaluate the effect of change in low-pressure system turbine efficiency.

Low-Pressure Turbine Efficiency. Any change in low-pressure turbine efficiency will affect H_c, hence r_n. It can be evaluated only through a measurement of the output developed by the condenser flow, since we cannot directly measure H_c.

To accomplish this objective it is first necessary to measure H_s, and from this value to determine the output of the extracted steam. By subtraction of this output from the total output of the low-pressure system the output of the condenser flow is determined. Comparison of this output with the expected output under the applicable operating conditions permits determination of any change in turbine efficiency that may have taken place. As shown previously in reference [2], equation (21)

$$\left.\frac{\Delta r_n}{r_n}\right]_{\eta} = \frac{-\Delta P_c}{P_t} \tag{19}$$

Since the effect of change in turbine efficiency is a change in H_s it may also be evaluated directly from the change in H_c [as shown by equation (22)].

Change in Inlet Enthalpy of Low-Pressure Turbine H_1. Now let us consider changes in steam conditions, which have been assumed to be at design values heretofore. A change in inlet enthalpy H_1 of the low-pressure turbine causes a change in heat supplied to the system. Assuming, for the moment, that h_f, H_s, H_c, and h_c remain unchanged, it may be shown that

$$\left.\frac{\Delta r_n}{r_n}\right]_{H_1} = -\frac{(r_n - 1)\dfrac{\Delta H_1}{H_1 - h_f}}{1 + r_n\left(\dfrac{\Delta H_1}{H_1 - h_f}\right)} \tag{20}$$

Change in Hotwell Enthalpy h_c. Although for monitoring the effectiveness of the heater system it is not necessary to consider Δh_c separately, since the effect is reflected in H_s, it is desirable to include herein an expression for its effect on r_n, for completeness.

$$\left.\frac{\Delta r_n}{r_n}\right]_{h_c} = -\frac{(r_n - 1)\left(\dfrac{H_s - H_c}{H_c - h_c}\right)\left(\dfrac{\Delta h_c}{H_s - h_c}\right)}{1 - \left[1 - (r_n - 1)\left(\dfrac{H_s - H_c}{H_c - h_c}\right)\right]\left(\dfrac{\Delta h_c}{H_s - h_c}\right)} \tag{21}$$

Equation (21) assumes that H_s, H_c, H_1, and h_f remain unchanged.

Change in Exhaust Enthalpy H_c. Where desired to analyze this effect separately

$$\left.\frac{\Delta r_n}{r_n}\right]_{H_c} = \frac{(r_n - 1)\left(\dfrac{\Delta H_c}{H_c - h_c}\right)}{1 - (r_n - 1)\left(\dfrac{\Delta H_c}{H_s - h_c}\right)} \tag{22}$$

Equation (22) assumes that H_s, H_1, h_c, and h_f remain unchanged.

Summary of Low-Pressure-System Equations. All equations for $\Delta r_n/r_n$ of the low-pressure system are collected herewith for ready reference

$$\left.\frac{\Delta r_n}{r_n}\right]_{H_s} = \frac{A\Big/\left(1 + \dfrac{\Delta H_s}{H_s - h_f}\right)}{1 - \left[\left(\dfrac{r_n}{r_n - 1}A\right)\Big/\left(1 + \dfrac{\Delta H_s}{H_s - h_f}\right)\right]} \tag{13}$$

$$\left.\frac{\Delta r_n}{r_n}\right]_{h_f} = \frac{B\Big/\left(1 - \dfrac{\Delta h_f}{H_s - h_f}\right)}{1 - \left[\left(\dfrac{r_n}{r_n - 1}B\right)\Big/\left(1 - \dfrac{\Delta h_f}{H_s - h_f}\right)\right]} \tag{18}$$

$$\left.\frac{\Delta r_n}{r_n}\right]_{H_1} = -(r_n - 1)\frac{\dfrac{\Delta H_1}{H_1 - h_f}}{1 + r_n\dfrac{\Delta H_1}{H_1 - h_f}} \tag{20}$$

$$\left.\frac{\Delta r_n}{r_n}\right]_{h_c} = -(r_n - 1)\frac{\left(\dfrac{H_s - H_c}{H_c - h_c}\right)\left(\dfrac{\Delta h_c}{H_s - h_c}\right)}{1 - \left[1 - (r_n - 1)\dfrac{H_s - H_c}{H_s - h_c}\right]\left(\dfrac{\Delta h_c}{H_s - h_c}\right)} \tag{21}$$

$$\left.\frac{\Delta r_n}{r_n}\right]_{H_c} = (r_n - 1)\frac{\dfrac{\Delta H_c}{H_c - h_c}}{1 - (r_n - 1)\left(\dfrac{\Delta H_c}{H_s - h_c}\right)} \tag{22}$$

Monitoring the Reheat System

Reference [3] presented the point of view that the reduction in heat rate associated with reheating is determined entirely by the magnitude of the fractional increase in heat supplied, $\Delta Q/Q$, that results from the addition (see equation (18) of reference [3]). Let us designate this quantity by S, that is,

$$S = \Delta Q/Q \tag{23}$$

and

$$G_r = (r_r - 1)S \tag{24}$$

or

$$G_r = [r_n(1 - G_r) - 1]S \tag{25}$$

Whereas reference [3] concerns itself with finding the improvement in heat rate, G_r, that resulted from superposing reheat on a low-pressure system, the present problem is to find the *change* in reheat heat rate that results from changes in the reheat system or other causes. It is clear, therefore, that we shall be concerned not with S itself but with $\Delta S/S$.

Reference [3] assumed a fixed low-pressure system and found the improvement in its heat rate resulting from the addition of reheat by determination of the value of S. Because the low-pressure

system was fixed, the heat rejected remained unchanged when reheat was added. That is, $\Delta q/q = 0$. On the other hand, even if S remains constant, as it will when H_1 and h_f of the low-pressure system remain unchanged, G_r will change if the low-pressure system changes in some other respect, as, for example, by a change in $\Delta q/q$ resulting from a change in turbine efficiency, or by a fault in the heater system. Thus G_r is a function not only of S, but also of r_n. This is also clear from equation (25), since $G_r = f(r_n, S)$.

The change in r_r that results from a change in r_n for fixed reheat conditions is given in reference [3] by equation (27). However, for present purposes it is more convenient to find the change in G_r due to changes in both r_n and S, by equation (26), and later to combine such changes with other existing effects to find the total change in plant heat rate. It may be shown that

$$\frac{\Delta G_r}{G_r} = \frac{\left(1 + \frac{r_r}{r_r - 1}\frac{\Delta r_n}{r_n}\right)\left(1 + \frac{\Delta S}{S}\right) - 1}{1 + \left(\frac{r_r}{r_r - 1}\right)\left(\frac{G_r}{1 - G_r}\right)\left(1 + \frac{\Delta r_n}{r_n}\right)\left(1 + \frac{\Delta S}{S}\right)} \tag{26}$$

in which r_r and G_r are the original values, before change in r_n and S.

Thus one effect on reheat heat rate is that which results from changes in the low-pressure system itself, even if there are no changes in the reheat system, that is, even if $\Delta S/S = 0$. A second effect is that which results from a change in S. Both of these effects change G_r, as shown by equation (26).

Changes in Reheat System. Let us now consider changes that may occur in the reheat system, including the interface between the reheat system and the low-pressure system, in an effort to evaluate $\Delta G_r/G_r$ for use in equation (8). By equations (6) and (24)

$$S = \left(\frac{H_2 - H_x}{H_1 - h_f}\right)\left(\frac{H_x - h_f}{H_x - h_{bf}}\right) \tag{27}$$

if we assume that the only heater above the reheat point is connected to the exhaust of the high-pressure turbine. Since this is the most common arrangement, and since additional heaters would further complicate the presentation, no other arrangement will be considered herein.

It is clear from equation (24) that G_r is not directly proportional to S, because r_r is, in itself, a function of S. It may be shown that, when $\Delta r_n = 0$,

$$\left.\frac{\Delta G_r}{G_r}\right]_{\Delta S} = \frac{\left(\frac{r_n - 1}{r_n G_r}\right) - 1}{1 + \left(\frac{r_n - 1}{r_n G_r}\right)\left(\frac{1}{\Delta S/S}\right)} \tag{28}$$

which is expressed in terms of r_n and may be most conveniently used when r_n is known. Alternatively, when it is more convenient to use r_r, equation (28) may be written in terms of this variable

$$\left.\frac{\Delta G_r}{G_r}\right]_{\Delta S} = (1 - G_r)\left[\frac{\left(\frac{r_r - 1}{r_r G_r}\right)}{1 + \left(\frac{r_r - 1}{r_r G_r}\right)\left(1 + \frac{G_r}{r_r - 1}\right)\left(\frac{1}{\Delta S/S}\right)}\right] \tag{29}$$

In both equations r_n, r_r, and G_r are the original values, before change in S. The value of $\Delta S/S$ remains to be found.

Considering equation (27), it appears that

$$S = f(H_2, H_x, H_1, h_f, h_{bf}) \tag{30}$$

That is, we must evaluate $\Delta S/S$ for changes in inlet enthalpy to both high-pressure turbine and low-pressure turbine, changes in feedwater temperature entering the high-pressure heater, changes in feedwater temperature leaving the high-pressure heater, and changes in exhaust enthalpy H_x. Observe that a change in the used energy of the high-pressure turbine, $U = H_2 - H_x$, may take place without change in the exhaust enthalpy H_x through changes in the inlet enthalpy to the high-pressure turbine H_2. However, in the general case it will involve a change in H_x that affects the heater, hence the effect on the heater must be considered separately. In other words, while U is a primary determinant of reheat gain, any change in its value usually results in a change in H_x, which in turn affects the high-pressure extraction, and therefore necessitates separate evaluation of this effect. An expression to be developed later [equation (43)] includes the effect of ΔH_x on both U and high-pressure extraction.

However, by equation (27), if H_x, H_1, h_f, and h_{bf} are constant

$$\left.\frac{\Delta S}{S}\right]_U = \frac{\Delta(H_2 - H_x)}{H_2 - H_x} = \frac{\Delta U}{U} \tag{31}$$

The general expression for change in S due to change in conditions surrounding the high-pressure system is complex, but frequently some of the terms drop out, so that the relationship is scarcely as formidable as it first appears. It is seen from equation (27) that, in general, for small increments

$$\frac{\Delta S}{S} = \frac{\frac{\Delta H_x - \Delta h_f}{H_x - h_f} - \frac{\Delta H_x - \Delta h_{bf}}{H_x - h_{bf}} - \frac{\Delta H_1 - \Delta h_f}{H_1 - h_f} + \frac{\Delta H_2 - \Delta H_x}{H_2 - H_x}}{\left(1 + \frac{\Delta H_1 - \Delta h_f}{H_1 - h_f}\right)\left(1 + \frac{\Delta H_x - \Delta h_{bf}}{H_x - h_{bf}}\right)} \tag{32}$$

in which only second-order cross products are neglected. Note that equation (31) may be derived directly from equation (32).

Thus it is seen that a fractional change in G_r may result from changes in the low-pressure cycle heat rate, changes in the used energy of the high-pressure turbine, or changes in conditions surrounding the high-pressure heater. The net effect is given by equation (26), using equation (32) to find $\Delta S/S$, and values of $\Delta r_n/r_n$ found by previously demonstrated methods. Knowing the net value of $\Delta G_r/G_r$, it may be used in equation (8) to find $\Delta r_r/r_r$.

Approximate Forms

It is possible, using the relationships of equations (9) and (26) to derive approximate forms for the change in reheat heat rate that results from changes in each of the determining parameters. Since the cost of a computer in a monitoring system is related to a considerable extent to the complexity of the equation which it must handle, the development of such approximate relationships obviously is desirable from an economic point of view. It remains to be determined, of course, whether such relationships yield satisfactory accuracy. It will be demonstrated in the "Examples" which follow that such approximate relationships are indeed sufficiently accurate, and may be used for all normal purposes.

To develop these approximate relations equation (9) is first written in an alternative form

$$\frac{\Delta r_r}{r_r} = \frac{\Delta r_n}{r_n}\left(1 - \frac{\left(\frac{G_r}{1 - G_r}\right)}{\left(\frac{\Delta r_n}{r_n}\right)}\frac{\Delta G_r}{G_r}\right) \tag{9a}$$

It is obvious in equation (26) that the terms $\Delta r_n/r_n$ and $\Delta S/S$ in the denominator are small compared to unity. They may therefore be neglected in a first approximation. Similarly, the cross product of these two terms in the numerator may be ignored in a first approximation. Using these approximations we may rewrite equation (26) in the form

$$\frac{\Delta G_r}{G_r} \approx \frac{\left(\frac{r_r}{r_r-1}\right)\frac{\Delta r_n}{r_n}}{1+\left(\frac{r_r}{r_r-1}\right)\left(\frac{G_r}{1-G_r}\right)} + \frac{\Delta S/S}{1+\left(\frac{r_r}{r_r-1}\right)\left(\frac{G_r}{1-G_r}\right)} \tag{33}$$

By substituting equation (33) in equation (9a) we find that

$$\frac{\Delta r_r}{r_r} = \frac{\Delta r_n}{r_n}\left(1 - \frac{\left(\frac{G_r}{1-G_r}\right)\left(\frac{r_r}{r_r-1}\right)}{1+\left(\frac{G_r}{1-G_r}\right)\left(\frac{r_r}{r_r-1}\right)}\right) - \left(\frac{\left(\frac{G_r}{1-G_r}\right)\frac{\Delta S}{S}}{1+\left(\frac{G_r}{1-G_r}\right)\left(\frac{r_r}{r_r-1}\right)}\right) \tag{34}$$

Simplifying this equation by letting

$$C = \left(\frac{G_r}{1-G_r}\right)\left(\frac{r_r}{r_r-1}\right) \tag{35}$$

we find that

$$\frac{\Delta r_r}{r_r} = \frac{\left(\frac{\Delta r_n}{r_n}\right)}{1+C} - \frac{\left(\frac{\Delta S}{S}\right)}{1+C}\left(\frac{G_r}{1-G_r}\right) \tag{36}$$

The relationship of equation (36) is the fundamental form of the first approximation. To use it, $\Delta r_n/r_n$ may be found by the methods previously presented. Similarly, $\Delta S/S$ may be found through the use of equation (32), changing one parameter at a time, or changing all parameters simultaneously. The form of equation (36) will be used in the Example to determine the approximate change in heat rate that results from change in any of the parameters.

As one might expect, any basic change in the low-pressure cycle that does not affect S affects the complete cycle in accordance with the ratio of the low-pressure-system output and the total system output. It is through this relationship that the combination $(1 + C)$ enters in equation (36); that is, it may be shown that

$$1 + C = \frac{\text{output of complete system}}{\text{output of low-pressure system}} \tag{37}$$

Summary of Linearized Relationships. Using equation (36) and previously developed values of $\Delta r_n/r_n$ and $\Delta S/S$ we may set down the approximate forms for all deviations. The relations given are those which yield $(\Delta r_r/r_r)$ for changes in the indicated variables

$$\left.\frac{\Delta r_r}{r_r}\right]_{H_e} = \frac{A}{1+C} \tag{38}$$

$$\left.\frac{\Delta r_r}{r_r}\right]_{h_f} = \frac{B}{1+C} - \frac{\left(\frac{G_r}{1-G_r}\right)\left(\frac{-\Delta h_f}{H_z-h_f}+\frac{\Delta h_f}{H_1-h_f}\right)}{1+C} \tag{39}$$

$$\left.\frac{\Delta r_r}{r_r}\right]_{H_1} = \frac{-(r_n-1)\frac{\Delta H_1}{H_1-h_f}}{1+C} + \frac{\left(\frac{G_r}{1-G_r}\right)\left(\frac{\Delta H_1}{H_1-h_f}\right)}{1+C} \tag{40}$$

$$\left.\frac{\Delta r_r}{r_r}\right]_{h_c} = \frac{-(r_n-1)\left(\frac{H_e-H_c}{H_e-h_c}\right)\left(\frac{\Delta h_c}{H_e-h_c}\right)}{1+C} \tag{41}$$

$$\left.\frac{\Delta r_r}{r_r}\right]_{H_c} = \frac{(r_n-1)\left(\frac{\Delta H_c}{H_e-h_c}\right)}{1+C} \tag{42}$$

$$\left.\frac{\Delta r_r}{r_r}\right]_{H_x} = -\frac{\frac{\Delta H_x}{H_x-h_f} - \frac{\Delta H_z}{H_x-h_{bf}} - \frac{\Delta H_x}{H_2-H_x}}{1+C}\left(\frac{G_r}{1-G_r}\right) \tag{43}$$

$$\left.\frac{\Delta r_r}{r_r}\right]_{h_{bf}} = -\frac{\frac{\Delta h_{bf}}{H_x-h_{bf}}}{1+C}\left(\frac{G_r}{1-G_r}\right) \tag{44}$$

$$\left.\frac{\Delta r_r}{r_r}\right]_{H_2} = -\frac{\frac{\Delta H_2}{H_2-H_x}}{1+C}\left(\frac{G_r}{1-G_r}\right) \tag{45}$$

It is evident that the eight relationships (38)–(45) provide for all of the changes that may take place in the basic parameters of the reheat cycle, and that when all changes are accounted for we may arrive at the total change in heat rate. More importantly it is to be noted that numerous combinations of these are possible, if one wishes to monitor a particular element of the system. For example, if it is desired to find the effect of the high-pressure turbine alone on heat rate, we see that

$$\left.\frac{\Delta r_r}{r_r}\right]_U = -\frac{\frac{\Delta U}{U}}{1+C}\left(\frac{G_r}{1-G_r}\right) + \frac{\frac{\Delta H_x}{H_x-h_f}\left(\frac{\Delta h}{H_x-h_{bf}}\right)}{1+C}\left(\frac{G_r}{1-G_r}\right) \tag{46}$$

which is found by combining equations (43) and (45). This equation, like other similar combinations of the linearized relationships, consists of a primary effect which is the first term, and a secondary effect, the magnitude of which is quite small. For all practical purposes in monitoring the effectiveness of the high-pressure turbine, the secondary effect may be ignored in most cases.

We have shown that Δh is an important determinant of heat rate. To devise an expression for its effect on heat rate we may combine equations (39) and (44), bearing in mind that

$$\Delta h = h_{bf} - h_f \tag{47}$$

and

$$\Delta(\Delta h) = \Delta h_{bf} - \Delta h_f \tag{48}$$

The result is

$$\left.\frac{\Delta r_r}{r_r}\right]_{\Delta h} = \frac{-\frac{\Delta(\Delta h)}{\Delta h}\left(\frac{\Delta h}{H_x-h_f}\right)}{1+C}\left(\frac{G_r}{1-G_r}\right) + \frac{B - \frac{\Delta h_f}{H_1-h_f} - \left(\frac{\Delta h_{bf}}{H_x-h_f}\right)\left(\frac{\Delta h}{H_x-h_{bf}}\right)}{1+C}\left(\frac{G_r}{1-G_r}\right) \tag{49}$$

in which the first term is the primary effect, as before, and the second term represents residual and much smaller effects.

Equations (46) and (49) provide the monitoring relationships for high-pressure turbine and high-pressure heater, respectively. The effect of a fault in the heater system is given directly by equation (38). A turbine fault is monitored either by equation (19) or by equation (42).

The usefulness of the linearized influence coefficients extends far beyond the examples that have been given. Special combinations are possible, to cover environmental effects, for example. The additive nature of the individual effects, by the principle of superposition, augments the versatility of the relationships, particularly when one has learned to identify the separate effects included within each equation. The author hopes to present, at a future date, the results of work currently in progress in this area, as well as other extensions of the monitoring problem.

Examples

To illustrate the application of the relationships it is desirable to use a simplified reheat cycle, and to apply certain changes to it. The basic cycle, known as the reference cycle, is that shown in Fig. 2. It is similar to Fig. 2 of reference [3], with the exception that certain of the enthalpy values have been rounded off for convenience.

The extraction for the low-pressure cycle, the extraction for the high-pressure heater, the heat rate of the low-pressure cycle, and the heat rate of the entire reheat cycle may be determined readily from the data given in Fig. 2. The method of calculation, which is used throughout all of the examples in which changes in the reference cycle are made, is shown herewith. Although the author is aware of the impracticability of making measurements in an actual plant that yield more than a few significant digits, the example used is an analytical model, not susceptible to measurement errors. The results are therefore carried to far more decimal places than test data could justify, primarily to demonstrate the accuracy of the relationships.

$$w_n = \frac{370 - 65}{1270 - 370} = 0.338888$$

$$r_n = \frac{1.338888(1525 - 370)}{1546.416667 - (1020 - 65)} = 2.614767$$

$$w_r = 1.338888 \times \frac{80}{880} = 0.121717$$

$$w = 1.338888 + 0.121717 = 1.460606$$

$$r_r = \frac{1.460606(1500 - 450) + 1.338888(1525 - 1330)}{1794.719697 - 955}$$

$$= 2.137284$$

From these results the value of G_r may be calculated, using equation (6). The result may be proved, as shown

$$G_r = 1.137284 \left(\frac{170}{1155}\right)\left(1 + \frac{80}{880}\right) = 0.1826100$$

Check:

$$G_r = 1 - \frac{2.137284}{2.614767} = 0.1826100$$

The foregoing calculations yield all of the necessary data for the reference cycle. The applicable conditions are tabulated in Table 1 for reference purposes. Having a firm base to which modifications may be made, certain changes will now be applied to the various parameters of the reference cycle, and the relationships of the paper used to calculate the changes in heat rate.

First let us consider a cycle which we shall designate as Cycle 1, Fig. 3, in which some fault occurs in the low-pressure feedwater heaters, raising the value of H_e from 1270 to 1280. Simultaneously it will be postulated that for some reason the feedwater temperature leaving the top low-pressure heater decreases from 370 to 360.

The new heat rate of the low-pressure system may be calculated as follows:

$$w_n = \frac{295}{1280 - 360} = 0.320652$$

$$r_n = \frac{1.320652(1525 - 360)}{1538.559778 - 955} = 2.636508$$

Similarly, the new reheat heat rate may be calculated, as follows:

$$w_r = 1.320652 \left(\frac{90}{880}\right) = 0.1350667$$

$$w = 1.320652 + 1.350667 = 1.4557187$$

$$r_r = \frac{1.4557187(1500 - 450) + 1.320652(1525 - 1330)}{1786.031808 - 955}$$

$$= 2.149174$$

Let us now calculate the change in heat rate due to ΔH_e, using equation (12)

$$\left.\frac{\Delta r_n}{r_n}\right]_{H_e} \approx A = (r_n - 1) w_n \frac{\Delta H_e}{H_e - h_e}$$

$$= 1.614767(0.338888)\frac{10}{1205} = 0.00454130$$

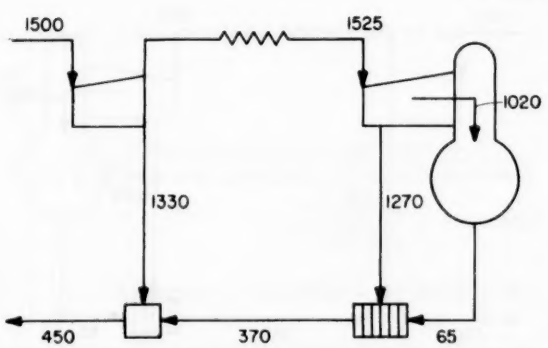

Fig. 2 Reference cycle

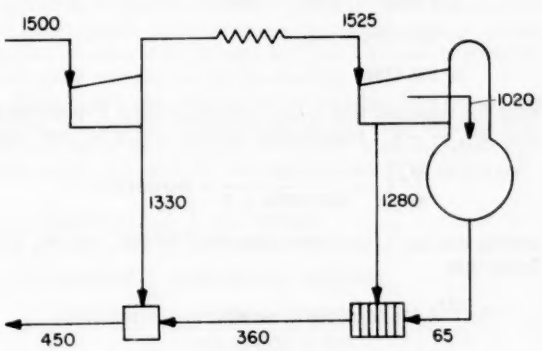

Fig. 3 Cycle 1 (change in H_e and h_f)

Table 1 Data for cycles of example

Cycle reference	h_{bf}	h_f	H_2	H_x	H_1	H_e	H_c	r_n[a]	r_r[a]	G_r[a]
	450	370	1500	1330	1525	1270	1020	2.614767	2.137284	0.1826100
1	450	360	1500	1330	1525	1280	1020	2.636508	2.149174	0.1848406
2	450	360	1500	1330	1525	1280	1025	2.659293	2.162183	0.1869333
3	460	360	1512	1340	1525	1280	1025	2.659293	2.154506	0.1898200

[a] Exact values.

Table 2 Summary of results of example

	Exact		Formula		Per cent error in			
Cycle reference	$\Delta r_n/r_n$	$\Delta r_r/r_r$	$\Delta r_n/r_n$	$\Delta r_r/r_r$	r_n	r_r	$\Delta r_n/r_n$	$\Delta r_r/r_r$
	...	...	...	...	...	...	...	...
1	0.008315	...	0.008502	...	0.0188	...	2.25	...
2	0.017029	0.011650	0.017145	0.011730	0.0116	0.0080	0.68	0.68
3	0.017029	0.008058	0.017145	0.008177	...	0.0119	...	1.48
3a*	...	0.008058	...	0.008348	...	0.0290	...	3.60

* By approximate forms.

Similarly, we may calculate the effect of the decrease in feedwater temperature leaving the top low-pressure heater, using equation (17)

$$\left.\frac{\Delta r_n}{r_n}\right]_{h_f} \approx B = -(r_n - 1)(1 + w_n)\left(\frac{H_1 - H_e}{H_1 - h_f}\right)\left(\frac{\Delta h_f}{H_e - h_c}\right)$$

$$= -1.614767(1.338888)\left(\frac{255}{1155}\right)\left(\frac{-10}{1205}\right) = 0.00396119$$

Adding the two effects we find the total change in low-pressure cycle heat rate, using the methods of the paper

By formula: $0.00454130 + 0.00396119 = 0.00850249$ (Cycle 1)

$$\text{Exact: } \frac{2.636508}{2.614767} - 1 = 0.00831461$$

As shown in Table 2, the formula yields a change in heat rate that is within 2.25 per cent of the actual change. More importantly, the heat rate of the low-pressure system is found with an accuracy of 0.0188 per cent. Thus it would appear that the accuracy of the proposed method in this situation is more than adequate.

Now let us consider that we superimpose on these changes a deterioration in the low-pressure turbine efficiency of such magnitude as to cause an increase in H_c from 1020 to 1025. To determine the change in heat rate equation (19) is used. First it is necessary to find the total power of the low-pressure system, as follows:

$$P_t = P_e + P_c$$

$$= 0.32065217(1525 - 1280) + 1.0(1525 - 1020)$$

$$= 78.55978 + 505$$

$$= 583.55978$$

Since the condenser flow is 1.0, we have, in effect, hypothecated that $\Delta P_c = -5$. Hence using equation (19) it is found that

$$\left.\frac{\Delta r_n}{r_n}\right]_\eta = \frac{5}{583.55978 - 5} = 0.00864215$$

Adding this loss to that previously found for ΔH_e and Δh_f, it is found that

$$\frac{\Delta r_n}{r_n} = 0.00850249 + 0.00864215 = 0.01714464$$

By Table 2 it is seen that the exact change in heat rate, calculated by basic methods previously illustrated, is 1.7029 per cent, as compared with 1.7145 per cent, using the relationships of the paper. This is an accuracy of 0.0116 per cent in heat rate, or 0.68 per cent in the loss.

An alternative approach to finding the loss is to use the change in H_c directly, as shown by equation (22)

$$\frac{\Delta r_n}{r_n} = \frac{1.636508\left(\frac{5}{1020 - 65}\right)}{1 - 1.636508\left(\frac{5}{955}\right)} = \frac{0.0085681}{0.9914319}$$

$$= 0.00864215$$

which is an exact check of the loss found previously.

It now has been demonstrated that the methods presented in the paper are adequate for predicting a change in the heat rate of the low-pressure cycle due to changes in H_e, changes in h_f, and changes in turbine efficiency. Although the effects of H_1 and h_c are not shown in this example, the relationships given in the text are applied in a similar manner.

It remains to be demonstrated that the methods presented herein also are applicable for changes in the reheat heat rate when such changes occur in the low-pressure cycle, and also when additional changes occur in the reheat portion of the cycle. First, let us determine that the methods given are applicable in predicting the reheat heat rate with changes only in the low-pressure system.

Unfortunately, it is impossible to have a change in the feedwater temperature leaving the low-pressure system without a simultaneous change in the feedwater temperature entering the

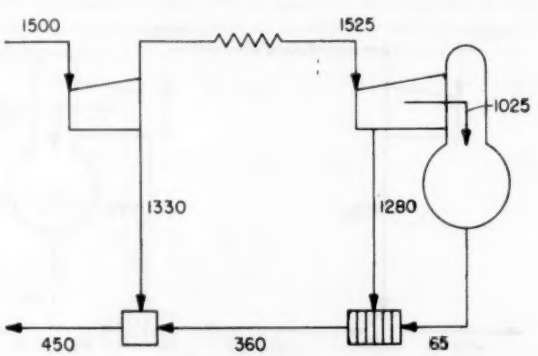

Fig. 4 Cycle 2 (change in H_e, h_f, and H_c)

high-pressure heater, since these are one and the same. Thus to maintain the reheat portion unchanged is impossible. We shall utilize the methods of the paper to determine the reheat heat rate for Cycle 2, as shown in Fig. 4, by using equations (32) and (26) to take care of the change in h_f.

To obtain a comparison between the analytical method presented in the paper and the exact value of the change in heat rate of the complete reheat system of Cycle 2, it is necessary to determine exact values for the nonreheat heat rate r_n and for the reheat heat rate r_r. The reheat of the low-pressure system with reduced turbine efficiency is seen to be

$$r_n = \frac{1538.55977805}{578.55977805} = 2.659293$$

To find the reheat heat rate of Cycle 2 we must first find the extraction from the high-pressure turbine exhaust, as follows:

$$w_r = 1.32065217\left(\frac{90}{880}\right) = 0.13506670$$

$$w = 1.32065217 + 0.13506670 = 1.45571887$$

The heat rate is then found, as follows:

$$r_r = \frac{1.45571887(1050) + 1.32065217(195)}{1786.0319856 - 960} = 2.162183$$

To find the net change in reheat heat rate of Cycle 2 with respect to the reference cycle, knowing the change in heat rate of the low-pressure system from the foregoing calculation, it is necessary to use equation (26) of the text to find $\Delta G_r/G_r$. The value of G_r is that pertaining to the reference cycle, the value of $\Delta r_n/r_n$ is that previously calculated, and the value of $\Delta S/S$ is found from equation (32) of the text.

Considering equation (32), it will be noted that the only variable which has experienced a change in the present example is h_f; that is, $\Delta h_f = -10$, as specified for Cycle 2. Under these conditions equation (32) reduces to

$$\frac{\Delta S}{S} = \frac{-\dfrac{\Delta h_f}{H_x - h_f} + \dfrac{\Delta h_f}{H_1 - h_f}}{1 - \dfrac{\Delta h_f}{H_1 - h_f}}$$

Inserting values from Cycle 2 we find that

$$\frac{\Delta S}{S} = \frac{-\dfrac{-10}{960} + \dfrac{-10}{1155}}{1 + \dfrac{10}{1155}} = 0.001743562$$

Inserting the applicable values in equation (26) we find that

$$\frac{\Delta G_r}{G_r} = \frac{(1 + 1.8792878 \times 0.01714464)(1.001743562) - 1}{1 + (1.8792878 \times 0.223406192)(1.01714464)(1.001743562)}$$

$$= \frac{0.034019452}{1.427738394} = 0.023827511$$

$$\left.\frac{\Delta r_r}{r_r}\right]_{r_n, h_f} = -0.023827511 \times 0.22340619 = -0.00532321345$$

Using equation (8), inserting the foregoing value and the previously found value of $\Delta r_n/r_n$ we find

$$\frac{\Delta r_r}{r_r} = (1.01714464)(1 - 0.00532321345) - 1 = 0.011730162$$

versus 0.011650 (exact)

It is seen, in summary, that the methods presented thus far have permitted calculation of the reheat heat rate with an error of only 0.008 per cent in heat rate. In fact, the error in calculation of the *change* in reheat heat is only 0.68 per cent, which is more than adequate for any reasonable purpose.

It is to be noted that this accuracy was achieved even though the approximate forms, equations (12) and (17), were used. If the exact forms, equations (13) and (18), had been used for calculating the change in low-pressure system, there would have been an improvement in the final accuracy. It would appear, on the other hand, that the cumbersome form of the exact relationships is scarcely necessary in view of the accuracy achieved with the first approximation. Obviously, it would be desirable to use the exact forms where the changes are large, to reduce the discrepancy.

Let us next consider Cycle 3. In this cycle both the inlet and exhaust enthalpy from the high-pressure turbine have changed, as well as the final feedwater enthalpy leaving the highest pressure heater; that is, let

$$\Delta H_1 = +12$$

$$\Delta H_x = +10$$

$$\Delta h_{bf} = +10$$

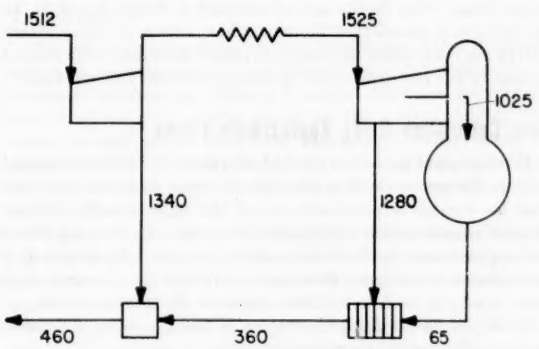

Fig. 5 Cycle 3 (change in H_x, h_f, H_c, H_x, h_{bf}, and H_2)

The preceding calculation did not involve any changes in the high-pressure system other than the change in h_f. This caused a change, ΔS, as derived from equation (32). For Cycle 3 we have allowed the changed low-pressure system to remain changed, but we have imposed additional changes in the high-pressure system, so that the value of $\Delta S/S$ found for Cycle 2 will now be modified, since other variables than h_f are changing.

First, let us find an exact value for the reheat heat rate r_r. As before, it is necessary to calculate the extraction quantity from the exhaust of the high-pressure turbine. Then the reheat heat rate may be calculated by the usual method. The results are

$$w_r = 1.32065217\left(\frac{100}{880}\right) = 0.15007411$$

$$w = 1.32065217 + 0.15007411 = 1.47072628$$

$$r_r = \frac{1.47072628(1512 - 460) + 1.32065217(1525 - 1340)}{1791.524698 - 960}$$

$$= 2.154506$$

Now, using equation (32) we may calculate the value of $\Delta S/S$

$$\frac{\Delta S}{S} = \frac{\frac{10-(-10)}{960} - \frac{10-10}{880} - \frac{0-(-10)}{1155} + \frac{12-10}{170}}{\left(1+\frac{10}{1155}\right)\left(1+\frac{0}{880}\right)}$$

$$= 0.023734536$$

Using equation (26), in which we insert the original value of r_r found for the reference cycle, the previously calculated value of $\Delta r_a/r_a$ for Cycle 2, $\Delta S/S$, and the original value of G_r, we may find the value of $\Delta G_r/G_r$

$$\frac{\Delta G_r}{G_r} = \frac{(1 + 1.8792878 \times 0.01714464)(1.023734536) - 1}{1 + (1.8792878 \times 0.22340619)(1.01714464)(1.023734536)}$$

$$= \frac{0.0567189689}{1.4371782688} = 0.039465507$$

Having the value of $\Delta G_r/G_r$, we may use equation (8) to find the net change in heat rate

$$\frac{\Delta r_r}{r_r} = (1.01714464)(1 - 0.039465507 \times 0.22340619) - 1$$

$$= 0.0081766399$$

The exact fractional change in reheat heat rate for all the changes that have been made in Cycle 3 with respect to the original reference cycle is 0.008058, as compared with the foregoing value. The results are summarized in Tables 1 and 2. In the latter it is shown that the reheat heat rate is accurate within 0.0119 per cent, while the *change* in reheat heat rate, with respect to that of the reference cycle, is accurate within 1.47 per cent.

Loss Calculation Using Approximate Forms

Having found the loss in reheat heat rate of Cycle 3 with respect to the reference cycle, it is desirable to break down the total loss into its various components, using the approximate relationships of equations (38)–(45), inclusive. Although these equations are approximate, in that they neglect second-order terms, it is nevertheless possible by their use to arrive at the change in heat rate caused by each individual change in the entire system.

First, let us establish the values of the necessary constants, based on the data of the reference cycle:

$$r_r = 2.137284$$

hence

$$\frac{r_r}{r_r - 1} = 1.879288$$

$$G_r = 0.1826100$$

hence

$$\frac{G_r}{1 - G_r} = 0.2234062$$

Thus

$$C = \left(\frac{r_r}{r_r - 1}\right)\left(\frac{G_r}{1 - G_r}\right) = 0.4198445$$

Consider first the change in H_s. Using equation (38) and the value of A found earlier, for Cycle 1, is it found that

$$\left.\frac{\Delta r_r}{r_r}\right]_{H_s} = \frac{0.004541}{1.4198} = 0.003198$$

that is, a loss of 0.4541 per cent in the low-pressure system results in a net loss in reheat heat rate of only 0.3198 per cent.

Similarly, using the loss ($B = 0.003961$) originally found for the change in h_f, in the low-pressure system, the net effect on the reheat rate may be found, although first it is necessary to find the $\Delta S/S$ component of equation (36) for use in the second term of equation (39):

$$\left.\frac{\Delta S}{S}\right]_{h_f} \approx \frac{10}{960} + \frac{-10}{1155} = 0.0017587$$

Then by equation (39)

$$\left.\frac{\Delta r_r}{r_r}\right]_{h_f} = \frac{0.003961}{1.4198} - \frac{0.001759}{1.4198}(0.2234) = 0.002513$$

For the change in turbine efficiency, which yielded a loss of 0.008642 on the low-pressure system, the change in reheat heat rate may be found

$$\left.\frac{\Delta r_r}{r_r}\right]_{\eta} = \frac{0.008642}{1.4198} = 0.006087$$

We may add these losses to find the total change in reheat heat rate due to all changes in the low-pressure system:

Due to ΔH_s	0.003198
Due to Δh_f	0.002513
Due to $\Delta\eta$	0.006087
Total change due to changes in low-pressure system	0.011798
Exact value, from Table 2	0.011650

Thus the approximate forms yield satisfactory accuracy in finding the total effect of changes in the low pressure system.

Consider now the changes in the high-pressure system. Under the conditions of Cycle 3, we have changed, with respect to the reference cycle, the values of H_x, h_{bf}, and H_2. The effect of each of these changes on $\Delta S/S$ must first be found by the use of equation (32), since $\Delta S/S$ is the numerator of each of the applicable relationships. Note that in using equation (32) only the numerator is used, because we are satisfied with a first approximation and the denominator represents second-order effects. In using the numerator, only changes in the variable of immediate concern are taken into account, with changes in the other variables considered to be zero for the moment. Thus we have, for the change in H_x

$$\left.\frac{\Delta S}{S}\right]_{H_x} = \frac{10}{960} - \frac{10}{880} - \frac{10}{170} = -0.059769$$

The change in r_r by equation (43) is

$$\left.\frac{\Delta r_r}{r_r}\right]_{H_x} = -\frac{-0.05977}{1.4198}(0.2234) = 0.0094045$$

Similarly, for the other changes we have

$$\left.\frac{\Delta S}{S}\right]_{h_{bf}} = \frac{+10}{880} = 0.011363$$

$$\left.\frac{\Delta r_r}{r_r}\right]_{h_{bf}} = -\frac{0.011363}{1.4198}(0.2234) = -0.001787$$

$$\left.\frac{\Delta S}{S}\right]_{H_2} = \frac{12}{170} = 0.070588$$

$$\left.\frac{\Delta r_r}{r_r}\right]_{H_s} = -\frac{0.07059}{1.4198}(0.2234) = -0.011068$$

Summarizing the losses due to all of the changes that have taken place we have

Due to ΔH_s	0.003198	
Due to Δh_f	0.002513	
Due to $\Delta\eta$	0.006087	
Total due to low-pressure system	0.011798	+0.011798
Due to ΔH_x	0.009405	
Due to Δh_{bf}	−0.001787	
Due to ΔH_2	−0.011068	
Total due to high-pressure system	−0.003450	−0.003450
Grand total loss		+0.008348
Exact loss		+0.008058

It is obvious from the foregoing that the approximate relationships provide excellent accuracy in determining change in plant heat rate due to changes in any of the parameters that determine it. We must also, however, demonstrate the applicability of the monitoring relationships, equations (46) and (49) as was done for the low-pressure-system criteria.

Let us make the transition from Cycle 2 to Cycle 3 by the monitoring relationships of equations (46) and (49) to test their accuracy. From Table 1 it is seen that

$$\frac{\Delta U}{U} = \frac{172 - 170}{170} = 0.011765$$

$$\Delta H_x = +10$$

$$\frac{\Delta(\Delta h)}{\Delta h} = \frac{100 - 90}{90} = +0.11111$$

$$\Delta h_f = 0$$

$$\Delta h_{bf} = +10$$

$$C = 1.86044 \times 0.22991 = 0.42773$$

By equation (46)

$$\left.\frac{\Delta r_r}{r_r}\right]_U = -\frac{0.011765}{1.42773}(0.22991) + \frac{\frac{10}{970}\left(\frac{90}{880}\right)}{1.42773}(0.22991)$$

$$= -0.0018944 + 0.0001698$$

$$= -0.0017246$$

By equation (49)

$$\left.\frac{\Delta r_r}{r_r}\right]_{\Delta h} = -\frac{0.11111\left(\frac{90}{970}\right)}{1.42773}(0.22991) + \frac{0 - 0 - \frac{10}{970}\left(\frac{90}{880}\right)}{1.42773}(0.22991)$$

$$= -0.0016601 - 0.0001698$$

$$= -0.0018299$$

Note that the secondary effects are only about 10 per cent of the primary effects. In fact, for the present example, the secondary effects are identical for the two components, by coincidence, because $\Delta h_{bf} = \Delta H_x$, numerically. The change in heat rate due to changes in the two components may be added to obtain the total effect, and compared with the exact value found from the data of Table 1, to establish the accuracy of equations (46) and (49)

$$\frac{\Delta r_r}{r_r} = -0.0017246 - 0.0018299 = -0.0035545$$

By Table 1

$$\frac{\Delta r_r}{r_r} = 1 - \frac{2.154506}{2.162183} = -0.0035506 \text{ (exact)}$$

Acknowledgment

The author wishes to thank the Bailey Meter Company, which sponsored this work, for permission to publish this third step in the performance-monitoring problem. Gratitude is also due Mr. H. H. Gorrie and Mr. H. T. Hoffman, of this company, and Mr. C. P. Welch of The Babcock & Wilcox Company, for their helpful suggestions on the manuscript.

References

1 J. Kenneth Salisbury, "Steam Turbines and Their Cycles," John Wiley & Sons, Inc., New York, N. Y., 1950, p. 162.

2 J. Kenneth Salisbury, "A New Performance Criterion for Steam-Turbine Regenerative Cycles," TRANS. ASME, Series A, JOURNAL OF ENGINEERING FOR POWER, vol. 81, 1959, pp. 389–402.

3 J. Kenneth Salisbury, "Analysis of the Steam-Turbine Reheat Cycle," TRANS. ASME, vol. 80, 1958, pp. 1629–1642. (This paper is an exposition of the properties of G_r.)

DISCUSSION

V. F. Estcourt[7]

The power industry should be indebted to the author for having completed this third paper in a series relating to power plant performance monitoring. This is a subject which is considerably more involved than might appear on the surface, and for this reason several papers have been necessary in order to lay the groundwork for the ultimate objective in developing a basis for the routine monitoring of both the over-all cycle and its principal components.

We have not yet had the opportunity of examining the author's paper in detail. Therefore, these comments are merely preliminary observations which may lead to further constructive thinking regarding some of the factors involved.

Performance monitoring requires instrumentation which will indicate the changes in performance of the cycle as a whole as well as identify the components which are responsible for such changes. One of the difficulties, which arises in any effort to measure over all performance in terms of output divided by input, is that the output is usually out of time phase with the input. Contrary to popular opinion, almost meaningless results are obtained if simultaneous values of output divided by input are recorded. This is because there are several points in the cycle where energy is being absorbed or given up, and this influences the value of heat input to the cycle without a corresponding change in the output.

The only solution to this difficulty which has been attempted up to the present time is to average the output and input over a period of minutes in order to minimize the inaccuracies produced by internal changes within the cycle. This situation makes it quite difficult to realize the ultimate goal which is to be able to identify changes in the cycle performance as they occur. Thus, since the cycle is frequently not in equilibrium the problem cannot be handled strictly from a static approach. The ultimate solution must take into consideration the dynamic factors involved.

[7] Pacific Gas and Electric Company, San Francisco, Calif. Fellow ASME.

Another question arises regarding the occurrence of simultaneous faults. Based upon our preliminary reading of the paper, it is not clear whether simultaneous faults in various parts of the cycle can always be segregated and identified individually. Another problem that may need further consideration is the fact that one or more faults in the cycle will, if corrected, result in a change in the output. Therefore, the various thermodynamic changes which can occur are also reflected in a change in the referenced output from the system.

In view of the foregoing, it is our feeling that still more work must be done on this subject before any system of monitoring can be set up which will make it possible to identify each individual fault in relation to the hardware which is the primary cause. It is hoped that the author will undertake to extend the excellent work which he has already accomplished to the point where the instrument manufacturers will feel the urge to develop more sophisticated instrument hardware for monitoring plant cycle performance.

Author's Closure

Mr. Estcourt has alluded to the transient nature of all changes, due to capacitance in the thermodynamic system that has been studied by the author. While these are recognized, they have not been given significant attention to date, largely because the steady-state analysis, normally considered as the first order of business, has presented a plethora of difficult problems, only too evident from the complexity of the presentations to date. Certainly, however, analysis of the dynamics of the transient system is desirable.

As to separation of faults, it is the intent of this approach to identify "areas" in which a deficiency exists, such as the low-pressure feedwater heating system. Once a fault is shown to exist in this area, and its magnitude identified, a detailed investigation and analysis of each of the subelements in the area is undertaken, using well-known methods. The cost of monitoring equipment will depend on the fineness of resolution that is required. Whether identification by automatic means of a faulty individual heater, for example, can be justified, is a moot question at the moment. Certainly at some point the cost of equipment will exceed its value to the operator.

The paper provides relationships for monitoring the areas of the high-pressure heater, high-pressure turbine, and low-pressure heaters. Since preprinting of the paper, a relationship for monitoring the low-pressure turbine has been developed and tested. Since it is required to complete the list of monitoring equations for the four major areas of the system, it is given herewith.

By combining Eqs. (40) and 42) we may arrive at a relationship that expresses the effect on heat rate of a fractional change in the low-pressure turbine used energy, u. As in the other equations, there is a primary effect, defined by the first term in the numerator of Eq. (50), below, and secondary effects, defined by the second and third terms:

$$\left.\frac{\Delta r_r}{r_r}\right]_u = \frac{-(r_n - 1)\,\frac{u}{H_1 - h_f}\left(\frac{\Delta u}{u}\right) + \left(\frac{\Delta H_c}{H_1 - h_f}\right)\left(1 - r_n\,\frac{w}{1+w}\right) + \left(\frac{\Delta H_1}{H_1 - h_f}\right)\left(\frac{G_r}{1 - G_r}\right)}{1 + C} \qquad (50)$$

The Application of the Deviation Concept of Turbine Cycle Monitoring

H. T. HOFFMAN
Manager of Application Engineering,
The Bailey Meter Company,
Wickliffe, Ohio

C. P. WELCH
Senior Analytical Engineer,
The Babcock & Wilcox Company,
Research Center, Alliance, Ohio.
Mem. ASME

In a companion paper, J. K. Salisbury has presented the theoretical aspects of a new approach to analyzing the steam turbine cycle. This paper presents the results of efforts at applying this new approach to the monitoring of the economics of turbine cycle operation.

Means are presented for identifying cycle faults and determining the change in heat rate resulting from these faults. Very little in the way of precision measurement and calculation is required. These techniques are, therefore, amenable to use by plant personnel with the tools already at hand. By the same token they also provide advantages when employing data-processing equipment.

Introduction

THIS paper is a report to the power industry on a program being carried on by The Bailey Meter Company designed to provide methods of boiler and turbine cycle analysis suitable for automatic data-processing techniques. The aims of this program are described and the analytical progress to date reported. It is hoped that through discussion of this and companion papers [1, 2, 3][1] the industry will contribute to the direction and implementation of this program.

In recent years there has been an increasing interest in monitoring the performance of the steam turbine cycle. The advent of both analog and digital computers has made the collection and rapid processing of data a simple task, so that now heat-rate computers for calculating over-all cycle performance are becoming commonplace. The authors suggest that this determination of over-all heat rate is not sufficient. Greater value rests with the ability to identify the sources of deterioration and the magnitude of the loss in heat rate associated with each source. A significant step forward would be accomplished, therefore, if the performance of the individual components of the cycle could be monitored in terms of the change in turbine cycle heat rate. This would make possible a comprehensive turbine cycle monitoring program which could effect economies in three broad areas of power-plant operation: (1) By identifying and evaluating faults or deterioration in terms of loss in heat rate, maintenance could be scheduled on the basis of balancing the loss being suffered against the cost of repair; (2) with accurate, up-to-date information on the cost of generation, load could be allocated on the basis of actual performance rather than expected performance; (3) operating procedures may be studied and changes evaluated in terms of their effect on the economy of operation.

If a monitoring program is to be successful it must be implemented by techniques which do not require large quantities of extremely accurate data or extensive calculations. Any program which does not meet these requirements will be expensive and cumbersome to implement even with modern automatic data collection and processing equipment. With this stimulus, the services of J. K. Salisbury were employed to study how simplified component monitoring might be accomplished. Over the past five years the authors have been working with Salisbury in applying his findings to real cycles and evaluating them with respect to commercial feasibility.

The first step of this study developed a means for evaluating the high-pressure turbine and its associated feedwater heater relative to the low-pressure portion of the cycle. This concept, known as the gain due to reheat G_r, was presented before ASME in 1957 by Salisbury [1].

The second step of this study developed a means of analyzing the performance of all feedwater heaters below the reheat point when taken as a group. The crux of this work concerned the flow-weighted enthalpy of steam extracted by these heaters and is called the effective enthalpy H_e. Salisbury reported this concept before ASME in 1958 [2].

[1] Numbers in brackets designate References at end of paper.

Contributed by the Power Division and presented at the Winter Annual Meeting, New York, N. Y., November 27–December 2, 1960, of THE AMERICAN SOCIETY OF MECHANICAL ENGINEERS. Manuscript received at ASME Headquarters, August 30, 1960. Paper No. 60—WA-166.

Nomenclature

r_r = the heat rate of the reheat cycle, Btu/Btu

r_n = the heat rate of condensing turbine. The inlet pressure is determined by the turbine characteristics as they exist in the reheat cycle, Btu/Btu

G_r = gain attributed to reheating. The improvement in r_n associated with a reheater, high-pressure turbine, and feedwater heating above the reheat point

H_e = the flow weighted enthalpy of the steam extracted for feedwater heating below the reheat point, Btu/lb

H_c = the enthalpy of the steam entering the condenser, i.e., the used energy end point, Btu/lb

E = the weight of steam extracted for feedwater heating above the reheat point, lb/hr

W = the total weight of steam extracted for feedwater heating below the reheat point, lb/hr

F = flow, lb/hr

H_{SLEP} = state line end point of low-pressure turbine, Btu/lb

H = the enthalpy of steam, Btu/lb

h = the enthalpy of water, Btu/lb

H_{z_s} = the isentropic expansion end point of the high-pressure turbine, Btu/lb

R = the enthalpy rise across a feedwater heater or heaters, Btu/lb

U = the high-pressure turbine used energy, Btu/lb

N = the high-pressure turbine efficiency, per cent/100

Δx = an *increment* in x

(Continued on next page)

A companion paper presented today by Salisbury [3] takes another step forward toward the ultimate goal. In his paper, the relationship is established between deviation from normal of eight key cycle enthalpies and the corresponding change in reheat heat rate. These key enthalpies are:

1 H_2—the main steam throttle enthalpy.
2 H_x—the exhaust enthalpy of the high-pressure turbine.
3 H_1—the reheat steam enthalpy.
4 H_s—the effective enthalpy of all extraction steam to the feedwater heaters below the reheat point.
5 H_c—the used energy end point of the low-pressure turbine
6 h_c—the condensate enthalpy entering the low-pressure heaters.
7 h_f—the feedwater enthalpy leaving the low-pressure heater group.
8 h_{bf}—the feedwater enthalpy leaving the highest pressure heater.

For every flow to the machine there is some normal value of each of these enthalpies. Any departure of these key enthalpies from the normal values as a result of environmental changes, i.e., steam conditions or condenser pressure, or, as a result of equipment malfunction, can be converted into a change in heat rate through Salisbury's equations.

The total deviation in performance of the cycle from some reference is the sum of the eight individual deviations. This concept has long been in use as illustrated by the corrections to heat rate for changes in steam conditions and condenser pressure. A significant aspect of this paper is the extension of the concept to include the physical condition of each cycle component. The result is a procedure for analyzing the performance of the entire turbine cycle which will be referred to as The Deviation Concept of Turbine Cycle Monitoring.

If Deviation Monitoring is applied to each component of the cycle and also to the cycle environment (i.e., steam conditions and condenser pressure), the operating heat rate may be determined by summing the deviations and adding these to the reference heat rate. Conversely, if the operating heat rate is known, Deviation Monitoring can be used to account for the difference between operating and reference heat rates. Cycle faults are given a value in terms of loss in heat rate and hence in terms of dollars.

One purpose of this paper is to show how accurately the summation of the changes in heat rate as determined from Salisbury's equations compares with the true change in heat rate for a real cycle as calculated from a complete new heat balance when various equipment faults are introduced into the cycle.

As a result of studying the effects of component malfunctions on enthalpies of the cycle, a single enthalpy difference was selected for each component as its criterion of performance. These criteria and their associated equipment are:

1	Feedwater heaters	
	A High pressure	$h_{bf} - h_f$
	B Low pressure	exit feedwater enthalpy − inlet feedwater enthalpy
2	High-pressure turbine	$H_2 - H_x$
3	Low-pressure turbine	$H_1 - H_c$

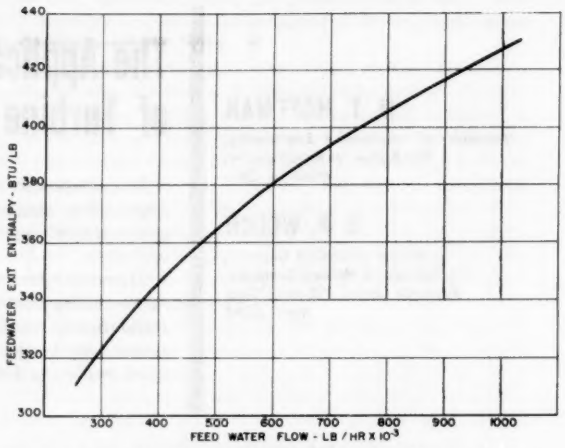

Fig. 1 Relationship between feedwater exit enthalpy and feedwater flow for a high-pressure heater

A second purpose of this paper is to illustrate the extent of the error introduced in the prediction of the change in heat rate by considering only this single criterion of component condition.

In summary the two objectives of this paper are:

1 To compare the accuracy of the summation of changes in heat rate as derived from deviations in eight key enthalpy values to the true change in heat rate for various component faults in the turbine cycle.

2 To illustrate the extent of the error introduced in the prediction of the change in heat rate by considering only the single criterion of component performance.

Method of Approach

The simplest means of implementing the Deviation Concept is to construct a series of curves which relate a deviation in the single criterion associated with each cycle component to a change in heat rate. These curves are constructed from the information normally available to the results engineer and without recourse to test procedures or extensive calculations. Generally the material required to construct the curves is in the form of design heat balances, expansion lines, stage pressure curves, and so on. Each enthalpy difference listed as a criterion of component performance consists of an enthalpy imposed on the component by the remainder of the cycle and one enthalpy essentially determined by the component performance. As will be explained later in this paper, it is possible to construct the afore-mentioned curves in terms of only the enthalpy affected by the component performance.

Feedwater Heaters. For each feedwater heater in the system two curves are plotted as illustrated in Figs. 1 and 2. For any heater a reference exit enthalpy can be obtained either from design cycle heat balances or from actual tests on the unit when it first goes into operation. This reference enthalpy can then be plotted as a function of feedwater flow through the heater as in Fig. 1. A

Nomenclature

$$C = \frac{(G_r)}{(1 - G_r)} \frac{(r_r)}{(r_r - 1)}$$

$$w = W/F_c$$

Subscripts

x = high-pressure turbine exhaust
c = condenser and hot-well
f = feedwater leaving the low-pressure heater group
bf = boiler feedwater—leaving the high-pressure heater
g, h, j, k = extractions to low-pressure heaters
1 = low-pressure turbine throttle
2 = high-pressure turbine throttle

A primed symbol represents a new as contrasted to a reference value. The reader should be aware that heat rate could be expressed in terms of Btu/kwhr or Btu/Btu. Care should be taken that the proper dimensions are used when substituting a specific numeric value for heat rate in an equation.

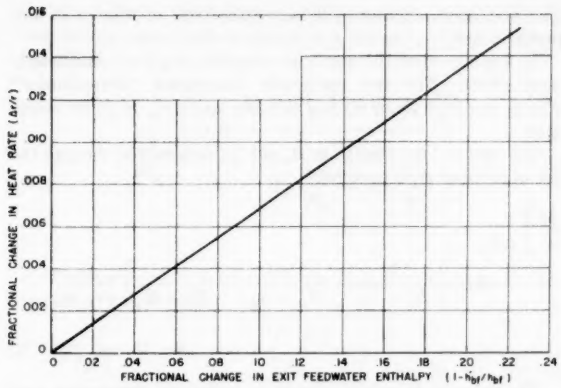

Fig. 2 Relationship between fractional change in exit feedwater enthalpy and fractional change in heat rate for a high-pressure heater

simple curve can be drawn which relates the deviation of exit feedwater enthalpy from its reference value to the resulting change in heat rate. A typical curve of this type is shown in Fig. 2 for the high-pressure heater. Similar curves would be constructed for each low-pressure heater. However, for some heaters there will be a load dependence, and load parameters might be necessary on the curve.

High-Pressure Turbine. For the high-pressure turbine two curves are plotted as illustrated in Figs. 3 and 4. One curve relates turbine exhaust pressure to expected exhaust enthalpy. The other curve relates deviations in exhaust enthalpy to changes in heat rate. As developed in this paper, these curves are limited in their application to the condition when the turbine is operating at a valve point and to design main steam conditions.

Low-Pressure Turbine. For the low-pressure turbine the simple relationship between a key variable and heat rate does not exist. As will be discussed later, the formulation of such a relationship requires prior knowledge of the nature of the turbine fault. However, some application of Deviation Monitoring is possible in most cases.

The used energy $H_1 - H_c$ has been specified as the criterion of performance of the low-pressure turbine. However, this is not a measurable quantity. The best that can be done at the present time is to provide calculating aids which enable one to obtain the reference used energy with some ease. A typical aid of this type is shown in Fig. 5 which has been constructed for a particular turbine utilizing previously published data [4]. It is necessary to predict the expected exhaust loss and subtract this from the result obtained from Fig. 5 to obtain the reference used energy. The results engineer is left to his own devices to obtain the *operating* used energy since the process of arriving at this will vary drastically from cycle to cycle. Once having the reference used energy and the deviation, the use of Salisbury's equations (40) and (42) of reference [3] enables a prediction of the change in heat rate.

Discussion and Construction of Curves

In the following sections of this paper the methods for constructing the curves just described are outlined and related to Salisbury's work.

Feedwater Heaters

The improvement in heat rate associated with any feedwater heater is a function of the feedwater enthalpy rise across the heater. However, the rise across a heater for any given feedwater flow is not entirely determined by the heater. The inlet enthalpy is determined by conditions external to the heater while

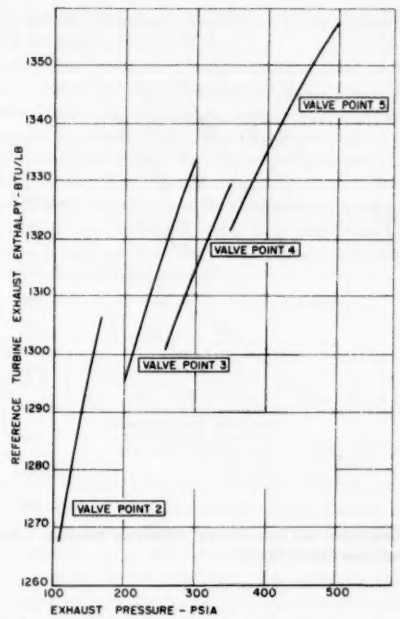

Fig. 3 Relationship between exhaust pressure and reference exhaust enthalpy for a high-pressure turbine

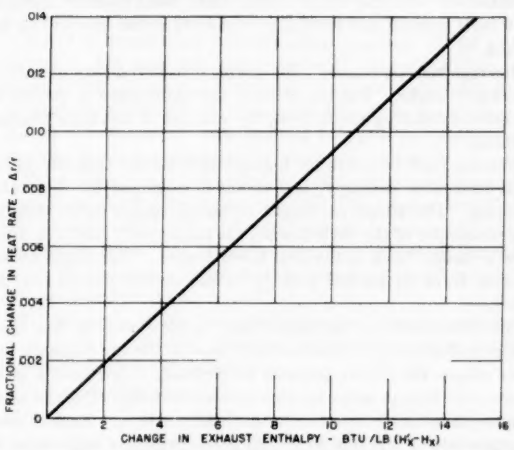

Fig. 4 Relationship between change in exhaust enthalpy and fractional change in heat rate for a high-pressure turbine

the exit enthalpy is determined essentially by the extraction steam pressure and the heater design. The small changes in exit enthalpy resulting from large changes in inlet enthalpy are considered to be insignificant.

When a fault occurs in any heater which reduces the effectiveness of its heat-transfer capabilities, the exit enthalpy decreases, causing the next higher heater to receive a lower temperature feedwater. The next higher heater will come very close to picking up the entire lost duty of the heater before it, maintaining a constant exit feedwater enthalpy within small limits.

From the Deviation Monitoring viewpoint, only that portion of a change in rise attributable to the condition of the heater under consideration is of interest. Therefore the rise to be observed is actual outlet enthalpy minus the expected inlet enthalpy. This, in effect, says that the quantity monitored as the index of heater condition is the exit enthalpy. It is apparent that

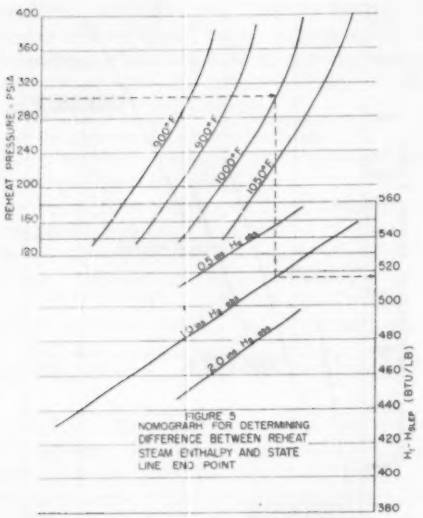

Fig. 5 Nomograph for determining difference between reheat steam enthalpy and state line end point

only those faults that affect exit enthalpy will be monitored by this index. Drain cooler faults and other internal leaks will go undetected. On the other hand, dirty heat-transfer surface, poor level control, and throttling in the extraction line will be detected.

The High-Pressure Heater. The heater considered here is the top feedwater heater. For the present, the application is limited to a heater extracting steam from the exhaust of the high-pressure turbine.

When a fault occurs in the high-pressure heater that affects the final feedwater enthalpy, less steam is extracted for feedwater heating. The steam no longer extracted passes down through the remainder of the cycle toward the condenser. Also less drain flow is flashed back to the next lower heater. This displacement of flow from its normal pattern causes several changes in the cycle.

The initial effect of the heater fault is the change in final feedwater enthalpy h_{bf}. The increased flow to the low-pressure turbine causes the reheat pressure to increase, which results in an increase in high-pressure turbine exhaust enthalpy H_z and a small improvement in the low pressure cycle heat rate r_n. Each of these components of loss due to a high-pressure heater fault must be evaluated to obtain the total loss.

The increase in H_z causes a loss in high-pressure turbine power, and thus represents a loss in heat rate. This loss is almost offset by the improvement in r_n. These two factors must, therefore, both be accounted for at the same time. If only one is accounted for, more error will result than if neither is accounted for.

The first approximation to the relationship between heater performance and change in heat rate is obtained through Salisbury's equation (49) which for Δh_f equal zero reduces to

$$\left.\frac{\Delta r}{r_r}\right]_{\Delta h_{bf}} = -\frac{\Delta h_{bf}}{H_z - h_{bf}} \frac{(G_r)}{(1 - G_r)} \frac{(1)}{(1 + C)}$$

(Eq. 49, ref. [3]) (1)

Since this is a linear expression in Δh_{bf} it is necessary to determine only one value of $\Delta r/r$ to be able to draw the first approximation, as has been done in Fig. 2. Generally the maximum value of $\Delta r/r$, for a complete heater outage, will be about 0.015. The first approximation will be within 0.002 of this value and probably low.

To improve upon the first approximation requires considerably more effort. The two previously mentioned "second-order" effects, the increase in H_z and the decrease in r_n, must be evaluated.

The effect of the change in H_z can be determined through the use of Salisbury's expression.

$$\left.\frac{\Delta r}{r_r}\right]_{\Delta H_z} = \frac{-\Delta H_z \left[\dfrac{1}{H_z - h_f} - \dfrac{1}{H_z - h_{bf}} - \dfrac{1}{H_2 - H_z}\right] \dfrac{G_r}{1 - G_r}}{1 + C}$$

(Eq. 43, ref. [3]) (2)

The value of H_z existing for the complete heater outage may be determined by increasing the design exhaust pressure of the high-pressure turbine in proportion to the increase in reheat steam flow and reading the new value of H_z from Fig. 3. The reference value of H_z is read from Fig. 3 at the design value of high-pressure turbine exhaust pressure. For a complete high-pressure heater outage, the value of $\Delta r/r_r$ from this cause ΔH_z will be on the order of 0.01.

The effect of the displaced extraction flow on r_n may be determined by one of two means. The increased flow to the low-pressure portion of the cycle will cause a change in H_1, h_f, H_s, H_c. Although Salisbury has presented expressions for evaluating changes in these variables, the problem of accurately estimating their new values is formidable. The alternate approach is to plot r_n versus reheat flow and read off the new value of r_n. Either approach may introduce large errors in evaluating the heater outage and hence should be used with care. The improvement in r_n due to the displaced extraction flow will be on the order of 0.01 and slightly less than the loss suffered from the increase in H_z. The authors suggest that, unless great care is taken, the second-order effect be neglected, as has been done in Fig. 2.

To construct Fig. 2, it is necessary to use only the total rise across the high-pressure heater in equation (1) simultaneously employing the values of the remaining variables in the equation from design heat balances. The use of $\Delta h_{bf}/h_{bf}$ as the abscissa in Fig. 2 reduces the load dependence of the plot to the vanishing point for the cycle used in the illustration.

Once the relationship between outlet enthalpy and heat rate has been established, it is necessary to measure only the flow through the heater and the outlet temperature. From the flow, the expected or reference enthalpy is determined. The calculated existing enthalpy and reference enthalpy are then used to enter the loss curve, Fig. 2.

In order to achieve an accuracy of 0.05 per cent in $\Delta r/r$, the accuracy of measurement required is moderate, ±5 per cent for flow and ±2 F for outlet temperature.

The Low-Pressure Heaters. A fault in a heater below the reheat point affects the heat rate through the effect it has on the enthalpy leaving the low-pressure heater group h_f and/or the effect it has on the weighted average enthalpy of extraction steam H_s. From a practical viewpoint, heaters with faults fall into two categories, (1) those which essentially affect only H_s, and (2) those which affect H_s, h_f, and the reheat throttle flow. Normally, only the top heater in the low-pressure group falls into the second category.

For a heater in the first category, any heater fault that changes the exit enthalpy of that heater manifests itself as a shift in duty to the next higher heater and thus increases H_s. The resultant loss in heat rate is determined by first relating the deviation in exit enthalpy to a change in H_s, and then relating the change in H_s to the change in heat rate.

The deviation in enthalpy rise across a feedwater heater resulting from a heater fault is related to a change in H_e by the expression:[2]

$$\frac{\Delta H_e}{H_e} = \frac{1 + \dfrac{W_h H_h \dfrac{\Delta R_h}{R_h} + W_j H_j \dfrac{\Delta R_j}{R_j}}{W H_e}}{1 + \dfrac{W_h \dfrac{\Delta R_h}{R_h} + W_j \dfrac{\Delta R_j}{R_j}}{W}} - 1 \qquad (3)$$

The change in H_e is related to the change in heat rate by using Salisbury's expression.

$$\frac{\Delta r}{r_r}\Big]_{\Delta H_e} = \frac{(r_n - 1)w\left(\dfrac{\Delta H_e}{H_e - h_c}\right)}{1 + C} \quad \text{(Eq. 38, ref. [3])} \quad (4)$$

A fault in the second category produces a shift in duty from a heater below the reheat point to a heater above the reheat point. This results in a reduction in reheat flow leading to a multiplicity of effects on the cycle. The reduced reheat flow reduces reheat pressure, shifting the low-pressure turbine expansion line and increasing the high-pressure turbine power. The shift in the low-pressure turbine expansion line changes H_e and H_c, the used energy end point. Thus the heater fault has caused a change in h_f, h_{bf}, H_x, H_1, H_e, and H_c.

Salisbury has developed expressions to relate a change in each of these enthalpies to a change in heat rate. However, it is virtually impossible to predict the changes in H_e and H_c without making a complete heat balance. These two factors account for about half the loss associated with the top low-pressure heater, and are not linearly related to the deviation in h_f, the exit enthalpy. Therefore the authors feel that at this time the top low-pressure heater does not lend itself to the same simple treatment that is possible with the other heaters.

The other low-pressure heaters are treated in much the same way as is the high-pressure heater. Curves similar to Figs. 2 and 3 are constructed from design heat balance data and equations (3) and (4).

Turbine

The usually accepted criterion for the condition of the turbine is its efficiency. However, the determination of a true change in efficiency due to change in physical condition and the relating of this change to change in heat rate is not as straightforward as might be expected.

High-Pressure Turbine. The efficiency of the high-pressure turbine is the combination of the efficiency of the first or control stage and the remaining so-called "single" stages. A change in inlet steam conditions or valve position changes the efficiency of the first stage and shifts the position of the single-stage state line. All this affects the over-all high-pressure turbine efficiency. A small change in the high-pressure turbine back pressure does not affect the first stage or single stages but does affect exhaust enthalpy and, hence, turbine efficiency. Before a change in efficiency attributable to change in physical condition can be obtained it is necessary to have a reference efficiency corrected to actual test condition.

The effect of a change in throttle steam conditions on efficiency is dependent upon the design of the first stage and cannot be evaluated without this knowledge. For this reason the evaluation of the physical condition of the turbine as presented in this paper is limited to design throttle conditions. With the inlet enthalpy limited to design value the criterion of turbine condition becomes exhaust enthalpy H_x.

The reference value of exhaust enthalpy must be corrected for the test value of exhaust pressure and valve position. A plot of exhaust enthalpy versus exhaust pressure with parameters of valve position can be constructed, using the single-stage expansion lines normally furnished by the turbine manufacturer. Such a plot is illustrated in Fig. 3.

The deviation in exhaust enthalpy found by comparing the test value of H_x to the reference value obtained from Fig. 3 can be related to change in heat rate using Salisbury's equation (46) which when H_2 is constant reduces to:

$$\frac{\Delta r}{r_r}\Big]_{\Delta H_x} = \frac{-\Delta H_x\left[\dfrac{1}{H_x - h_f} - \dfrac{1}{H_x - h_{bf}} - \dfrac{1}{H_2 - H_x}\right]\dfrac{G_r}{1 - G_r}}{1 + C}$$

(Eq. 46, ref. [3]) (5)

When the turbine efficiency changes, other secondary effects occur. The higher exhaust enthalpy causes less steam to be extracted by the high-pressure heater. This displaced extraction steam is passed on to the low-pressure turbine, increasing the throttle pressure to this machine. The pressure level is raised in the upper part of the cycle, i.e., exhaust pressure and high-pressure heater shell pressure, and a small change in boiler feedwater enthalpy occurs. In using these techniques the authors have found that these second-order effects are negligible at least for losses in high-pressure turbine efficiency up to 4 per cent.

Fig. 4 is constructed by evaluating equation (5) for various values of ΔH_x and different cycle loads. Since equation (5) is linear in ΔH_x, it need be evaluated for only a single value of ΔH_x to establish the curve. For the cycle studied by the authors, the variation in the result with load was so small that a single mean line was drawn as representative of all load values.

From Figs. 3 and 4, the condition of the high-pressure turbine may be monitored by measuring only the exhaust temperature and pressure with the throttle conditions at design and the turbine on a valve point. To obtain an accuracy of ± 0.05 per cent in $\Delta r/r_r$, the exhaust pressure must be measured to ± 2 psi and the exhaust temperature to ± 1.5 F.

Deviations in H_x can be related either to changes in used energy or changes in efficiency if desired, and curves similar to Fig. 3 constructed for these parameters.

This is possible since:

$$N = \frac{H_2 - H_x}{H_2 - H_{xs}} = \frac{U}{H_2 - H_{xs}} \qquad (6)$$

and for fixed values of H_2 (to which this application is limited)

$$-\Delta H_x = \Delta U = \Delta N(H_2 - H_{xs}) \qquad (7)$$

Low-Pressure Turbine. The efficiency of the low-pressure turbine that has meaning in evaluating changes in heat rate is the efficiency to the used energy end point. This efficiency is dependent upon reheat steam temperature, reheat steam pressure, condenser pressure, and the steam flow to the condenser as well as the physical condition of the turbine.

When each of these determinants of turbine efficiency has been accounted for the only remaining variable that can cause a difference between reference efficiency and test efficiency is the used energy end point H_c. Therefore the used energy end point becomes the index of the condition of the turbine.

Determination of the reference value of used energy end point requires a knowledge of the design practices of the turbine manufacturer. The authors have used the turbine performance information presented by Hegetschweiler and Bartlett [4] for

[2] Derived in Appendix.

their studies. From this material a nomograph, such as Fig. 5, was constructed. It gives the value of throttle enthalpy minus state line end point for the test conditions of reheat steam temperature and pressure and condenser pressure. To this is added the exhaust loss corresponding to the test condenser flow and pressure to obtain the expected value of used energy. The expected used energy subtracted from the test initial enthalpy gives the expected value of used energy end point.

The deviation in used energy end point found by comparing the expected and test values can be related to change in heat rate using Salisbury's expression:

$$\left.\frac{\Delta r}{r_r}\right]_{\Delta H_c} = \frac{(r_n - 1)\dfrac{\Delta H_c}{H_e - h_c}}{1 + C}$$

(Eq. 42, ref. [3]) (8)

There is a secondary effect on heat rate which cannot be ignored. A deviation in turbine efficiency will cause a change in H_e unless the result were to lie below the last extraction opening. If the turbine efficiency became worse, H_e would increase, adding to the increase in heat rate. Determining the reference value of H_e for other than design conditions has not yet been undertaken by the authors, although Salisbury has indicated the means for accounting for changes in condenser pressure. If the test were conducted at other than design conditions, or the reference value of H_e otherwise determined for comparison with a test H_e, any existing ΔH_e may be related to change in heat rate using equation (4).

There is an alternate approach to determining the condition of the low-pressure turbine and any associated loss in heat rate. For those cycles not complicated by steam-driven auxiliary equipment or other special equipment arrangements, Deviation Monitoring may be applied to the heaters and high-pressure turbine. All of the changes in heat rate thus found when summed would account for most of the difference between test heat rate and reference heat rate. The unaccounted for difference is chargeable to the low-pressure turbine and the errors of the operation. The entire operation should be accurate to approximately 1 per cent and relatively constant. A plot of the unaccounted difference against time (day, week, or month) should give a picture of the change in condition of the low-pressure turbine and approximately the magnitude of any associated loss in heat rate.

Examples of Application

Illustrations of the application of the foregoing monitoring procedures are presented here to illustrate two points: First, how well Salisbury's expressions predict the change in heat rate for a real cycle; and second, how well the application described in this paper predicts the change in heat rate.

The numbers used in the examples were obtained by using a digital computer program that calculated heat balances for the cycle shown in simplified form in Fig. 6. Any cycle fault could be simulated with this program. The cycle used in this example actually exists and field tests have demonstrated that the primary characteristics of the major cycle components have been accurately described in the computer program.

The computer was used to evaluate cycle faults because the changes in heat rate experienced in many cases are smaller than the resolution and accuracy of even the best full-scale heat-rate test. Also it is impossible to purposely introduce many faults without doing permanent damage to the cycle.

In the following examples the items headed "Primary Effect" are accounted for by the described application. Those listed as "Secondary Effect" are the remainder of Salisbury's key enthalpies which have been affected by the faults of the example.

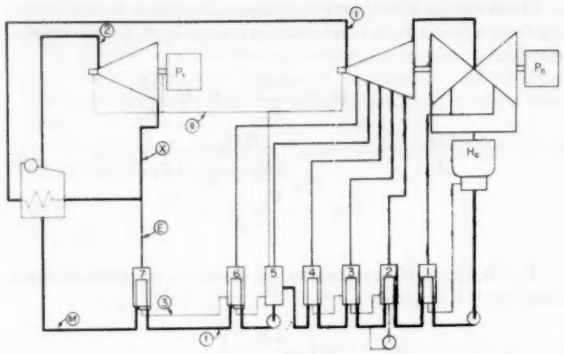

Fig. 6 A practical reheat cycle

Example No. 1, High-Pressure Heater Fault. Extraction line throttled to reduce heater shell pressure.

Primary effect: The final feedwater enthalpy was reduced from 421.5 Btu/lb to 395.5 Btu/lb. Δh_{bf} is 26 Btu/lb and the loss in heat rate from this factor is

$$\left.\frac{\Delta r}{r_r}\right]_{\Delta h_{bf}} = +0.00429 \quad (9)$$

Secondary effects:

1 The high-pressure turbine exhaust enthalpy increased 3.3 Btu/lb, resulting in a loss in heat rate of:

$$\left.\frac{\Delta r}{r_r}\right]_{\Delta H_x} = +0.00314 \quad (10)$$

2 The reheat steam enthalpy decreased by 0.4 Btu/lb, resulting in an increase in heat rate of:

$$\left.\frac{\Delta r}{r_r}\right]_{\Delta H_1} = +0.00030 \quad (11)$$

3 The feedwater enthalpy entering the high-pressure heater (leaving the low-pressure group) increased 2.53 Btu/lb, resulting in an improvement in heat rate of:

$$\left.\frac{\Delta r}{r_r}\right]_{\Delta h_f} = -0.00070 \quad (12)$$

4 The used energy end point decreased by 0.92 Btu/lb, resulting in an improvement in heat rate of:

$$\left.\frac{\Delta r}{r_r}\right]_{\Delta H_c} = -0.00113 \quad (13)$$

Total secondary effect	= +0.00161
Primary effect	= +0.00429
Total predicted $\Delta r/r$	= +0.00590
True value $\Delta r/r$	= +0.00553
Prediction error $\Delta r/r$	= +0.00037

Example No. 2, Low-Pressure Heater Fault. Heater No. 3 extraction line throttled to reduce heater shell pressure.

Primary effect: The exit feedwater enthalpy was reduced from 183.2 Btu/lb to 168.9 Btu/lb. The change in heater rise was 14.3 Btu/lb and the change in H_e as determined from equation (3) is:

$$\Delta H_e]_{\Delta R} = +4.0 \text{ Btu/lb} \quad (14)$$

The true change in H_e as determined by the computer is:

Table 1 Summary of numerical examples

$\frac{\Delta r}{r_r}$ component	Example no. 1 (HPH)	2 (LPH)	3 (HPT)	4 (LPT)
Δh_{bf}	+0.00429[a]	...	−0.00001	...
ΔH_x	+0.00314	...	+0.00717[a]	...
ΔH_1	+0.00030	...	−0.00001	...
Δh_f	−0.00070	...	−0.00002	−0.00001
ΔH_e	...	+0.00105[a]	−0.00001	+0.00598
ΔH_e	−0.00113	+0.00002	−0.00004	+0.03321[a]
Predicted total $\frac{\Delta r}{r_r}$	+0.00590	+0.00107	+0.00710	+0.03918
True total $\frac{\Delta r}{r_r}$	+0.00553	+0.00110	+0.00725	+0.04077
Prediction error $\frac{\Delta r}{r_r}$	+0.00037	−0.00003	−0.00015	−0.00159

[a] Accounted for by the described application.

$$\Delta H_e = +4.1 \text{ Btu/lb} \tag{15}$$

The loss in heat rate corresponding to a ΔH_e of 4.0 Btu/lb is:

$$\left.\frac{\Delta r}{r_r}\right]_{\Delta H_e} = +0.00105 \tag{16}$$

Secondary effect: The only measurable secondary effect is a change in used energy end point of +0.02 Btu/lb.

The resulting loss in heat rate is:

$$\left.\frac{\Delta r}{r_r}\right]_{\Delta H_e} = 0.00002 \tag{17}$$

Primary effect	= +0.00105
Secondary effect	= +0.00002
Total predicted $\Delta r/r$	= +0.00107
True value of $\Delta r/r$	= +0.00110
Prediction error $\Delta r/r$	= −0.00003

Example No. 3, High-Pressure Turbine Fault. The high-pressure turbine efficiency was decreased by 3.76 per cent.

Primary effect: The high-pressure turbine exhaust enthalpy increased from 1343.5 Btu/lb to 1351.0 Btu/lb.

ΔH_x is +7.5 Btu/lb, resulting in a loss in heat rate of:

$$\left.\frac{\Delta r}{r_r}\right]_{\Delta Hx} = +0.00717 \tag{18}$$

Secondary effects:

1 The final feedwater enthalpy increased by 0.08 Btu/lb, resulting in a gain in heat rate of:

$$\left.\frac{\Delta r}{r_r}\right]_{\Delta h_{bf}} = -0.00001 \tag{19}$$

2 The reheat steam enthalpy decreased by 0.01 Btu/lb, resulting in a loss in heat rate of:

$$\left.\frac{\Delta r}{r_r}\right]_{\Delta H_1} = +0.00001 \tag{20}$$

3 The feedwater enthalpy leaving the low-pressure heater group increased by 0.06 Btu/lb, resulting in a gain in heat rate of:

$$\left.\frac{\Delta r}{r_r}\right]_{\Delta h_f} = -0.00002 \tag{21}$$

4 H_e decreased by 0.05 Btu/lb, resulting in a gain in heat rate of:

$$\left.\frac{\Delta r}{r_r}\right]_{\Delta H_e} = -0.00001 \tag{22}$$

5 The used energy end point decreased by 0.03 Btu/lb, resulting in a gain in heat rate of:

$$\left.\frac{\Delta r}{r_r}\right]_{\Delta H_e} = -0.00004 \tag{23}$$

Total secondary effect $\Delta r/r_r$	= −0.00007
Total primary effect $\Delta r/r_r$	= +0.00717
Total predicted $\Delta r/r_r$	= +0.00710
True value $\Delta r/r_r$	= +0.00725
Prediction error $\Delta r/r_r$	= −0.00015

Example No. 4, Low-Pressure Turbine Fault. The low-pressure turbine efficiency was decreased by 4.72 per cent.

The direct effect on heat rate is through the increase in used energy end point of 27.1 Btu/lb. The resulting loss in heat rate is:

$$\left.\frac{\Delta r}{r_r}\right]_{\Delta H_e} = +0.03321 \tag{24}$$

This fault was uniformly distributed through the low-pressure turbine causing H_e to increase by 22.9 Btu/lb. The resulting loss in heat rate is:

$$\left.\frac{\Delta r}{r_r}\right]_{\Delta H_e} = +0.00598 \tag{25}$$

The feedwater enthalpy leaving the low-pressure group increased by 0.05 Btu/lb, resulting in a gain in heat rate of:

$$\left.\frac{\Delta r}{r_r}\right]_{\Delta h_f} = -0.00001 \tag{26}$$

Total predicted $\Delta r/r_r$	= +0.03918
True value $\Delta r/r_r$	= +0.04077
Error in prediction $\Delta r/r_r$	= −0.00159

The preceding results are shown in tabular form in Table 1.

Summary

By reference to Table 1 (Predicted total $\Delta r/r_r$ versus True total $\Delta r/r_r$) it is evident that the summation of all the changes in heat rate due to the deviations in key enthalpies results in a very good approximation of the true change in heat rate.

As seen by comparing only the primary effect with the true total change in heat rate, secondary effects are certainly negligible for the high-pressure turbine and low-pressure heater faults. In the case of the high-pressure heater, the primary effect is not as good an approximation of the true change as for the foregoing equipment, but it still provides a resolution and accuracy better than is obtainable from a full-scale test which is at best only reproducible to ±0.25 per cent.

Secondary effects, primarily a change in H_e, play an important part when faults occur in the low-pressure turbine as indicated by the difference between the primary effect ΔH_e and the true change in heat rate. This difference amounts to an error of 0.7 per cent in heat rate. It is therefore evident that secondary effects must be accounted for in this case.

The application technique outlined in this paper is amenable to either manual or automated implementation. The curves presented as an aid to manual application may be calculated in one day for the average cycle, and one man can collect and analyze the data, often using station instrumentation. The exception of course is the low-pressure turbine. In the automated application with on-line computation, substantial equipment and programming savings can be realized over conventional methods of analysis.

It is evident that there are aspects of turbine-cycle performance monitoring not yet embraced in either the theory, as reported by Salisbury, or in the analytical application as reported herein. Therefore the authors consider that this paper is a report of progress to date rather than a complete exposition. The program of developing simplified techniques for isolating and evaluating faults in the turbine cycle is continuing on a broad front.

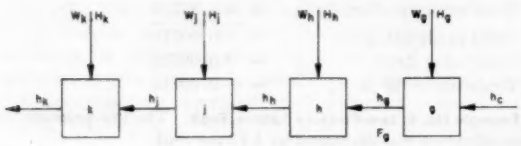

Fig. 7 An ideal contact heater system

APPENDIX

Derivation of Relationship Between Change in Enthalpy Rise Across a Feedwater Heater and Change in H_e[3]

Consider an ideal low-pressure heater system consisting of contact heaters as in Fig. 7. For any heater, for example heater h, the extraction flow is given by

$$\left.\begin{aligned} W_h &= \frac{F_g(h_h - h_g)}{H_h - h_h} \\ &= \frac{F_g R_h}{H_h - h_h} \text{ where } R = h_h - h_g \\ &= K_h R_h \text{ where } K_h = F_g/(H_h - h_h) \end{aligned}\right\} \quad (27)$$

The extraction flow to each heater can be similarly expressed and H_e can be written as

$$H_e = \frac{K_e R_e H_e + K_k R_k H_k + K_j R_j H_j + K_h R_h H_h}{K_e R_e + K_k R_k + K_j R_j + K_h R_h} \quad (28)$$

If a fault occurs in the h heater, the duty lost by heater h will be shifted to heater j with an accompanying equal but opposite change in rise for the two heaters. The new effective enthalpy will be:

$$H_e' = \frac{K_e R_e H_e + K_k(R_k + \Delta R_k)H_k + K_j(R_j + \Delta R_j)H_j + K_h R_h H_h}{K_e R_e + K_k(R_k + \Delta R_k) + K_j(R_j + \Delta R_j) + K_h R_h} \quad (29)$$

The fractional change in H_e can be written as

$$\frac{\Delta H_e}{H_e} = \frac{1 + \dfrac{K_k \Delta R_k H_k + K_j \Delta R_j H_j}{W H_e}}{1 + \dfrac{K_k \Delta R_k + K_j \Delta R_j}{W}} - 1 \quad (30)$$

Multiplying by $\frac{R_k}{R_k}$ and $\frac{R_j}{R_j}$

$$\frac{\Delta H_e}{H_e} = \frac{1 + \dfrac{K_k R_k \dfrac{\Delta R_k H_k}{R_k} + K_j R_j \dfrac{\Delta R_j H_j}{R_j}}{W H_e}}{1 + \dfrac{K_k R_k \dfrac{\Delta R_k}{R_k} + K_j R_j \dfrac{\Delta R_j}{R_j}}{W}} - 1 \quad (31)$$

Since $K_k R_k = W_k$ and $K_j R_j = W_j$

$$\frac{\Delta H_e}{H_e} = \frac{1 + \dfrac{W_k \dfrac{\Delta R_k H_k}{R_k} + W_j \dfrac{\Delta R_j H_j}{R_j}}{W H_e}}{1 + \dfrac{W_k \dfrac{\Delta R_k}{R_k} + W_j \dfrac{\Delta R_j}{R_j}}{W}} - 1 \quad (32)$$

Conditions of derivation:

The expression for ΔH_e is valid if the following conditions are essentially fulfilled:

1 There is no change in extraction steam enthalpy for any heater.

2 The only feedwater enthalpy affected by the fault is the exit enthalpy of the heater under consideration.

As a result of these conditions of derivation, changes in heater rise resulting from changes in the cycle external to the heaters are not properly related to ΔH_e. For example, local turbine damage could cause a change in heater rise that would not be properly related to ΔH_e. Such a change in rise would be a false indication of a heater fault.

[3] Originally developed by J. K. Salisbury.

References

1 J. Kenneth Salisbury, "A New Performance Criterion for Steam-Turbine Regenerative Cycle," TRANS. ASME, Series A, JOURNAL OF ENGINEERING FOR POWER, vol. 81, 1959, pp. 389–402.

2 J. Kenneth Salisbury, "Analysis of the Steam-Turbine Reheat Cycle," TRANS. ASME, vol. 80, 1958, pp. 1629–1642.

3 J. Kenneth Salisbury, "Power-Plant Performance Monitoring," published in this issue, pp. 409–422.

4 H. Hegetschweiler and R. L. Bartlett, "Predicting Performance of Large Steam Turbine-Generator Units for Central Stations," ASME Paper No. 56—SA-52.

DISCUSSION

V. F. Estcourt[4]

The authors have presented the results of their preliminary studies "to provide methods of boiler and turbine cycle analysis suitable for data-processing techniques."

They conclude that there are aspects of turbine-cycle performance monitoring not yet embraced in either theory or application. They have, however, attempted to present some new relationships between the thermodynamic values in various parts of the plant cycle with the thought that these may open the way to new methods of employing data-processing techniques.

[4] Pacific Gas and Electric Company, San Francisco, Calif. Fellow ASME.

Although it is perhaps true that the study of these thermodynamic relationships as presented by the authors may assist in pointing the way to new techniques of measurement, it is our feeling that there is already an urgent demand for the development of hardware which will yield more precise measurements. This is already evident from a reading of the companion paper by J. Kenneth Salisbury[6] wherein dependence is placed upon the accurate measurement of feedwater flow at two different points in the cycle.

When it is realized that commercial flowmetering devices usually carry a guarantee of accuracy equal to plus or minus 2 per cent, it is evident that we have a long way to go in the development of satisfactory hardware. Although, as a result of special orifice calibration and other special techniques, it is possible to obtain a flowmeter accuracy of the order of plus or minus 0.5 per cent, this still leaves much to be desired both in terms of accuracy and the complicated procedures necessary to obtain even this degree of precision.

There is a technological lag in the development of primary measuring devices. Perhaps what is needed is a completely new look at some of these problems in terms of fundamentals rather than merely an attempt to improve present day hardware.

J. Kenneth Salisbury[6]

Although the authors have demonstrated the validity of the writer's relationships through the use of a computer, using the individual enthalpy changes, the authors and the writer are in agreement that the basic monitoring equations for a reheat powerplant system must involve changes in *enthalpy differences*, rather than changes in the enthalpies themselves. That is, the monitoring relationships for various elements of the system are:

High-pressure heater—Equation (49)
High-pressure turbine—Equation (46)
Low-pressure heater—Equation (42)
Low-pressure turbine—Equation (50)

in which the equation numbers refer to the writer's companion paper. Although Equation (42) deals with an enthalpy change, ΔH_s, rather than a change in an enthalpy difference, the writer has become convinced that even here a better criterion may be $\Delta(H_1 - H_s)$.

Let us now address ourselves to the Appendix of the authors' paper. As credited in the footnote, the equations of this Appendix were developed by the writer in an early effort to find a method of monitoring faults of individual heaters. The derivation was based on the gross assumption (later found to be insufficiently accurate) that heater extraction quantity is proportional to rise across the heater, as stated in the last line of the authors' Equation (27). Since the original work was done, the writer has come to believe that Equation (32) of the authors' paper is not adequate for monitoring individual heaters, and further, that such monitoring is indeed a complex procedure that must rely, in last analysis, on the measurement of all flows and temperatures at the heater, and subsequent comparison of these data with guarantees.

The fallacy in the assumption of the proportionality of extraction and heater rise is evident from the definition of K_h in Equation (27). For K_h to remain constant, F_g and $(H_h - h_h)$ must both be constant (or proportional to each other, which is highly unlikely). Thus when a fault occurs, resulting in a decrease in h_h, it is required that H_h also decrease by *exactly the same amount*. If the fault that has occurred is due to fouling of the heater, or due to an obstruction in the extraction line, H_h probably will not change at all, and the original assumption is therefore incorrect. Conceivably, the change in rise across the heater may occur due to a change in turbine shell pressure, so that H_h and h_h would tend to change by approximately the same amount. Clearly, this situation is quite different, and would yield a different result. Obviously the *source* of a change in rise is of paramount importance, and a given change in rise on a heater causes a different loss, depending on whether a change in rise is caused by fouling, or by a change in turbine shell pressure. Thus a change in rise across the heater does not completely determine the change in heat rate that results without further qualification as to the source of the change in rise.

Consider, for the moment, that through some unusual combination of circumstances the value $(H_h - h_h)$ does remain constant, as h_h decreases. The change in h_h will decrease the extraction quantity, w_h. The rise across heater j will increase, but $(H_j - h_j)$ will remain constant. However, the change in w_h changes F_h, destroying the proportionality of rise and extraction for heater j, which was the basic original assumption.

Referring to the authors' conditions, following Equation (32), it is clear that the extraction steam enthalpy *must* change by exactly the same amount as the heater outlet enthalpy, but that even this is not a sufficient condition to make the result valid, since the heater condensate flows vary when the heater rises change, destroying the proportionality of rise and extraction quantity. It is obvious that the manner in which the condensate varies is an extremely complex function of what has happened at each of the lower heaters, affecting their extractions, hence the condensate flow to the heater in question.

The writer has given much thought and attention to the problem of monitoring individual heaters. He has not found, to date, any suitable "short-cut" approach that avoids the many individual measurements now necessary to check performance of a given heater. He has, however, presented in Ref. [1] of the authors' paper, a method by which the heater system, taken as a single thermodynamic entity, can be monitored as to its effect on plant heat rate, through the criterion H_s. Although this approach requires two precision flow measurements, which present some problems, it seems to represent the best shortcut found to date for monitoring purposes.

The application of the H_s method in monitoring the heater system requires repeatability of the flow measurements, rather than absolute accuracy. The writer has proposed that the difficulties of careful calibration may be avoided. It is suggested that during the initial operating period one may use guarantee heat balance data to work backward through the relationships of Ref. [1] of the authors' paper and arrive at a "pseudo" calibration of the flowmeters which may then be used for all future work. Whether this calibration is indeed correct is quite unimportant, since for all practical purposes we are interested only in determining changes of the heater system that may occur subsequent to the initial operating period. Such an approach obviously is "second best," by comparison with accurately calibrated flowmeters. Whether it offers any real advantage or not remains to be determined by trial.

Authors' Closure

The authors will not disagree with Mr. Estcourt in his statement that "there is already an urgent demand for the development of hardware which will yield more precise measurement." However, there is also an urgent demand for turbine cycle analysis techniques which can be used and understood without large expenditures of effort on the part of the user. It is to this second demand that the authors direct their paper. Satisfying the second demand should serve to identify where equipment development is needed to stimulate interest in astute cycle analysis, and provide the justification for the higher cost of more sophisticated equipment.

[6] J. Kenneth Salisbury, "Power-Plant Performance Monitoring," published in this issue, pp. 409–422

[6] Consulting Engineer, Atherton, Calif. Fellow ASME.

Mr. Salisbury comments on certain specific details of the monitoring techniques presented by the authors. A proper reply to these comments would be longer than the original paper. It suffices to say that it was not the authors' intent to present a complete and rigorous practical turbine monitoring procedure. This paper was intended to provide numerical examples of the validity of Mr. Salisbury's equations as presented in his companion paper and to point the direction the authors are following in developing a turbine cycle monitoring technique.

However, the authors do feel it necessary to answer Mr. Salisbury's comments on the derivation of the low pressure heater monitoring expression (equation 32). The derivation contains assumptions as Mr. Salisbury points out and as pointed out in the Appendix to the paper. These assumptions are not rigorously met in the actual situation; however, extensive checking of the results obtained by use of equation (32) indicates that reasonable precision is obtained in almost every situation of heater faults. The authors recognized, as stated in the Appendix, that cycle faults external to the heater system which affect heater performance are not properly evaluated.

Perhaps it will help place this work in proper perspective if the objectives of the authors' work is restated. It is the objective of the authors to develop a turbine cycle monitoring technique (later to be extended to the entire power plant) which can be used by power-plant personnel not steeped in cycle design practice. Such a technique must be simple to implement—thus the use of precalculated loss curves, and easy to develop—thus the approximate equations presented. It must be recognized that some rigor must be given up to achieve simplicity.

The paper as written represents the progress made as of approximately June, 1960, and only an outline at that. A complete presentation of the authors' turbine cycle analysis techniques is beyond the scope of an ASME paper. These techniques are the subject of the Bailey Turbine Cycle Analysis Workshop, a two-week program. The written material for this workshop is in excess of 200 pages.

It is the authors' hope that this and similar papers will stimulate increased interest in turbine cycle analysis at the power-plant level, for it is the man in everyday contact with the cycle who will be able to realize savings through a better knowledge of why his unit performs the way it does

G. CHIANTORE[1]
D. BORGESE[1]
F. BALDO[1]
J. H. POTTER[2]

Optimizing a Regenerative Steam-Turbine Cycle

Conventional design procedures require complete and accurate heat balances on each of a number of alternative regenerative cycles in order to determine the optimum cycle for a given set of conditions. This paper presents an analytical method, developed at the Edisonvolta, S.p.A., of Milan, Italy, by which the number of heat balances required to optimize the cycle is reduced a minimum.

Introduction

THE selection of the best steam-turbine regenerative cycle for a new power installation is normally determined by heat-balance studies of several alternative arrangements. The complexity of modern steam power cycles is reflected in the heat balances, and a great amount of time must be spent in the conventional heat-balance comparisons of the alternatives. As a result, many efforts have been made to set up rapid or shortcut methods for arriving at the optimum cycle [1–8].[3]

This paper reports upon an analytical design method developed at the Edisonvolta, S.p.A., Milan, Italy, in which a minimum number of heat balances is required for the optimization of the feedwater-heater system. The method involves the analysis of a "basic" cycle, decided upon by the utility management and the manufacturer, as being appropriate for the installation. This implies a selection of the turbine, at least as far as capacity and steam conditions are concerned, and the estimated locations of the bleed points. The basic cycle *is not* a generalized or simplified or fictitious cycle; building the method upon a generalized cycle would reduce the accuracy of the results to the degree obtainable with the present shortcut methods. Each case must be referred to a basic cycle involving only the specified capacity and steam conditions for that particular installation. It is also assumed that the alternatives to the base cycle may produce more or less power, cost more or less money, and operate at rated load at a greater or lower heat rate than the base cycle. When these alternatives are compared to the base cycle, it is further assumed that:

(*a*) Each unit of power generated can be used; each unit of power missing could have been used; each unit of power will have the same value and will be capitalized in the same way.

(*b*) The change in heat rate will be capitalized, taking account of the probable fuel-cost changes and the probable plant-capacity factor over the life of the installation.

(*c*) To the foregoing costs, the incremental equipment costs of the alternatives will be algebraically added.

If the turbine described in the manufacturer's proposal is still in the preliminary design stages, a study can be made to fix the number and location of the bleed points and, consequently, the final feedwater temperature. If the proposed turbine has been fully designed, the only possible investigation is the determination of the feasibility of the turbine load changes, and the economics of the elimination of one or more feedwater heaters. In either event, simplified heat balances or other shortcut methods may be used [1, 3, 4, 5].

Optimization of the heater terminal differences, the use of condensate-drain pumps, and the location of the boiler feed pump require greater accuracy in calculation. Either detailed heat balances must be used, or the optimization method to be presently described.

The theory underlying the proposed method is that any modification of a cycle may be simulated by fictitious additions and subtractions of heat in the basic cycle, since these have the same effects on turbine capacity and heat rate. This is similar to the

[1] Steam Power Division, Edisonvolta, S.p.A., Milan, Italy.
[2] Gibbs and Hill, Inc., New York, N. Y. Mem. ASME.
[3] Numbers in brackets designate References at end of paper.
Contributed by the Power Division and presented at the Winter Annual Meeting, New York, N. Y., November 27–December 2, 1960, of THE AMERICAN SOCIETY OF MECHANICAL ENGINEERS. Manuscript received at ASME Headquarters, August 8, 1960. Paper No. 60—WA-179.

Nomenclature

P_b = power of basic cycle, kw
r_b = heat rate of basic cycle, Btu/kw hr = Q_b/P_b
Q_b = heat furnished by boiler in basic cycle, Btu/hr
ΔP = change in turbine capacity, kw
Δr = change in heat rate, Btu/kw hr
ΔQ = change in heat furnished by boiler, Btu/hr
ΔI = enthalpy difference in heater between entering steam and drains, Btu/lb
Δi = enthalpy rise of feedwater in heater, Btu/lb
Δi_c = enthalpy drop of drains in heater, Btu/lb
ε' = entering feedwater-enthalpy increase, Btu/lb
ε'' = leaving drains-enthalpy increase, Btu/lb
δ = entering steam-enthalpy decrease, Btu/lb
W = feedwater flow, lb/hr
$\mathfrak{W}$ = leaving-drains flow, lb/hr
W_v = extraction-steam flow, lb/hr
f = (feedwater extracted)/(over-all feedwater flow), lb/lb
q = main variation, Btu/hr
q_c = heat introduced into feedwater between two consecutive heaters, Btu/hr
q_p = heat introduced by a pump, Btu/hr

Definitions

"Heater upstream of another heater"—means "preceding" in the direction of feedwater flow.

"Inlet terminal difference"—the temperature difference between the leaving drains and entering feedwater.

"Outlet terminal difference"—the temperature difference between saturated steam at heater and outlet feedwater.

perturbation techniques employed in the solution of many of the complex problems in the physical sciences. These fictitious additions and subtractions of heat in the basic cycle are to be identified as "main variations." A linear relationship is assumed to exist between the main variations and the thermodynamic effects in the cycle; that is, changes in turbine capacity and heat rate. It is further assumed that the thermodynamic effects of one or more modifications are equal to the algebraic sum of the thermodynamic effects due to each of the corresponding main variations.

To recapitulate, any modifications to the cycle may be expressed by the corresponding main variations, and the over-all thermodynamic effects M of the modification may be expressed as

$$M = (a)V_1 + (b)V_2 + \ldots \quad (1)$$

where $a, b, \ldots$ are the main variations corresponding to the modification, measured by taking as a unit the "main unit variation," and $V_1, V_2, \ldots$ are the corresponding thermodynamic effects of the main unit variation. This is a fictitious addition of heat of a fixed value, which may be selected arbitrarily, usually between 1 and 2 per cent of Q_b.

The procedure for applying the foregoing theory consists first in the determination of the complete full-load heat balance of the basic cycle.

The main-unit variation is then applied successively and individually to the condenser, to each of the feedwater heaters, and to the boiler, and the corresponding thermodynamic effects are calculated by heat balances. The introduction of this extra heat in the condenser, for which the same loading and cooling-water flow is maintained, results in a loss of vacuum with a consequent increase in the enthalpy of the steam to the condenser. A loss of power, ΔP, ensues. As the heat supplied by the boiler is unchanged, the heat rate is affected adversely.

In the several feedwater heaters the introduction of the main-unit variation causes a reduction in the bled steam with the probability of greater power development and reduction in heat rate

The main-unit variation introduced after the last high-pressure heater will decrease that needed in the boiler and reduce the heat rate; however, the bled steam flows remain the same and there is no change in power.

The changes are related to the basic cycle values as

$$\Delta r/r_b = \Delta Q/Q_b - \Delta P/P_b \quad (2)$$

Calculations of the thermodynamic effects of the modifications are facilitated by grouping the effects of the main-unit variations as shown in Table 1.

Table 1 Thermodynamic effects due to A main-unit variation of------ Btu/hr

Heat addition in	Cdr	1st htr	2nd htr		nth htr	Boiler
ΔP, kw						
ΔQ, Btu/hr						
Δr, Btu/kw hr						

The steam saturation temperatures in the several feedwater heaters are used as loci forming the abscissa of a graph in which the quantities listed in Table 1 are plotted. Representative graphs are shown in Figs. 1, 2, and 3.

The thermodynamic effects of a main-unit variation in a 60-mw nonreheat cycle are shown in Fig. 1. If Fig. 1 were being used in a study to determine the number of feedwater heaters, approximate values of ΔP, ΔQ, and Δr could be obtained by reading the respective ordinates at the saturation temperatures intermediate to those shown. However, it is important to note that to maintain the accuracy of the method, the addition of other heaters would require a new Table 1 and a complete recalculation of the values in it.

Larger and more complex cycles have been represented in Figs. 2 and 3 to show the effects of reheating and higher throttle conditions. The trend of the curves in Figs. 1, 2, and 3 may be explained as follows:

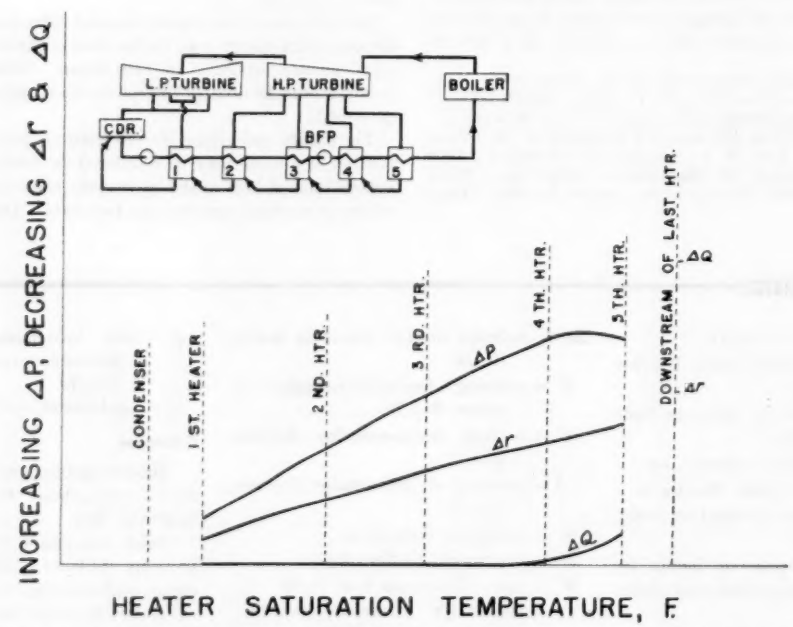

Fig. 1 Thermodynamic effects of a main-unit variation of 10 million Btu/hr on a 60-mw cycle; throttle conditions 850 psig, 900 F

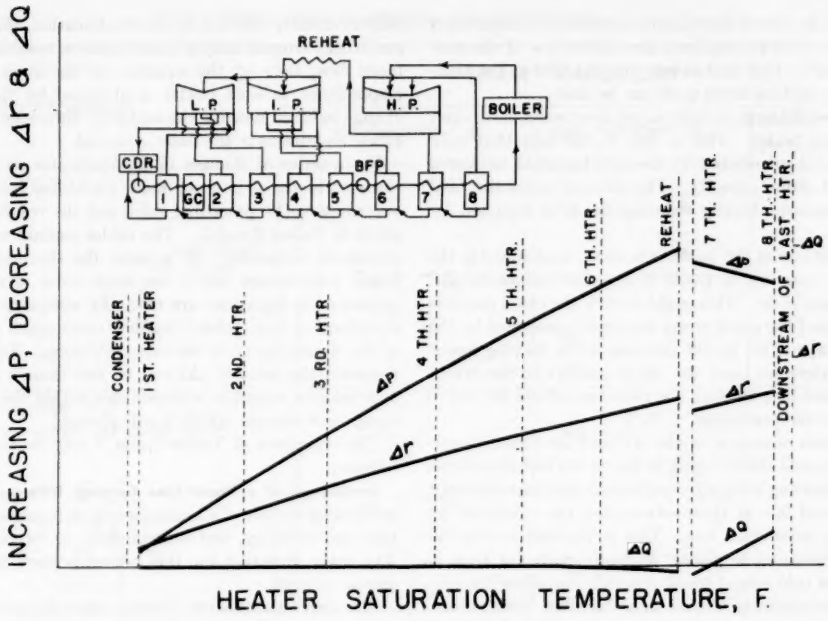

Fig. 2 Thermodynamic effects of a main-unit variation of 50 million Btu/hr on a 300-mw cycle; throttle conditions 2400 psig, 1050 F, reheat 1000 F

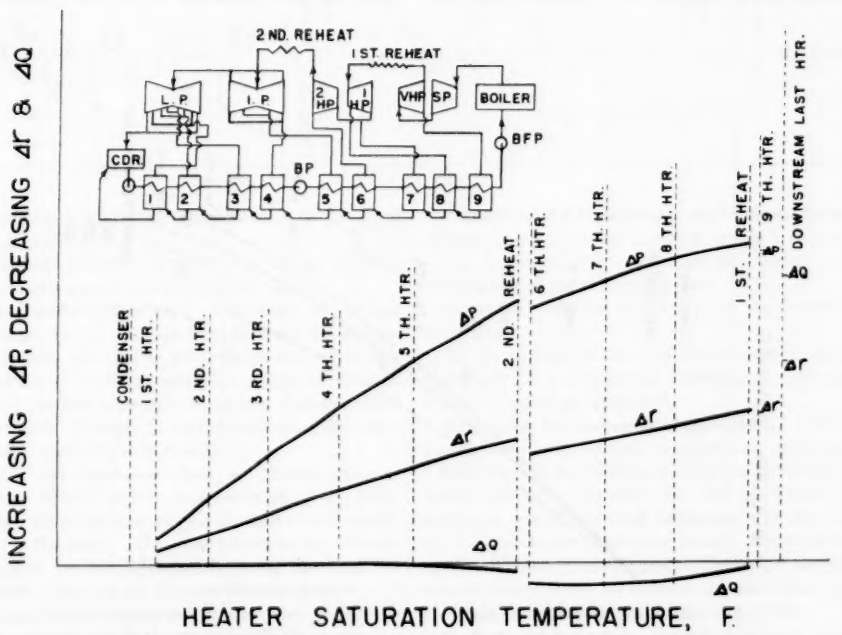

Fig. 3 Thermodynamic effects of a main-unit variation of 50 million Btu/hr on a 350-mw cycle; throttle conditions 5000 psig, 1200 F, reheat to 1050 F, second reheat to 1050 F

1 The ΔP and Δr-curves show improvement as the saturation temperatures rise. This follows from the second law of thermodynamics and from the fact that as less steam is bled at the high-pressure end of the turbine more work can be done.

2 The ΔP-curve flattens, or even slopes downward, in the last portion toward the boiler. This is due to the fact that only a portion of the heat introduced in the last heater is recovered as an increase in turbine capacity. The balance raises the final feed-water temperature, thereby reducing the heat supplied by the boiler.

3 If the exhaust end of the machine is small, heat added in the L-P heater could conceivably result in negative values for ΔP and positive changes in Δr. This might occur if the bleed pressure was very low, so that the small power increment produced by the extra steam flow was offset by the increase in the leaving losses.

4 Where reheaters are used, the ΔQ is positive to the extent that increased steam flow through the reheaters offsets the rise in the final feedwater temperature.

5 The step down occurring in the ΔP and Δr-curves in correspondence to the cold reheat bleed, is due to the fact that steam extracted after reheating is highly superheated and, consequently, again by the second law of thermodynamics, its utilization for feedwater heating involves a loss. This is the reason why the bleed after the reheating is placed normally quite far from it. Consequently, the cold reheat bleed generally furnishes the feedwater with a larger quantity of heat than the other bleed points.

The economic value corresponding to a main-unit variation can be determined from the graphs described previously when the criteria and values of fuel cost, plant-capacity factor, cost of money, and cost of installation are established. In Fig. 4 this value is plotted against the heater saturation temperatures for the cycle shown in Fig. 2. Curves A and B are based on equal plant-capacity factors and fuel costs, but B exceeds A in cost of construction. Curve C represents variations in these items. Any number of curves could have been plotted in Fig. 4, depending upon the combinations of the variables involved.

The general rules to determine the main variations corresponding to a modification are as follows: (*a*) First determine the heaters directly affected by the modification, (*b*) a heat balance is performed around each of these heaters, resulting in a change in bleed flow, then (*c*) the equation of the main variation in correspondence to each heater is obtained by the product of the change in bleed flow for the enthalpy difference between entering steam and drains in the basic cycle, ΔI.

For a series of changes in the feedwater circuits covering the cases normally of interest, main variations have been evaluated according to the preceding rules and the resulting equations are given in Tables 2 and 3. The tables contain both exact and approximate equations. In general, the thermodynamic and economic inaccuracies are of the same order of magnitude, so the approximate equations are normally adequate. As an example, modification A in Table 2 involves elimination of the second term of the denominator in the exact equation. For the changes anticipated the term $\mathcal{E}''/\Delta I$ will be less than 2 per cent, and the approximate equation is reasonable within the cost range of the equipment changes which it will govern.

The equations of Tables 2 and 3 may be commented upon as follows:

A—Change of a Heater-Inlet Terminal Difference. Reducing the subcooling surface of a heater causes an increase in drain temperature and enthalpy, and consequently an increase in bleed steam. The main variation for this heater is then negative, i.e., a removal of heat.

The only other heater directly affected by the modification is the upstream one, into which the drains enter at a higher enthalpy. As a consequence, less bleed steam is required. Main variation of the upstream heater has the same value but opposite sign to that of the modified heater.

If the lowest pressure heater is modified, the change in the heat furnished by drains to it will involve a change, of equal amount but opposite sign, in the heat discharge in the condenser.

B—Change of a Heater-Outlet Terminal Difference. Increasing the condensing and/or desuperheating area of a heater causes an increase in bleed steam and a rise in the outlet feed temperature. Again, the main variation for the other heater directly affected

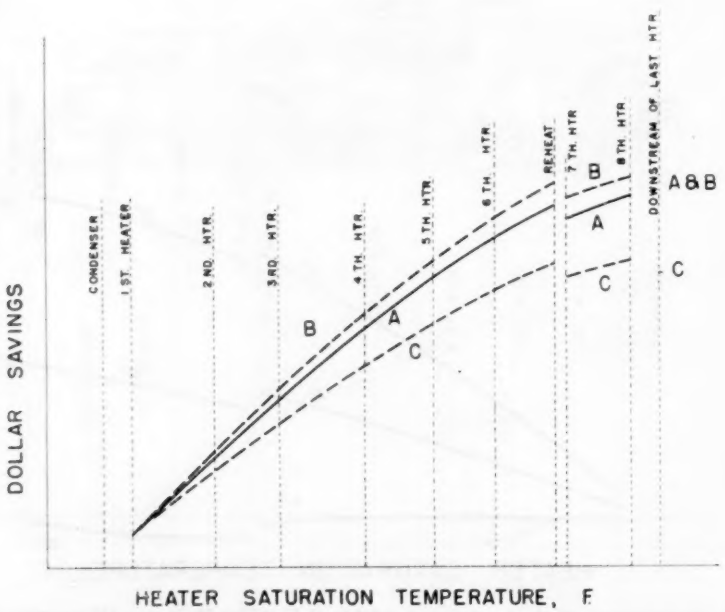

Fig. 4 Economical value of thermodynamic effects of cycle shown in Fig. 2

Table 2 Main variations for most usual changes

MODIFICATION		MAIN VARIATIONS at heater a	at heater b	at heater other than "a" & "b"
A) Change in inlet T.D 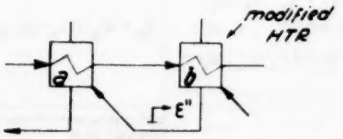	excess	$q_a = -q_b$	$q_b = \frac{-\varepsilon'' w_b}{1-\frac{\varepsilon''}{\Delta I_b}}$	
	reduction		$q_b = -\varepsilon'' w_b$	
B) Change in outlet T.D C) Alteration in dia. of one xtr piping 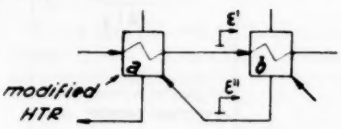	excess	$q_a = -q_b$	$q_b = \frac{\varepsilon' W - \varepsilon'' w_b}{1-\frac{\varepsilon''}{\Delta I_b}}$	
	reduction		$q_b = \varepsilon' W - \varepsilon'' w_b$	
D) Addition of heat recovering units in the F.W. system 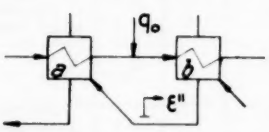	excess	$q_a = -(q_b - q_o)$	$q_b = \frac{q_o - \varepsilon'' w_b}{1-\frac{\varepsilon''}{\Delta I_b}}$	
	reduction		$q_b = q_o - \varepsilon'' w_b$	
E) Addition of B.F.P. in F.W. cycle 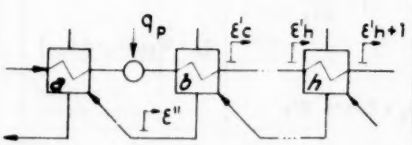	excess	$q_a = -(q_b - q_p)$	$q_b = \frac{q_p - \varepsilon'' w_b - \varepsilon'_c W}{1-\frac{\varepsilon''}{\Delta I_b}}$	at heaters where pressure is changed $q_h = W(\varepsilon'_h - \varepsilon'_{h+1})$
	reduction		$q_b = q_p - \varepsilon'' w_b - \varepsilon'_c W$	

by the modification, i.e., the downstream heater, is of the same amount, but with opposite sign.

If the highest pressure heater is modified, the change in feedwater temperature causes a main variation for the boiler.

C—Change in Extraction-Piping Diameter. Variations in piping diameter cause changes in the pressure drop between the extraction point and the heater, reflected in the pressure and saturation temperature in the heater. As the terminal temperature difference at the heater outlet remains constant, there is a change in the feed-outlet temperature. Changes in extraction-piping diameter give, therefore, a main variation as in case B.

D—Heat Introduced Into Feedwater From an Outside Source. Here the modification affects the heater downstream of the point of application in the same manner as case B, and consequently the main variation is the same. The main variation for the upstream heater is equal to the difference between the heat recovered and the main variation for the downstream heater.

E—Addition of Booster Pumps in Feedwater Circuit. An additional pump causes a temperature rise in the water, with effects similar to case D, and a rise in pressure reflected in enthalpy rises downstream.

F—Addition of a Drain Pump in the Feedwater Circuit. Introducing a drain pump as shown in case F, Table 3, causes:

(*a*) A rise in temperature of the heater drains due to the elimination of the subcooling zone.

(*b*) A slight change of enthalpy to the downstream heater due to mixing.

(*c*) At all heaters between the condenser and the drain pump there will be a substantial reduction in feedwater flow and an equal reduction in drain flow.

G—Separate Desuperheating of Bleed Steam. Sometimes there is justification for a separate desuperheating of the bleed steam at a high point in the feedwater circuit as shown in Table 3. If this desuperheater is downstream of the last heater, there is only an enthalpy rise of the final feedwater. If the desuperheating is done between two feedwater heaters the criteria of case D will apply. The heat balance around the heater receiving the desuperheated steam shows an increase in bleed flow, and consequently the main variation for this heater is negative.

H—Feedwater Extraction. Partial feedwater flow may be combined with separate desuperheating [9] as shown in Table 3. The general relations developed for case G will apply for the heater

Table 3

F) Addition of heater drain pump in F.W. cycle 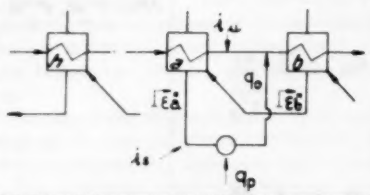	exact	$q_a = \frac{W_a(\Delta i_a - \varepsilon''_a)}{1 + \frac{\Delta i_a - \varepsilon''_a}{\Delta I_a}} - (q_b - q_o)$	$q_b = \frac{q_o - \varepsilon''_b W_b}{1 - \frac{\varepsilon''_b}{\Delta I_b}}$ in which $q_o = \frac{(i_s - i_w)W_a}{1 + \frac{\Delta i_a - \varepsilon''_a}{\Delta I_a}} + q_p$	at upstream heaters $q_h = \frac{W_a}{1 + \frac{\Delta i_a - \varepsilon''_a}{\Delta I_a}}(\Delta i_h - \Delta i_{ch})$
	approx	$q_a = W_a(\Delta i_a - \varepsilon''_a) + (q_b - q_o)$	$q_b = q_o - \varepsilon''_b W_b$ in which $q_o = (i_s - i_w)W_a + q_p$	$q_h = W_a(\Delta i_h - \Delta i_{ch})$
G) Extraction steam separate desuperheating 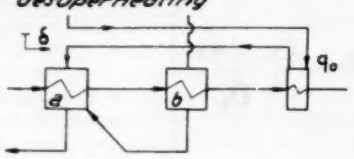	exact	$q_a = -\frac{W_{va}\delta}{1 - \frac{\delta}{\Delta I_a}}$		at desuperheater location $q_o = \frac{W_{va}\delta}{1 - \frac{\delta}{\Delta I_a}}$
H) F.W extraction 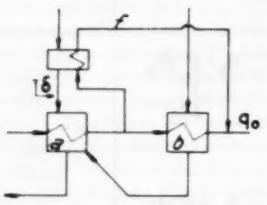	exact	$q_a = \frac{-W_{va}\delta}{1 - \frac{\delta}{\Delta I_a}}$	$q_b = f\,W\,\Delta i_b$	at point where ex. tracted water is readmitted $q_o = -(q_b + q_a)$
I) Replacement of a surface heater by a contact heater 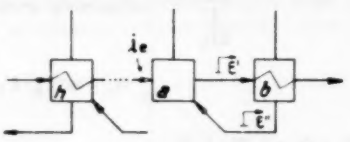	exact	$q_a = \frac{(i_{cu} - i_e)W_a - q_b}{1 + \frac{i_{cu} - i_e}{\Delta I_a}}$ in which i_{cu} is the en. thalpy of drains leaving the heater in the basic cycle	$q_b = \frac{\varepsilon' W - \varepsilon'' W_b}{1 - \frac{\varepsilon''}{\Delta I_b}}$	at upstream heaters $q_h = W_a(\Delta i_h - \Delta i_{ch})$
	approx.	$q_a = (i_{cu} - i_e)W_a - q_b$	$q_b = \varepsilon' W - \varepsilon'' W_b$	

receiving the desuperheated steam and for the re-entry point. The main variation for each heater between the water-extraction point and re-entry point is proportional to the change in feedwater flow.

I—Replacement of a Surface Heater by a Contact Heater. Should a surface heater be substituted by a contact heater, the heaters affected by the modification are the same as in case F, but the heat balances around the heaters are slightly different.

Applications of Method for Optimizing Terminal Temperature Differences of Feedwater Heaters

Once the first part of the calculation has been performed, Table 1 has been completed, and graphs similar to those of Figs. 1, 2, 3, and 4 have been drawn, the evaluation of economic gain due to any modification is very quick and easy. As an example, optimization of outlet-terminal temperature differences of the heaters may be performed as follows:

1 Using the approximate formulas in Tables 2 and 3, the main variations are seen to be proportional to the changes in terminal temperature differences. To evaluate the main variations, the first part of Table 4 is prepared on the basis of a change of 1 deg F in terminal difference; other changes are obtainable by proportion.

2 The second part of Table 4 is then prepared, using the result of the preliminary calculation reported in Table 1.

Table 4

Heater no.	1	2	3		n
W, lb/hr					
W_b, lb/hr					
ε', Btu/lb					
ε'', Btu/lb					
q_b, Btu/hr					
ΔP, kw					
Δr, Btu/kw hr					
ΔQ, Btu/hr					
Value $					

3 The value of the thermodynamic effect of the modification is then algebraically added to the cost of heaters.

From the basic design the terminal temperature differences and heater surfaces are known. The cost of changes in the terminal temperature differences may be estimated, or may be obtained from the heater manufacturer. This determination is facilitated by the use of Table 5, relating the heater area changes from the basic design due to small changes in the terminal temperature differences.

Table 5

Heater no.	Heater-area increments	
	TTD greater than basic	TTD below basic
1		
2	Surface areas decreasing	Surface areas increasing
3		
n		

This is then followed by Table 6, in which the heater cost and thermodynamic-effects values are combined for several terminal temperature differences.

Table 6

Heater	TTD above basic					TTD below basic				
1st Heater cost										
1st Thermo. value										
Total $										
2nd Heater cost										
2nd Thermo. value										
Total $										
*n*th Heater cost										
*n*th Thermo. value										
Total $										

In order to limit the number of calculations, several values from Table 6 can be plotted and the optimum value determined graphically. This has been indicated, for one heater only, in Fig. 5. A final tabulation can then be made, listing the optimum terminal temperature difference for each heater and the over-all saving referred to the basic cycle.

Discussion

It is readily apparent that with the large array of variables the number of calculations can become excessive. Experience in the application of the method and a knowledge of the performance of similar cycles will reduce the number of alternatives and hence the time for computation. Once the optimum values are determined for each of the modifications, the best feedwater-heater cycle for the plant can be found modifying the basic cycle by each of the changes which will improve it. The designer then prepares a final heat balance of the optimized cycle to determine the turbine and station heat rates and the net power output. This also serves to check the assumption upon which the changes were made.

A qualitative indication of the best places in which to initiate changes can be found from a study of Fig. 4. As examples, the choice of the final feedwater temperature and the locations of the heaters can be weighed. As a first approximation, the gain to be realized from an introduction of heat upstream of the economizer is an index of the maximum regeneration justifiable. This is the criterion for the location of the highest pressure extraction.

The approximate and exact equations given in Tables 2 and 3 have been compared in Table 7 for a modern large steam-turbine cycle. It is apparent that great accuracy can be obtained with the approximate equations.

Table 7

Values obtained by:	ΔP, kw	Δr, Btu/kw hr
Heat balance	+2705	−2.6
Approx equation	+2696	−1.9
Exact equation	+2709	−2.2

Conclusions

As it was the purpose of this paper to present in concise form the Edisonvolta method, detailed calculations have been omitted.[4] Superficially, the Edisonvolta approach appears complicated. However, an extremely logical and systematic method has been presented for analyzing the effects of even the small changes in the regenerative steam-turbine cycle. Italian experience has verified by comparison with traditional heat-balance

[4] For a more detailed study see reference [12].

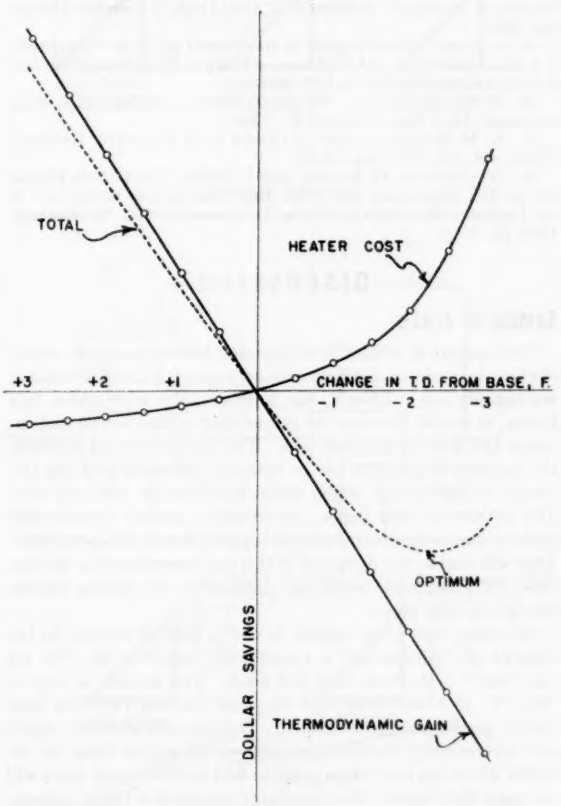

Fig. 5 Optimization of outlet terminal difference for one of the heaters shown in Fig. 2

procedure the usefulness and accuracy of the method, which has been used to optimize, among others, the cycle of the new Edison-volta installation at La Spezia, Italy. The first unit of this is a 320-mw plant, in which the steam conditions are 2400 psig, 1050 F, with reheat at 1000 F, and an absolute back pressure of 1.5 in. Hg. It is to be hoped that the proposed method will be taken up by the design engineers in this country.

Acknowledgments

The authors wish to express their thanks to Dr. Ing. G. Amedei and Mr. G. Fossati for their valuable co-operation. Thanks are also due to Mr. A. Gnesutta and Mr. J. B. Prather.

References

1 J. K. Salisbury, "Steam Turbines and Their Cycles," John Wiley & Sons, New York, N. Y., 1950.

2 J. K. Salisbury, "Analysis of the Steam-Turbine Reheat Cycle," TRANS. ASME, vol. 80, 1958, pp. 1629–1642.

3 H. Bollier, "The Gain Obtainable From Regenerative Feed Heating," *Escher-Wyss News*, vol. 23/24, 1950–1951, pp. 29–39.

4 A. Keller, "The Evaluation of Steam-Power-Plant Losses by Means of the Entropy-Balance Diagram," TRANS. ASME, vol. 72, 1950, pp. 949–953.

5 C. A. Meyer, G. J. Silvestri, and J. A. Martin, "Availability Balance of Steam Power Plants," TRANS. ASME, vol. 81, 1959, pp. 35–42.

6 J. Bartels, "Thermodynamics of Supercritical-Pressure Steam-Power Plants," TRANS. ASME, vol. 77, 1955, pp. 705–714.

7 A. C. Holmes and R. S. Hollitch, "A Steam Properties Program for Medium and Large Computers," ASME Paper No. 57—A-278, 1957.

8 A. Paquet, "La Condensation et le Poste d'Eau d'une Centrale Electrique Moderne," *Bulletin de L'Aim*, Liège, November–December, 1958.

9 J. Ricard, "Amelioration du Rendement du Cycle a Surchauffe et a Resurchauffe par des Soutirages d'Eau aux Rechaffeurs," *Chaleur et Industrie*, vol. 39, 1958, pp. 27–49.

10 E. F. Church, Jr., "Steam Turbines," McGraw-Hill Book Company, Inc., New York, N. Y., 1950.

11 R. M. Stephani, "How to Choose Your Feedwater Heaters," *Power*, vol. 101, 1957, pp. 82–84.

12 G. Chiantore, D. Borgese, and F. Baldo, "Un Metodo Rapido per la Determinazione del Ciclo Rigenerativo piu Economico di un Impianto Termelettrico," *La Termotecnica*, vol. 14, January, 1960, pp. 3–24.

DISCUSSION

Samuel H. Arnow[5]

The method of adding or subtracting bits of energy to reflect changes in basic or auxiliary components of a thermal cycle is not entirely new. Thus if, say, a drain cooler were added to a heater, it would decrease the steam bled to that heater and increase the flow to the next one. The designer would multiply the decrease in quantity by the enthalpy difference and add this energy to the turbine, which would give him the new heat rate. The authors of this paper, nevertheless, deserve considerable commendation for generalizing this approach and citing examples. This will enable the designers of thermal power stations to visualize the effect and assess the desirability of making various changes in basic cycles.

However, this writer wishes to add a note of caution to the concept of "optimizing" a regenerative steam cycle. To get the "best" cycle is all well and good. The trouble is what is "best"? Is it the cycle with the least thermal rate, the least costly, or the least troublesome? One can, for example, figure out theoretically the minimum size of blowdown lines, as the writer did in his early days, only to find out that such pipes will not pass the "muck" that invariably comes with the blowdown, or that the steam fitters failed to properly ream out the lines. Similarly, an optimized solution might indicate an extraction at a certain pressure point in the turbine, but it would be well to investigate the prosaic fact that this best approach might place this extraction opening smack in the center of a blade. Surely there must be some "practical" conferences with the turbine manufacturers who generally are hard-headed businessmen who have some rather old-fashioned ideas that it might cost, say, $200,000 to develop a new blade path to accommodate such an extraction point. One would have to save a goodly number of Btu's to justify that.

Further, it seems to this writer that, in general, a general solution suffers from the fact that it is just that—a "general solution—" and must of necessity include many factors not relevant to specific problems at hand. Any user of such methods must perforce spend much time deciphering the various ramifications before he can eliminate all the factors which do not apply to his case. He might perhaps find it better to just use a "local" solution and obtain an answer which, while somewhat less accurate, is nevertheless adequate.

[5] Consulting Engineer, C. H. Wheeler Manufacturing Company, Philadelphia, Pa. Mem. ASME.

David Aronson[6]

Even in these days of the ready availability of computer facilities there is considerable advantage to the method of small changes proposed by the authors. The man carrying out calculations at his desk is likely to get a feeling for possible cycle improvements or to consider modifications, which is not the case when preparing the program for computer handling. The computer can only follow the program fed into it. An argument can be made for each method of carrying out cycle studies, but the opportunities for creative thinking while running desk calculations should be kept in mind.

John Cruise[7]

Sample Study of Surface Change Effects Upon Cycle Efficiency

Symbols

R = over-all heat transfer rate
W_f = weight of feed, lb/hr = 1.0
w_d = weight of drain, lb/hr = 1.0
c/ρ_m = mean specific heat
S = surface, sq ft
$\log_E \Delta T$ = $\log_E$ mean temperature difference (basic feed − drain)

basic heat balance = $W_f c/p_m \Delta T_f = w_d c/p_m \Delta T_d$
$= RS(\log_E \Delta T)$

[6] Consulting Engineer, Worthington Corporation, Harrison, N. J. Mem. ASME.

[7] Consulting Engineer, Combustion Engineering, Inc., New York, N. Y.

DRAIN THERMAL EFFICIENCY $= \frac{\Delta i - E''}{\Delta i} = 1 - \frac{E''}{\Delta i}$

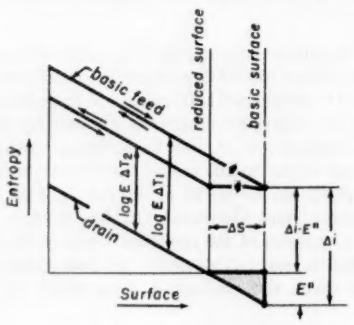

NOTE: Within the limit of change, the transfer rate, pressure drop, and $\log_E \Delta T$ are considered constant. The transfer rate and pressure drop are assumed compensated for in a final heater design by a change in diameter or length or both. The $\log_E \Delta T$ is of small degree.

Heat balance based on the drain system

$$w_d c/p_m \Delta T_{d1} = RS(\log_E \Delta T) = \text{basic cycle}$$

$$w_d c/p_m \Delta T_{d2} = R(S \pm \Delta S) \log_E \Delta T$$

$$\frac{w_d c/p_m \Delta T_{d1}}{w_d c/p_m \Delta T_{d2}} = \frac{RS \log_E \Delta T_1}{R(S \pm \Delta S) \log_E \Delta T_2}$$

$$\frac{c/p_m \Delta T_{d1}}{c/p_m \Delta T_{d2}} \approx \frac{S}{(S \pm \Delta S)} \approx \frac{\Delta H_1}{\Delta H_2}$$

It is thus established that a change in surface is approximately proportional to a change in enthalpy.

Premise Above Plotted Out. Scheme showing relationship of two concepts to achieve basic cycle conditions—(1) change in surface, (2) change in bleed flow.

Δi_a = enthalpy difference in the heater between entering steam and leaving drains

Q = main variation, Btu/hr

Wv_a = extraction steam flow, lb/hr

δ = decrease in entering steam enthalpy

f = fraction of feedwater extracted from over-all flow

thermal efficiency heater "A" = $\dfrac{\Delta i_a - \delta}{\Delta i_a} = 1 - \dfrac{\delta}{\Delta i_a}$

$$Q = \frac{-Wv_a \delta}{1 - \dfrac{\delta}{\Delta i_a}}$$

Case G, Table 3

BLEED STEAM DESUPERHEATED BY EXTRACTED FEED IN A SEPARATE DESUPERHEATER

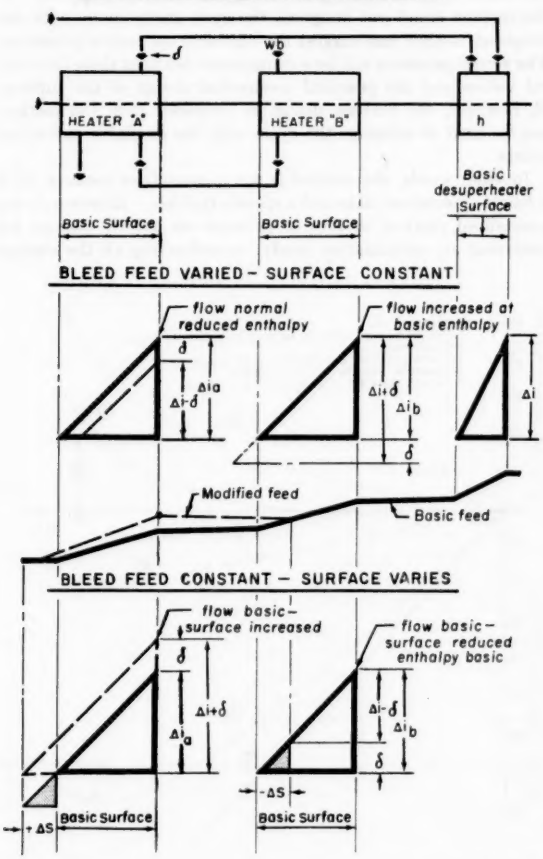

Case H, Table 3

FEEDWATER EXTRACTION FOR DESUPERHEATING BLEED STEAM

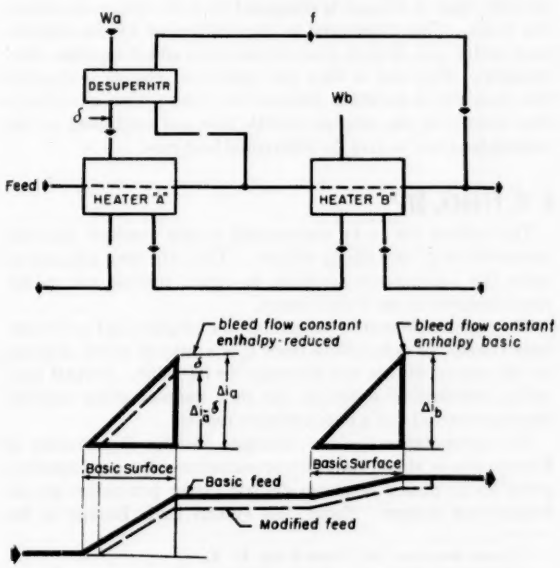

Plot Comparison: Surface Versus Flow Change

1 – SURFACE VARIES

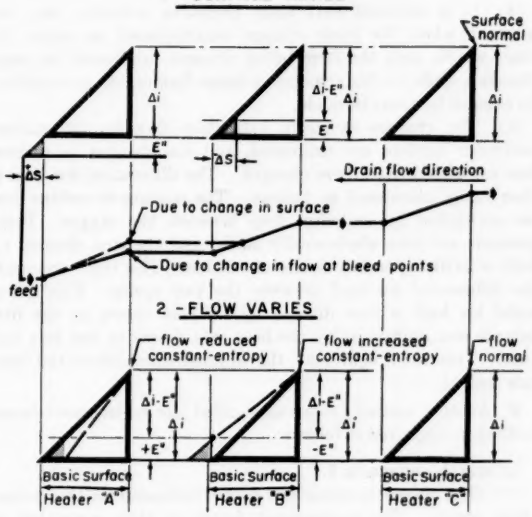

Anthony Fiala, Jr.[8]

This paper was quite interesting. It seems quite complex, but I suspect that after use it will not seem as long or complex.

In our organization, we do not make as many comparative balances as formerly for the following reason. We feel that, based on experience, we can optimize the turbine cycle with very few balances.

However, when we are looking for cycle differences, we use either of the two following methods to approximate the differential heat rate or capability of the turbine.

1 (*a*) It is assumed that one balance has been computed and put on paper.

(*b*) It is assumed that stage pressures, enthalpy, etc., are constant when the cycle change contemplated is made. In other words, only the item being changed is allowed to vary. Once in a while, if a big change in exhaust flow occurs, a correction for exhaust loss may be made.

(*c*) The changes in steam extraction flow to the various feedwater heaters are estimated, and the changes in turbine flow calculated from these changes. The differential kw load is then easily calculated as follows. The changes in turbine flow are multiplied by enthalpy drop between the stages. These products are then algebraically added and the sum divided by 3460 or 3470, depending on size of turbine. This then represents the differential kw load between the two cycles. This differential kw load is then divided by kw load shown on the first balance and multiplied by the heat rate shown on the first balance. This then represents the approximate differential heat rate desired.

2 Another method, sometimes called the replacement factor method, is employed as follows:

(*a*) and (*b*) same as in 1.

(*c*) The change in extraction flow is estimated for the various bleed points. The replacement factor is then computed as follows for each point. This is equal to the enthalpy drop from the stage in question, to the exhaust enthalpy including exhaust loss, divided by the total enthalpy drop through the turbine.

The increase or decrease of the turbine flow in the turbine to the next stage or exhaust is computed from the change in extraction flows. This differential is then multiplied by the replacement factor and all such products are then added together algebraically. This sum is then the equivalent change in throttle flow required to maintain constant kw load. This quantity is then divided by the original throttle flow and multiplied by the existing heat rate to give the differential heat rate.

C. C. Franck, Sr.[9]

The authors are to be commended on the excellent material presented on a very timely subject. They are very gracious to make the information available to steam turbine and power plant designers in the United States.

The paper represents considerable deliberation and a tremendous amount of calculations since it is a subject which depends on the utmost in care and accuracy for its value. Several individual calculations made by our own thermal group indicate that the material is of a highly reliable nature.

This presentation by the Thermal Electric Department of Edisonvolta in Milan, Italy, is representative of the considerations given to all phases of steam electric power generation on the Edisonvolta system. Today this system leads Europe in the efficiency and reliability of its steam electric power generating stations.

The writer has been privileged to participate actively in the growth of the Edisonvolta system during the postwar era. Selection of operating steam conditions and cycle considerations have been based on the same sound reasoning as exemplified by the subject paper. We are appreciative that the work of these fine engineers is shared with those who must give considerations to similar problems.

[8] Ebasco Services, Inc., New York, N. Y.

[9] Consulting Engineer, Steam Division, Westinghouse Electric Corporation, Lester Plant, Philadelphia, Pa. Fellow ASME.

Authors' Closure

Mr. Aronson's discussion points out a characteristic of the proposed method that, in the light of our experience, is very important. This is the realization that the person using the method has an over-all picture of the cycle and of the effects of the changes as they are made. In this connection, curves such as those in Fig. 2 and Fig. 4 are useful in estimating the sign and magnitude of a possible change. It is because the operator can see the effects of changes as they occur, and can think about the problem while the calculation is in progress, that gives this method some advantages over complete computer analysis.

Mr. Arnow expresses concern over the possibility of putting the theoretical results of the study in practice. In particular, he fears that said results call for such impossible, or at least impractical, things as modification of the turbine blade design. We wish to point out that the proposed method has different applications and therefore gives different results according to the phase of the over-all plant design in which it is applied. If the turbine is not yet designed, the cycle study made with the proposed method can suggest the optimum extraction pressures: The actual pressures will be a compromise between these theoretical values and the practical mechanical design of the turbine. If, however, the turbine design is complete, then the method can be used to optimize the cycle with the available extraction points.

In other words, the method is not a *generalized* method, as it is based upon actual data and a specific turbine. However, it is a generalized method in that it presents an orderly routine for preparing an optimization study, co-ordinating all the various

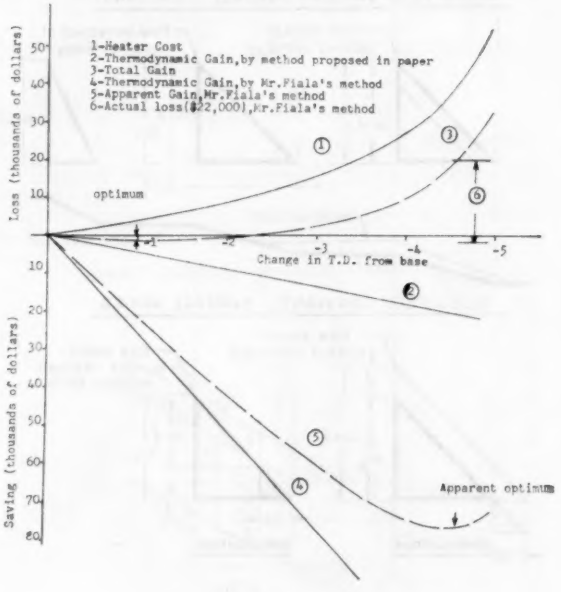

Fig. 6

calculations—essentially similar in nature—in order to shorten the study without sacrificing the precision and reliability of the results.

Referring to Mr. Fiala's discussion, we are concerned with the possibility of making wrong choices which over-simplified methods may encourage. In the complex cycles of modern units so many variations are possible that the over-all economic loss due to an accumulation of single small inaccurate choices can be considered.

To give an idea of the order of magnitude involved, the outlet terminal differences of the heaters in the cycle of Fig. 2 were optimized using Mr. Fiala's method and also our own. For some heaters the results are only slightly different, while for others the difference is greater. As an example, the optimization of No. 6 heater is shown on Fig. 6. In this case the simplified method involves an increase in the heater surface, and therefore an additional cost, not actually justified. The over-all loss due to this single inaccurate choice is about $22,000, indicating the value of the more thorough study.

We wish to confirm Mr. Fiala's feeling that the method, although apparently complicated, actually is fairly simple in nature and not difficult to apply.

Lastly for us, who developed the method, as well as for all the people of Edisonvolta Thermo Electric Department, Mr. Franck's discussion is cause for deep satisfaction, especially since the support and appraisal comes from such an eminent authority in the field.

A Study of Sulfur Reactions in Furnace Deposits[1]

M. WEINTRAUB[2]
S. GOLDBERG[3]
A. A. ORNING[4]

A study was made of absorption of sulfur from synthetic flue gas by coal ash. When fly ash was placed in a temperature gradient like that in a deposit on a boiler tube, maximum absorption was found in the coldest layer. When held at constant temperature, maximum absorption was found at 1100 F. The amount of absorption was highest for fly ash from furnaces in which serious deposit formation was observed. It was also highest for fly ash containing the highest content of sodium and potassium. The sulfur is probably absorbed as mixtures of normal sulfates, pyrosulfates, and such compounds as potassium-ferric trisulfate. A liquid phase of these compounds in contact with tube metal causes corrosion. The maximum sulfur absorption found at 1100 F coincides with a maximum at the same temperature that has been observed for external tube-metal corrosion.

Introduction

EXTERNAL corrosion of certain heat-transfer surfaces in high-pressure, coal-fired boilers is associated with adherent deposits that are rich in alkali metals and sulfur. These elements generally are combined as normal sulfates, pyrosulfates [1–3][5] or more complex compounds, such as potassium ferric trisulfate [2.]

These deposits may contain various amounts of coal ash, and they may be overlaid with ash and slag. They may be found on tube surfaces in areas of flame impingement, principally furnace-wall tubes, or on superheater and reheater tubes. Compounds in these deposits are responsible for bonding ash to tube-metal surfaces [4]. The evidence to date also indicates that corrosion of the metal of such surfaces is significant whenever conditions are favorable for the compounds in the deposit to become liquid. When a liquid phase is present, metal in contact with the liquid will be attacked.

The sulfates found in the deposits do not occur as such in the coal. They must be the result of chemical reactions during combustion, or of reactions between immediate products of combustion and compounds previously deposited on the metal surfaces.

An example of the latter might be as follows: Alkali-metal oxides are deposited on the metal and then react with sulfur compounds in the products of combustion to form normal sulfates or pyrosulfates. Reactions with the metal and with oxides of aluminum and iron in the ash then produce such compounds as potassium ferric trisulfate. Whenever conditions are such that a liquid phase appears, the reactions speed up, and severe corrosion may result.

Another example of reactions that might explain the presence of a layer of sulfur-rich compounds between the tube metal and a covering layer of coal ash might be as follows: The primary deposit on the tubes is coal ash which may contain up to 6 or 7 per cent of sodium and potassium (calculated to the corresponding oxides). As the layer of ash thickens, temperatures and temperature gradients within the layer become favorable for the alkali metals to diffuse through the deposit. Sulfur oxides in the products of combustion also diffuse through the ash. The end result is that the deposit becomes progressively richer in alkali-metal sulfates at the metal-deposit interface.

The purpose of the present investigation by the Bureau of Mines was to study the reactions between samples of fly ash and compounds of sulfur in flue gas. The absorption of sulfur by fly ash when exposed to synthetic flue gas was observed both when the fly ash was placed in a temperature gradient and when placed in a constant-temperature zone. The temperature gradients used were like those found in ash layers on boiler tubes. The observations, at constant temperatures with the same ash, gave comparative data so that the effect of the temperature gradient could be determined. Oxides of sulfur were supplied in the gas stream. Other components were limited to those in the fly ash. Results obtained under these conditions indicated what further work should be done.

Apparatus

The study of reactions with fly ash in a high-temperature gradient required special apparatus. Requirements were that a layer of fly ash should rest on a steel surface with a controlled metal-surface temperature about 700 F. The top of the fly-ash layer was to be exposed to a source of heat with a radiant intensity comparable to that found near a boiler-furnace outlet. These conditions were obtained with the apparatus shown in Fig. 1. The fly ash was held on top of a rectangular air-cooled duct of cold-rolled steel. This assembly was placed along the axis of a tubular heating element of silicon carbide. Side plates, formed of thin sheets of steel, completed a sample tray on top of the duct. No refractory tube was used to confine the gas stream. Such a tube, between the sample and the heating element, would have introduced an intermediate radiant-heat-transfer surface. This would have required an excessive heating-element temperature to obtain the desired intensity of radiation on the sample. Since the silicon-carbide tube was somewhat porous, it was necessary to seal the entire furnace case. Water-

---

[1] Work on manuscript completed June, 1960.

[2] Chemical Engineer, Combustion Section, Branch of Bituminous Coal, Division of Solid Fuels Technology, Bureau of Mines, U. S. Department of the Interior, Pittsburgh, Pa.

[3] Chemist, Combustion Section, Bureau of Mines, U. S. Department of the Interior, Pittsburgh, Pa.

[4] Chief, Combustion Section, Bureau of Mines, U. S. Department of the Interior, Pittsburgh, Pa. Mem. ASME.

[5] Numbers in brackets designate References at end of paper.

Contributed by the ASME Research Committee on Corrosion and Deposits From Combustion Gases and presented at the Winter Annual Meeting, New York, N. Y., November 27–December 2, 1960, of THE AMERICAN SOCIETY OF MECHANICAL ENGINEERS. Manuscript received at ASME Headquarters, August 8, 1960. Paper No. 60—WA-183.

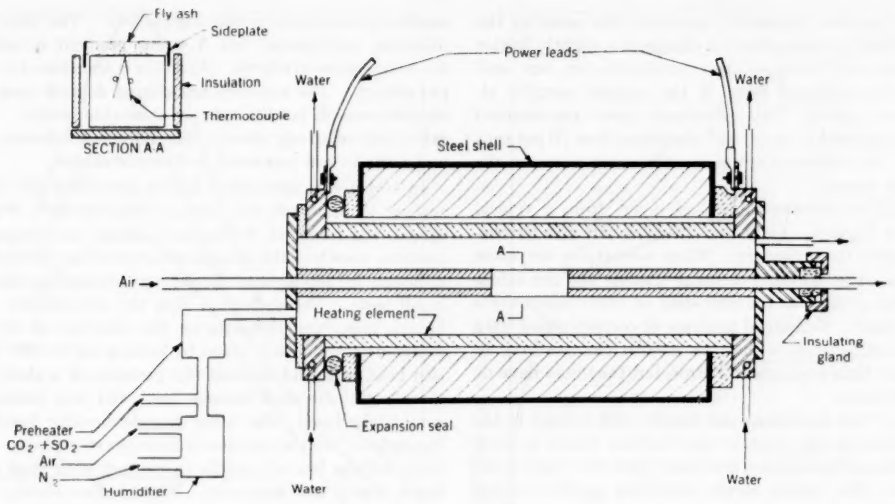

Fig. 1 Apparatus for maintaining an ash sample in a high-temperature gradient and a synthetic atmosphere

cooled holders served as electrical contactors for the heating element and as fittings for introducing the furnace atmosphere.

The furnace temperature was determined with a platinum-platinum, 10 per cent rhodium thermocouple placed near the silicon-carbide wall and shielded from the cooled surface. A controller held this temperature within 5 deg F of the desired value. Temperatures were measured at three points on the surface supporting the fly-ash sample by chromel-alumel thermocouples silver-soldered into holes drilled in the surface of the steel duct. These thermocouples were threaded through the cooling air-supply line.

Procedures

Two types of tests were made. In the first, the equipment described was used to subject the ash to a high-temperature gradient. In the second, measurements were made of changes that occurred in the fly ash when it was maintained under a synthetic atmosphere at uniform temperatures in a porcelain boat which was placed within a heated quartz tube.

For a gradient test, a weighed quantity of ash was placed on the sample tray in a layer about $^1/_4$ in. thick. A synthetic flue-gas atmosphere was provided by metered flows of nitrogen, air, and a mixture of carbon dioxide and sulfur dioxide from a pressure cylinder. The purpose of premixing the CO_2 and SO_2 was to limit the SO_2 concentration in case of failure of either the air or nitrogen supply. Moisture was added to the atmosphere by bubbling the air and nitrogen through a thermostated flask of distilled water. The humidity was checked by measurement of the water evaporated over a given length of time. A typical synthetic flue-gas analysis was oxygen 2.2 per cent, nitrogen 74.6, carbon dioxide 14.9, sulfur dioxide 0.4, and water vapor 7.9 per cent. When the per cent sulfur dioxide was varied, other components were maintained in the foregoing proportions. The total flow was held at 0.143 cfm, equivalent to 0.115 fps over the sample.

When the flue-gas atmosphere was established, the furnace temperature was raised, for the gradient tests, at a rate of about 600 deg F per hr up to 2000 F. Air flow through the sample holder was adjusted to keep the surface under the sample below 700 F. When the furnace temperature reached 2000 F, the control was set to maintain this temperature, and the cooling air was adjusted to keep the hotter end of the sample-holder surface at 750 F, while the cooler end was at approximately 600 F.

After conditions were maintained for the desired period, the furnace was cooled while flow of the test atmosphere was continued. The sample holder was removed from the furnace, and the auxiliary side plates were removed to expose a vertical section of the sample. The sample was then divided into portions according to visible differences in each of three layers. Any material that was misplaced in handling and thus not ascribed to one of the three layers was collected as "undifferentiated residue" so that complete mass balances could be obtained. The four portions were weighed and subjected to chemical analyses.

For the tests in the uniform-temperature apparatus, a flow of 0.0035 cfm of the desired atmosphere was established. This corresponded to a linear velocity over the sample of 0.110 fps at 1100 F. The furnace temperature was set. A weighed quantity of fly ash was then placed in a porcelain boat, and the boat was inserted into the cold end of the furnace tube. After 15 min, to permit the sample to be permeated by the test atmosphere, the boat was pushed into the hot zone of the furnace. At the end of 24 hr the boat was drawn into a glass T where it was cooled while the furnace atmosphere flowed over it. The ends of the T were then stoppered, and the T and boat were transported to the balance room where the boat and its contents were weighed with minimum exposure to the atmosphere. The sample was returned to the furnace for an additional period, again cooled and reweighed. This process was repeated until the change in weight per hour was less than 1 per cent of the total weight change to that point.

Experimental Results

The fly ash, M-1, used in the temperature-gradient studies, was obtained from the electrostatic precipitator of a pulverized-coal-fired, slag-tap furnace which had given considerable difficulty with ash deposits. The coal used, an Illinois No. 6 seam coal, had 18.7 per cent ash and 5.6 per cent sulfur. The ash was 98 per cent through 200 mesh and had the analysis given in Table 1. After exposure to thermal radiation at 2000 F for periods in the order of 50 hr or more, the samples invariably showed three distinct layers differing in color, hardness, and state of agglomeration. The bottom layer, which had been in contact

with the cooled surface, physically appeared the same as the original fly ash with the exception of a change to a slightly lighter color. The intermediate layer was reddish-brown but still retained the unconsolidated form of the original sample, although somewhat caked. The uppermost layer was sintered and hard, was violet-red in color, and comprised over 70 per cent of the sample. No visible differences were noted between the two ends of the sample.

Chemical analyses for the individual layers from a typical test are given in Table 2. Only the sulfur-trioxide and ferrous-iron contents show large changes. When corrections are made for dilution, caused by addition of sulfur trioxide and the oxidation of iron, the changes in concentration of other components are extremely small. Statistical analyses of corresponding data from the series of tests show that the smaller changes may be real; i.e., greater than experimental error, but they may have no practical significance.

A summary of test conditions and results with respect to the sulfur distribution in top, middle, and bottom layers is given in Table 3. The sulfur balances are based upon the weights and concentrations of the various layers, including undifferentiated residue, as compared to the original ash. The data lead to the following conclusions: (*a*) A sulfur gradient is established by the temperature gradient. (*b*) Sulfur is transferred to or from the gas stream. The amounts transferred depend upon the sulfur-dioxide content, but the data are somewhat erratic. (*c*) Changes take place relatively slowly; the difference between a 56-hr test and a 163-hr test was small, but unmistakable.

Table 1 Ash analyses

	B-1	B-2	C-1	M-1
Ignition loss	0.5	7.5	2.4	2.8
Silicon, as SiO_2	41.9	49.6	49.6	38.6
Aluminum, as Al_2O_3	26.3	20.1	25.4	15.7
Ferric iron, as Fe_2O_3	13.0	9.7	10.9	19.6
Ferrous iron, as FeO	3.4	3.7	7.9	2.0
Titanium, as TiO_2	1.2	1.0	1.1	0.9
Phosphorus, as P_2O_5	0.8	0.3	0.4	0.3
Calcium, as CaO	2.1	3.2	1.7	5.7
Magnesium, as MgO	1.2	1.0	0.9	0.9
Sodium, as Na_2O	0.3	0.3	0.4	3.1
Potassium, as K_2O	2.8	2.6	1.9	2.7
Sulfur, as SO_3	0.5	0.6	0.3	8.0
Chlorine, as Cl_2	0.02	0.01	0.02	0.06

Table 2 Analytical results of typical temperature-gradient test

Material	Fly ash M-1
Test no.	1-7
Furnace temperature, deg F	2000
Plate temperature, deg F	700
Time at maximum temperature, hr	56
SO_2 in atmosphere, per cent by volume	1.0

	Composition, per cent				
Component	Original ash	Top layer	Middle layer	Bottom layer	Undifferentiated residue
Ferric oxide	19.6	22.3	19.9	17.7	18.2
Ferrous oxide	2.0	0.1	0.4	1.0	0.6
Calcium oxide	5.7	5.5	5.5	4.6	4.8
Sodium oxide	3.1	3.2	3.1	2.7	2.8
Potassium oxide	2.7	2.7	2.9	2.7	2.7
Sulfur trioxide	8.0	6.5	13.5	19.7	18.2

Table 3 Tests run in gradient furnace with fly ash M-1

Test no.	Hr at max temp	Pct SO_2 in atm.	Pct S in bottom layer of ash	Pct S in middle layer of ash	Pct S in top layer of ash	Pct sulfur balance
1-1	164	0.00	5.2	3.6	0.9	[a]
1-2	3	0.3	6.2	4.5	2.2	88.5
1-4	19	0.3	Mechanical failure[b]			
1-5	44.5	0.3	8.3	7.4	2.1	135.2
1-6	42.3	0.0	5.1	3.4	1.6	56.1
1-7	56	1.0	7.9	5.4	2.6	100.0
1-9	163	1.1	9.8	6.5	2.3	100.0

[a] Weights of layers not determined.

[b] Failure of plate cooling air permitted plate to reach furnace temperature with interesting results discussed in text.

In test 1-4 a mechanical failure permitted the sample plate surface to approach the furnace temperature. When the ash sample was removed, it was fused, black, and magnetic. In no previous tests had this change occurred in any portion of the ash, although the top layer of the ash was presumably close to 2000 F in all tests. The deduction that the temperature of the steel has an important influence on the direction of the fly ash-atmosphere reaction was tested by heating ash to 2000 F in a porcelain boat with and without the presence of a steel plate. The sample without steel became brick red and sintered, but not completely fused; the other sample became fused and black throughout, even where remote from the steel plate. A sample of ferric sulfate heated rapidly in contact with steel also became fused, black, and magnetic. When heated slowly, it remained red, apparently because it was decomposed to the oxide before it could react with the steel. It therefore appears that in a furnace both the time and temperature of contact between ash and steel may have important effects on subsequent or simultaneous reactions between the ash and the flue gas.

The establishment of a sulfur-concentration gradient coincident with a temperature gradient suggested that, under some conditions, equilibrium relations existed among sulfur content of the fly ash, temperature, and gas composition. Constant-temperature tests were made to determine these relations in the temperature range from 800 to 1800 F. Analyses of the samples of fly ash used are given in Table 1. Data for tests with fly ash M-1 are shown in Fig. 2. The gas supplied consisted of SO_2 and O_2 in the concentrations indicated, 15.0 per cent carbon dioxide, and nitrogen. Data are also shown for fly ash M-1 after exposure to air, instead of flue gas, at various temperatures. The data show that the sulfur content of the ash reached a maximum when the temperature was 1100 F in an atmosphere of flue gas. They also show that the sulfur content of the ash increased with the sulfur dioxide and with the oxygen content of the inlet gas stream. The dependence upon the sulfur-dioxide content appears more clearly when data of Fig. 2, excepting those at 10 per cent O_2, are replotted as shown in Fig. 3. The sulfur content of the fly ash increased rapidly as the sulfur-dioxide content was raised to 0.4 per cent and became nearly constant when the sulfur dioxide exceeded 2.5 per cent. The data at 10 per cent oxygen in the flue gas show similar variation but are not sufficient for sound conclusions.

Oxygen reacted with sulfur dioxide to produce sulfur trioxide. The fly ash catalyzed this reaction. Sulfur-trioxide fumes and condensation of sulfuric acid were observed at the exit of the tube. These products were not detected when the gas was passed through the tube and over the sample boat in the absence of fly ash. The equilibrium content of sulfur trioxide depends upon the gas composition and decreases with increasing temperature. Fig. 4 shows the sulfur content of the fly ash plotted against the calculated equilibrium content of sulfur trioxide in the gas stream. Data are not shown in the range below 1100 F. The approximation to a single curve for sulfur in the ash versus the equilibrium content of sulfur trioxide in the gas stream, without regard to the temperature or the oxygen content of the gas, indicated that the sulfur content of the ash reached an equilibrium with the sulfur-trioxide content of the gas when the temperature was above 1100 F. The sulfur trioxide in turn had reached equilibrium with respect to the temperature and the oxygen and sulfur-dioxide content of the gas.

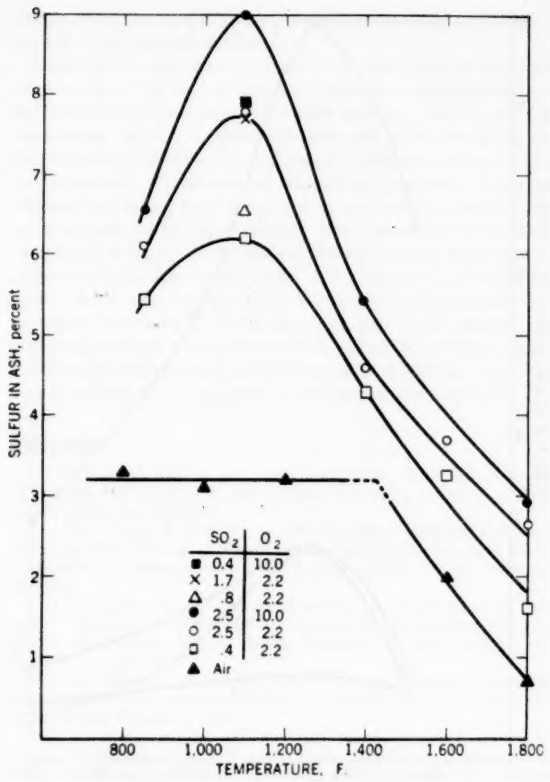

Fig. 2 Sulfur in M-1 ash after exposure to synthetic flue gas at various temperatures. Original sulfur content was 3.2 per cent (8.0 per cent as SO_3). The synthetic flue gas contained the indicated percentages of SO_2 and O_2, 15 per cent CO_2, and the remainder N_2.

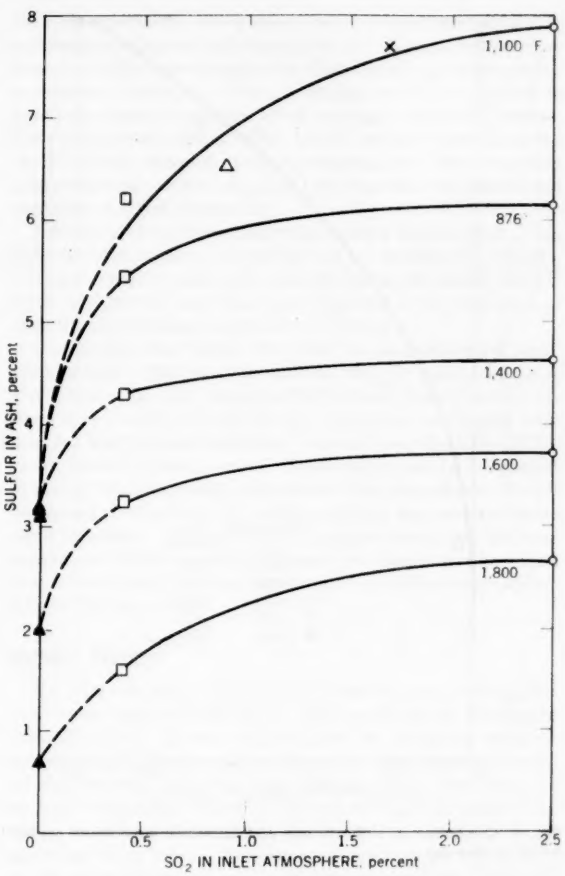

Fig. 3 Effect of sulfur-dioxide concentration on sulfur in ash. Gas contained indicated amount of SO_2, 2.2 per cent O_2, 15 per cent CO_2, and remainder N_2, except gas was air when per cent SO_2 was zero.

The existence of an equilibrium in the range from 1100 to 1800 F was shown further by special tests. A sample of ash was heated in a synthetic flue-gas atmosphere at 1100 F until maximum absorption of sulfur was obtained. The sample was then pulverized and reheated under the same conditions, except that the temperature was 1400 F. The sample lost sulfur. Another sample was heated to constant weight at 1800 F, was pulverized, and was reheated at 1400 F. The sample gained sulfur.

A similar test for reversibility was made for the range below 1100 F. A sample that had been heated at 1100 F was repulverized and reheated at 860 F. The sulfur content increased slightly instead of decreasing. A reasonable explanation is that the concentration of sulfur trioxide in the system below 1100 F is limited by the rate of oxidation of sulfur dioxide.

Tests were made with other samples of fly ash to seek a relation between sulfur absorption, ash composition, and deposit-forming tendency. The ash analyses are given in Table 1, and absorption data are shown in Fig. 5. The fly-ash samples were from pulverized-coal-fired boiler furnaces. M-1 was from a slag-tap furnace firing southern Illinois coal. There were pronounced fireside deposit difficulties. C-1 was from a slag-tap furnace with no problems of deposit formation above the slagging zone. The West Virginia coal had a content of 11 per cent ash and 2.5 per cent sulfur. The furnaces, from which samples B-1 and B-2 were obtained, had moderate deposit formation. There was frequent need to use soot blowers, although no outages for cleaning were required between yearly overhaul periods. The coal burned in the furnace producing B-1 was from eastern Kentucky and contained 13.2 per cent ash and 3.1 per cent sulfur. The furnace which yielded B-2 burned coal from western Kentucky that had 9.3 per cent ash and 2.6 per cent sulfur. The inlet-gas composition for these tests was 2.5 per cent sulfur dioxide, 10 per cent oxygen, 15 per cent carbon dioxide, and the remainder nitrogen. Each of the samples showed a maximum sulfur absorption at 1100 F. The absorption, at the maximum, was widely different for the different samples. The amount of sulfur absorption for the different fly-ash samples increased with the amount of trouble with deposits that was observed for the different furnaces. A comparison with analyses in Table 1 also showed that the maximum absorption of sulfur increased with the total content of sodium and potassium oxides.

Discussion of Results

The experimental data on sulfur absorption by fly ash at first seemed contradictory. The constant-temperature tests showed low absorption at temperatures below 1100 F. The gradient tests showed maximum absorption in the bottom layer where the temperature was certainly below 1100 F since this layer was thin, was protected by the overlying ash, and rested directly on the metal surface at 700 F. The contradiction no longer appeared when it was assumed that the oxidation of sulfur dioxide to trioxide was catalyzed by the fly ash. The catalysis was observed in the constant-temperature tests. A decreasing rate of the catalytic reaction was assumed to explain the low absorption

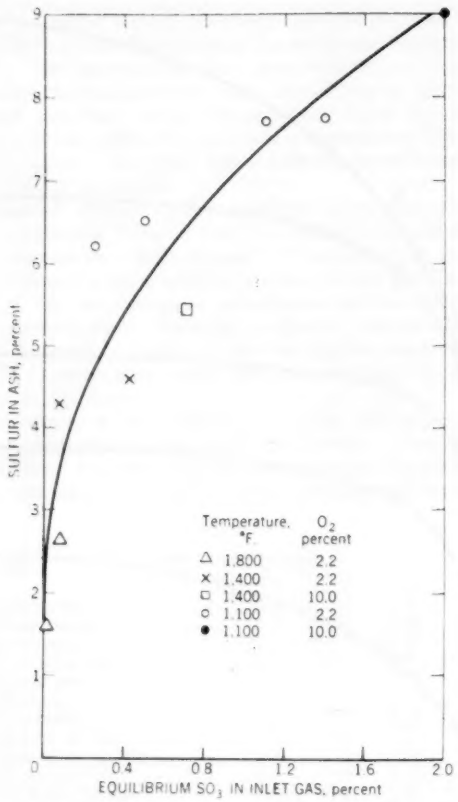

Fig. 4 Correlation of sulfur in ash and calculated equilibrium content of SO_3 in flue gas

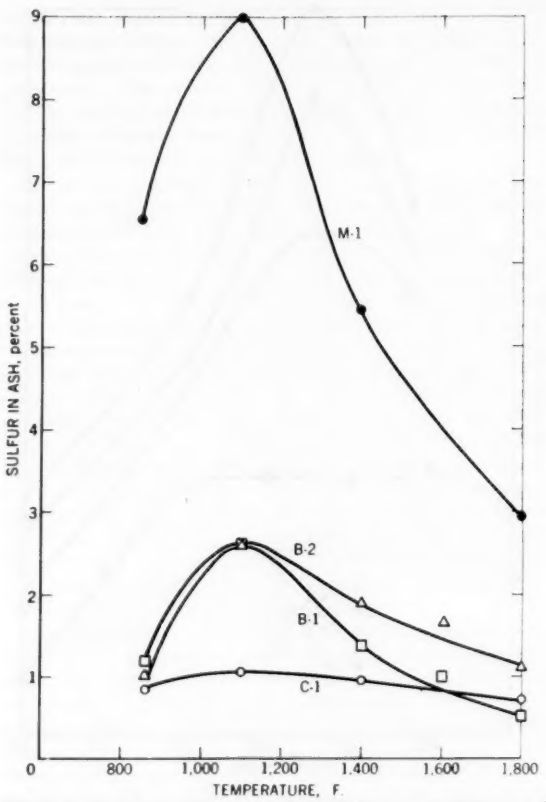

Fig. 5 Sulfur in ash after exposure to synthetic flue gas at various temperatures. Synthetic flue gas contained 2.5 per cent SO_2, 10 per cent O_2, 15 per cent CO_2, and remainder N.

of sulfur at temperatures below 1100 F. Decreasing equilibrium content of sulfur trioxide in the gas explained low absorption at temperatures above 1100 F. Since the layer of fly ash in the gradient tests was exposed to radiation at 2000 F and rested on a surface at about 700 F, temperatures about 1100 F must have existed at some level in the layer. The catalytic oxidation of the sulfur dioxide became "frozen" near its highest level as the gas permeated through the fly ash to the cooler bottom layer. The concentration of sulfur dioxide reached the highest levels attained in the constant-temperature tests. Accordingly, a comparison of the data in Fig. 5 and Table 3 showed that the maximum absorption was the same in both the gradient and constant-temperature tests.

The maximum absorption at 1100 F coincided with a maximum that has been observed for corrosion of superheater and reheater tubes [5]. Maximum corrosion involves additional conditions, namely, contact with the metal and solution of the corrosion product. These conditions are provided by a fused salt layer in contact with the metal. Ferric oxide reacts with sodium and potassium sulfates, in the presence of sulfur trioxide, to form sodium and potassium ferric trisulfates [2]. The reaction products melt at about 1100 F and decompose to solid products at higher temperatures. The result is a maximum in corrosion rates at the same temperature level as that found for the absorption of sulfur by the ash. Other maxima should be expected. Pyrosulfates are stable and become liquid at lower temperatures. The normal sulfates of sodium and potassium become liquid at higher temperatures. In each instance the compounds producing a liquid phase become unstable with a further rise in temperature. The liquid phase disappears at the intermediate temperature levels. Corrosion can be minimized by design so that metal surfaces are at the intermediate temperatures rather than at those temperatures where a liquid phase can exist in contact with the metal.

The absorption of sulfur is only part of the transport of material involved in the concentration of bonding agents and of layers of corrosive material. The pattern of absorption of sulfur is reasonably explained by permeation of sulfur dioxide into the ash deposit and catalytic oxidation to sulfur trioxide by the ash. Iron and aluminum are available as oxides in the ash or as corrosion products. Sodium and potassium are present in the ash but at too low a concentration. They must either migrate from overlying layers of ash or they must be transported in some volatile form from the combustion zone. The gradient tests showed large differences in concentration of sulfur in the different layers. Differences in concentration of sodium and potassium were of no significance as compared with concentrations of these elements observed in layers of corrosive material. The bottom layer in the gradient tests was much like the original ash while the layer of material at the interface over corroded areas was generally quite unlike either the overlying ash deposit or the fly ash in the gas stream. These facts indicate that sodium and potassium are released from the coal ash and carried in the combustion products in a volatile form, possibly as oxides or hydroxides. These compounds may diffuse through the ash layer and react with sulfur trioxide at the site of deposit. Therefore, hindering the oxidation of sulfur dioxide to sulfur trioxide in the gas

stream would not be effective unless the catalytic oxidation in the ash layer was also hindered.

Additional work is needed to determine the form in which the alkali metals, lithium, sodium, and potassium, are released from the fuel and are transported in the gas stream. Basic and acidic compounds, such as sodium hydroxide and sulfur dioxide probably may coexist as separate compounds in the gas stream at high temperatures. Alleviation of difficulties observed with ash deposits by burning part of the coal in suspension over traveling-grate stokers might have resulted from reactions of the basic compounds with fly ash in the gas streams so that they were no longer available for reaction with sulfur trioxide in the ash deposit. Such observations show the need for fundamental information on reactions between acidic and basic materials at high temperatures where liquid water cannot be present. Additional work is also needed to show how deposit-forming tendencies may be related to ash analyses and to operating conditions.

References

1 W. T. Reid, R. C. Corey, and B. J. Cross, "External Corrosion of Furnace Wall Tubes—I History and Occurrence," TRANS. ASME, vol. 67, 1945, pp. 279–288.

2 R. C. Corey, B. J. Cross, and W. T. Reid, "External Corrosion of Furnace Wall Tubes—II Significance of Sulfate Deposits and Sulfur Trioxide in Corrosion Mechanism," TRANS. ASME, vol. 67, 1945, pp. 289–302.

3 R. C. Corey, H. A. Grabowski, and B. J. Cross, "External Corrosion of Furnace Wall Tubes—III Further Data on Sulfate Deposits and the Significance of Iron Sulfide Deposits," TRANS. ASME, vol. 71, 1949, pp. 951–963.

4 C. H. Anderson and E. K. Diehl, "Bonded Fireside Deposits in Coal-Fired Boilers—A Progress Report on the Manner of Formation," ASME Paper No. 55—A-200.

5 J. G. Koopman, E. M. Marselli, James Jonakin, and R. C. Ulmer, "Development and Use of a Probe for Studying Corrosion in Superheaters and Reheaters," *Proceedings, American Power Conference*, vol. 21, 1959, pp. 236–245. Wharton Nelson and Carl Cain, Jr., "Corrosion of Superheaters and Reheaters of Pulverized-Coal-Fired Boilers," TRANS. ASME, Series A, JOURNAL OF ENGINEERING FOR POWER, vol. 82, 1960, pp. 194–204.

DISCUSSION

Wharton Nelson[6]

The authors have indicated that statistical analysis of the data from Table 2 shows that changes in ash composition other than ferric oxide and sulfur trioxide may be real, but they attach no practical significance to such differences. I believe that these analyses indicate the migration of molten complex potassium iron and/or aluminum sulfates toward the cooler metal surface. A complete material balance cannot be made from the data presented since only part of the components are listed in this table. However, due to the increase of sulfur trioxide content of the bottom layer every component tabulated has decreased in percentage from that of the original ash with the exception of sulfur trioxide and potassium oxide. The average per cent decrease for ferric oxide (allowing for that contributed by oxidation of ferrous oxide), calcium oxide, and sodium oxide is 15.2 per cent. A corresponding decrease in potassium oxide (assuming no migration) would give a value of 2.3 per cent rather than the 2.7 per cent obtained. Although this difference is small, perhaps because of the relatively short exposure compared to boiler service, it nevertheless indicates that the potassium has been concentrated at the cooler surface by a migration process.

Both metal-side temperature and ash temperature gradient would influence the rate of migration of alkali-containing compounds through the ash deposit, since a molten state is requisite for such movement. For instance, adjustment of the gradient to a value extending upward from about 1025 F metal temperature would make the experiment more characteristic of modern boiler superheater conditions. Such a change would be expected to speed movement of complex alkali sulfates to the metal surface. These compounds melt at about 1025 F and have been identified in SH-RH ash deposits. Our experimental data show that they migrate through an ash deposit and are responsible for accelerated corrosion of metal underneath.

Additional absorption experiments using a thicker layer of ash (one rich in potassium since sodium has less tendency to migrate), a longer exposure time, and metal temperatures nearer SH-RH level may produce more conclusive evidence of the migration of complex alkali sulfates indicated by Table 2.

Our experiments did not show that the temperature for maximum corrosion rate was the same as that for maximum sulfur absorption. Fig. 1 of the paper by Cain and Nelson[7] showed instead that as sulfur trioxide pickup (which can be equated with complex alkali sulfate formation) decreased over the 1050–1275 F range, corrosion rate increased. These results may be interpreted in the light that increasing temperature level overrode the effect of decreasing concentration of complex sulfates and produced more rapid corrosion. Fig. 4 of this same paper shows that the temperature at which maximum corrosion rate occurs can be varied over a wide range by changing the ratio of sodium-to-potassium salts in the ash mixture.

Authors' Closure

The statistical analyses, to which Nelson referred, were applied to an entire series of tests rather than merely to the illustrative data of Table 2. It was concluded that the changes in composition with depth, excepting iron and sulfur, "may" have no practical significance. This was an expression of the fact that the amount of migration observed was not sufficient to account for the layers of corrosive material that have been found under ash layers on boiler tubes. Broader considerations were presented in the introduction and in the discussion of results. Without denying the appearance of migration in the ash deposit, it was concluded that sodium and potassium may be transported as volatile compounds from the combustion zone. If these alkali metals are carried only by particulate matter, the supply available for migration is limited to that in the fly-ash particles deposited. If they are carried from the flame as volatile compounds, diffusion through the ash layer can provide a continuous source that can lead to further deposit of corrosive and bonding materials wherever concentrations and temperatures are favorable for such deposit formation.

The representation of a molten state as requisite for migration of alkali-containing compounds through the ash layer is an oversimplification. Mixed alkali iron trisulfates become liquid within the range of SH-RH temperatures. Corresponding mixtures of pyrosulfates become liquid at boiler-tube temperatures. In either instance, the range from fusion to thermal decomposition temperatures is limited. Thermal decomposition, diffusion of volatile decomposition products, recombination, condensation to liquid or solid products, and capillary flow of liquids may all occur provided the heat-transfer rate and the thickness of the ash layer are such that the necessary temperatures are present at various depths within the ash layer.

Experiments with the ash in a temperature gradient were conducted under temperature conditions where the formation of corrosive deposits under ash layers on boiler tubes had been observed. While evidence of migration was found, the typical corrosive deposit at the cold surface was not produced. This was attributed to the limited amount of alkali metals available in the

[6] Combustion Engineering, Inc., Kreisinger Development Laboratory, Chattanooga, Tenn.

[7] Published in this issue, pp. 468-474.

ash. Work at higher temperatures would provide greater mobility but would not increase the amount of alkali metals available for migration. It was felt that the more fruitful direction of attack would be to seek information on the form in which these metals are released from the flame and transported in the gas stream to the deposit site.

The purpose of the statement that maximum absorption of sulfur corresponded with a maximum that had been observed for corrosion, was to introduce the concept that corrosion is the result of several conditions that appear together. The statement was correct. Other corrosion maxima at somewhat different temperatures, reported in one of the papers to which reference was made, and in another now available,[7] show as Nelson stated that the exact location of the maximum depends upon the composition of the deposit.

The important fact is that maxima exist and that there are overlapping ranges about the maximum in which elevated sulfur absorption and corrosion occur.

The Role of Chemical Thermodynamics in Analyzing Gas-Side Problems in Boilers

R. H. BOLL
Research Engineer,
The Babcock & Wilcox Company,
Research Center, Alliance, Ohio

H. C. PATEL[1]
Analytical Engineer,
The Babcock & Wilcox Company,
Research Center, Alliance, Ohio

Part 1 deals with equilibrium concentrations of twenty-nine gaseous and five condensed constituents which were calculated for the combustion gases from two coals. Temperatures ranged from 440 to 3140 F and fuel-air ratios from 90 to 130 per cent of theoretical air. Results are presented in graphical and tabular form paying particular attention to sodium, sulfur, and chlorine compounds. A few of the many possible inferences relevant to fouling, corrosion, and air pollution are pointed out. Starting from the equilibrium-gas-composition results of Part 1, the regions of thermodynamic stability of various sodium and iron compounds are obtained in Part 2 as functions of temperature and fuel-air ratio. It is shown that purely thermodynamic considerations impose an upper temperature limit upon corrosion mechanisms involving complex iron sulfates. An explanation is advanced for the severe fouling tendency of high alkali coals.

Part 1—Minor Constituents of Gas

Introduction

GAS-SIDE fouling and corrosion in boilers (and gas turbines) as well as air pollution are problems of increasing importance in the production of electrical power from coal. The composition of combustion gas is basic to the study of these phenomena for it transports various gaseous compounds, and in it may occur various chemical reactions which contribute to each of them.

Gas-composition information may be obtained in two ways—by measurement and by calculation from basic chemical principles. Measurement is generally to be preferred where:

1 Adequate analytical techniques exist.

2 The required information relates mainly to what is occurring, not to what would occur if circumstances were changed.

Almost invariably, however, the first requirement cannot (presently) be met where minor constituents—NaOH, NaCl, HCl, SO_2, SO_3, NO, and so on—are concerned. Moreover, solving a problem implies changing circumstances, so that the second requirement is not met except by costly trial and error. By contrast, chemical thermodynamics provides means for predicting the concentrations of a wide variety of chemical species over a wide range of operating conditions, without first developing and operating several pieces of highly specialized and costly apparatus. The results of such calculations are, of course, limited by the necessary assumption of equilibrium and by the accuracy of basic data; but these limitations are often slight, or at least acceptable (see "Discussion").

Chemical thermodynamics has been used extensively [1, 2][2] for determining concentrations of thermally important species, CO_2, H_2O, CO, OH, H, and so on, because a knowledge of their concentrations is essential for predicting flame temperatures. However, the thermally unimportant minor constituents, NaOH, HCl, SO_2, NO, and so forth, appear not to have received much attention in the past. The objective of the present work is to provide general background for the further study of fouling, corrosion, and air pollution by determining equilibrium concentrations of minor constituents as functions of temperature, fuel-air ratio, and (to some extent) fuel.

Scope and Method of Calculation

Table 1 lists the constituents assumed to be present (or potentially present) in the combustion gas together with the sources of thermodynamic data which were used to obtain values of equilibrium constants. It will be noted that sodium, sulfur, and chlorine compounds have been included. Several solid or liquid-sodium compounds have also been included to provide a guide to the form and condensation temperatures to be expected of alkalis. Potassium compounds were omitted because of paucity of thermodynamic data and because of their probable similarity to sodium compounds. Table 2 shows the conditions of fuel, fuel-air ratio, and temperature for which equilibrium calculations were made. The two coals were selected for their difference with respect to behavior in a boiler. Both are high in sulfur, but the Pana, which is especially high in alkali and chlorine, produces a highly fouling and corrosive deposit [15], whereas the Wright contains less of these elements and is innocuous with respect to superheater fouling. Table 3 compares ultimate analyses of these coals and their contributions to the elemental compositions of the corresponding gases. In determining the elemental composition of the gases, it was assumed in all cases that:

1 Ninety-five per cent of the nonash sulfur appears in the combustion gas, the remainder going into the ash.

2 Forty per cent of the sodium content of the coal appears in the gas.

3 Twenty per cent of the potassium content of the coal appears in the gas.

4 All of the potassium content of the gas may be handled as though it were sodium.

5 Except for Na, K, and S, no ash constituents enter the combustion gas.

The foregoing percentages, or "appearance factors," were estimated from data obtained with an experimental cyclone furnace.

The columns headed "In gas as calculated" of Table 3 together with fuel-air ratio provide the essential information for calculating the complete elemental composition of the combustion gas. With elemental composition in hand, the calculation of equilibrium concentrations of the various constituents requires the setting up and solving of a number of simultaneous algebraic

[1] Present address, Tata Chemicals, Mithapur, Saurashtra, India.

[2] Numbers in brackets designate References at end of paper.

Contributed by the Research Committee on Corrosion and Deposits From Combustion Gases and presented at the Winter Annual Meeting, New York, N. Y., November 27–December 2, 1960, of THE AMERICAN SOCIETY OF MECHANICAL ENGINEERS. Manuscript received at ASME Headquarters, August 8, 1960. Paper No. 60—WA-182.

Table 1 Constituents of equilibrium mixture

Constituent	Phase[a]	References[b] $\Delta H_{f298}°$	$C_p°$ or $H_T°-H_{298}°$	$S_{298}°$	$S_T°-S_{298}°$
A	g	14	7	7	7
C	g	14	7	7	7
CO	g	14	12	14	12
CO_2	g	14	12	14	12
Cl	g	14	7	7	7
Cl_2	g	14	12	14	7
H	g	14	7	7	7
H_2	g	14	12	14	12
HCl	g	14	12	14	12
H_2O	g	14	12	14	12
H_2S	g	14	12	14	12
N	g	14	7	7	7
N_2	g	14	12	14	12
NH_3	g	14	12	14	12
NO	g	14	12	14	12
NO_2	g	14	12	14	12
Na	g	8	8	8	8
NaCl	g	14	12	11	12
NaOH	g	14	6	14	6
Na_2SO_4[c]	g	...	...	...	...
O	g	14	7	7	7
O_2	g	14	12	14	12
OH	g	14	12	14	12
P_4O_{10}	g	14	12	5	12
S	g	14	12	14	12
S_2	g	14	12	11	12
SO_2	g	14	12	14	12
SO_3	g	14	12	14	12
NaCl	s,l	14	12	14	12
Na_2CO_3	s,l	14	13	14	13
Na_2O	s,l	14	12	14	12
NaOH	s,l	14	12	10	12
Na_2SO_4	s,l	9	4	4	4

[a] g = gas, l = liquid, s = solid.

[b] Numbers designate References at end of paper. $\Delta H_{f298}°$ = heat of formation at 298 K (77 F). $C_p°$ = specific heat. $H_T°-H_{298}°$ = enthalpy above 298 K (77 F). $S_{298}°$ = absolute entropy at 298 K (77 F). $S_T°-S_{298}°$ = entropy above 298 K (77 F).

[c] Thermodynamic properties estimated from properties of Na_2SO_4 (s, l) and vapor pressure data of Bowden [3].

equations. This was done by using a modification of Brinkley's method [16, 17]. It was assumed throughout that:

1 Total pressure is 1 atm.

2 All gaseous constituents behave ideally.

3 All condensed constituents are pure compounds.

Table 2 Temperatures and theoretical air ratios for which calculations were made

Temperature deg K	Temperature deg F	Per cent theoretical air: Pana coal 90	Pana coal 100	Pana coal 110	Pana coal 130	Wright coal 90	Wright coal 100	Wright coal 110
500	540	x	x	x	x	x	x	x
600	620	x	x	x	x	x	x	x
800	980	x	x	x	x	x	x	x
1000	1340	x	x	x	x	x	x	x
1200	1700	x	x	x	x	x	x	x
1400	2060		x	x	x			
2000	3140	x	x	x	x	x	x	x

4 When condensed constituents occur, they flow along and remain in intimate contact with the gas whence they came.

Numerical work was carried out on an IBM-650 computer and spot-checked by hand via back calculation of equilibrium constants.

Results

Results are plotted in Figs. 1 through 8 and Tables 4 through 10 give detailed results of the equilibrium calculations.[3] Figs. 1–3 give equilibrium concentrations of sodium, sulfur, and chlorine compounds in the combustion gas from Pana coal while Figs. 4–6 do the same for Wright coal. Figs. 7 and 8 apply to miscellaneous compounds in the gas from either coal. Each figure contains four plots, two for constant fuel-air ratio and varying temperature and two for constant temperature and varying fuel-air ratio. Note that the ordinate in these plots is always the logarithm of partial pressure in atmospheres, which means that the plots are really eight-cycle semilogarithmic. Since the total pressure was 1 atm throughout, (−2) at the top of the plots corresponds to 1 per cent by volume while (−6) in the middle corresponds to 1 part per million. The symbols (c) and (g) are used after the formulas of those compounds which might be present in either condensed or gaseous states; (c) stands for condensed solid or liquid and (g) for gas.

In the following we note a few of the inferences about the behavior of the minor constituents of combustion gas which may be drawn from these results. It should be remembered that both gases contain about the same amount of sulfur, but the Pana contains about five times as much sodium as the Wright, and the Wright contains negligible chlorine.

Alkali Compounds (Figs. 1 and 4). Combustion gas can transport considerable quantities of alkali vapors from the combustion zone

[3] In these tables all entries are partial pressures in atmospheres except "total mols," which are pound mols per pound of dry coal. Floating point notation is used. The quantity 1.234 02-, means 1.234 × 10^{-2} or 0.01234. All constituents are gaseous except those marked (c) which are condensed liquids or solids.

Table 3 Comparison of coal analyses

	Pana coal: Original coal	Pana coal: In gas	Pana coal: In gas as calc'd	Wright coal: Original coal	Wright coal: In gas	Wright coal: In gas as calc'd
C	67.8	67.8	67.8	69.5	69.5	69.5
H.....	4.7	4.7	4.7	4.9	4.9	4.9
N.....	1.4	1.4	1.4	1.4	1.4	1.4
S	4.5	4.275	4.275	4.9	4.655	4.655
O	8.0	8.0	8.0	7.6	7.6	7.6
Na_2O....	0.62	0.248	0.278	0.04	0.016	0.049
K_2O	0.23	0.046	0	0.25	0.050	0
Cl.....	0.66	0.66	0.66	0.01	0.01	0.01
Other ash	12.09	0	0	11.40	0	0
H_2O.....	6.9	6.9	6.9	10.0	10.0	10.0
Totals..	106.90	94.029	94.013	110.00	98.131	98.114

NOTES:

(a) Entries are lb per 100 lb of dry coal.

(b) "In gas" column obtained from coal analysis via appearance factors.

(c) "In gas as calc'd" column identical with "in gas" column except that K_2O has been converted to its Na_2O equivalent.

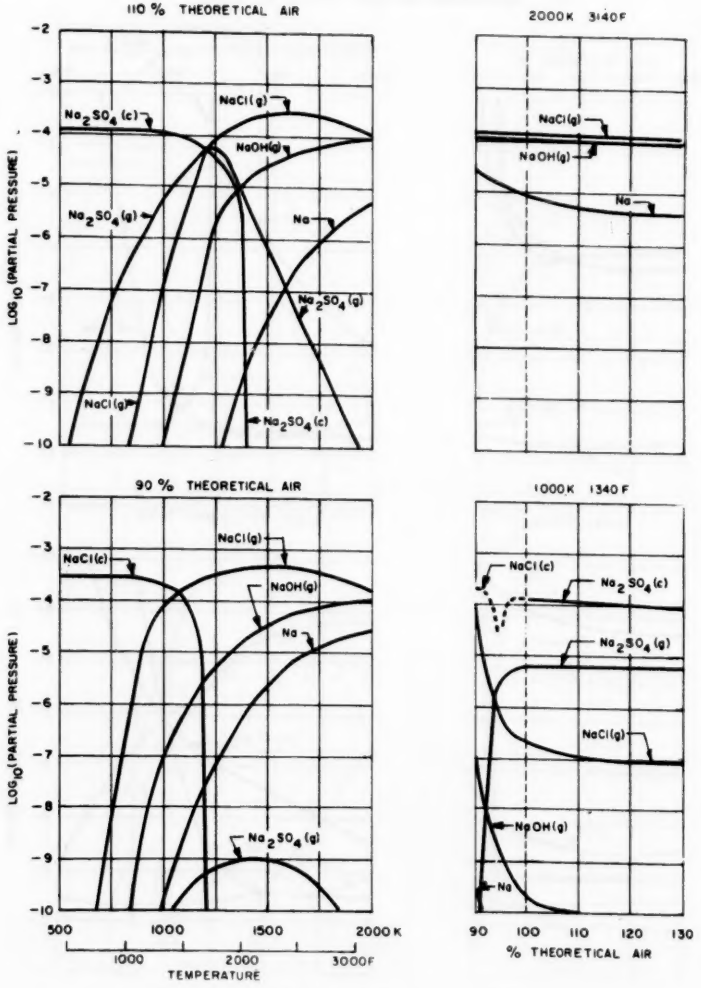

Fig. 1 Pana coal—sodium compounds

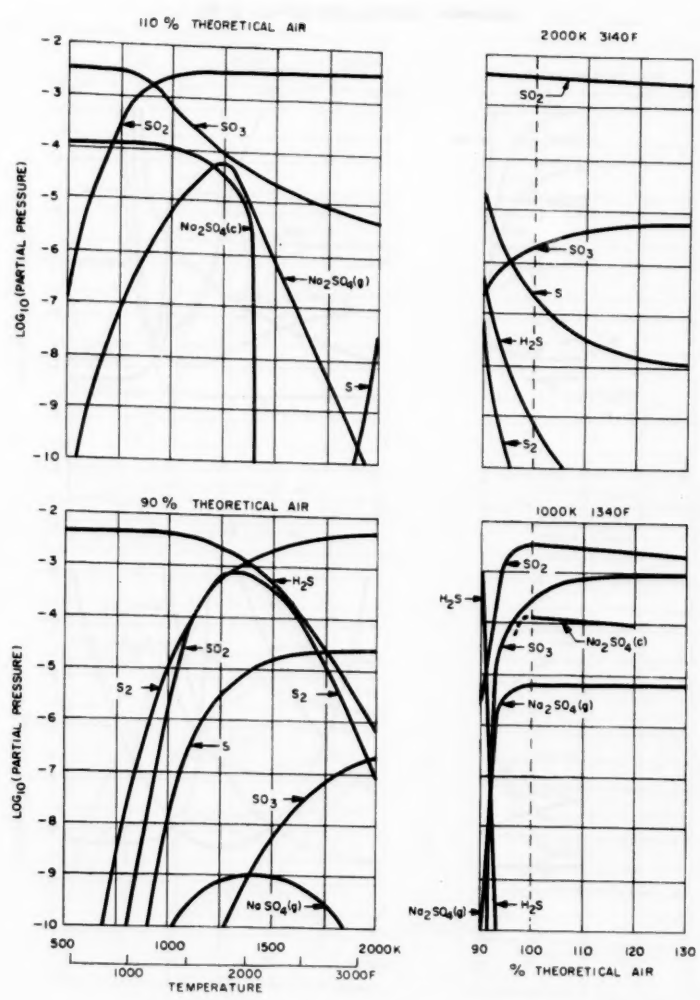

Fig. 2 Pana coal—sulfur compounds

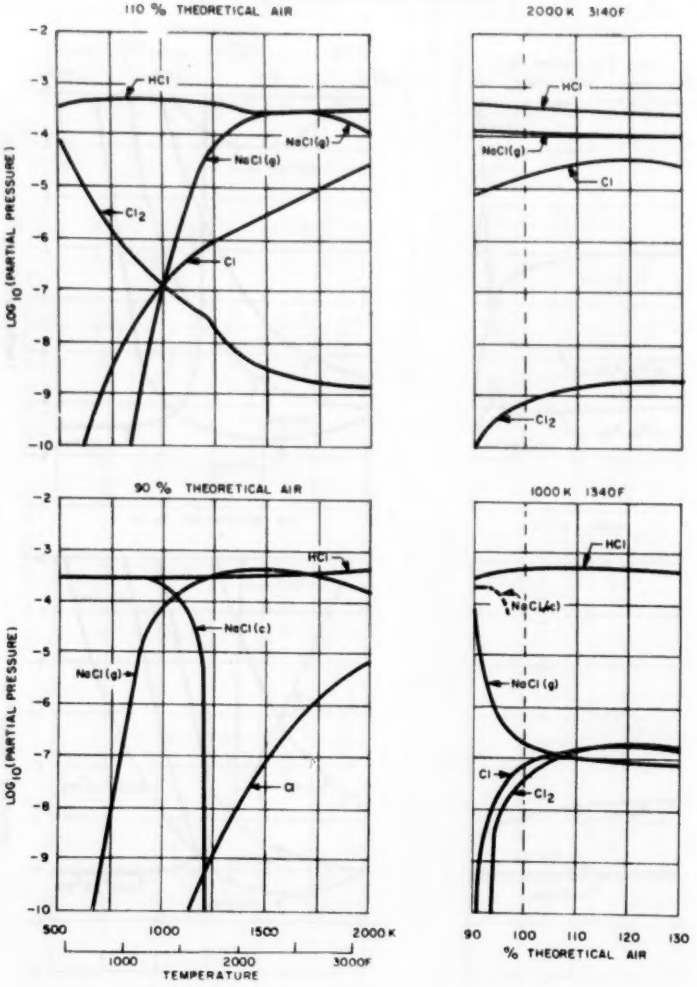

Fig. 3 Pana coal—chlorine compounds

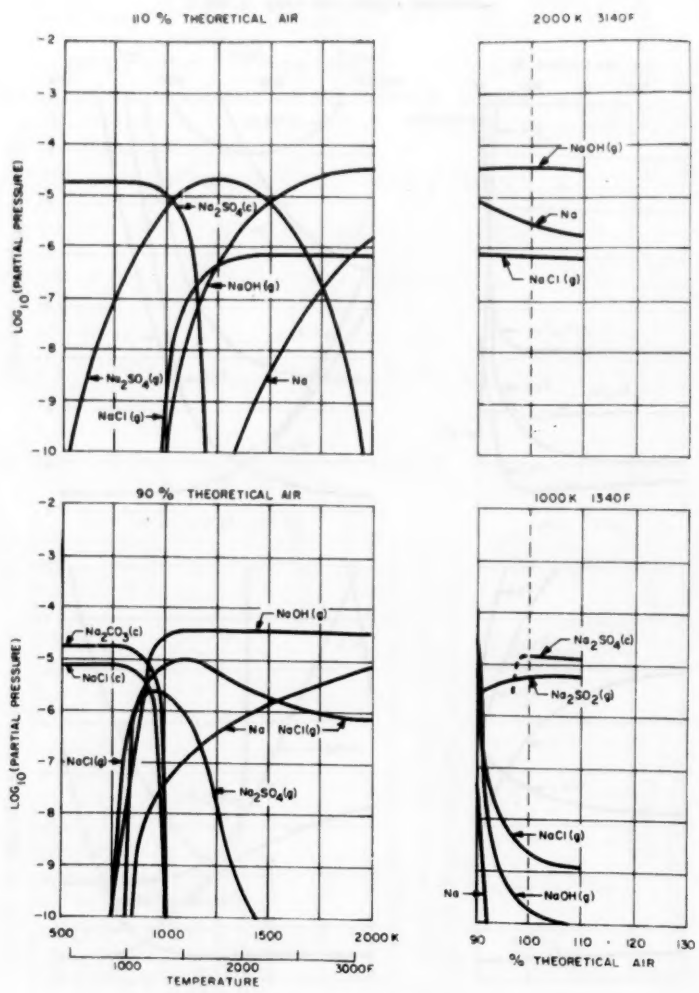

Fig. 4 Wright coal—sodium compounds

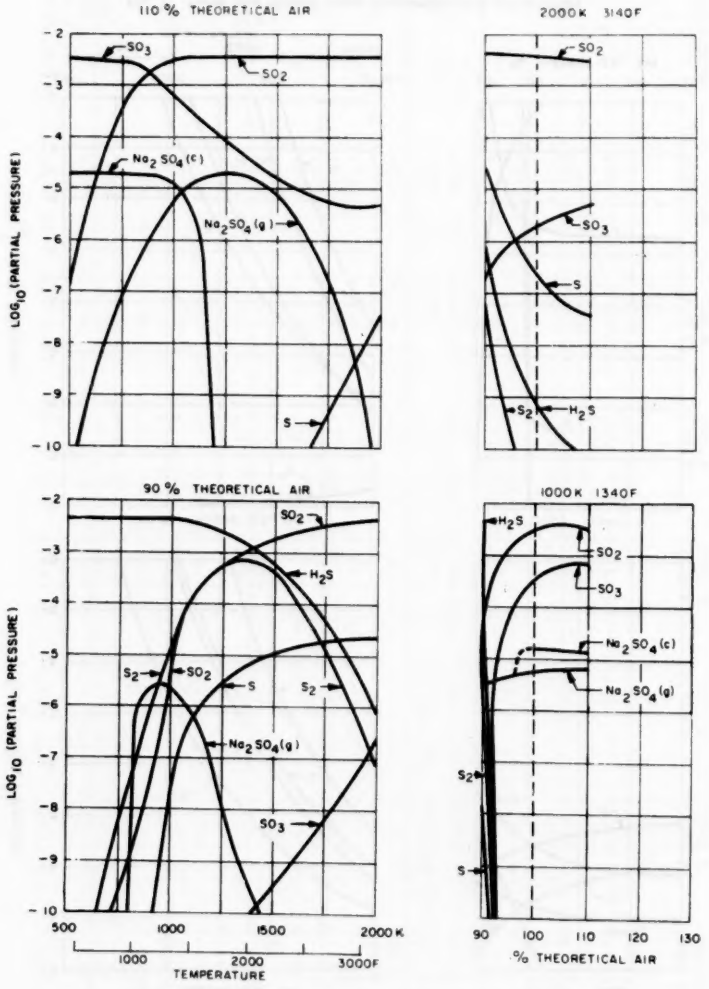

Fig. 5 Wright coal—sulfur compounds

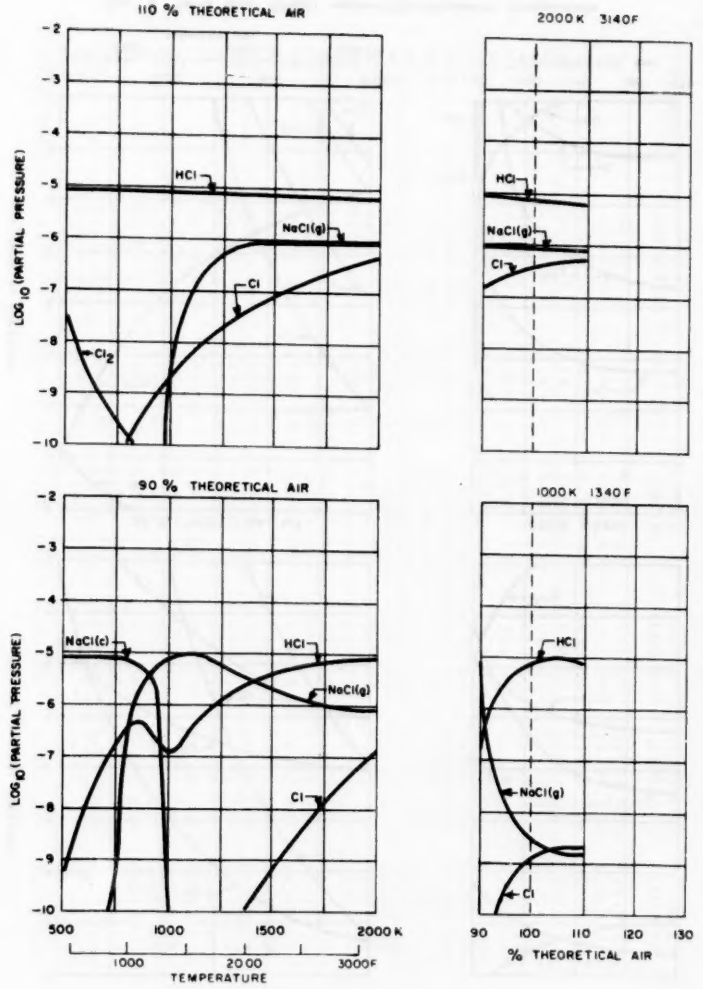

Fig. 6 Wright coal—chlorine compounds

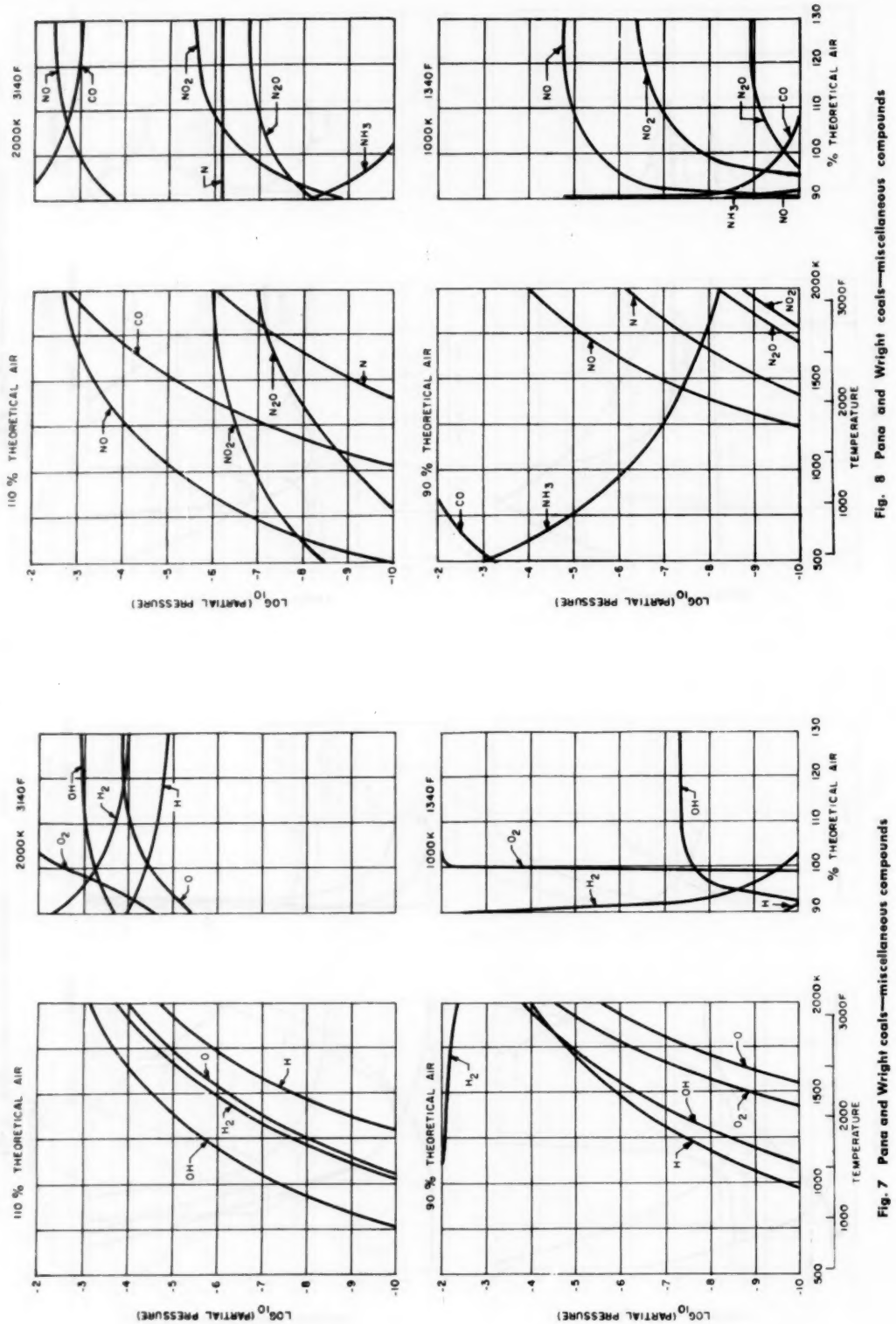

Fig. 7 Pana and Wright coals—miscellaneous compounds

Fig. 8 Pana and Wright coals—miscellaneous compounds

Table 4 Equilibrium composition of combustion gas from Pana Coal—90 per cent theoretical air

TEMPERATURE	500 K (540 F)	600 K (620 F)	800 K (980 F)	1000 K (1340 F)	1200 K (1700 F)	2000 K (3140 F)
A	8.624 03-	8.616 03-	8.615 03-	8.614 03-	8.606 03-	8.575 03-
C	.000 51-	.000 51-	5.892 41-	2.718 33-	3.168 28-	4.867 18-
CO	4.109 04-	1.914 03-	8.339 03-	1.434 02-	1.907 02-	3.291 02-
CO2	1.761 01-	1.744 01-	1.680 01-	1.620 01-	1.571 01-	1.426 01-
CL	1.952 23-	1.114 19-	6.864 15-	6.043 12-	5.827 10-	7.504 06-
CL2	1.952 26-	3.421 23-	5.574 19-	2.464 16-	1.528 14-	1.009 10-
H	1.053 21-	6.981 18-	3.741 13-	2.361 10-	1.756 08-	1.128 04-
H2	2.339 02-	2.318 02-	1.694 02-	1.097 02-	8.039 03-	4.841 03-
HCL	3.012 04-	3.009 04-	3.009 04-	3.010 04-	3.044 04-	4.245 04-
H2O	7.638 02-	7.782 02-	8.423 02-	9.022 02-	9.419 02-	9.973 02-
H2S	4.168 03-	4.165 03-	4.164 03-	4.138 03-	2.993 03-	7.344 07-
N	3.553 35-	6.492 29-	4.551 21-	2.390 16-	3.411 13-	7.404 07-
N2	7.096 01-	7.094 01-	7.094 01-	7.093 01-	7.087 01-	7.060 01-
NH3	1.007 03-	1.287 04-	5.634 06-	5.605 07-	1.135 07-	5.397 09-
NO	5.602 32-	3.905 26-	1.200 18-	5.099 14-	6.532 11-	9.810 05-
NO2	.000 51-	3.612 43-	2.029 31-	4.287 24-	3.630 19-	2.231 09-
N2O	1.155 35-	5.579 30-	1.097 22-	3.643 18-	4.021 15-	4.918 09-
NA	3.701 32-	8.545 25-	1.006 15-	2.152 10-	3.052 08-	2.565 05-
NACL	2.140 16-	1.764 12-	1.213 07-	8.467 05-	2.722 04-	1.466 04-
NAOH	1.601 24-	7.303 19-	8.445 12-	1.368 07-	3.675 06-	1.069 04-
NA2SO4	2.755 32-	7.293 26-	4.929 17-	3.844 11-	6.239 10-	1.527 12-
O	7.012 46-	2.826 37-	2.548 26-	1.340 19-	3.966 15-	4.305 06-
O2	1.736 45-	5.925 37-	6.414 26-	5.017 19-	2.229 14-	3.458 05-
OH	1.719 27-	1.706 22-	3.905 16-	3.060 12-	1.228 09-	1.954 04-
P4O10	1.498 06-	1.496 06-	1.496 06-	1.496 06-	1.495 06-	1.489 06-
S	6.459 22-	1.304 17-	4.662 12-	1.353 08-	2.109 06-	2.216 05-
S2	2.609 15-	2.450 12-	2.652 08-	1.208 05-	4.110 04-	8.074 08-
SO2	6.311 19-	3.528 15-	5.660 10-	1.858 06-	3.422 04-	4.121 03-
SO3	5.384 36-	1.091 29-	4.407 21-	2.293 15-	1.367 11-	2.196 07-
NACL (c)	2.807 04-	2.805 04-	2.803 04-	1.956 04-		
TOTAL MOLS	3.198 01-	3.201 01-	3.201 01-	3.202 01-	3.205 01-	3.216 01-

Table 5 Equilibrium composition of combustion gas from Pana coal—100 per cent theoretical air

TEMPERATURE	500 K (540 F)	600 K (620 F)	800 K (980 F)	1000 K (1340 F)	1200 K (1700 F)	1400 K (2060 F)	2000 K (3140 F)
A	8.812 03-	8.812 03-	8.804 03-	8.797 03-	8.795 03-	8.793 03-	8.773 03-
C	.000 51-	.000 51-	.000 51-	7.388 49-	3.714 39-	3.166 32-	5.423 20-
CO	1.420 24-	1.073 19-	6.280 14-	2.365 10-	6.632 08-	3.723 06-	3.657 03-
CO2	1.624 01-	1.623 01-	1.622 01-	1.621 01-	1.620 01-	1.620 01-	1.580 01-
CL	4.765 13-	2.253 11-	4.031 09-	7.987 08-	4.781 07-	1.188 06-	2.112 05-
CL2	1.162 05-	1.399 06-	1.923 07-	4.304 08-	1.029 08-	1.743 09-	7.993 10-
H	7.335 32-	6.107 26-	1.131 18-	3.170 14-	3.299 11-	4.827 09-	3.534 05-
H2	1.135 22-	1.774 18-	1.548 13-	1.976 10-	2.839 08-	9.884 07-	4.752 04-
HCL	5.120 04-	5.324 04-	5.344 04-	5.340 04-	4.693 04-	2.947 04-	3.744 04-
H2O	9.884 02-	9.883 02-	9.874 02-	9.866 02-	9.867 02-	9.872 02-	9.761 02-
H2S	.000 51-	2.322 41-	7.580 30-	3.751 23-	1.294 18-	2.257 15-	6.711 10-
N	3.593 35-	6.565 29-	4.601 21-	2.415 16-	3.448 13-	6.272 11-	7.487 07-
N2	7.256 01-	7.256 01-	7.250 01-	7.244 01-	7.242 01-	7.240 01-	7.219 01-
NH3	3.441 34-	8.710 29-	1.574 22-	1.370 18-	7.617 16-	7.027 14-	1.678 10-
NO	1.511 11-	6.554 10-	1.555 07-	3.127 06-	1.959 05-	7.257 05-	9.891 04-
NO2	2.019 11-	1.006 10-	3.372 09-	1.595 08-	3.229 08-	5.337 08-	2.243 07-
N2O	3.151 15-	9.470 14-	1.437 11-	2.257 10-	1.219 09-	4.141 09-	5.014 08-
NA	1.809 48-	4.176 38-	2.962 25-	3.292 17-	8.798 12-	5.257 09-	8.540 06-
NACL	2.553 22-	1.743 17-	2.097 11-	1.712 07-	6.437 05-	2.382 04-	1.374 04-
NAOH	1.454 30-	5.181 24-	9.637 16-	1.705 10-	5.904 07-	1.567 05-	1.111 04-
NA2SO4	1.208 11-	9.630 10-	2.297 07-	6.135 06-	4.913 05-	1.914 06-	1.557 11-
O	1.870 25-	4.690 21-	3.267 15-	8.130 12-	1.176 09-	4.773 08-	4.293 05-
O2	1.235 04-	1.632 04-	1.054 03-	1.847 03-	1.961 03-	1.998 03-	3.438 03-
OH	3.194 17-	2.476 14-	1.514 10-	2.492 08-	6.847 07-	7.341 06-	6.104 04-
P4O10	1.378 06-	1.378 06-	1.376 06-	1.375 06-	1.375 06-	1.375 06-	1.372 06-
S	.000 51-	9.505 40-	9.283 28-	6.806 21-	2.582 16-	4.770 13-	2.063 07-
S2	.000 51-	.000 51-	1.051 39-	3.058 30-	6.160 24-	1.896 19-	6.998 12-
SO2	1.627 06-	7.082 05-	1.852 03-	3.441 03-	3.686 03-	3.811 03-	3.815 03-
SO3	3.703 03-	3.634 03-	1.849 03-	2.577 04-	4.367 05-	1.251 05-	2.027 06-
NA2SO4(c)	1.291 04-	1.291 04-	1.288 04-	1.227 04-	4.725 05-		
TOTAL MOLS	3.477 01-	3.477 01-	3.480 01-	3.483 01-	3.484 01-	3.484 01-	3.492 01-

Table 6 Equilibrium composition of combustion gas from Pana coal—110 per cent theoretical air

TEMPERATURE	500 K (540 F)	600 K (620 F)	800 K (980 F)	1000 K (1340 F)	1200 K (1700 F)	1400 K (2060 F)	2000 K (3140 F)
A	8.857 03-	8.857 03-	8.854 03-	8.845 03-	8.842 03-	8.840 03-	8.830 03-
C	.000 51-	.000 51-	.000 51-	.000 51-	3.423 40-	2.971 33-	9.126 21-
CO	1.080 25-	9.370 21-	1.382 14-	6.704 11-	1.924 08-	1.090 06-	1.444 03-
CO2	1.483 01-	1.483 01-	1.483 01-	1.481 01-	1.481 01-	1.480 01-	1.464 01-
CL	1.167 12-	6.595 11-	7.761 09-	1.357 07-	8.410 07-	2.020 06-	2.982 05-
CL2	6.978 05-	1.199 05-	7.127 07-	1.243 07-	3.182 08-	5.036 09-	1.593 09-
H	2.043 32-	1.823 26-	5.359 19-	1.704 14-	1.795 11-	2.638 09-	2.229 05-
H2	8.804 24-	1.580 19-	3.475 14-	5.713 11-	8.401 09-	2.952 07-	1.891 04-
HCL	3.494 04-	4.650 04-	4.874 04-	4.878 04-	4.491 04-	2.738 04-	3.334 04-
H2O	9.216 02-	9.210 02-	9.206 02-	9.196 02-	9.194 02-	9.200 02-	9.117 02-
H2S	.000 51-	1.678 45-	3.499 32-	8.251 25-	3.432 20-	6.277 17-	4.434 11-
N	3.601 35-	6.581 29-	4.613 21-	2.421 16-	3.456 13-	6.287 11-	7.506 07-
N2	7.290 01-	7.290 01-	7.288 01-	7.280 01-	7.277 01-	7.274 01-	7.256 01-
NH3	7.455 36-	2.320 30-	1.678 23-	2.135 19-	1.229 16-	1.150 14-	4.224 11-
NO	1.820 10-	6.874 09-	6.478 07-	1.011 05-	6.182 05-	2.270 04-	2.327 03-
NO2	2.922 09-	1.104 08-	5.834 08-	1.663 07-	3.209 07-	5.208 07-	1.238 06-
N2O	3.804 14-	9.955 13-	6.000 11-	7.314 10-	3.857 09-	1.298 08-	1.183 07-
NA	5.460 49-	1.339 38-	1.197 25-	1.148 17-	2.964 12-	2.755 09-	5.472 06-
NACL	1.888 22-	1.636 17-	1.632 11-	1.014 07-	3.814 05-	2.122 04-	1.243 04-
NAOH	1.469 30-	5.188 24-	7.664 16-	1.030 10-	3.407 07-	1.400 05-	1.054 04-
NA2SO4	1.208 11-	9.630 10-	2.297 07-	6.135 06-	4.913 05-	4.638 06-	3.219 11-
O	2.248 24-	4.907 20-	1.357 14-	2.621 11-	3.704 09-	1.489 07-	1.007 04-
O2	1.784 02-	1.787 02-	1.819 02-	1.920 02-	1.945 02-	1.945 02-	1.894 02-
OH	1.069 16-	7.733 14-	2.979 10-	4.321 08-	1.173 06-	1.252 05-	9.037 04-
P4O10	1.259 06-	1.259 06-	1.258 06-	1.257 06-	1.256 06-	1.256 06-	1.255 06-
S	.000 51-	7.713 43-	1.909 29-	5.179 22-	2.314 17-	4.442 14-	3.425 08-
S2	.000 51-	.000 51-	4.447 43-	1.771 32-	4.947 26-	1.644 21-	1.928 13-
SO2	1.238 07-	6.292 06-	6.574 04-	2.722 03-	3.276 03-	3.456 03-	3.487 03-
SO3	3.384 03-	3.378 03-	2.726 03-	6.575 04-	1.222 04-	3.539 05-	4.349 06-
NA2SO4(c)	1.180 04-	1.179 04-	1.177 04-	1.116 04-	4.938 05-		
TOTAL MOLS	3.806 01-	3.806 01-	3.807 01-	3.811 01-	3.813 01-	3.813 01-	3.818 01-

Table 7 Equilibrium composition of combustion gas from Pana coal—130 per cent theoretical air

TEMPERATURE	500 K (540 F)	600 K (620 F)	800 K (980 F)	1000 K (1340 F)	1200 K (1700 F)	1400 K (2060 F)	2000 K (3140 F)
A	8.921 03-	8.921 03-	8.919 03-	8.911 03-	8.908 03-	8.906 03-	8.898 03-
C	.000 51-	.000 51-	.000 51-	.000 51-	1.211 40-	1.052 33-	3.266 21-
CO	5.758 26-	4.999 21-	7.426 15-	3.669 11-	1.057 08-	5.992 07-	7.993 04-
CO2	1.264 01-	1.264 01-	1.264 01-	1.263 01-	1.262 01-	1.262 01-	1.253 01-
CL	1.204 12-	7.369 11-	8.842 09-	1.534 07-	9.537 07-	2.300 06-	3.300 05-
CL2	7.426 05-	1.497 05-	9.251 07-	1.563 07-	4.093 08-	6.525 09-	1.951 09-
H	1.521 32-	1.357 26-	4.004 19-	1.285 14-	1.356 11-	1.993 09-	1.687 05-
H2	4.878 24-	8.757 20-	1.940 14-	3.248 11-	4.794 09-	1.685 07-	1.083 04-
HCL	2.683 04-	3.869 04-	4.149 04-	4.158 04-	3.847 04-	2.355 04-	2.792 04-
H2O	8.163 02-	8.157 02-	8.154 02-	8.147 02-	8.145 02-	8.149 02-	8.072 02-
H2S	.000 51-	1.946 46-	4.492 33-	1.487 25-	6.790 21-	1.261 17-	9.045 12-
N	3.614 35-	6.604 29-	4.630 21-	2.430 16-	3.469 13-	6.310 11-	7.532 07-
N2	7.342 01-	7.342 01-	7.340 01-	7.334 01-	7.331 01-	7.328 01-	7.305 01-
NH3	3.085 36-	9.611 31-	7.026 24-	9.188 20-	5.317 17-	4.977 15-	1.836 11-
NO	2.920 10-	1.102 08-	1.032 06-	1.580 05-	9.633 05-	3.535 04-	3.611 03-
NO2	7.495 09-	2.829 08-	1.474 07-	4.050 07-	7.764 07-	1.259 06-	2.972 06-
N2O	6.124 14-	1.602 12-	9.588 11-	1.148 09-	6.032 09-	2.029 08-	1.841 07-
NA	4.677 49-	1.147 38-	9.914 26-	8.400 18-	2.088 12-	2.034 09-	4.120 06-
NACL	1.668 22-	1.566 17-	1.540 11-	8.389 08-	3.048 05-	1.783 04-	1.036 04-
NAOH	1.497 30-	5.286 24-	7.526 16-	8.860 11-	2.815 07-	1.212 05-	9.290 05-
NA2SO4	1.208 11-	9.630 10-	2.297 07-	6.135 06-	4.913 05-	5.161 06-	3.720 11-
O	3.593 24-	7.841 20-	2.153 14-	4.084 11-	5.751 09-	2.311 07-	1.558 04-
O2	4.559 02-	4.562 02-	4.580 02-	4.661 02-	4.688 02-	4.683 02-	4.529 02-
OH	1.272 16-	9.199 14-	3.532 10-	5.076 08-	1.375 06-	1.468 05-	1.057 03-
P4O10	1.073 06-	1.073 06-	1.073 06-	1.072 06-	1.071 06-	1.071 06-	1.070 06-
S	.000 51-	1.613 43-	4.390 30-	1.641 22-	8.025 18-	1.564 14-	1.220 08-
S2	.000 51-	.000 51-	2.352 44-	1.778 33-	5.948 27-	2.037 22-	2.449 14-
SO2	6.599 08-	3.359 06-	3.806 04-	2.094 03-	2.738 03-	2.929 03-	2.972 03-
SO3	2.885 03-	2.882 03-	2.504 03-	7.879 04-	1.585 04-	4.654 05-	5.733 06-
NA2SO4(c)	1.005 04-	1.005 04-	1.003 04-	9.426 05-	3.589 05-		
TOTAL MOLS	4.465 01-	4.465 01-	4.466 01-	4.470 01-	4.471 01-	4.472 01-	4.476 01-

Table 8 Equilibrium composition of combustion gas from Wright coal—90 per cent theoretical air

TEMPERATURE	500 K (540 F)	600 K (620 F)	800 K (980 F)	1000 K (1340 F)	1200 K (1700 F)	2000 K (3140 F)
A	8.579 03-	8.572 03-	8.571 03-	8.570 03-	8.564 03-	8.531 03-
C	.000 51-	.000 51-	5.138 41-	2.474 33-	2.973 28-	4.865 18-
CO	3.675 04-	1.726 03-	7.750 03-	1.362 02-	1.839 02-	3.268 02-
CO2	1.739 01-	1.724 01-	1.664 01-	1.605 01-	1.556 01-	1.407 01-
CL	3.185 29-	3.239 24-	8.519 18-	2.537 15-	1.593 12-	1.278 07-
CL2	5.195 38-	2.891 32-	8.586 25-	4.343 23-	1.142 19-	2.926 14-
H	1.043 21-	6.930 18-	3.748 13-	2.383 10-	1.784 08-	1.164 04-
H2	2.294 02-	2.284 02-	1.699 02-	1.117 02-	8.298 03-	5.159 03-
HCL	4.867 10-	8.684 09-	3.741 07-	1.275 07-	8.453 07-	7.463 06-
H2O	8.276 02-	8.405 02-	9.007 02-	9.590 02-	9.988 02-	1.056 01-
H2S	4.374 03-	4.370 03-	4.370 03-	4.339 03-	3.145 03-	8.321 07-
N	3.544 35-	6.476 29-	4.540 21-	2.384 16-	3.403 13-	7.386 07-
N2	7.061 01-	7.059 01-	7.059 01-	7.058 01-	7.053 01-	7.025 01-
NH3	9.761 04-	1.255 04-	5.648 06-	5.747 07-	1.188 07-	5.922 09-
NO	6.172 32-	4.270 26-	1.276 18-	5.308 14-	6.694 11-	7.721 05-
NO2	.000 51-	4.330 43-	2.299 31-	4.657 24-	3.822 19-	2.196 09-
N2O	1.270 35-	6.085 30-	1.163 22-	3.782 18-	4.111 15-	4.861 09-
NA	2.269 26-	2.939 20-	8.107 13-	5.060 08-	3.132 07-	8.802 06-
NACL	2.140 16-	1.764 12-	1.213 07-	8.358 06-	7.634 06-	8.567 07-
NAOH	1.073 18-	2.734 14-	7.264 09-	3.388 05-	3.935 05-	3.761 05-
NA2SO4	1.647 20-	1.327 16-	4.317 11-	2.596 06-	7.448 08-	1.862 13-
O	7.745 46-	3.098 37-	2.715 26-	1.398 19-	4.074 15-	4.277 06-
O2	2.118 45-	7.120 37-	7.285 26-	5.464 19-	2.353 14-	3.413 05-
OH	1.881 27-	1.856 22-	4.169 16-	3.223 12-	1.282 09-	2.004 04-
S	6.909 22-	1.389 17-	4.876 12-	1.393 08-	2.147 06-	2.357 05-
S2	2.985 15-	2.779 12-	2.901 08-	1.281 05-	4.258 04-	9.129 08-
SO2	8.235 19-	4.515 15-	6.723 10-	2.083 06-	3.676 04-	4.325 03-
SO3	7.760 36-	1.530 29-	5.579 21-	2.684 15-	1.508 11-	2.290 07-
NA2CO3(c)	1.952 05-	1.951 05-	1.968 05-			
NACL(c)	8.494 06-	8.479 06-	7.991 06-			
TOTAL MOLS	3.320 01-	3.322 01-	3.323 01-	3.323 01-	3.326 01-	3.338 01-

Table 9 Equilibrium composition of combustion gas from Wright coal—100 per cent theoretical air

TEMPERATURE	500 K (540 F)	600 K (620 F)	800 K (980 F)	1000 K (1340 F)	1200 K (1700 F)	2000 K (3140 F)
A	8.773 03-	8.773 03-	8.765 03-	8.757 03-	8.756 03-	8.735 03-
C	.000 51-	.000 51-	.000 51-	7.462 49-	3.762 39-	5.462 20-
CO	8.515 23-	2.387 19-	6.470 14-	2.363 10-	6.634 08-	3.648 03-
CO2	1.604 01-	1.604 01-	1.603 01-	1.601 01-	1.601 01-	1.561 01-
CL	9.078 16-	2.143 13-	5.608 11-	1.128 09-	7.068 09-	3.605 07-
CL2	4.220 11-	1.266 10-	3.721 11-	8.580 12-	2.248 12-	2.328 13-
H	5.877 31-	9.427 26-	1.188 18-	3.279 14-	3.415 11-	3.653 05-
H2	7.285 21-	4.226 18-	1.709 13-	2.115 10-	3.041 08-	5.077 04-
HCL	7.817 06-	7.816 06-	7.809 06-	7.799 06-	7.181 06-	6.604 06-
H2O	1.046 01-	1.046 01-	1.045 01-	1.044 01-	1.044 01-	1.033 01-
H2S	1.107 44-	6.663 40-	1.003 29-	4.436 23-	1.523 18-	7.675 10-
N	3.584 35-	6.550 29-	4.590 21-	2.409 16-	3.440 13-	7.470 07-
N2	7.222 01-	7.222 01-	7.215 01-	7.209 01-	7.208 01-	7.186 01-
NH3	1.766 31-	3.196 28-	1.821 22-	1.513 18-	8.425 16-	1.849 10-
NO	2.484 13-	2.904 10-	1.488 07-	3.085 06-	1.930 05-	9.773 04-
NO2	5.471 15-	1.981 11-	3.094 09-	1.556 08-	3.142 08-	2.195 07-
N2O	5.168 17-	4.187 14-	1.371 11-	2.221 10-	1.198 09-	4.943 08-
NA	1.374 47-	6.099 38-	2.941 25-	3.201 17-	5.671 12-	2.983 06-
NACL	3.693 24-	2.422 19-	2.897 13-	2.350 09-	6.134 07-	8.191 07-
NAOH	1.458 30-	5.189 24-	9.639 16-	1.696 10-	3.890 07-	3.975 05-
NA2SO4	1.208 11-	9.630 10-	2.297 07-	6.135 06-	2.133 05-	1.957 12-
O	3.082 27-	2.083 21-	3.133 15-	8.041 12-	1.162 09-	4.251 05-
O2	3.355 08-	3.220 05-	9.697 04-	1.807 03-	1.913 03-	3.373 03-
OH	4.218 18-	1.698 14-	1.525 10-	2.550 08-	6.999 07-	6.249 04-
S	5.506 45-	1.144 38-	1.113 27-	7.523 21-	2.837 16-	2.209 07-
S2	.000 51-	.000 51-	1.513 39-	3.736 30-	3.949 03-	8.019 12-
SO2	1.040 04-	1.683 04-	2.043 03-	3.720 03-	4.621 05-	4.005 03-
SO3	3.899 03-	3.835 03-	1.956 03-	2.756 04-	7.432 24-	2.108 06-
NA2SO4(c)	2.187 05-	2.187 05-	2.162 05-	1.569 05-		
TOTAL MOLS	3.608 01-	3.608 01-	3.611 01-	3.614 01-	3.615 01-	3.623 01-

Table 10 Equilibrium composition of combustion gas from Wright coal—110 per cent theoretical air

TEMPERATURE	500 K (540 F)	600 K (620 F)	800 K (980 F)	1000 K (1340 F)	1200 K (1700 F)	2000 K (3140 F)
A	8.818 03-	8.818 03-	8.815 03-	8.805 03-	8.802 03-	8.792 03-
C	.000 51-	.000 51-	.000 51-	.000 51-	3.395 40-	9.068 21-
CO	1.072 25-	9.310 21-	1.372 14-	6.640 11-	1.905 08-	1.431 03-
CO2	1.466 01-	1.466 01-	1.465 01-	1.464 01-	1.463 01-	1.447 01-
CL	2.299 14-	9.819 13-	1.103 10-	1.927 09-	1.233 08-	5.108 07-
CL2	2.707 08-	2.657 09-	1.440 10-	2.505 11-	6.842 12-	4.673 13-
H	2.105 32-	1.879 26-	5.524 19-	1.754 14-	1.847 11-	2.295 05-
H2	9.344 24-	1.679 19-	3.692 14-	6.053 11-	8.898 09-	2.005 04-
HCL	7.089 06-	7.138 06-	7.141 06-	7.130 06-	6.776 06-	5.879 06-
H2O	9.737 02-	9.737 02-	9.734 02-	9.723 02-	9.720 02-	9.639 02-
H2S	.000 51-	1.959 45-	4.069 32-	9.495 25-	3.921 20-	4.962 11-
N	3.593 35-	6.567 29-	4.603 21-	2.416 16-	3.449 13-	7.490 07-
N2	7.259 01-	7.259 01-	7.256 01-	7.248 01-	7.246 01-	7.225 01-
NH3	8.133 36-	2.537 30-	1.834 23-	2.324 19-	1.337 16-	4.600 11-
NO	1.808 10-	6.823 09-	6.434 07-	1.006 05-	6.157 05-	2.316 03-
NO2	2.890 09-	1.090 08-	5.768 08-	1.652 07-	3.191 07-	1.229 06-
N2O	3.771 14-	9.860 13-	5.947 11-	7.266 10-	3.833 09-	1.175 07-
NA	5.264 49-	1.291 38-	1.154 25-	1.106 17-	1.813 12-	1.882 06-
NACL	3.584 24-	2.349 19-	2.237 13-	1.388 09-	3.420 07-	7.321 07-
NAOH	1.452 30-	5.131 24-	7.584 16-	1.020 10-	2.140 07-	3.724 05-
NA2SO4	1.208 11-	9.630 10-	2.297 07-	6.135 06-	1.967 05-	3.978 12-
O	2.238 24-	4.882 20-	1.351 14-	2.616 11-	3.697 09-	1.005 04-
O2	1.768 02-	1.768 02-	1.803 02-	1.912 02-	1.938 02-	1.884 02-
OH	1.096 16-	7.930 14-	3.057 10-	4.438 08-	1.205 06-	9.280 04-
S	.000 51-	8.470 43-	2.090 29-	5.625 22-	2.497 17-	3.616 08-
S2	.000 51-	.000 51-	5.331 43-	2.088 32-	5.758 26-	2.149 13-
SO2	1.344 07-	6.837 06-	7.132 04-	2.943 03-	3.521 03-	3.663 03-
SO3	3.658 03-	3.651 03-	2.944 03-	7.093 04-	1.311 04-	4.555 06-
NA2SO4(c)	1.999 05-	1.999 05-	1.975 05-	1.382 05-		
TOTAL MOLS	3.948 01-	3.948 01-	3.949 01-	3.953 01-	3.955 01-	3.959 01-

to heat-transfer surfaces. In the case of Pana coal, the sum of NaCl and NaOH, each at a partial pressure of about 0.0001 atm, could amount to an equivalent of roughly 275 lb of Na_2O per hr for a boiler producing 1,000,000 lb of steam per hr. If only one tenth of this quantity were evenly distributed as Na_2SO_4 (solid) throughout the superheater surface of such a boiler, the rate of build-up would be about 1/16 in. per month.

At combustion temperatures, e.g., about 3140 F, the stable alkali compounds are NaCl(g), NaOH(g), and Na(g). When results in Figs. 1 and 4 are compared, it appears that NaCl(g) is the most stable of these for its concentration seems to be controlled by the available chlorine.

The condensing temperature of alkali compounds is affected by both fuel-air ratio and amount of alkali present. With Pana coal, the range is about 1400 to 1700 F[4] in going from 90 to 110 per cent of theoretical air; with Wright coal, 1200 to 1400 F. The identity of the condensed compound is affected by the fuel-air ratio and the chlorine content of the gas. It is Na_2SO_4(c) with both coals at 110 per cent of theoretical air, but at 90 per cent of theoretical air it is NaCl(c) with Pana coal and a mixture of Na_2SO_3(c) and NaCl(c) with Wright coal.

Sulfur Compounds (Figs. 2 and 5). Since the sulfur contents of both coals are about equal and considerably in excess of the alkali contents, the only differences in the behavior of sulfur compounds are those due to alkali-sulfur compounds, i.e., Na_2SO_4(c) and Na_2SO_4(g). SO_2 predominates at combustion temperatures regardless of the fuel-air ratio; but, at lower temperatures, it tends to change to SO_3 or H_2S depending upon the fuel-air ratio. The temperature at which the SO_2 and SO_3 concentrations are equal at 110 per cent of theoretical air is about 1150 F. At 90 per cent of theoretical air, there is a region around 2000 F where S_2 temporarily achieves a concentration roughly equal to both the H_2S and SO_2 concentrations, i.e., 0.1 per cent.

[4] The temperatures given are those at which condensation is about half complete; condensation is substantially complete about 200 deg F below the given temperatures.

Chlorine Compounds (Figs. 3 and 6). At combustion temperatures, the stable chlorine compounds are, in order, HCl(g), NaCl(g), and Cl(g), irrespective of the fuel-air ratio; the Cl concentration is about an order of magnitude below the HCl, and NaCl is in between. As temperature drops, HCl remains predominant at 110 per cent of theoretical air; its concentration amounts to about 400 ppm with Pana coal, but only about 7 ppm with Wright coal. However, at 90 per cent of theoretical air, NaCl(g) or NaCl(c) tends to predominate as temperature drops, the degree depending upon the coal.

Miscellaneous Compounds (Figs. 7 and 8). The behavior of these compounds does not differ between the two coals. Probably the most significant one is NO, Fig. 8, because of its role in air pollution. It will be noted that its concentration at combustion temperatures, 3140 F, increases from about 100 ppm at 90 per cent of theoretical air to about 2300 ppm at 110 per cent theoretical air, thus indicating the advantage to be gained by properly controlled combustion. The NO concentration falls off very rapidly, however, with decreasing temperature.

Discussion

Equilibrium Limitation. For reasons of brevity and clarity, we have described the equilibrium composition of combustion gas as if it were always the actual composition. Of course, the two are not invariably the same because sufficient time is not always available to achieve equilibrium. Whether or not equilibrium is actually achieved in a given instance depends upon the circumstances; namely, the species under consideration, the temperature, the rate of change of temperature with time, catalysts, and so on. Unfortunately, no precise criterion is available for predicting the degree of approach to equilibrium in the present systems. Although departures from equilibrium place distinct limitations upon the utility of equilibrium results, they do not, however, render them useless because:

1 Reaction rates generally increase exponentially with in-

creasing temperature; this means that the equilibrium composition is likely to approximate the actual composition at the higher temperatures.

2 The nature of depatures from equilibrium at the lower temperatures is known; the departures are characterized by the persistence of concentrations typical of the higher temperatures.

3 Knowledge of equilibrium concentrations is a prerequisite to the prediction of actual concentrations from kinetic considerations (where reaction mechanisms and rate constants are known).

4 Although quantitatively suspect, the trends displayed by equilibrium compositions with respect to temperature and fuel-air ratio should be qualitatively accurate.

Accuracy of Basic Thermodynamic Data. Accuracy of the basic thermodynamic data referred to in Table 1 is generally excellent except for the sodium compounds. For these, it is fair to good, i.e., the individual free-energy functions are probably accurate to within about ±1 or 2 kcal per mol, and equilibrium constants within a factor of 1.5 to 3. Such inaccuracies would scarcely be noticed in the plotted results. In fact, they are probably of lesser significance than errors arising from our assumption as to the amount (and kind) of alkalis actually present in the gas.

Transport and Condensation of Alkalis. By using the results of Figs. 1 through 8 as a base, and estimating kinetic factors, one may arrive at an estimate of the actual behavior of any species of interest. For example, in view of the complicated over-all reaction required to form Na_2SO_4 from NaOH or NaCl and other gaseous constituents, e.g.,

$$4NaOH + 2SO_2 + O_2 \rightarrow 2Na_2SO_4 + 2H_2O,$$

we would not expect $Na_2SO_4(g)$ to be formed in equilibrium concentrations. Consequently, not much alkali should condense directly as the sulfate. Rather, the results presented suggest that, for Pana coal, alkali is transported and condensed as the chloride. This would make the condensing temperature about 1400 F (half condensed) regardless of fuel-air ratio, or about 300 deg F lower than the sulfate condensing temperature, but still above superheater metal temperatures. Once condensed, however, the time available for reaction becomes several orders of magnitude greater than the time available for the formation of $Na_2SO_4(g)$ during passage of the gas from the combustion chamber through the boiler. Thus a relatively prompt conversion (measured in hours) of chloride to sulfate seems probable on the tube surface (or blade, in case of turbines)

On account of the low chlorine content of Wright coal and the consequent tendency for NaOH to predominate even at quite low temperatures, Fig. 4, one might expect hydroxide to be the transporting and condensing species. If so, the condensing temperature would be about 1000 F rather than 1200 F for chloride and 1400 F for sulfate As with Pana coal, a relatively prompt conversion to sulfate should follow condensation. However, the low condensing temperature suggests that condensation would occur slowly, if at all, on superheater tubes—a behavior which might explain the low fouling tendencies of Wright coal.

It should be noted that condensing temperatures will be influenced somewhat by the kind and amounts of alkalis actually present in the combustion gas if these differ greatly from our assumptions. This circumstance points up the need for additional experimental data on alkali distribution, i.e., "appearance factors."

SO_3 and NO. It is known that SO_3 actually achieves only a few per cent of its equilibrium concentration on exit from a boiler [18, 19]. This is fortunate for if the equilibrium concentration (about 0.3 per cent) were to be obtained, air-heater corrosion would become more severe. On the other hand, it seems probable that SO_3 actually achieves its equilibrium concentrations within the stagnant crevices of porous fly-ash deposits on heat-transfer surfaces—especially if a catalyst like iron oxide is also present. With respect to NO, the steep drop in equilibrium concentration with decreasing temperature, Fig. 8, implies that almost the total amount of NO formed in the flame might be decomposed by the time the combustion gas is discharged from the stack if a suitable decomposition catalyst could be found.

Conclusion

A number of conclusions might be drawn from the plots of equilibrium composition which have resulted from this study. Some of them—relating to transportation and condensation of alkalis and to behavior of SO_3 and NO—have been pointed out in the Discussion to illustrate the use of such results. In drawing and using such conclusions, one should always keep probable kinetic factors in mind. Even where the kinetics are tentative, however, equilibrium results and their implications may be useful in indicating approaches to problems of fouling, corrosion, and air pollution which were not previously apparent. It is our hope that the present results will, indeed, be found useful as background in solving these important gas-side problems.

Part 2—Mechanisms of Superheater Fouling and Corrosion

Introduction

As is well known, severe corrosion of superheater tubes sometimes occurs in coal-fired boilers with steam temperatures exceeding about 1000 F. The chances of finding more effective and economical countermeasures against this troublesome phenomenon would be improved considerably if the mechanism by which it occurs were precisely known. A number of mechanisms have been proposed [20–27]. They may be divided into two general categories: (*a*) Accelerated oxidation, where the ultimate

Nomenclature

C_p = molar specific heat, cal/gm mol K
F = free energy, cal
H = enthalpy, cal
p = partial pressure, atm
R = universal gas constant, cal/gm mol K
S = entropy, cal/K
T = temperature, K

Subscripts

1, 2, 3, etc. = particular values
298 = at 298 K (77 F)
f = pertaining to formation from the elements
O, S, etc. = atomic oxygen, atomic sulfur, etc.
T = at temperature, T

Superscripts

0 = pertaining to standard state or states, i.e., pure solid, pure liquid, or pure gas at one atmosphere pressure

Symbols

Δ = increment in a quantity
(s) = solid
(l) = liquid
(g) = gas

corrosion product is always tube-metal oxide, and (*b*) attack by some agent other than oxygen where the ultimate corrosion product is not the oxide but some compound such as FeS, $FeSO_4$, $Fe_3Na(SO_4)_3$, and so on. Both categories may be subdivided further according to the method of destruction of the normally protective oxide scale or the nature of the attacking agent, e.g., whether HCl, $Na_2S_2O_7$, and so forth.

One purpose of the studies reported herein was to determine the conditions of temperature and effective fuel-air ratio under which the mechanism of corrosion might be expected to belong to one or the other of the categories. This differentiation can be accomplished by determining the thermodynamic stability of iron compounds. In the region where Fe_2O_3 is the stable iron compound, only mechanisms in the first category are possible; mechanisms in the second category are excluded by the thermodynamic impossibility of forming their corrosion products. In regions where the stable iron compound is other than Fe_2O_3, it seems highly probable that the mechanism is one in the second category, and that the corrosion product is the stable iron compound. The value of such a differentiation is, of course, obvious; it considerably narrows the field requiring further investigation.

It is also well known that relatively high concentrations of alkali metals are found in corrosive deposits [22, 27, 28, 29]. It seems quite probable, therefore, that alkali compounds within the deposits on the tube are at least involved in the mechanism of superheater corrosion. The second purpose of the present work was to identify the thermodynamically stable sodium[5] compound. Although the stable compound is not necessarily the one first deposited on the tube, it is quite likely to be the one present, because a relatively long time has been available for conversion. In any event, the identity of the stable compound at least tells the direction in which a given initially deposited compound will tend to change and, therefore, something about the nature of reactions taking place within a deposit.

Scope of Study

In Part 1 we considered the possibility that one or more of five sodium compounds might condense from the equilibrium gas at lower temperatures. The present work extends the number of sodium compounds to nine and introduces 12 iron compounds. Here, however, we are not concerned with the gaseous states of these compounds. Instead, the thermodynamic objective is to determine which of these 21 solid or liquid compounds would be stable under varying conditions of temperature and effective fuel-air ratio of the gas in contact with them. In addition to extending the number of condensed compounds, the present work also interpolates between calculated points so as to permit stabilities to be represented as areas in the temperature-fuel-air-ratio plane.

The compounds whose stabilities were investigated are listed in Table 11, together with sources of thermodynamic data and estimates of accuracy of the derived free-energy functions. Both presence and absence of SiO_2 were assumed in order to account for the possibility of silicate formation through reactions with fly ash or vaporized silica.

The present work was based upon the equilibrium gas-composition results of Part 1 and a few additional calculations at 70 per cent of theoretical air. Calculations were made using the gas from both Pana and Wright coals. The Pana gas is much higher in sodium and chlorine content than is the Wright, but both contain about the same amount of sulfur. The temperature range considered was from 600 to 2000 F, and the range of fuel-air ratio was from 80 to 130 per cent of theoretical air.

[5] Throughout this study it was assumed, for simplicity, that the behavior of sodium is characteristic of the behavior of alkali metals present in deposits.

Calculation Method

Our method of calculation is similar to that used by Richardson and Jeffes [37] for determining the stabilities of various oxides. Principal assumptions are as follows:

1 The stable compounds are in equilibrium with the layer of combustion gas that is next to the tube and at the same temperature as the tube.

2 Constituents of the combustion gas are in equilibrium with each other.

3 Each compound, if it is present at all, is present as the pure solid or liquid.

4 The quantities of iron and sodium compounds in the deposits are small in comparison with the quantity of combustion gas with which they are in equilibrium, so that the composition of the gas is not affected by the composition of the deposits.

The first two assumptions should be valid within porous deposits because of the relatively long time available for attainment of equilibrium. The third was made partly for simplicity and partly because of lack of data. It will cause some error, and the magnitude will be discussed later. The fourth seems reasonable if one postulates some diffusion of combustion gas in and out of the porous deposits.

The basis of the stability determination is the fact that the existence of a negative value for the free-energy change, ΔF, of a given chemical reaction means that the reaction will tend to proceed until one of the reactants is used up or else concentration changes have been brought about so as to make ΔF equal to zero. The essence of the present calculation method lies in writing reactions such as:

$$6FeO(s) \rightarrow 6Fe(s) + 6\,O(g),\ \Delta F_1 \quad (1)$$

$$2Fe_3O_4(s) \rightarrow 6Fe(s) + 8\,O(g),\ \Delta F_2 \quad (2)$$

$$3Fe_2O_3(s) \rightarrow 6Fe(s) + 9\,O(g),\ \Delta F_3 \quad (3)$$

$$6FeS(s) \rightarrow 6Fe(s) + 6\,S(g),\ \Delta F_4 \quad (4)$$

$$6FeSO_4(s) \rightarrow 6Fe(s) + 6\,S(g) + 24\,O(g),\ \Delta F_5 \quad (5)$$

$$3Na_2Fe_2O_4(s) \rightarrow 6Fe(s) + 6Na(g) + 12\,O(g),\ \Delta F_6 \quad (6)$$

ΔF_1, ΔF_2, and so on, stand for the numerical values of ΔF for their respective reactions for the circumstances under which the reactions might occur; i.e., for partial pressures of atomic oxygen, atomic sulfur, and so forth, equal to those present in the equilibrium gas. These partial pressures are the same for each reaction and, on account of assumption 4, are unaffected by the occurrence of any of the reactions. If the reverse of one of the foregoing reactions be written and added to another of the reactions, for example:

$$6Fe(s) + 6S(g) \rightarrow 6FeS(s),\ -\Delta F_4 \quad (4a)$$

$$\underline{6FeO(s) \rightarrow 6Fe(s) + 6\,O(g),\ \Delta F_1} \quad (1)$$

$$6FeO(s) + 6S(g) \rightarrow 6FeS(s) + 6\,O(g), \Delta F_7 = \Delta F_1 - \Delta F_4, \quad (7)$$

there results a reaction (7), expressing the conversion of one iron compound into another; besides constituents of the gas, reaction (7) involves only two iron compounds. If the ΔF for this new reaction, ΔF_7, is negative, then the right-hand compound, FeS, will be stable in preference to the left hand, FeO. ΔF_7 will be negative if ΔF_4, corresponding to FeS, is larger than ΔF_1. Since each of the reactions (1) through (6) is written to involve the same number of iron atoms, each of the reactions can be combined in this way with any other of the reactions. To determine the stable iron compound, then, it is only necessary to inspect the ΔF-values, ΔF_1, ΔF_2, and so on, and pick the compound cor-

responding to the highest, for, by the foregoing argument, this compound must be favored over all other iron compounds. Elemental iron may be included as one of the possibly stable forms of iron merely by noting whether or not the highest ΔF-value is negative; if it is, then elemental iron is the stable form, because the most stable compound would tend to decompose to form elemental iron and a gas constituent (or constituents).

It makes no difference what oxygen compound (or compounds) is used to supply the oxygen "sink" in reactions (1)–(6), provided the constituents of the gas are in equilibrium with one another. For example, reaction (1) could have been written:

$$6FeO(s) \rightarrow 6Fe(s) + 3\ O_2(g), \quad \Delta F = \Delta F_1' \tag{8}$$

but since $O_2(g)$ and $O(g)$ are in equilibrium with each other,

$$3\ O_2(g) \rightarrow 6\ O(g), \quad \Delta F = 0 \tag{9}$$

Adding reactions (8) and (9), we obtain:

$$6FeO(s) \rightarrow 6Fe(s) + 6\ O(g), \quad \Delta F = \Delta F_1 = \Delta F_1' \tag{10}$$

Since reaction (10) is identical with reaction (1), the ΔF-values for reactions (1)–(6) are not changed by using $O_2(g)$ in place of $O(g)$. Similar arguments will easily show that combinations such as CO/CO_2 and H_2/H_2O can also be used in place of atomic oxygen in reactions (1)–(6) without changing the ΔF-values.

Values of ΔF for reactions (1)–(6) are given by [38, 39],

$$\Delta F_1 = \Delta F_1^\circ + 6RT \ln p_0 \tag{11}$$

$$\Delta F_2 = \Delta F_2^\circ + 8RT \ln p_0 \tag{12}$$

. . .

. . .

. . .

$$\Delta F_6 = \Delta F_6^\circ + 6RT \ln p_{Na} + 12RT \ln p_0 \tag{13}$$

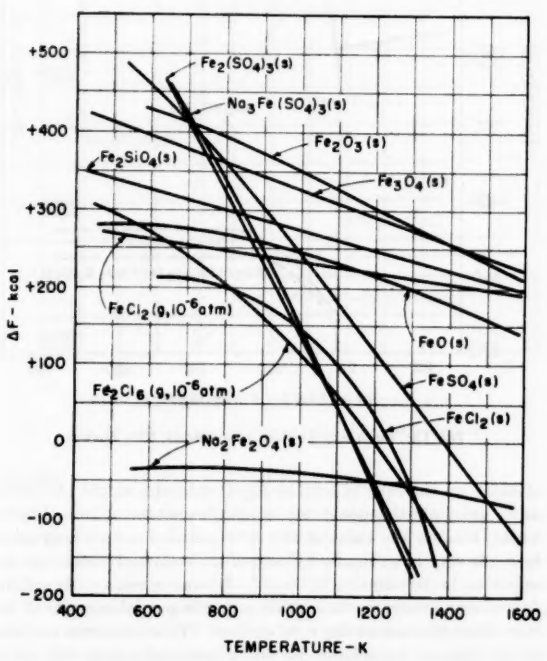

Fig. 9 ΔF versus temperature for decomposition to six Fe atoms—Pana coal, 100 per cent theoretical air

Table 11 Compounds considered

Compound formula	Phase	References for thermodynamic data: ΔH_{f298}°	C_p° $H_T^\circ - H_{298}^\circ$ $S_T^\circ - S_{298}^\circ$	S_{298}°	Estimated reliability of data
Fe	s	14	12	14	good
FeO	s	14	12	14	good
Fe_3O_4	s	14	12	14	good
Fe_2O_3	s	14	12	14	good
FeS	s,l	14	12	14	good
$FeSO_4$	s	14	31	(*a*)	questionable
$Fe_2(SO_4)_3$	s	(*b*)	(*c*)	(*a*)	questionable
$FeCl_2$	g	(*d*)	(*d*)	(*d*)	fair
$FeCl_2$	s,l	14	12	14	good
$FeCl_3$	g	30	30	30	good
Fe_2SiO_4	s	14	12	14	good
$Na_2Fe_2O_4$	s	14	(*g*)	(*h*)	questionable
$Na_3Fe(SO_4)_3$	s	(*i*)	(*j*)	(*k*)	questionable
Na_2O	s	14	12	14	good
NaOH	s,l	14	12	10	good
Na_2S	s,l	(*e*)	(*e*)	(*e*)	fair
NaCl	s,l	14	12	14	good
Na_2SO_4	s,l	9	4	4	good
$Na_2S_2O_7$	s,l	(*f*)	(*f*)	(*f*)	fair
Na_2CO_3	s,l	14	13	14	good
Na_2SiO_3	s,l	14	12	14	good
$Na_2Si_2O_5$	s,l	32	12	32	good

NOTES:

(*a*) Estimated from plot of S_{298}° versus molecular weight for sulfates; data on sulfates from Rossini [14] and Kelley [12].

(*b*) Calculated from ΔH_{298}° of $Fe_2(SO_4)_3$(aq) given by Rossini [14] and a heat of solution of −60,600 cal estimated by Giaque [33].

(*c*) Estimated from heat capacity of similar sulfates by Giaque [33].

(*d*) Estimates from extrapolated vaporization data of Kelley [30] and known thermodynamic data for $FeCl_2$(s, l) from Rossini [14] and Kelley [12].

(*e*) Free-energy function calculated from free-energy data of Richardson and Jeffes [35].

(*f*) Calculated from free-energy data of Flood and Förland [36].

(*g*) Heat capacity assumed to be the sum of the individual heat-capacity values for Na_2O and Fe_2O_3.

(*h*) Estimated from known entropies of Na_2O and Fe_2O_3 and ΔS_{298}° for the reaction,

$$Na_2O + Fe_2O_3 \rightarrow Na_2Fe_2O_4$$

ΔS_{298}° for the reaction estimated from ΔS° for similar reactions [14]:

$$CaO + B_2O_3 \rightarrow CaB_2O_4 \text{ and } FeO + Fe_2O_3 \rightarrow Fe_3O_4.$$

(*i*) Estimated from ΔH_{f298}° for Na_2SO_4 and $Fe_2(SO_4)_3$ and ΔH_{298}° for the reaction, $\frac{3}{2}\ Na_2SO_4 + \frac{1}{2}\ Fe_2(SO_4)_3 \rightarrow Na_3Fe(SO_4)_3$

ΔH_{298}° for the reaction (−3.0 ± 0.5 kcal) obtained by Krieger [34] from heat-of-solution measurements.

(*j*) Estimated [33] to be sum of heat capacities of $^1/_2Fe_2(SO_4)_3$ and $^3/_2Na_2SO_4$.

(*k*) Estimated from the entropies of $Fe_2(SO_4)_3$ and Na_2SO_4 and an estimated [33] value of $\Delta S_{298}^\circ = -1.5$ cal/Kfor the reaction:

$$\frac{3}{2}\ Na_2SO_4 + \frac{1}{2}\ Fe_2(SO_4)_3 \rightarrow Na_3Fe(SO_4)_3.$$

Logarithm terms arise in equations (11)–(13) because, for a perfect gas:

$$\text{Gas (1 atm)} \rightarrow \text{Gas } (p \text{ atm}), \quad \Delta F = RT \ln p \tag{14}$$

The values of ΔF° in equations (11)–(13) depend only upon temperature; they were computed from the basic data referred to in Table 11. The logarithmic terms, however, depend upon gas composition, which is a function of both temperature and fuel-air ratio; their values were computed from the equilibrium gas compositions obtained in Part 1.

The ΔF-functions, equations (11), and so on, were plotted versus fuel-air ratio at constant temperature and versus temperature at constant fuel-air ratio for all twelve iron compounds. Fig. 9 is typical of these plots. In terms of temperature and fuel-air ratio the regions of stability for the various compounds were

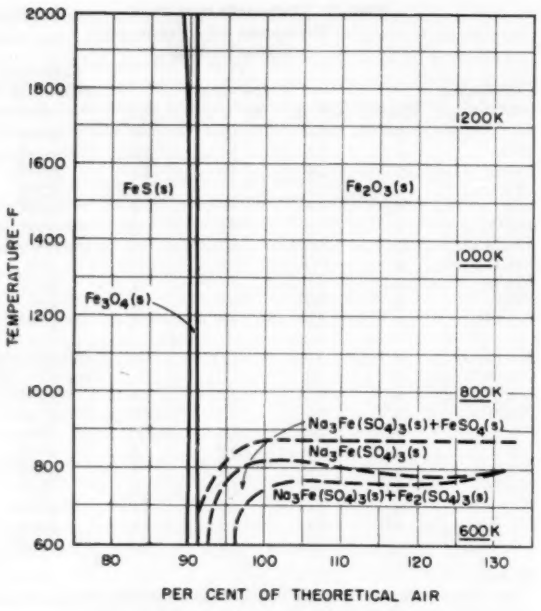

Fig. 10 Pana gas, iron compounds, SiO_2 present

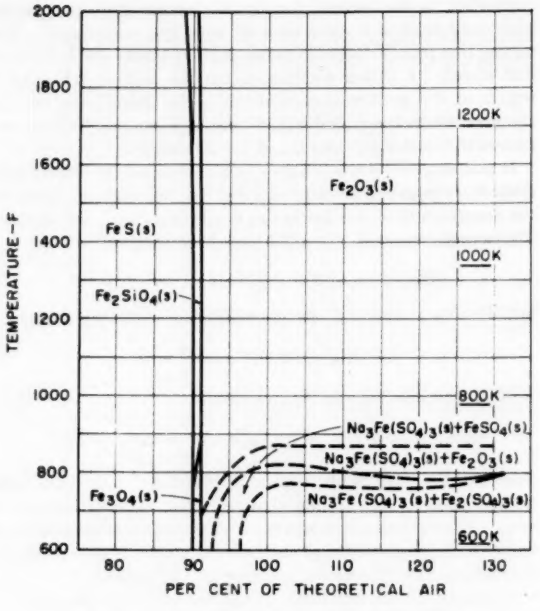

Fig. 11 Pana gas, iron compounds, SiO_2 absent

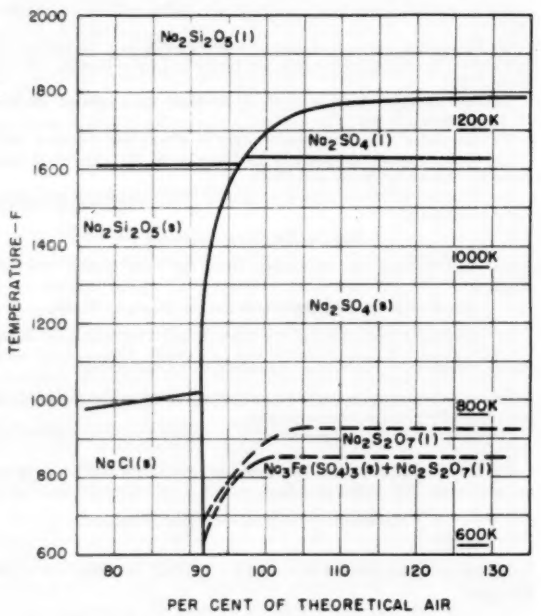

Fig. 12 Pana gas, sodium compounds, SiO_2 present

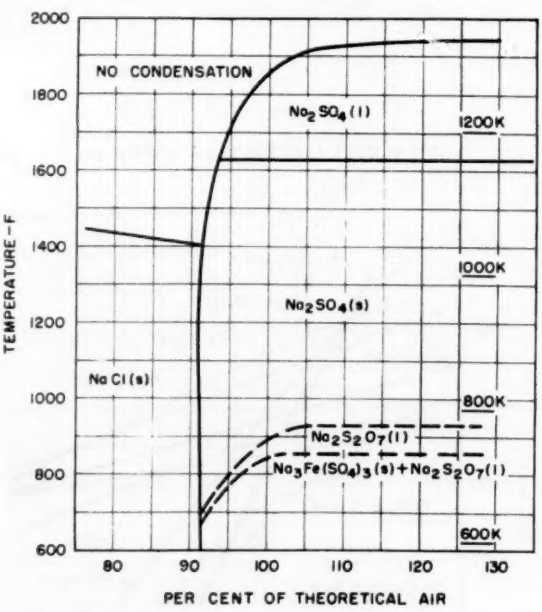

Fig. 13 Pana gas, sodium compounds, SiO_2 absent

easily determined from the plots by following an extension of the principle mentioned previously, namely, that compound is stable whose curve lies above all the others. Sodium compounds were handled in exactly the same fashion except that the decomposition reactions were written so as to involve Na(g). This meant that whenever the highest ΔF-value was negative, no sodium compound was condensed.

Iron chlorides were given special treatment because of the possibility of their formation and subsequent vaporization. Since the equilibrium gas was assumed to contain no iron compounds, instability on the tube of solid or liquid chlorides would not necessarily preclude the possibility of the formation of iron-chloride vapor, because the value of the ΔF-function for the vapor could be made very large simply by assuming the partial pressure of the vapor to be infinitesimally small. It was necessary, therefore, to make an arbitrary assumption as to the partial pressure of the iron-chloride vapor at the tube surface. This value was taken to be 10^{-6} atm on the assumption that a lower value than this would result in a diffusion rate into the gas stream that would be too low to cause rapid corrosion.

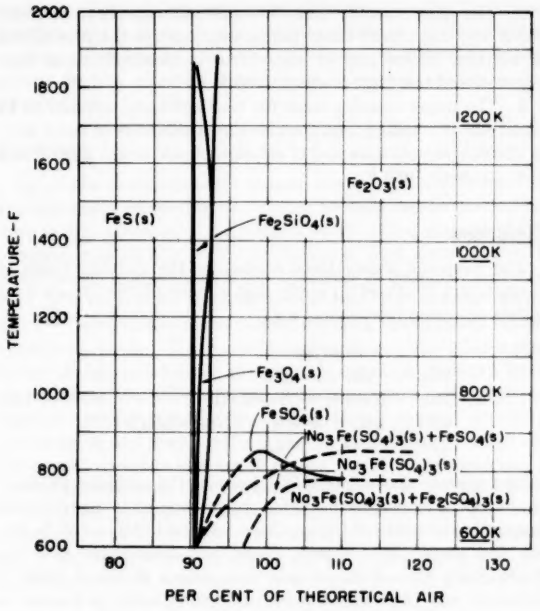

Fig. 14 Wright gas, iron compounds, SiO_2 present

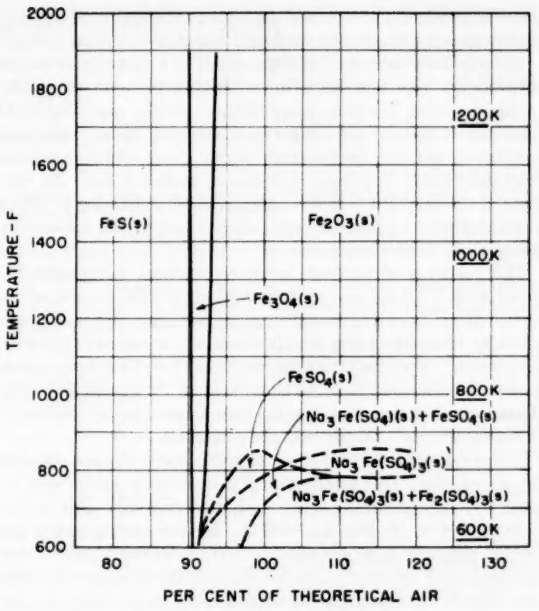

Fig. 15 Wright gas, iron compounds, SiO_2 absent

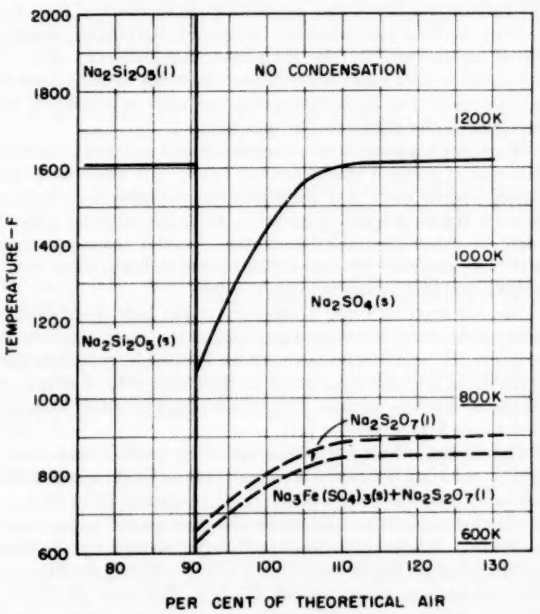

Fig. 16 Wright gas, sodium compounds, SiO_2 present

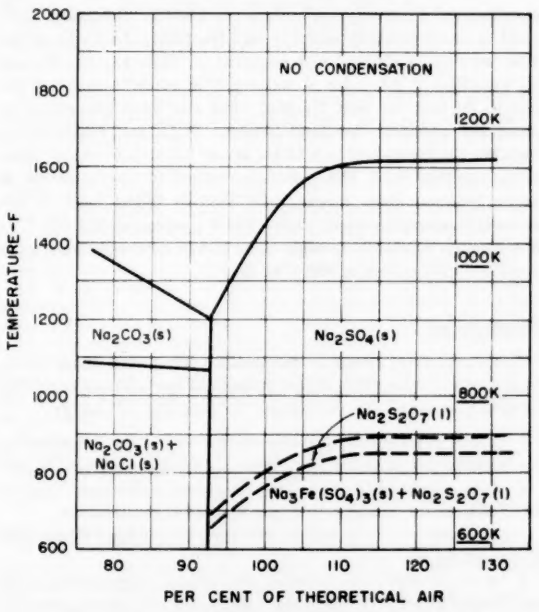

Fig. 17 Wright gas, sodium compounds, SiO_2 absent

Results

Figs. 10–17 show the regions of thermodynamic stability of the various compounds in terms of temperature and fuel-air ratio of the gas with which they are in equilibrium. Four diagrams are for Pana combustion gas and four for Wright combustion gas. Two of the diagrams for each gas apply to iron compounds and two to sodium compounds. Of the two for iron compounds, one applies when SiO_2 is assumed absent (or not available for reaction), and one applies when SiO_2 is assumed present; the same is true of the two diagrams for sodium compounds.

Compounds appearing in Table 11 but not in the diagrams were found to be thermodynamically unstable within the ranges of temperature and fuel-air ratio considered. Where SiO_2 is assumed to be present, it has invariably been assumed to exist in stoichiometric excess of sodium and iron. This assumption simplifies the diagrams without sacrificing accuracy, because the regions where both Si-Na or Si-Fe compounds might co-exist if silica were not in excess are easily constructed by superimposing the diagrams for silica present and silica absent. Where Na-Fe compounds are concerned, iron has always been assumed to be present in stoichiometric excess of sodium. This assumption complicates the dia-

grams somewhat, but it keeps the regions of stability of iron sulfates from being masked by the formation of sodium-iron sulfates.

Dashed lines are used in Figs. 10–17 for boundaries whose positions are uncertain due to uncertainty in the basic thermodynamic data for $Na_2S_2O_7$, $Na_3Fe(SO_4)_3$, $FeSO_4$, and $Fe_2(SO_4)_3$. Such uncertainties are important because these particular boundaries tell the temperature limits above which corrosion mechanisms involving these substances cannot occur. An estimate of the magnitude of the uncertainty is ±100 deg F, which corresponds to a probable error of ±5 kcal in the free-energy functions of these compounds.

The positions of vertical, or nearly vertical, boundaries between 90 and 100 per cent of theoretical air are also somewhat uncertain due to the rapid change in gas composition and consequent difficulty of interpolating the ΔF-functions, equations (11)–(13), in this area. Such uncertainties are thought to be of little consequence because they could be eliminated by further computation of gas composition and because the boundaries must, in any event, lie between 90 and 100 per cent theoretical air.

It was assumed, for simplicity, that the stable compounds exist as pure phases. This assumption is known to be untrue with respect to Na_2SO_4-$Na_2S_2O_7$ [36], and it is probably also untrue with respect to Na_2SO_4-$Na_3Fe(SO_4)_3$, for the corresponding potassium compounds show solubility in the solid state [40]. When solutions occur between stable compounds, the boundary between them should be a more or less broad band rather than a sharp line. Within this band, composition changes gradually from almost pure A to almost pure B. The "width" of the band can be calculated if activity coefficients are known. Assuming them equal to unity (activity equal to mol fraction), the width of the band between Na_2SO_4(s) and $Na_2S_2O_7$(l) (Figs. 12, 13, 16, and 17) would be of the order of 400 deg F in going from 1 mol per cent to 99 mol per cent Na_2SO_4. For the same concentration range, the width of the band between Fe_2O_3 and $Na_3Fe(SO_4)_3$, Figs. 10, 11, 14, and 15 would be about 200 deg F wide. This, taken together with the estimated effect of uncertainties in thermodynamic data, means that $Na_2S_2O_7$ might exist in low concentrations up to about 1200–1250 F (instead of 900–950 F as shown), and $Na_3Fe(SO_4)_3$ might exist in low concentrations up to about 1050 F (instead of 850 F as shown).

Observations

Study and comparison of the stability diagrams, Figs. 10–17, leads to many interesting observations and speculations regarding gas-side corrosion. In particular, we note the following:

1 There is no significant difference between the diagrams for iron compounds in going from Pana to Wright combustion gas.

2 SiO_2 produces in the iron diagrams a narrow band of Fe_2SiO_4(s) in the vicinity of 90 per cent of theoretical air.

3 FeS makes its appearance at a surprisingly high 90 per cent of theoretical air.

4 A major difference between the sodium diagrams for Pana and Wright combustion gas is the appearance of high-temperature liquids, Na_2SO_4(l) and $Na_2Si_2O_5$(l), on the oxidizing side of the Pana diagram. This is due to the high sodium content of the Pana gas.

5 On the reducing side of the diagrams for sodium compounds, the high chlorine content of Pana gas makes NaCl(s), Fig. 13, stable in preference to Na_2CO_3(s) which is stable with the Wright gas, Fig. 17.

6 Again on the reducing side, when SiO_2 is present, $Na_2Si_2O_5$(s) takes precedence over both Na_2CO_3(s) and NaCl(s) except that NaCl(s) remains with Pana gas below about 1000 F.

7 There is only a slight difference in the stability limit for $Na_2S_2O_7$(l) between Pana and Wright gas; there is no difference for $Na_3Fe(SO_4)_3$(s).

8 The upper stability limit for $Na_2S_2O_7$(l) appears to be about 950 F with high alkali coal; taking into account the possibilities of solution effects and of some error in thermodynamic data might extend this limit to about 1250 F.

9 The upper stability limit for $Na_3Fe(SO_4)_3$(s) appears to be about 850 F; taking into account the possibilities of some error in thermodynamic data and of solution effects might extend this limit to about 1050 F.

Discussion

The foregoing observations relative to the stability limits of $Na_2S_2O_7$ and $Na_3Fe(SO_4)_3$ imply that a pyrosulfate-complex iron-sulfate corrosion mechanism, e.g.,

$$\left.\begin{aligned} &\xrightarrow{\text{catalyst}} \\ &SO_2 + {}^1/_2O_2 \longrightarrow SO_3 \\ &SO_3 + Na_2SO_4 \rightarrow Na_2S_2O_7(l) \\ &3Na_2S_2O_7(l) + Fe_2O_3 \rightarrow 2Na_3Fe(SO_4)_3 \\ &2Fe + {}^3/_2\,O_2 \rightarrow Fe_2O_3, \end{aligned}\right\} \qquad (15)$$

cannot operate above 850–1050 F because the corrosion product, $Na_3Fe(SO_4)_3$, cannot form. This observation finds experimental support in the works of Corey, Cross, and Reid [20] and of Anderson and Diehl [22]. Corey, Cross, and Reid found that the $Na_3Fe(SO_4)_3$ present in deposits decomposes at about 1050 F. Anderson and Diehl found that $Na_3Fe(SO_4)_3$ could be formed in synthetic boiler gas (0.5 per cent SO_2, 2.5 per cent O_2) at 1000 F, but not at 1100 F. Severe corrosion occurring above 1050 F [26, 27] may be due to another mechanism or to the fact that the stability limit for the potassium compound, $K_3Fe(SO_4)_3$, is some 200 F higher than that for the sodium compound [22, 40]. If one assumes that another mechanism does not operate, then it would appear that the sodium-potassium ratio in deposits is an important factor in superheater corrosion.

Of course, it is possible that our estimates of inaccuracy in basic data and of solution effects are too small. In any event, the present results show that there must be an upper temperature limit for the mechanism of equation (15). Its value (or values) might be determined quite accurately if better thermodynamic data were available for complex alkali-iron sulfates, alkali pyrosulfates, and their solutions in one another.

The observations 1 and 7, relevant to the lack of differences between the Pana and Wright gas, suggest that the mechanism of equation (15) might operate even with low-alkali coals, although probably at a slower rate, owing to the slower rate of arrival of alkalis at the tube surface. This observation is not at variance with recent field experience [41].

The finding of Fe_2SiO_4, observation 2, implies that under slightly reducing conditions siliceous material might dissolve the normally protective tube-metal oxide, exposing the metal to accelerated oxidation, albeit under less than normal oxygen concentration. Similarly, the finding of FeS at so high a percentage of theoretical air implies that even a mildly reducing condition at the tube surface would convert Fe_2O_3 to FeS with all the deleterious effects which follow therefrom. Metallic iron itself would be capable of producing a reducing condition approximately equivalent to 90 per cent theoretical air provided oxygen (or oxygen-bearing compounds) from the combustion gas were excluded by impermeable deposits. There is experimental evidence [27] that reactions such as

$$4Fe + Na_2S_2O_7 \rightarrow Na_2SO_4 + FeS + 3FeO \qquad (16)$$

actually occur beneath enamel deposits. It remains to be shown, however, what conditions make a deposit impermeable to oxygen.

The finding of stable high-temperature liquids with the high alkali Pana gas but not with the low-alkali Wright, observation 4, seems quite significant in view of the difference in fouling

tendencies between the two coals. It seems possible that these liquids might form on fly-ash particles, either on or off the tube, causing severe fouling; or they might seal an otherwise loosely porous deposit, allowing reducing conditions to develop at the tube surface.

Conclusion

By purely thermodynamic means, this study has succeeded in approximately separating the regions wherein accelerated oxidation, on the one hand, and sulfation, on the other, can operate as corrosion mechanisms. The results are in good agreement with experimental observations when allowance is made for probable error in certain basic thermodynamic data, for solution effects, and for slight differences in behavior among the different alkali-metal compounds. It has also been shown that sulfidation is predicted thermodynamically if oxygen is somehow excluded from the metal surface. These results demonstrate how useful thermodynamic studies can be in distinguishing among corrosion mechanisms, and they spotlight the data required for more accurate and complete distinction among corrosion mechanisms.

Also evident from the thermodynamic results are several interesting and potentially important facts relevant to fouling and high-temperature corrosion. Not the least of these is the finding that high-temperature liquids, $Na_2SO_4(l)$ and $Na_2Si_2O_5(l)$, are stable above 1600 F in contact with high-alkali combustion gas.

References

1 J. W. Myers, S. A. Goldberg, and R. W. Smith, Jr., "Calculation of Theoretical Flame Temperatures in Furnaces," TRANS. ASME, vol. 80, 1958, pp. 202–216.

2 H. C. Hottell, G. C. Williams, and C. M. Satterfield, "Thermodynamic Charts for Combustion Processes," John Wiley & Sons, Inc., New York, N. Y., 1949.

3 A. T. Bowden, P. Draper, and H. Rowling, "The Problem of Fuel-Ash Deposition in Open-Cycle Gas Turbines," *Proceedings, The Institution of Mechanical Engineers*, series A, vol. 167, 1953, pp. 291–300.

4 J. P. Coughlin, "High Temperature Heat Contents, Heats of Transition, and Heat of Fusion of Anhydrous Sodium Sulfate," *Journal of The American Chemical Society*, vol. 77, 1955, pp. 868–870.

5 J. P. Coughlin, "Contributions to the Data on Theoretical Metallurgy XII. Heats and Free Energies of Formation of Inorganic Oxides," U. S. Bureau of Mines Bulletin 542, U. S. Government Printing Office, Washington, D. C., 1954.

6 W. F. Giauque, private communication to The Babcock & Wilcox Company, Boiler Division, June 23, 1958.

7 V. N. Huff, S. Gordon, and V. E. Morrel, "General Method and Thermodynamic Tables for Computation of Equilibrium Composition and Temperature of Chemical Reactions," NACA Report 1037, 1951.

8 D. R. Hull and G. C. Sinki, "Thermodynamic Properties of the Elements," American Chemical Society, Washington, D. C., 1956.

9 K. K. Kelley, "Contributions to the Data on Theoretical Metallurgy VII. The Thermodynamic Properties of Sulphur and Its Inorganic Compounds," U. S. Bureau of Mines Bulletin 406, U. S. Government Printing Office, Washington, D. C., 1937.

10 K. K. Kelley, "Contributions to the Data on Theoretical Metallurgy IX. Entropies of Inorganic Substances. Revision (1940) of Data and Methods of Calculation," U. S. Bureau of Mines Bulletin 434, U. S. Government Printing Office, Washington, D. C., 1941.

11 K. K. Kelley, "Contributions to the Data on Theoretical Metallurgy XI. Entropies of Inorganic Substances. Revision (1948) of Data and Methods of Calculation," U. S. Bureau of Mines Bulletin 477, U. S. Government Printing Office, Washington, D. C., 1950.

12 K. K. Kelley, "Contributions to the Data on Theoretical Metallurgy X. High Temperature Heat-Content, Heat-Capacity, and Entropy Data for Inorganic Compounds," U. S. Bureau of Mines Bulletin 476, U. S. Government Printing Office, Washington, D. C., 1949.

13 M. M. Popov and D. M. Ginzburg, "Specific Heat of Na_2CO_3, Na_2SO_4, and NaOH at High Temperatures," *Zhurnal Obshchei Khimii*, vol. 26, 1956, pp. 971–980. Translated by Associated Technical Services, Inc., East Orange, N. J., Translation No. RJ-859, 1957.

14 F. D. Rossini, D. D. Wagman, E. H. Evans, S. Levine, and I. Jaffe, "Selected Values of Chemical Thermodynamic Properties," National Bureau of Standards Circular 500, U. S. Government Printing Office, Washington, D. C., 1952.

15 P. Sedor, E. K. Diehl, and D. H. Barnhart, "External Corrosion of Superheaters in Boilers Firing High-Alkali Coals," TRANS. ASME, Series A, JOURNAL OF ENGINEERING FOR POWER, vol. 82, 1960, pp. 181–193.

16 S. R. Brinkley, Jr., "Note on the Conditions of Equilibrium for Systems of Many Constituents," *Journal of Chemical Physics*, vol. 14, 1946, pp. 563–564.

17 S. R. Brinkley, Jr., "Calculations of the Equilibrium Composition of Systems of Many Constituents," *Journal of Chemical Physics*, vol. 15, 1947, pp. 107–110.

18 P. H. Crumley and A. W. Fletcher, "Formation of Sulfur Trioxide in Flue Gases," *Journal of the Institute of Fuel*, vol. 29, 1956, pp. 322–327.

19 H. F. Johnstone, "The Corrosion of Power Plant Equipment by Flue Gases," University of Illinois, Engineering Experiment Station," Bulletin No. 228, 1931.

20 R. C. Corey, B. J. Cross, and W. T. Reid, "External Corrosion of Furnace-Wall Tubes II. Significance of Sulphate Deposits and Sulphur Trioxide in Corrosion Mechanism," TRANS. ASME, vol. 67, 1945, pp. 289–302.

21 R. C. Corey, H. A. Grabowski, and B. J. Cross, "External Corrosion of Furnace-Wall Tubes III. Further Data on Sulphate Deposits and the Significance of Iron Sulphide Deposits," TRANS. ASME, vol. 71, 1949, pp. 951–963.

22 C. H. Anderson and E. K. Diehl, "Bonded Fireside Deposits in Coal-Fired Boilers—A Progress Report on the Manner of Formation," ASME Paper No. 55—A-200.

23 E. L. Simons, G. V. Browning, and H. A. Liebhafsky, "Sodium Sulfate in Gas Turbines," *Corrosion*, vol. 11, 1955, pp. 505t–514t.

24 K. Wickert, "Chemische Umsetzungen im Feuerraum der Schmeltzkammerkessel," *Brennstoff-Wärme-Kraft*, vol. 9, 1957, pp. 105–118.

25 M. Werner, "Die Korrosion in Hochtemperaturkesseln," *Werkstoffe und Korrosion*, vol. 10, 1957, pp. 587–596.

26 A. Rahmel, "Oxydation hitzebeständiger Stähle: Einflusz von Alkalisulfat-Ablagerungen bei gleichzeitiger Anwesenheit von Schwefel (VI)-oxydspuren in den Ofengasen," *Archiv für das Eisenhüttenwesen*, vol. 31, 1960, pp. 59–65.

27 W. Nelson and C. Cain, Jr., "Corrosion of Superheaters and Reheaters of Pulverized-Coal-Fired Boilers," TRANS. ASME, Series A, JOURNAL OF ENGINEERING FOR POWER, vol. 81, 1960, pp. 194–204.

28 W. T. Reid, R. C. Corey, and B. J. Cross, "External Corrosion of Furnace-Wall Tubes—I. History and Occurrence," TRANS. ASME, vol. 67, 1945, pp. 279–288.

29 H. W. Nelson, et al., "A Review of Available Information on Corrosion and Deposits in Coal- and Oil-Fired Boilers and Gas Turbines," Report of ASME Committee on Corrosion and Deposits from Combustion Gases, ASME, New York, N. Y., 1959.

30 K. K. Kelley, "Contributions to the Data on Theoretical Metallurgy III. The Free Energies of Vaporization and Vapor Pressures of Inorganic Substances," U. S. Bureau of Mines Bulletin 383, U. S. Government Printing Office, Washington, D. C., 1935.

31 K. K. Kelley and G. E. Moore, "The Specific Heats at Low Temperatures of Anhydrous Sulfates of Iron, Magnesium, Manganese, and Potassium, *Journal of The American Chemical Society*, vol. 64, 1942, pp. 2949–2951.

32 O. Kubaschewski and E. L. Evans, "Metallurgical Thermochemistry," John Wiley & Sons, Inc., New York, N. Y., 1956.

33 W. F. Giaque, private communication to The Babcock & Wilcox Company, Boiler Division, February 19, 1958.

34 I. M. Krieger, private communication to The Babcock & Wilcox Company, Research Division, July 31, 1958.

35 F. D. Richardson and J. H. E. Jeffes, "The Thermodynamics of Substances of Interest in Iron and Steel Making," *Journal of the Iron and Steel Institute*, vol. 171, 1952, pp. 165–175.

36 H. Flood and T. Förland, "The Acidic and Basic Properties of Oxides II. The Thermal Decomposition of Pyrosulfates," *Acta Chemica Scandinavica*, vol. 1, 1947, pp. 781–789.

37 F. D. Richardson and J. H. E. Jeffes, "The Thermodynamics of Substances of Interest in Iron and Steel Making from 0°C to 2400°C—I Oxides," *Journal of the Iron and Steel Institute*, vol. 160, 1948, pp. 261–270.

38 R. R. Wenner, "Thermochemical Calculations," McGraw-Hill Book Company, Inc., New York, N. Y., 1941.

39 B. F. Dodge, "Chemical Engineering Thermodynamics," McGraw-Hill Book Company, Inc., New York, N. Y., 1944.

40 A. Rahmel and W. Jäger, "Untersuchungen über das System Kaliumsulfat-Eisen (III)-Sulfat," *Zeitschrift für Anorganische und Allgemeine Chemie*, vol. 303, 1960, pp. 90–95.

41 J. P. Winkin, discussion of "External Corrosion of Superheaters in Boilers Firing High-Alkali Coals," TRANS. ASME, Series A, JOURNAL OF ENGINEERING FOR POWER, vol. 82, 1960, pp. 192–193.

CARL CAIN, JR.
Research Engineer,
Combustion Engineering,
Inc., Kreisinger Development
Laboratory, Chattanooga, Tenn.

WHARTON NELSON
Chemical Section Leader,
Combustion Engineering, Inc.,
Kreisinger Development
Laboratory, Chattanooga, Tenn.

Corrosion of Superheaters and Reheaters of Pulverized-Coal-Fired Boilers, II

This paper deals with studies of high-temperature fireside corrosion of reheater and superheater tubes in pulverized-coal-fired boilers. Factors affecting the temperature range and rate of corrosion by molten complex alkali sulfates are described. The influence of sulfides, produced by reaction of complex sulfates with tube metal, on corrosion rate is discussed. The similarity of coal-ash to oil-ash corrosion mechanism is brought out. Methods for distinguishing liquid phase from gas-phase corrosion on ferritic alloys are presented.

Introduction

A PREVIOUS paper [1][1] presented results of laboratory and field studies of high-temperature fireside corrosion of reheater and finishing superheater tubes in modern pulverized-coal-fired boilers. Complex iron and/or aluminum alkali sulfates were shown to be formed in fireside ash deposits and to become corrosive when molten on tubes having steam temperatures above about 950 F. The molten compounds migrate through the ash deposit to tube-metal surface as a result of the thermal gradient existing in the deposit, and react with the metal according to the following equation:

$$3Fe + SO_4^{=} \rightarrow Fe_3O_4 + S^{=} \quad (1)$$

Tube metal — Molten complex sulfate — Iron oxide — Sulfide

The skin-temperature range for this rapid liquid-phase attack is bracketed by (*a*) the melting point of the mixture of complex alkali sulfates present, and (*b*) their thermal-stability limit. Its range is about 1025–1300 F. Presence of ash deposits on a tube together with metal temperature within these limits are both necessary for rapid corrosion to occur by this mechanism. Stainless-steel shields attached to tube surfaces effectively prevent corrosion, since the skin temperature of the shields is above the 1300 F temperature limit for formation of these corrosive compounds.

Continued studies of the corrosion process have developed additional data concerning the temperature boundaries, corrosion rates, and methods for distinguishing liquid-phase from gas-phase attack on low-chrome ferritic alloys.

Factors Affecting Liquid-Phase Corrosion Temperature Range and Rate

Effect of Temperature on Corrosion Rate. The effect of temperature on the rate of corrosion produced by molten complex sulfates was described in the earlier paper. Briefly, the rate of corrosion increases with temperature once the melting point of the corroding complex sulfate mixture is reached. With further increase in temperature its thermal-stability limit is exceeded, and no more complex sulfate can be formed. At metal temperatures above this limit, the corrosion rate again assumes the considerably lower gas-phase oxidation rate.

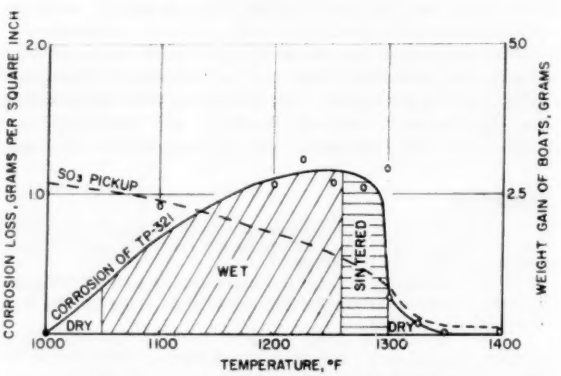

Fig. 1 Liquid-phase corrosion of TP-321 alloy

Fig. 1 shows a complex sulfate-corrosion curve for TP-321 alloy (18 Cr, 8 Ni, Ti stabilized) as a function of temperature. This curve and others in this paper were produced in the following manner: A standard sized ($1^1/_2$ in. × $^1/_4$ in. × $^1/_8$ in.) weighed coupon of test alloy was suspended in a porcelain boat by platinum wire hangers. The coupon was covered with a complex sulfate-generating mixture consisting of sodium sulfate, potassium sulfate, and iron oxide (molar ratio — 1.5:1.5:1 in this case) and placed in a tubular muffle furnace at the desired temperature. Synthetic flue gas of composition 15.0 CO_2, 3.6 O_2, 81.15 N_2, and 0.25 per cent SO_2 was passed over the boat at atmospheric pressure for the duration of the test at a velocity of about 0.6 cfh. Reaction of the corrosion mixture with sulfur trioxide, produced by the catalytic action of Fe_2O_3 on sulfur dioxide and oxygen in the flue gas, resulted in formation of complex sulfates by the following reaction:

$$3(K \text{ or } Na)_2SO_4 + Fe_2O_3 + 3SO_3 \rightleftarrows 2(K \text{ or } Na)_3\,Fe(SO_4)_3 \quad (2)$$

Equilibrium for the reaction was established in about 30 hr. Tests were run for 100 hr. The coupon was then removed, pickled in inhibited acid, and reweighed to determine corrosion loss.

The physical state of the hot corrosion mixtures at the end of the test is indicated in Fig. 1 by different shadings under the curve. The dotted curve shows weight gain of the boat containing the test coupon and corrosion mixture and is an indication of the amount of complex sulfates formed by reaction (2) as a function of temperature. At lower temperatures the equilibrium

[1] Numbers in brackets designate References at end of paper.

Contributed by ASME Research Committee on Corrosion and Deposits From Combustion Gases and presented at the Winter Annual Meeting, New York, N. Y., November 27–December 2, 1960, of THE AMERICAN SOCIETY OF MECHANICAL ENGINEERS. Manuscript received at ASME Headquarters, August 8, 1960. Paper No. 60—WA-180.

favors production of complex sulfates. As the temperature increases above approximately 1100 F, the equilibrium concentration of the complex decreases. Even so, the corrosion rate continues to increase due to the greater reactivity of complex sulfate with metal at higher temperatures. At about 1300 F the concentration of complex becomes so low that the corrosion rate drops abruptly to that of flue-gas attack. On stainless steel the gas-phase corrosion rate is negligible compared to that due to molten complex sulfates.

With the same reactants present, it was postulated that this graph might be extended downward to 600 F and upward to 1600 F to include two other corrosion zones which would be predicted to occur due to the formation of other types of sulfates. In the vicinity of 600 F, sodium and potassium pyrosulfate, which are corrosive to metal, would be expected to form and become molten, producing a second corrosion peak. At about 1540 F another corrosion peak might be encountered due to melting of the normal sodium and potassium sulfates. Thus a two-peak curve would result over the whole temperature range found on heat-transfer surfaces throughout the boiler; i.e., from water walls to superheater tubes. The third high-temperature peak due to normal sulfates might occur only on noncooled supports in high-gas-temperature regions.

Experiments were run in the laboratory to confirm these ideas. Corrosion was noted in each of the other two zones, but it occurred in each case at a lower rate than that due to the molten complex sulfates. Potassium and sodium pyrosulfate are, in the absence of sufficient iron oxide, extremely corrosive to metal, and the very low rate in the pyrosulfate range was the result of the competing reaction:

$$Fe_2O_3 + 3K_2S_2O_7 \rightarrow 2K_3Fe(SO_4)_3 \qquad (3)$$

The end-product complex sulfate formed by this reaction was not molten at 600 to 900 F and hence produced no corrosion. These results are analogous to field experience with pulverized-coal-fired boilers, where a great excess of iron oxide is present in the fly ash and no corrosion occurs on water-wall tubes. With other types of firing which concentrate alkalies in the ash deposits, water-wall corrosion may be accelerated due to a deficiency of iron oxide for reaction (3).

In the molten normal sulfate range, lower corrosion rates were observed due to a less labile sulfate radical in the compound. The sulfate associated with iron in potassium iron trisulfate is apparently more loosely bound and, hence, considerably more reactive than that in the normal salt. This is also true of the "extra" sulfur trioxide in potassium pyrosulfate.

The relation of melting point, corrosive range, and sulfur content of the various alkali sulfates may be seen in Fig. 2. Each type of compound has its characteristic corrosion temperature range; i.e., range in which it is molten and stable. Both melting point and stability of these compounds decrease with increasing sulfur content. Mixtures of the various kinds of alkali sulfates o a particular type or of different types can greatly lower the temperature for initial attack.

Effect of Variation of Complex Sulfate Composition. The temperature range of liquid-phase corrosion varies to a great extent with composition of the liquid phase. Many compounds which would influence the melting point of the mixture and its thermal-decomposition temperature are formed under normal boiler operating conditions. Among these are the normal alkali and alkaline-earth sulfates, pyrosulfates, and complex iron and aluminum trisulfates. Only an extensive investigation would elucidate the effect of all the various constituents on corrosion-temperature limits. A study of several of the more important variables, however, has been completed.

Variation of the sodium-to-potassium ratio greatly affects the melting point of the complex sulfates in an ash deposit. Fig. 3 presents the melting points observed in a synthetic flue-gas atmosphere of various molar ratio mixtures of the two complex compounds, sodium iron trisulfate and potassium iron trisulfate. Sodium iron trisulfate melts at 1155 F in a synthetic flue-gas atmosphere while potassium iron trisulfate melts at about 1145 F. Mixtures of the two, however, show a wide variation of melting points with a minimum occurring between a 1 to 1 and 2 to 1 molar mixture of potassium to sodium compound. This minimum, 1026 F, is about 120 deg F lower than the melting point of either compound alone. Thus the minimum temperature for onset of liquid-phase corrosion may vary considerably as a result of this single type of composition change.

Variation of the corrosion rate is likewise effected by changes in the sodium-to-potassium ratio. Fig. 4 shows the corrosion curve for TP-321 samples in a 1:1 molar sodium-to-potassium corrosion mixture and in a 3:1 mixture. The peak corrosion temperature, employing the 3:1 mixture occurs about 150 deg F lower than that observed with the 1:1 mixture and the corrosion rate is considerably slower. The sodium compound is less stable than the potassium and, consequently, the richer sodium mixtures are less stable. As a result, the corrosion mixture is less fluid at a given temperature owing to the presence of unreacted solid sodium sulfate and iron oxide. This decreased fluidity hampers contact with the metal surface and impedes corrosive action.

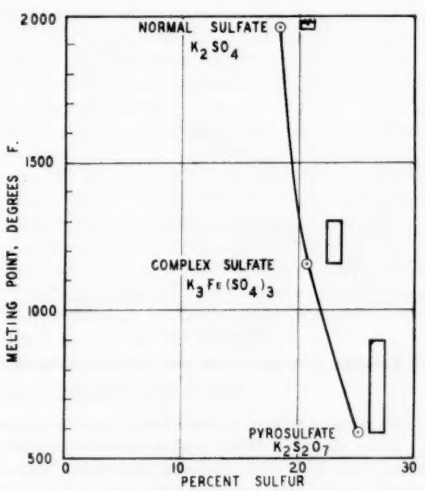

Fig. 2 Melting points of alkali sulfates as a function of sulfur content

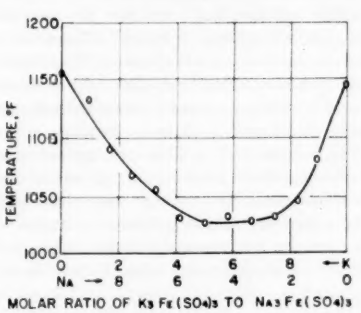

Fig. 3 Melting-point curve for system $K_3Fe(SO_4)_3$–$Na_3Fe(SO_4)_3$

Pure samples of several compounds identified by x-ray diffraction as constituents of corrosive-ash-deposit inner layers have been prepared in the laboratory from normal sulfates, iron or aluminum oxide, and sulfur trioxide. Melting points of these compounds are given in Table 1. The complex iron and aluminum trisulfates are sufficiently stable that melting points could be obtained in a synthetic flue-gas atmosphere. The disulfates, however, decompose considerably below their melting points and so an atmosphere very high in sulfur trioxide has to be provided to prevent decomposition prior to melting. Because of this instability, it is doubtful that the disulfates exist in the deposits during operation. They are probably formed later by hydrolysis due to contact with atmospheric moisture. Ferric sulfate, found in some deposits, is probably also formed by such an action, since it is unstable at superheater and reheater temperatures even in concentrated sulfur-trioxide atmospheres. High sulfur-trioxide concentrations in flue gas, resulting from burning high-sulfur coals, would considerably enhance the stability of all of these compounds, and corrosion would be expected to increase due to the greater quantities of liquid complex sulfates present.

Table 1 Melting points of corrosive-ash constituents in synthetic flue-gas atmosphere

Compound	Melting point, deg F
$K_3Fe(SO_4)_3$	1145
$K_3Al(SO_4)_3$	1210
$Na_3Fe(SO_4)_3$	1155
$Na_3Al(SO_4)_3$	1195
$KFe(SO_4)_2$	1281*
$NaFe(SO_4)_2$	1274*

* In high-sulfur-trioxide atmosphere.

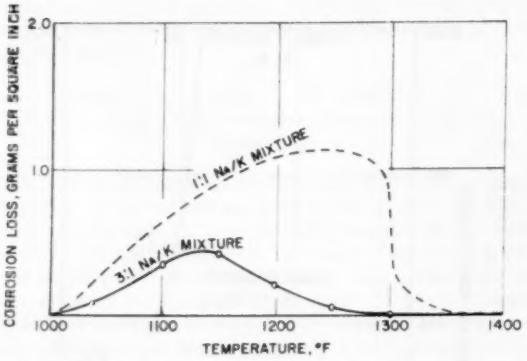

Fig. 4 Variation of corrosion rate with sodium-to-potassium ratio

Effect of Sulfides and Carbides. Sulfides are produced by the corrosive reaction of molten complex sulfates on metal and frequently sulfide penetration into the metal structure is observed. Sulfide penetration of a TP-321 reheater tube is shown in Fig. 5. The intergranular sulfide penetration occurred only under an ash deposit, while the adjacent surface, showing no penetration, was exposed to flue gas only. This severe penetration ahead of the general corrosion front results in considerable increase in the over-all corrosion rate by causing premature separation of metal grains. However, since sulfide penetration depends on liquid-phase corrosion for generation of the sulfide, the two effects are concomitant. Laboratory experiments have shown, however, that sulfides alone are quite injurious to metals, particularly the low-chrome ferritics. In one experiment with T-22 alloy ($2^1/_4$ Cr, 1 Mo), 8.7 per cent of the weight of a coupon was corroded away when covered with ferrous sulfide for 24 hr at 1100 F. This rate is extremely high when compared to the flue-gas oxidation rate at the same temperature. In another experiment, a TP-321 coupon was exposed to ferrous sulfide at 1200 F for 24 hr and lost 0.6 per cent of its weight. These experiments show that rapid corrosion might occur as a result of large build-up in the scale of sulfide which is itself a product of the corrosion reaction.

Surface carburization of tubes in the zones of highest corrosion has sometimes been observed even though carbon in the fly ash is very low. The effect of this carburization is similar to the effect of sulfide penetration, in that grains are prematurely separated from the metal surface, and the corrosion rate is increased. It is believed that carburization occurs at the sites of accelerated liquid-phase corrosion as a result of the reaction:

$$CO_2 + 5Fe \rightarrow 2FeO + Fe_3C \qquad (4)$$

Tube metal under attack by molten complex sulfates is in a sensitized condition and does not have the protective scale which would normally prevent reaction with carbon dioxide of the flue gas. The flue gas probably reaches these sensitized areas through voids in the molten layer and fissures in the oxide scale.

Comparison of Laboratory Corrosion Rates of Alloys. The rate of corrosion of several alloys by molten complex sulfates in laboratory experiments has been found roughly proportional to the gas-phase oxidation resistance of the alloy as shown in Fig. 6. The weight losses shown are for 100 hr exposure and, of course, this short-term exposure does not reflect the parabolic nature of most corrosion processes. It does indicate, however, the relative resistance of the alloys under the conditions employed,

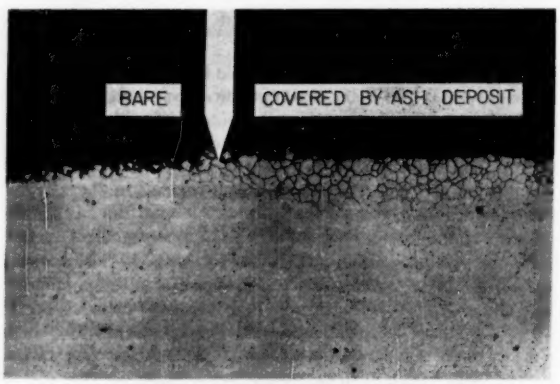

Fig. 5 Sulfide penetration of TP-321 alloy reheater tube

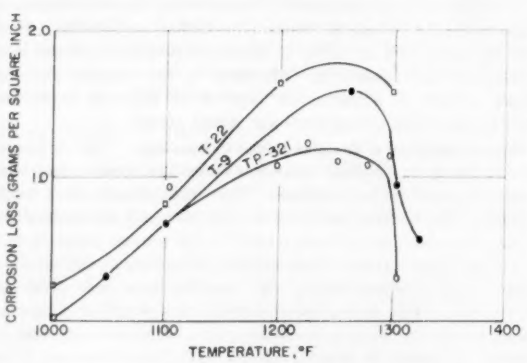

Fig. 6 Effect of alloying constituents on corrosion rate

and suggests that the severity of corrosion could possibly be lessened to a tolerable extent by substitution of highly alloyed tubing, as pointed out by Sedor, et al. [2]. Complete elimination of corrosion in the liquid-phase temperature range, however, will probably not be achieved by substitution of any known alloy since even the very high-chrome and high-chrome-nickel alloys are attacked much more rapidly by molten complex sulfates than by flue gas.

Comparison of Coal-Ash and Residual-Oil-Ash Corrosion

An abundance of literature exists concerning corrosion by ash from burning residual oil in gas turbines and boilers. Much is known about its mechanism and the preventative measures required. Less is known about high-temperature corrosion by coal ash, since the problem is still relatively new, due to the fairly recent advent of steam temperatures above 950 F. Several parallels between the two types of corrosion are evident. In both cases a liquid-phase mechanism and low-melting complex alkali-sulfur compounds are involved. In oil ash the corrosive species consist of sodium sulfate-vanadium oxide combinations, while the corrosive liquid-phase compounds in coal-ash deposits are combinations of sodium and potassium sulfates with iron or aluminum oxides and sulfur trioxide. In both cases, the combinations produce a mixture which is liquid at the operating skin temperature of the metal. These liquids are extremely corrosive, since they are capable of penetrating the usually protective oxide scale of the metal and, once this is accomplished, they do not allow regeneration of a protective scale. In both cases a sulfide scale is formed by the reaction of sulfated materials with the tube metal. Sulfide scales are generally porous and nonprotective and allow the corrosive reaction to proceed with much less inhibition than a corresponding thickness of oxide scale. Sulfidation of metal structure is usually involved with corrosion by both kinds of ash, although sometimes when liquid-phase attack is occurring at a rapid rate, general corrosion obliterates the results of sulfide penetration.

The mechanism of accelerated corrosion for both kinds of ash is similar in that the liquid phase serves to provide oxygen at the metal surface in a highly reactive state. This process has been studied by Cunningham and Brasunas [3] in the case of oil-ash corrosion. Coal-ash corrosion may be viewed in terms of the cyclic process shown in Fig. 7. In the cycle only oxygen and tube metal are consumed and the end product is iron oxide. Thus a small amount of corrosion agent may be responsible for a great amount of metal loss. This may be true also for residual-oil-ash corrosion, wherein the liquid vanadium oxide-sodium sulfate compounds serve chiefly to provide oxygen in a reactive state at the metal surface. Oxygen and tube metal would be the only reactants consumed and iron oxide the net end product in this case as well.

The two corrosion processes fortunately differ in that a comparatively low maximum temperature limits corrosion in the coal-ash case. The hump shape of the coal-ash corrosion versus temperature curve allows effective use of shields which operate at temperatures above the liquid-phase temperature limit. The molten corrosive compounds in oil ash are stable up to very high temperatures, hence shields would not prevent oil-ash corrosion. To alleviate their destructiveness, additives must be used to increase their melting points (and thus eliminate the liquid state) or water washing must be employed to remove the alkali salts from the oil.

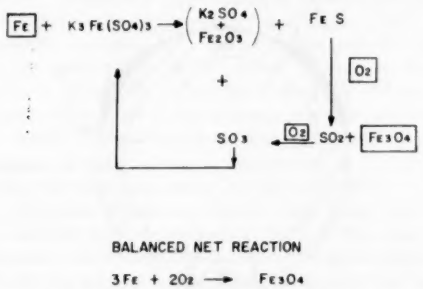

Fig. 7 Diagram of coal-ash corrosion cycle

Use of Shields as a Remedial Measure

The use of shields for eliminating liquid-phase corrosion was discussed in the previous paper. Operation of these TP-304 stainless-steel shields at 1400–1500 F places their temperature above the molten complex sulfate-formation range and below their rapid gas-phase-attack range and, hence, no appreciable corrosion of the shields occurs. Shielding is still the most effective means known to eliminate rapid liquid-phase attack. No corrosion of shields has been observed after more than three years of service in several boilers of up to 1050 F steam temperature, and tube attack has been eliminated. At scheduled outages, replacement of only a few shields dislodged due to soot-blowers and/or to faulty welds has been necessary. Such replacement has averaged less than 1 per cent.

Selection of the proper alloy for shields is an important consideration. At one installation, the lead pendant-outlet reheater tubes of a unit were shielded with ferritic-type 430 (16 Cr) shields which were fabricated and installed exactly as austenitic TP-304 shields had been in other units. After one year of operation, these shields of ferritic alloy had almost completely disintegrated. The normal operating temperature of shields, 1400–1500 F, was below the upper use temperature for this alloy, and so the failure was quite disturbing. It was noted that, during operation, these ferritic shields had accumulated 6-in-thick layers of ash deposits. By comparison, very little ash deposit has ever been seen on the TP-304 shields. It is believed that the thick ash deposits lowered the shield temperature to within the liquid-phase corrosion range, perhaps 1250–1300 F, and that rapid corrosion by molten complex sulfates occurred. These disintegrated shields were subsequently replaced with TP-304 shields which have now been operating for about a year without appreciable ash build-up or damage. Thus an austenitic rather than a ferritic alloy seems to be necessary for shields.

Detection of Liquid-Phase Attack

Remedial measures for alleviation of corrosion depend upon the type of attack causing corrosion. Both liquid and gas-phase corrosion produce black iron-oxide scale as the ultimate end product, hence it is easy to confuse the two types. Rapid corrosion of stainless steel used in finishing superheaters and reheaters is almost always the result of liquid-phase attack, and here little question arises as to the remedial measure necessary. Low-chromium ferritics, on the other hand, are always used at temperatures closer to their much lower gas-phase-scaling temperature limits. With these alloys, determination of the type of attack is extremely important in order to apply the proper remedial measures. For example, if molten complex sulfate is causing rapid corrosion of ferritic tubes in a particular application, the problem will not be obviated by substituting higher chromium alloys or stainless steels. Corrosion may be decreased by such substitution but not eliminated, since all alloys tested to date are vulnerable in some degree to liquid-phase attack. In this case, shielding would be the proper preventative measure. If accelerated corrosion is the result only of overheating a particular alloy (which produces attack by flue gas and/or steam), however, substitution of a higher chrome alloy would be the answer.

Several characteristics have been observed by which liquid-phase attack may be distinguished from gas-phase oxidation:

Determination of Type of Corrosion by Sulfur Prints and Scale Analyses. The value of sulfur prints in locating sites of high sulfide concentrations on corroded tube surfaces was discussed in the previous paper [1]. Sulfides were shown to be a product of liquid-phase corrosive action, and a positive sulfur print indicates this mechanism.

Fig. 8 shows a series of sulfur prints of the windward areas of several corroded ferritic reheater tubes in use longer than two years. Nos. 1 and 6 of T-22 alloy had thick layers of external oxide and no ash deposits which indicated attack by flue gas. Although external corrosion of these two samples was severe, no sulfide could be detected on their surface by sulfur prints. Nos. 2 and 3 (also T-22) had severe external corrosion only under heavy ash deposits. On these samples, high concentrations of sulfide were detected by sulfur prints on the surface only at corroded areas, indicating liquid-phase corrosion. The other sulfur prints, Nos. 4 (T-9) and 5 (TP-430), were made on liquid-phase-corroded test alloy tubes which had bonded ash deposits. The slower rate of wastage of these higher chromium-alloy tubes is indicated by their lighter prints which resulted from lower sulfide concentrations.

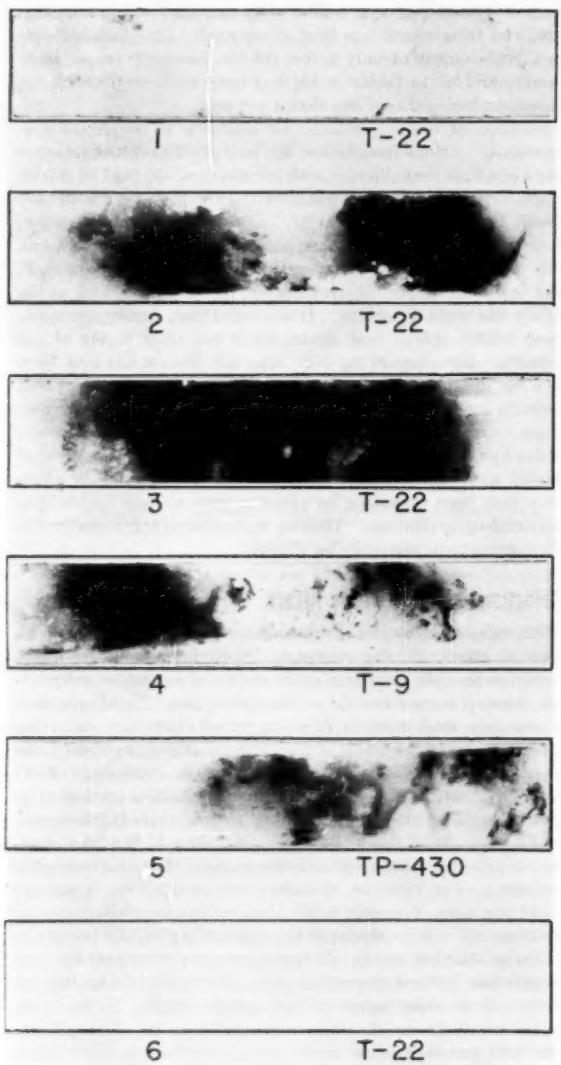

Fig. 8 Sulfur prints from corroded tube surfaces

To determine more precisely the quantities of sulfide involved, analyses were run on laboratory corroded coupons and scaled surface of various portions of field-exposed tubes. These analyses are shown in Table 2. Gas-phase attack on laboratory test coupons and also on leeward (rear) surfaces of tubes produced only 0.1 to 2.0 mg of ferrous sulfide per square centimeter compared to 24 to 109 for liquid-phase-attacked surfaces. Corresponding measurements of sulfide on contiguous gas and liquid-attacked areas on the same tube showed this same difference in concentration. Thus quantitative measurement of sulfide content of adherent scale and qualitative detection of it by sulfur prints are both reliable methods for identifying the type of attack on corroded ferritic alloy.

Visual Surface Appearance. The surface appearance of corroded ferritic and austenitic tubing is also indicative of the type of attack which has occurred. This difference is quite obvious in a comparison of the surfaces of coupons corroded by liquid and gas-phase mechanisms. Fig. 9 is an enlarged view of two series of laboratory coupons after exposure for 5 days to a 1:1 molar ratio of sodium:potassium iron trisulfate at various

Table 2 Sulfide concentration of corrosion scale

Station	Alloy	Type of exposure	Area	Sulfide (mg FeS/cm²)	Sulfur print
Laboratory (39 days)	T-22	Flue gas	Entire surface	0.1	No
Laboratory (4 days)	T-22	Liquid	Entire surface	24.3	Yes
Laboratory (4 days)	T-22	Liquid	Entire surface	26.2	Yes
Boiler 1 (30 months)	T-22	Flue gas	B	0.9	No
		Liquid	D	28.7	Yes
Boiler 1 (30 months)	T-9	Flue gas	B	0.6	No
		Liquid	C + D	24.4	Yes
Boiler 2[a] (4 years)	T-22	Flue gas	B	0.2	No
		Liquid	C	0.2	No
Boiler 3 (17 months)	T-22	Flue gas	B	2.0	No
		Liquid	D	109.0	Yes

[a] Natural gas fired, no gas deposits on tubes.

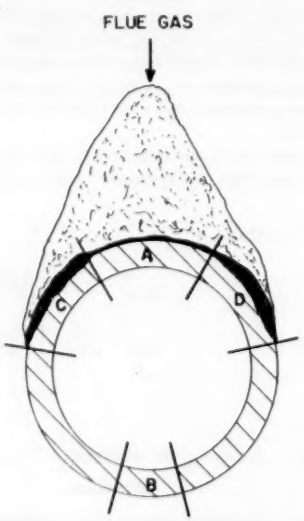

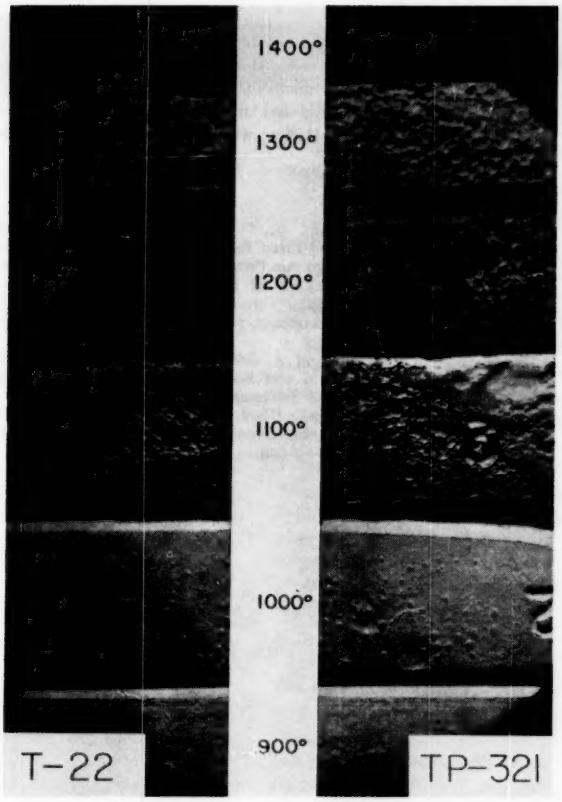

Fig. 9 Surface appearance of liquid- and gas-phase corroded laboratory samples

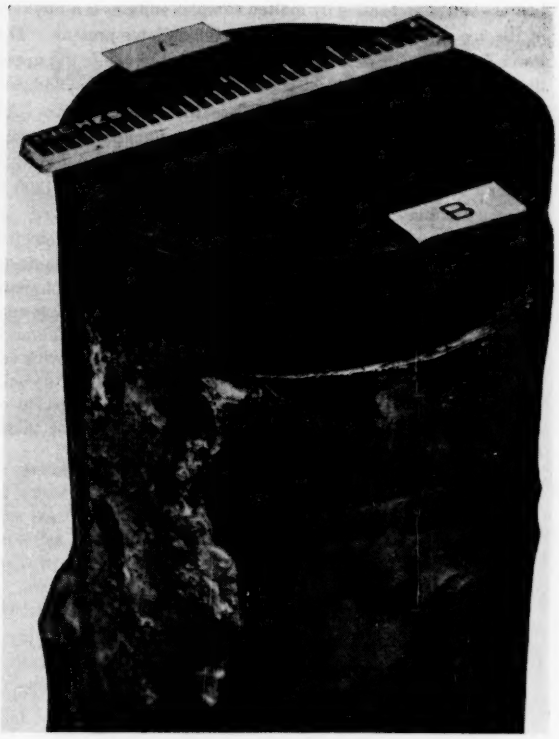

Fig. 10 Surface appearance of liquid- and gas-phase corroded tube sample

temperatures from 900 to 1400 F under a synthetic flue-gas atmosphere. A pitted surface may be seen on the coupons exposed in the liquid-forming range at 1100, 1200, and 1300 F while at 900 and 1000 F practically no corrosion had occurred, since the temperature was below the melting point of the mixture, Fig. 1. The T-22 coupon was attacked severely by flue gas at 1400 F which was 300 deg F above its gas-phase scaling limit. The striking difference in surface condition may be seen readily in the illustration. At 1400 F, the T-22 coupon was smooth and evenly corroded, while at 1200 F the liquid-phase attack produced deep and uneven pitting. This same distinction in surface appearance of metal corroded by liquid and gas-phase mechanisms was also noted for TP-321 alloy.

A comparison of liquid and gas-phase attack on a field-corroded T-22 tube is shown in Fig. 10. On the upper pickled ring, the pitted "alligatored" appearance of liquid-phase attack on the windward surface exposed to liquid-phase corrosion under ash deposits contrasts with the relatively smooth surface of contiguous gas-phase-attacked metal. Where a heavy ash deposit is in place on a ferritic tube, the tube surface becomes "notched" at the edge of the deposit-coated surface due to the greater attack by complex sulfates than by flue gas.

Microscopic Surface Condition. Penetration of sulfur into the metal has been discussed earlier in relation to effect on corrosion rates. Extensive sulfidation results only when corrosion by molten complex sulfates produces sulfides at the metal surface. Penetration of sulfides is also indicative of liquid-phase attack. On TP-321 the penetration of sulfides is marked and easily observed after etching. It is generally intergranular in nature. The low chromium-ferritic alloys, however, have shown sulfide penetration rather erratically by the present etching technique. Metallographic examination to date is not a reliable test for the presence of liquid-phase attack on ferritic tubes.

Gaging the Potential Corrosiveness of a Deposit

Complex iron and aluminum alkali sulfates are the only known materials occurring in coal-fired superheater and reheater deposits that are molten, stable, and corrosive at these skin temperatures. Other factors being equal, the proportion and amount of these substances present in the inner layer of an ash deposit next to the tube metal or oxide scale is a gage of the potential corrosiveness of the deposit. A simple method may be employed to determine the amount of complex sulfates present in an inner deposit layer. It is based on the fact that complex sulfates hydrolyze when placed in water, according to the equation:

$$2K_3\,Fe(SO_4)_3 + 6H_2O \rightarrow 3K_2SO_4 + 2Fe(OH)_3 + 3H_2SO_4 \quad (5)$$

The iron hydroxide is insoluble, and the pH of the solution will be low due to the sulfuric acid liberated. This sulfuric acid may be titrated potentiometrically with standard base to obtain the per cent of "excess sulfate," defined by Anderson and Diehl [4] or the equivalent per cent of complex sulfate present in the deposit. Results, of course, will be influenced by the care with which the corrosive inner ash-deposit layer adjacent to the tube is separated from the inert friable outer ash-deposit layers and products of metal corrosion.

Conclusions

The temperature range of rapid liquid-phase corrosion of re-

heaters and superheaters by molten complex sulfates is a function of the species and proportion of complex sulfates present. The lower limit for corrosion may vary considerably, while the upper limit is relatively constant at about 1300 F. Sulfidation and carburization of metal structure increase the corrosion rate. All alloys tested are subject in some degree to liquid-phase attack. Shielding of corrosion-prone surfaces remains the best remedial measure to date. Only those surfaces between 1025 and 1300 F which accumulate ash deposits are subject to such attack.

Liquid-phase corrosion on austenitic alloys may be detected by inspection of the tube surface for pitted and notched condition and metallographically for penetration of sulfides. On ferritic alloys determination of sulfide content of scale overlaying corroded areas or using a sulfur-print technique reveals a difference between liquid and gas-phase corrosion. The potential corrosiveness of a deposit may be estimated by determination of the acid content of a water solution of its inner corrosive layer adjacent to the tube surface. Proper preventative measures may be taken once the type of corrosion has been identified.

Acknowledgments

The authors wish to acknowledge the work of the following individuals in connection with this investigation: Mr. P. V. Andreae, who conducted metallurgical examinations, Mr. J. R. M. Long, who investigated melting points and thermal stabilities, and Mr. C. W. Holley, who developed sulfide analytical techniques.

References

1 W. Nelson and C. Cain, Jr., "Corrosion of Superheaters and Reheaters of Pulverized-Coal-Fired Boilers," TRANS. ASME, Series A, JOURNAL OF ENGINEERING FOR POWER, vol. 82, 1960, pp. 194–204.

2 P. Sedor, E. K. Diehl, and D. H. Barnhart, "External Corrosion of Superheaters in Boilers Firing High-Alkali Coals," TRANS. ASME, Series A, JOURNAL OF ENGINEERING FOR POWER, vol. 82, 1960, pp. 81–193.

3 G. W. Cunningham and A. deS. Brasunas, "The Effects of Contamination by Vanadium and Sodium Compounds in the Air Corrosion of Stainless Steels," *Corrosion*, vol. 12, 1956, p. 389t.

4 C. H. Anderson and E. K. Diehl, "Bonded Fireside Deposits in Coal-Fired Boilers—A Progress Report on the Manner of Formation," ASME Paper No. 55—A-200.

Journal of ENGINEERING FOR POWER

Information for Authors

• Manuscripts should be submitted in final form to the Editor. Each manuscript must be accompanied by a statement that it has not been published elsewhere nor has it been submitted for publication elsewhere. A paper which would occupy more than 8 pages of the Journal may be returned to the author for abridgment.

• The author should state his business connection, the title of his position, and his mailing address. A short abstract (50 to 100 words) should be included on the first page immediately preceding the introductory paragraph of the paper.

Three copies of the manuscript are required. One of these must be a carefully prepared printer's copy, typed in double spacing, on one side of the page only, with wide margins, on $8^1/_2$ by 11-in. opaque white paper. Mimeographed manuscripts, if prepared with exceptional care, can be accepted provided they are completely edited.

• As far as possible, all mathematical expressions should be typewritten. Greek letters and other symbols not available on the typewriter should be carefully inserted in ink. Care should be taken to distinguish between capital and lowercase letter, between zero (0) and the letter (*O*), between the numeral (1) and the letter (*l*), etc. A letter representing a vector cannot be printed with an arrow above or below it. The letter should be underscored with a single wavy line, wherever it appears in the text, to designate boldface type.

• A list of symbols carefully marked for the use of the editor (thus: κ, Greek l.c. kappa), if it has not been included in the body of the paper, should accompany the manuscript on a separate page.

• Before preparing a manuscript the author should study printed articles in the Journal, with special attention to the form and style of mathematical expressions, tables, footnotes, references, and abstract. Numbers that identify mathematical expressions should be enclosed in parentheses. Numbers that identify references at the end of the paper should be enclosed in brackets. Care should be taken to arrange all tables and mathematical expressions in such a way that they will fit into a single column when set in type. Equations that might extend beyond the width of one column (fractions that should not be broken or long expressions enclosed in parentheses) should be rephrased to go on two or more lines within column width. Fractional powers are preferred to root signs and should always be used in more elaborate formulas. The solidus should be used instead of the horizontal line for fractions wherever possible.

• A normal paper should not exceed 8 pages in the Journal. It is about 8000 words or 20 double-spaced typewritten pages exclusive of drawings. A Technical Brief should not exceed 750 words or about one page in the Journal inclusive of drawings.

• Originals and two copies of figures must accompany the manuscript. Line drawings should not be larger than $8^1/_2 \times 11$ in. and should be planned for reduction to column width. Lettering should be large enough to be clearly legible when the illustration is reduced. The originals of line drawings must be in India ink on white or pale blue tracing paper or tracing cloth. Photographs of equipment or test specimens must be glossy prints and should be used sparingly. Captions for figures should be typed double-spaced and included as the last page of the manuscript. The figure number and author's name should be written in the margin or on the back of each illustration.

• Titles of papers should be brief.

• Authors can obtain copies of the ASME Manual MS-4, "An ASME Paper," from the Editor and are urged to do so before drafting their papers in final form.

• Papers published in Journals of the Transactions of the ASME must be presented at a Meeting, either in person or by title.

• An author is entitled to 25 preprints free of charge (in the case of two authors, 15 each; three or more authors, 10 each). Larger quantities of preprints or reprints can be ordered from Editorial Department, The American Society of Mechanical Engineers, 345 East 47th Street, New York 17, N. Y. Quotations will be sent on request.

Please address all communications to:

Editor, ASME,

United Engineering Center

345 East 47th Street,

New York 17, N. Y.

ASME Publications Committee

Publications of The American Society of Mechanical Engineers

TECHNICAL DATA ON FUEL In this Sixth Edition texts and tables have been reset, the subject matter has been rearranged, the contents of the book extensively revised, tables have been recalculated where necessary, or replaced on the basis of more recent data, and a number of new topics added. **Contents:** Atomic Weights, Mathematical Tables, Units and Conversion Factors. Selected Principles and Methods of Technical Calculations, including fluid flow, fluidized flow, heat transfer, calculation of flame temperature, I-t diagram, combustion with oxygen and oxygen-enriched air. Techniques of Measurement and Special Conversion Tables, including temperature measurement, flow measurement, barometer corrections, viscometry, calorimetry. Selected Properties of Substances, including viscosity, saturated air and gas, thermodynamic properties of steam, refrigerants and heat-transfer media, thermal conductivity, specific heat, thermodynamic functions. Metals and Alloys. Refractory Materials. Gaseous, Liquid, Solid, and Nuclear Fuels. **1961 $8.75 to ASME members and nonmembers**

IDEAS, INERTIA AND ACHIEVEMENTS In this book are the comments and suggestions of a hundred engineering executives, scientists, and engineers of eighty-eight leading organizations and institutions on reducing the time-lag between scientific discovery and engineering application. They range from the need of systems that interrelate internal research and development activity with published material from all sources to management's responsibility in organizing communications, personnel, capital, patents, and steps in planning corporate programs; possibe approaches to the process of applying new discovery to development of useful hardware; the bearing that the functions of universities and research institutes, as well as government agencies have on the relation of research to application; and the steps taken to deal with the time lag problem under the Soviet system. **1960 $5.00 to ASME members and nonmembers**

MATERIALS HANDLING HANDBOOK Here has been condensed and organized virtually the entire literature of modern materials handling, stressing the economies and short-cuts of the greatest importance to industry; and giving the actual operating experiences of hundreds of companies in all segments of manufacturing and industry. **Contents:** Definition and Scope. Analyzing Materials Handling Problems. Materials Handling Factors. Factory Planning. Materials Positioning in Production. Materials Handling Research. Materials Handling and Production Control. Communication Systems. Training Personnel. Handling Bulk Materials. In-Process Handling of Bulk Materials. Unit Handling of Various Shapes. Unit Handling in Manufacturing. Scrap Classification and Handling. Uses of Containers in Industry. Industrial Packaging. Palletization. Warehousing and Yard Handling. Truck Terminal Handling. Air Terminal Handling. Belt Conveyors. Elevating Conveyors. Chain Conveyors. Trolley Conveyors. Cable Conveyors. Haulage Conveyors. Vibrating and Oscillating Conveyors. Pneumatic Conveyors. Package Conveyors. Portable Conveyors. Fixed Cranes, Derricks, and Cableways. Traveling Cranes and Towers. Portable Cranes. Elevators. Winches. Auxiliary Crane Equipment. Positioning Equipment. Powered Industrial Trucks. Industrial Hand Trucks. Industrial Tractors. Highway Trucks and Truck-Trailers. Railroad Freight Cars. Marine Carriers. Air Carriers. Pallets and Containers. **1958 $20.00**

DIAPHRAGM CHARACTERISTICS, DESIGN AND TERMINOLOGY Defines a diaphragm and its performance characteristics, describes methods of measuring and representing them, shows how they are related and used, describes and illustrates the effects of design details and manufacturing methods on the characteristics. In the appendixes, the terms and notations used are defined, the equipment and measurement methods used described, applications of the diaphragms classified, and the various equations presented. **1958 $3.75**

Please note: **Members' prices are 20% less except where stated otherwise.**

You save handling and mailing charges by sending payment with order.

SMALL PLANT MANAGEMENT In this revised second edition the basic material in the original book, published in 1950, has been updated to provide the small business man with the kind of good sound information he needs to obtain maximum utilization of his management skills. **Contents:** Part 1—The Economic and Industrial Importance of Small Plants. Small Plant Financing and Banking. Community Progress Created by Small Plants. Government Interest in Small Plants. Part 2—Top-Management Planning for the Small Plant. Organizing the Small Plant. Operating the Small Plant. Supervising and Controlling the Small Plant. Part 3—How to Fulfill the Legal Requirements. How to Get Best Workers and Labor Relations. How to Get Along With the Union. How to Buy Best Facilities and Materials. How to Obtain Best Productivity. How to Do Technical Research. How to Get Best Sales. How to Do and Use Accounting. How to Pay and Save in Taxes. How to Make Savings and Use Profits. Part 4—The General Outlook for Small Plants in the United States. Quality Control in the Small Business. A Management Check List. Bibliography. Index. **1960 $10.50**

FIFTY YEARS PROGRESS IN MANAGEMENT, 1910–1960 This is both a chronical of a half century's progress in management and a portent of things to come. It comprises five ten-year progress reports. That for the period 1950–1960 focuses attention on progress made in formulating a testable philosophy of management; management as a profession; practices in general and operational management; management science, management education, and management internationally. Earlier reports extend back to the 1910–20 decade when the modern themes of management came into prominence. They accurately reflect the thinking and progress in such areas as administrative organization, job evaluation and standardization, wage plan, profit sharing, industrial hazards, occupational diseases, human factor, budgetry control, industrial marketing and many other management activities. **1960 $10.50**

HANDBOOK OF CONSULTING PRACTICE FOR MECHANICAL ENGINEERS Sets forth the proper approach in obtaining professional engineering services, in establishing the fundamental structure for engineering agreements, and in determining the general conditions that should apply to the conduct of engineering assignments under various types of agreements. Part 1 of the book contains the basic recommendations prepared by the Engineers Joint Council while Part 2 covers those practices which are important to the mechanical engineer but which are not discussed elsewhere in the book. **1960 $2.00**

DIRECTORY OF CONSULTING ENGINEERS Contains the names and addresses of ASME members who are consulting engineers, also those of consulting engineering companies with which members are associated. The listing is both alphabetical and geographical, with the latter including a brief statement of specialty of each entry. **1957 $2.50**

RECOMMENDED PRACTICES FOR THE DESIGN OF MARINE PROPULSION UR BINE LUBRICATING SYSTEMS Provides the marine industry with a reliable guide for improving the design of marine turbine lubricating systems. Three groups of systems (gravity, pressure and pressure/gravity) are recommended. Requirements for materials, piping, valves, oil coolers, oil heating, oil strainers, and fire hazard are included. These practices were developed by representatives of equipment builders, ship designers, and government agencies.
ASME Standard No. 111 **1960 $1.50**

RECOMMENDED PRACTICES FOR CLEANING OF TURBINE LUBRICATING SYSTEMS Offers procedures for preparing new turbine lubricating systems, the cleaning of systems after service, and the purification of turbine oils. **1952 $1.00**

RECOMMENDED PRACTICES FOR THE DESIGN OF TURBINE LUBRICATING SYSTEMS Presents recommendations for the design and construction of turbine lubricating oil systems which will enable the turbine oil to deliver the maximum of its functional possibilities.
ASME Standard No. 108 **1955 $1.00**

GUIDE TO RESEARCH IN AIR-POLLUTION This guide is divided into four sections, the first summarizing the status of air-pollution research as a whole; the second listing the 370 projects under investigation during 1959 alphabetically by states and thereunder alphabetically by name of those conducting the research; and the third and fourth sections providing indexes to these projects by subject and by investigator.
Fourth Edition **1961 $4.00**

INSTRUMENTS FOR THE STUDY OF ATMOSPHERIC POLLUTION Lists hundreds of devices ranging from filter samplers to gas chromatography, many others of corollary nature, and gives the names and addresses of the suppliers. Third Edition **1959 $2.00**

MANUFACTURERS OF DUST AND FUME CONTROL EQUIPMENT Lists available commercial equipment for collecting and separating dust and fumes from gases, gives useful information about the equipment, the names and addresses of the manufacturers, the type of equipment each produces, and, where possible, the trade names under which the equipment is sold. **1960 $1.50**

POWER REACTORS This second edition includes foreign as well as domestic nuclear reactors for producing electric power. For each plant the following information is given on a standardized form: Plant location; reactor type; status; estimated plant costs; electric power data, nuclear data; information on the fuel elements; also on the reactor from core overall dimensions to moderator, reflector, shielding, refueling, core heat flux, etc.; reactor control; the primary and secondary coolant systems; and the steam system. Schematic diagrams show heat removal and utilization cycle. **1959 $3.75**

RESEARCH AND TEST REACTORS The 93 facilities in this book are located in various parts of the world. For each reactor the following information is presented, also on a standardized form: Reactor location, cost of reactor facilities, operating design power, principal use of reactor, the applicable fuel, nuclear data, the reactor, and the primary coolant. **1959 $7.50**

FLUID METERS, THEIR THEORY AND APPLICATION Provides authentic, reliable information on fluid meters and metering techniques. Section A defines the terms used to designate thirty-eight types of fluid meters, describes some of the special methods useful in tests which involve fluid flow and its measurement, lists the symbols employed in fluid metering, defines the special terms used in connection with fluid meters, and discusses the methods of measuring the quantities to which they are applied. Section B considers some of the distinctive features of fluid meters, presents the theory of fluid measurement, and describes in full the development of practical working equations from theoretical relations. Section C gives the figures and tables useful in solving practical fluid measurement problems along with examples to illustrate the proper use of the data presented. **1959 $8.00**

FLOW MEASUREMENT Offers the best available information on the construction and installation of the three most extensively used differential head metering units, namely, thin plate orifice, flow nozzle, and venturi tube. After outlining the advantages and disadvantages of these units, the report takes up their construction, recommends types of pressure connections to use, illustrates location of pressure taps used with orifices and flow nozzles, shows the general arrangement to be used when a flow nozzle is mounted in plenum chamber, discusses the system by which differential pressure can be measured, and presents the values of flow coefficients in tabular form. The report also shows how the primary elements are installed, includes examples to illustrate the appropriate methods of applying data, and gives tolerances for discharge coefficients, flow coefficients, and the expansion factors.
PTC 19.5.4 **1959 $5.00**

United Engineering Center, 345 E. 47th Street, New York 17, N. Y.